Myeloid cells at the onset of colitis in the context of IRF5 deficiency



Dorothée Lisa Berthold

Wadham College

University of Oxford

A thesis submitted for the degree of

Doctor of Philosophy

Michaelmas 2022

Abstract

Innate immune cells are at the frontline of balancing the host response to microbiota and dietary antigens in the intestine. Dysregulation of the intestinal immune system can lead to chronic inflammation like inflammatory bowel disease (IBD). Emerging evidence supports a regional specialization of immune cells due to different microenvironments along the gastrointestinal tract. Macrophages are known to play a pivotal role in homeostasis and in orchestrating the initiation and maintenance of inflammation. Neutrophils are the first immune cells to be recruited to the site of inflammation and are used as a hallmark of disease in IBD. The tissue microenvironment and the microbiota are two major factors influencing immune cell function in the intestine.

Interferon Regulatory Factor 5 (IRF5) is a transcription factor expressed in myeloid cells, activated during inflammation and mediating the transcription of pro-inflammatory mediators. Recently, its role in murine colitis was uncovered alongside a previously undefined role in controlling neutrophil activation.

In this thesis, we set out to investigate the the spatiotemporal patterns of myeloid cell infiltration over a time course of *Helicobacter hepaticus* + aIL10R mediated model of murine colitis. We discovered a distinct infiltration of neutrophils in areas of higher inflammation, together with a two-fold monocyte recruitment wave. Recent studies have demonstrated the ability of neutrophils to tailor their functions to mount tissue-specific and transcriptionally regulated inflammatory responses. Despite their central role in the onset of inflammation, modulation of their function and its effect in diseases is understudied. As *Irf5-/-* mice were completely protected from colitis at peak of inflammation, we aimed to unravel the mechanisms by which immune cells interact and set up the pro-inflammatory microenvironment. By deleting a IRF5 specifically in neutrophils using a novel genomic mouse model, we deciphered the crucial role of neutrophils in mediating monocyte recruitment through lower CCL2 secretion. Our results thus open a new area of investigation as well as lead to novel therapeutic avenues targeting neutrophil activation.

Furthermore, we investigated immune-microbe crosstalk at the onset of *Helicobacter hepaticus* + aIL10R-mediated colitis, by modulating the microbiome through cohousing. We found a major role of the microbiome in regulating neutrophil function, acting via IRF5. Microbiome sequencing revealed a selection of bacterial species significantly associated with inflammation, warranting further investigation in the exact molecular mechanisms involved. We found higher lipocalin 2 secretion by *Irf5-/-* neutrophils, which could lead to an altered microbiome, as well as affect the function of other immune cells.

All in all, the modulation of IRF5 specifically within neutrophils led to vast changes at the onset of intestinal inflammation, despite only a few genes being differentially regulated between WT and *Irf5-/-* neutrophils. This thesis not only highlights neutrophils as pivotal players in intestinal inflammation, but also offers means to dissect the underlying mechanisms and identify new pathways to target in order to circumvent IBD.

Acknowledgements

I would like to first and foremost acknowledge my supervisor Prof. Irina Udalova for the continuous support and guidance over the course of my PhD, also to explore novel ideas (like cohousing mice) and helping me to shape my project and focus on crucial experiments. Furthermore, I would like to thank Irina for reading and critiquing my thesis, helping me to shape and structure it. My thanks extend to my co-supervisor Prof. Fiona Powrie, who has provided me with scientific guidance on the mucosal immunology part of this project.

Thank you to my thesis committee members, Prof. Tal Arnon, Prof. Holm Uhlig and Prof. Siamon Gordon for all their input and guidance over the years of my DPhil. Special thanks also goes to Prof. Wolf-Dietrich Hardt, for your mentorship extending since my Masters, for your career advice and support.

I would like to acknowledge the financial support granted by the Kennedy Trust for Rheumatology Research for funding my scholarship.

I would also like to acknowledge all of the animals used in this study and throughout the history of scientific research. They have paid the ultimate sacrifice in our quest to advance scientific knowledge and ultimately save human lives, a fact for which we should be eternally grateful for.

A special thanks goes to each member of the Udalova lab for their continuous daily support, be it through listening to one of my rants, looking at crappy data, helping me in the lab, sending memes, sharing life or by having lunch at 12 sharp. I am beyond grateful to having been able to do my PhD in such a great lab, surrounded by wonderful people who are endlessly inspiring to me:

Thank you Kristina, for all your help inside the lab with your optimism, amazing staining protocols and reading my first chapter of this thesis, and outside the lab, for being such a kind and supportive friend, endless science discussions over dinner and being enthusiastic for any adventure. Lockdown wouldn't have been manageable without you, I'm forever grateful.

Bara, it has been amazing to share this PhD journey with you, through highs and lows, we've always pulled through and found an appropriate meme. Thank you for listening to all my blabla and complaining, and for all the wonderful conversations we had in the lab, scooping poop, and outside, not scooping poop.

A big dank je wel also to Erinke, for helping me with all the scRNA-seq experiments (third time is the charm) and with countless takedowns and reading my second thesis chapter whilst on holidays! You have been such a supportive friend throughout my PhD, listening to so many absurd ideas and providing critical input, and sharing the love for cheese.

Thank you to Alastair, whose project I was continuing, for all your help and support in my first year, teaching me the techniques and basics needed for this project and not losing your patience when I couldn't even prepare an excelsheet for my first *in vivo* experiment.

I would also like to give a big thanks to Hayley, without your lab management skills and countless times of takedown help and the wonderful defactinib experiments I couldn't have made it.

Thank you Laura, for your shared enthusiasm about poop samples and the microbiome and for reading my discussion.

I would also like to thank the members of the Powrie lab, for all the scientific discussions and help throughout the years, I'm glad I was able to be a honorary half-Powrie!

Thank you to Claire, for scoring all my histology in good spirits and being a big support for my germ-free experiments.

My thanks extend to Sam, and his countless hours spent with me on the cryostat or microscope when I first started, enduring my frustrations.

A big thank you also goes to Rebecca, who has helped me tremendously with the microbiome data and parenting Hh so many times over the years - no one I'd rather share the Hh baby with.

I would also really like to thank Alina, for being my partner in crime in regards to proximal versus distal takedowns (double the work!!) and neutrophils in colitis. It has been amazing to work with you!

Thank you to Xinyue, for bringing microbiology and Salmonella back into the Powrie lab, and for reading and supporting me throughout my thesis writing.

Nick, thank you for providing so much feedback over the years re microbiome, be it my literature review or now the microbiome part of my project. I would also like to thank Jethro, the discussions with you and Nick were super helpful in shaping the third chapter of my thesis.

When I came to Oxford, I had to start anew, and I'm beyond grateful to have met the people that shaped the four years I was here, for all the experiences, laughs and conversations we had. I'm looking forward to welcoming you in Switzerland, and also to visit you all in the different corners of the world.

My biggest thank you goes to Marta, my beloved housemate and dearest friend. I can't imagine Oxford without you, you have been my home and comfort, seeing all my highs and lows. Thank you for enduring to live with me, listening to me, for all the conversations, laughs, tears, meals, and comforting silences, film nights, boardgame nights, pancakes, walks etc we had.

Thank you Matt - our extended housemate - for the "science girls" coffees in the BDI, always being there to listen and help (especially with my tons of excel sheets, where you provided an easy python script to ease countless hours of image analysis)! It was very inspiring to see everything you did beside your PhD, even if unachievable for a mere mortal.

Thank you Cat, for being my friend since day 1, our medicine dinner at Wadham, you are such a caring and wonderful friend. Kate, our lockdown walks and shared experiences, of

course also seeing the film you made, were so uplifting and wonderful. Thank you Klem, for all the memes and laughs over the years, sharing our wonderful PhD experience. Mariana, it was such a lucky punch that you ended up in the Kennedy, after having shared lab space back in Zurich. Thank you for all your support over the years, and for learning how to canoe with me. Thank you Erik, also a former lab member ending up in Oxford, for showing me how to lose in squash, and all the discussions around my Salmonella experiments and my PhD experience. It was great to already have a friend in England when I arrived, so I'm beyond grateful for Lorraine, and all the visits between Oxford and the Lake District, which have shown me the beauty of North England and the escape from Oxford city life.

I couldn't have done it without my friends back in Switzerland, I am beyond grateful for all the amazing friends I have back home, who were willing to endure this journey with me, skyping and visiting and supporting me whenever I needed you.

Thank you to Seraina, you are such a wonderful friend, being able to just share the mood as is, for all the laughs and cries over the years, and your visits to Oxford.

Danja, my oldest friend, you were such a rock throughout this time, always there for me and supporting me with kind messages, care packages and visits.

Thank you Celina, even if we are not in the same country, talking with you for endless hours and your visits to Oxford were invaluable.

Rahel, it was wonderful to share this experience with you, travelling to South Africa together and hearing about your latest adventure.

Thank you Anna for your support over the years, our holidays in Sicily in the middle of a covid-ridden year was truly one of my saving graces.

Thank you M@u, for all the fübis and memes provided over the years.

I would also like to thank Annika, my previous supervisor and friend, for all the support over the years and helping me to become an independent scientist.

Thank you to Madelon, my friend from the Netherlands, for sharing cheese, laughs and our love of books. Looking forward to our next exchange visit!

Eternal gratitude extends to my parents, and my brother Matthias who have been beyond supportive of my journey to Oxford, even if it wasn't easy at times. Even though having 5000km between us, I have felt your love and support daily, and I always knew I could rely on you no questions asked. Thank you for all the visits, allowing me to show you my daily Oxford life, and the spontaneous and planned calls, sharing life.

Finally, I would like to thank Dave, for your never-ending support, your love I experience daily and telling me when to stop complaining and start doing something. I couldn't have done this without you.

Contributions

I declare that the thesis presented is the result of my own work. All experimental data presented in this thesis are original and were performed by myself unless indicated otherwise in the text.

The experiments described below were performed with assistance from others:

- Dr. Kristina Zec performed the CXCL1 staining on the colon (Figure 3.8d)
- Dr. Alastair Corbin generated the bulk RNA-seq dataset from sorted neutrophils from a mixed-bone marrow chimera at d21 Hh + aIL10R, which was used for hypothesis generation (Figure 4.26a)
- Dr. Zhichao Ai performed the stimulation of Hoxb8 neutrophils with zymosan (Figure 4.27a) and analysed immature and mature neutrophils at steady state and d7 Hh + aIL10R (Figure 4.30)
- Dr. Claire Pearson assisted with histopathology scoring of all *in vivo* experiments (Figure 4.6b, 4.9b, 4.19b, 4.23b)
- Rebecca Jeffery analysed the microbiome sequencing dataset (Figure 5.14 & Figure 5.18, 5.16, 5.17)
- Dr. Laura Myhill carried out the experiment identifying neutrophil populations using Ly6G, CD177 and CD101 as markers (Figure 4.12, Figure 4.13 & Table 4.1)
- FACS was conducted by Mr. Jonathan Webber of the Kennedy Institute of Rheumatology Flow Cytometry Facility
- Histology was sectioned and stained by the Kennedy Institute of Rheumatology Histology team (Dr. Bryony Stott, Dr. Ida Parisi, and Ms Rhiannon Cook)
- Various lab members assisted with the takedowns of Hh + aIl10R colitis experiments

This thesis is made available under a Creative Commons Attribution Non-Commercial No Derivatives Licence. The copyright rests with the author alone. Researchers are free to copy or distribute this thesis on the condition that the author is recognised, and that such copying or distribution is not for a commercial purpose.

Approximate word count: 36400

Contents

List of Figures **x**

List of Tables **xiv**

List of Abbreviations **xv**

1 Introduction **1**

1.1 Regional differences along the gastrointestinal tract 2
1.1.1 Architecture of the gastrointestinal tract 2
1.1.2 The intestinal tissue microenvironment 4
1.1.2.1 Dietary factors 5
1.1.2.2 The microbiome and dysbiosis 7
1.2 The intestinal immune system 12
1.2.1 Innate immune system 13
1.2.1.1 Myeloid cells 13
1.2.1.2 Lymphoid cells 16
1.2.2 Adaptive immune system 17
1.3 The *Helicobacter hepaticus* model of colitis and its relation to IBD in humans 19
1.3.1 Inflammatory bowel disease 19
1.3.2 The *Helicobacter hepaticus* + anti-IL10R model of colitis 20
1.3.3 The value of experimental mouse models for studying IBD pathogenesis 21
1.4 IRF5 as a regulator of immune cell function 22
1.4.1 Signalling pathway of IRF5 22
1.4.2 The role of IRF5 in various immune cell populations 23
1.5 Hypothesis and aims 26

2 Material and Methods **28**

2.1 *In vivo* models 29
2.1.1 Animals 29
2.1.2 *Helicobacter hepaticus* culture 30
2.1.3 *Helicobacter hepaticus* and aIL10R model of colitis 31
2.1.4 Assessment of *Helicobacter hepaticus* colonisation 31
2.1.5 Histoscoring 34
2.1.6 *Salmonella* Typhimurium culture 34
2.1.7 *Salmonella* Typhimurium infection model 34
2.1.8 Assessment of CFU 34
2.1.9 Cecal gentamicin protection assay 35

2.2 Cell isolation protocols . . . 35
2.2.1 Isolation of intestinal lamina propria leukocytes . . . 35
2.2.2 Isolation of blood leukocytes . . . 36
2.2.3 Splenocyte isolation . . . 36
2.2.4 Bone marrow isolation . . . 37
2.3 Flow cytometry . . . 37
2.3.1 Extracellular labelling of cells . . . 37
2.3.2 Intracellular labelling of cells . . . 40
2.3.3 Flow cytometry acquisition and analysis . . . 40
2.3.4 FACS . . . 40
2.4 Protein and RNA analysis . . . 41
2.4.1 CCL2, CCL3 & Lipocalin 2 ELISA . . . 41
2.4.2 Dynabeads RNA extraction . . . 41
2.4.3 RNA extraction with Qiagen Miniprep . . . 42
2.4.4 cDNA generation . . . 42
2.4.5 Taqman RT-qPCR reaction . . . 43
2.5 Confocal microscopy . . . 44
2.5.1 Sample preparation and embedding . . . 44
2.5.2 Immunofluorescence labelling of colons - unfixed sections . . . 44
2.5.3 Immunofluorescence labelling of colons - PLP fixed sections . . . 45
2.5.4 Image acquisition and processing . . . 46
2.5.5 Image analysis and quantification . . . 47
2.6 Cell culture and *in vitro* stimulation . . . 48
2.6.1 Freezing and thawing of cell lines from liquid nitrogen . . . 48
2.6.2 Maintenance and differentiation of Hoxb8 cells . . . 48
2.6.3 *In vitro* stimulation . . . 49
2.7 Statistical analysis . . . 50

3 Unravelling spatial differences of the tissue microenvironment and immune cell infiltration over the course of murine intestinal inflammation 51
3.1 Regional specialization of intestinal macrophages along the gastrointestinal tract . . . 52
3.2 Aims . . . 55
3.3 Results . . . 56
3.3.1 Myeloid cells are the first responders in Hh + aIL10R-mediated inflammation . . . 56

3.3.2 Swiss rolls as a powerful tool to investigate cellular and tissular changes during intestinal inflammation . . . 58
3.3.3 Characterization of CX3CR1-GFP Ly6G-tdTomato double-reporter mice . . . 60
3.3.4 Distinct infiltration of myeloid cells at specific sites over the course of intestinal inflammation . . . 62
3.3.5 *Helicobacter hepaticus* localisation over the course of intestinal inflammation does not indicate a preferred colonisation site . . . 66
3.3.6 The tissue environment starts to differ as early as d4 Hh + aIL10R between the distinct proximal and distal microenvironments . . . 67
3.3.7 Neutrophils correlate with areas of higher inflammation at the onset of inflammation . . . 71
3.3.8 Changes in the macrophage subset pool occur distinctly in the proximal and distal colon over the timecourse of inflammation . . . 73
3.3.9 Macrophage subsets occupy distinct niches in the colon at steady state 75
3.3.10 Macrophage subset markers and their localisation blur during inflammation . . . 79
3.4 Discussion . . . 81
3.4.1 The tissue microenvironment leads to distinct spatiotemporal immune cell infiltration in the colon . . . 81
3.4.2 Inflammation-dependent changes of the tissue microenvironment leads to differential localisation of macrophage subsets . . . 83
3.5 Conclusion . . . 86
3.6 Future directions & limitations . . . 87

4 The role of IRF5 in myeloid cells at the onset of colitis 89
4.1 Interferon regulatory factor 5 in colitis . . . 90
4.2 Aims . . . 92
4.3 Results . . . 94
4.3.1 *Irf5-/-* mice display a distinctly different cellular landscape in the inflamed colon as early as d7 Hh + aIL10R . . . 94
4.3.2 Expression of IRF5 in CX3CR1+ cells is required for the onset of intestinal inflammation and recruitment of neutrophils and monocytes 102
4.3.3 Characterization of a novel neutrophil-specific Ly6G-Cre strain . . . 106
4.3.4 Expression of IRF5 in neutrophils is required for the onset of intestinal inflammation . . . 116

4.3.5 Deletion of IRF5 specifically in neutrophils is sufficient to prevent the onset of intestinal inflammation altogether . . . 121
4.3.6 The tissue microenvironment is significantly different in Ly6G^{Irf5} mice at d7 Hh + aIL10R . . . 125
4.3.7 CCL2 secreted from IRF5-proficient neutrophils leads to the infiltration of monocytes into the inflamed colon . . . 127
4.3.8 The set-up of an *in vitro* system to study the effects of neutrophils and monocytes in isolation . . . 131
4.3.9 Immature neutrophils accumulate in the colons of inflamed mice . . 132
4.4 Discussion . . . 136
4.4.1 Depletion of IRF5 leads to a distinct myeloid landscape at the onset of colitis . . . 136
4.4.2 IRF5 in neutrophils plays an indispensable role in amplifying intestinal inflammation . . . 137
4.5 Conclusion . . . 144
4.6 Future directions & limitations . . . 145

5 IRF5-dependent neutrophil-microbiota crosstalk at the onset of intestinal inflammation 147
5.1 Crosstalk between neutrophils and the microbiota . . . 148
5.1.1 Regulation of neutrophils by the microbiome . . . 150
5.1.2 Neutrophil responses toward the microbiota and gut infection . . . 151
5.2 Aims . . . 154
5.3 Results . . . 156
5.3.1 IRF5-deficient neutrophils are not deficient in clearing SPI-2 deficient *Salmonella in vivo* . . . 156
5.3.2 IRF5-deficient neutrophils produce more lipocalin 2 . . . 161
5.3.3 IRF5-deficiency in neutrophils leads to inflammation in cohoused mice 164
5.3.4 Higher Lcn2 levels in the cecum of cohoused Ly6G^{Irf5} mice . . . 167
5.3.5 Hh colonisation does not account for the differences between genotypes 167
5.3.6 Metagenomic microbiome sequencing reveals differences in overall microbiota composition . . . 170
5.3.7 Dysbiosis ratios not altered between inflamed and protected conditions 173
5.3.8 Differences at steady state between cohoused and separately housed mice . . . 175
5.3.8.1 Ly6G^{cre} mice at steady state . . . 175
5.3.8.2 Ly6G^{Irf5} mice at steady state . . . 175

5.3.9 Specific microbiota species are associated with inflammation status independently of the genotype of the mice 178
5.4 Discussion 180
5.4.1 The ability of *Irf5-/-* neutrophils in controlling pathogen infection . 180
5.4.2 The effect of microbiome composition on IRF5 function in neutrophils 181
5.5 Conclusion 186
5.6 Future directions & limitations 186

6 General Discussion **189**
6.1 Summary of results 189
6.2 Intrinsic and extrinsic regulation of the BM niche during inflammation . . 190
6.3 The tissue microenvironment as a scaffold for intestinal inflammation . . . 192
6.4 New insights in neutrophil-monocyte interactions during intestinal inflammation 197
6.5 Deciphering the priming of immune cells by the microbiota 201
6.6 Future directions 205
6.7 Conclusion 206

Appendices

A Appendix 1 **208**

References **211**

List of Figures

1.1 Architecture of the gut mucosal wall . . . 2
1.2 Anatomy of the intestinal mucosa in the small intestine and colon . . . 3
1.3 Spatial distribution of microorganisms along the gastrointestinal tract . . . 10
1.4 Spatial rearrangement of main bacterial phyla in IBD . . . 11
1.5 Components of the innate and adaptive immune system . . . 12
1.6 Cells expressing IRF5 in the colonic lamina propria . . . 22
1.7 Model of proposed role of IRF5 at peak of in intestinal inflammation . . . 25
1.8 Experimental set up . . . 27

3.1 Differences along the gastrointestinal tract include physical, chemical, dietary and microbial factors. . . . 54
3.2 Myeloid cells infiltrate the colon at different timepoints over the course of intestinal inflammation. . . . 57
3.3 Hh + aIL10R colitis induces severe colitis and leads to epithelial elongation and an increase in macrophage numbers. . . . 59
3.4 Characterization of CX3CR1-GFP Ly6G-tdTomato double-reporter mice in intestinal inflammation. . . . 61
3.5 Myeloid cells infiltrate the colon at distinct sites over the course of intestinal inflammation. . . . 63
3.6 Myeloid cells infiltrate the colon at distinct sites over the course of intestinal inflammation. . . . 64
3.7 *Helicobacter hepaticus* colonization along the timecourse of murine colitis . . . 65
3.8 Immune cell-recruiting chemokines are expressed distinctly in the proximal and distal colon . . . 69
3.9 Expression of pro-inflammatory cytokines starts in the proximal colon at d4 Hh + aIL10R . . . 70
3.10 Intestinal inflammation in Hh + aIL10R model starts in the distal colon . . . 72
3.11 The macrophage pool starts to differ at d7 Hh + aIL10R . . . 74
3.12 CD206+ macrophages and CD11c+ macrophages are distinctly localised at steady state . . . 77
3.13 Flow cytometry gating for CD206+ and CD11c+ macrophages reveals higher percentage of double-positive cells at d21 Hh + aIL10R . . . 80
3.14 Overview of spatiotemporal changes between the proximal and distal colon along the course of intestinal inflammation . . . 85

4.1 IRF5 at the crossroad for setting up chronic intestinal inflammation . . . 90
4.2 Experimental set up chapter 4 . . . 93

4.3 Representative gating scheme for progenitors in the bone marrow 95
4.4 Representative gating scheme for myeloid cells in the colon 96
4.5 No changes in myeloid cell pools in colon, bone marrow and blood at d4 Hh + aIL10R in *Irf5-/-* 97
4.6 Increased recruitment of leukocytes and myeloid cells in the colon at d7 Hh + aIL10R in *Irf5-/-* 99
4.7 Ly6C^{hi} monocytes are decreased in the blood of *Irf5-/-* mice at d7 Hh + aIL10R 100
4.8 Lower proportions of mature monocytes and neutrophils in the bone marrow of *Irf5-/-* mice at d7 Hh + aIL10R 101
4.9 CX3CR1^{Irf5} mice exhibit a significant reduction of pathology at the onset of inflammation 103
4.10 No difference in Ly6C^{hi} monocytes and neutrophils in the blood at d7 Hh + aIL10R 104
4.11 Development deficiency of monocytes and neutrophils in the bone marrow of CX3CR1^{Irf5} during inflammation 105
4.12 Examining the labelling efficiency of different neutrophil markers CD101 and CD177 107
4.13 Ly6C^{int} CD11b+ composition in bone marrow, blood and colon 110
4.14 Representative gating scheme for identification of various cell types for characterization of Ly6G-Cre tdTomato+ expressing cells 111
4.15 Expression of Ly6G-driven Cre measured by td-Tomato in various cell types across different tissues 112
4.16 Composition of Ly6^{int} CD11b+ using t-SNE to identify distinct cell populations 113
4.17 *Irf5* is not expressed in epithelial cells and fibroblasts at d7 Hh + aIL10R . 114
4.18 Neutrophils exhibit a reduction in *Irf5* expression in Ly6G^{Irf5} mice 115
4.19 Lower recruitment of Ly6C^{hi} monocytes into the colon of Ly6G^{Irf5} mice at the onset of inflammation 117
4.20 No differences in Ly6C^{hi} monocytes numbers in the blood 118
4.21 Lower production of mature monocytes in the bone marrow of Ly6G^{Irf5} mice 119
4.22 *Helicobacter hepaticus* colonization is not different at d7 Hh + aIL10R between Ly6G^{cre} and Ly6G^{Irf5} mice 120
4.23 *Irf5*-deficient neutrophils prevent intestinal inflammation 122
4.24 The cytokine landscape is distinctly set up at d7 Hh + aIL10R in Ly6G^{Irf5} mice 123
4.25 The chemokine landscape is distinctly set up at d7 Hh + aIL10R in Ly6G^{Irf5} mice 124

4.26 *Ccl2* expression is lower in *Irf5-/-* tissue and *Irf5-/-* neutrophils during inflammation . . . 126
4.27 IRF5-deficient neutrophils produce lower levels of CCL2 *in vitro* . . . 128
4.28 Titration of *Helicobacter hepaticus* sIAg and LPS on Hoxb8 neutrophils . . 129
4.29 Neutrophils secrete a soluble factor stimulating monocyte pro-inflammatory cytokine secretion . . . 130
4.30 Change in the proportion of neutrophil populations in the inflamed colons of WT mice . . . 133
4.31 Ly6G^{cre} mice have higher percentages of immature neutrophils in the colon at d7 Hh + aIL10R . . . 134
4.32 Ly6G^{cre} mice have higher percentages of immature neutrophils in the colon at d21 Hh + aIL10R with unchanged levels in the blood . . . 135
4.33 Model for the onset of colitis in WT, *Irf5-/-*, CX3CR1^{Irf5}, Ly6G^{Irf5} mice . 143

5.1 The double-edged sword of neutrophils . . . 148
5.2 Microbiome-mediated modulation of neutrophil recruitment and function . 150
5.3 Neutrophil-mediated modulation of the microbiome . . . 152
5.4 Experimental set up chapter 5 . . . 155
5.5 Ly6G^{Irf5} mice have lower CFU values over the course of *Salmonella* Typhimurium infection . . . 158
5.6 No differences in bacterial loads of systemic organs and the cecum at d5 p.i. 159
5.7 No differences in immune cell populations of the cecal tissue at d5 p.i. . . . 160
5.8 Trend towards higher Lcn2 production in Ly6G^{Irf5} mice approaching chronic infection of S. Tm . . . 162
5.9 *Irf5-/-* neutrophils produce higher quantities of Lcn2 after stimulation . . . 163
5.10 The effect of Ly6G^{Irf5}-mediated protection is dependent on the microbiome 165
5.11 Higher levels of Lcn2 are found in the cecum of cohoused Ly6G^{Irf5} mice at d7 Hh + aIL10R . . . 166
5.12 *Helicobacter hepaticus* colonisation is significantly lower in cohoused Ly6G^{cre} mice . . . 169
5.13 Alpha diversity is comparable across samples . . . 171
5.14 Microbiome analysis reveals specific clustering based on inflammation status 172
5.15 Dysbiosis ratios are comparable between the different conditions at d7 Hh + aIL10R . . . 174
5.16 *Porphyromonadaceae* are significantly higher in cohoused Ly6G^{cre} mice . . 176
5.17 Several distinct bacterial species are elevated in cohoused Ly6G^{Irf5} mice at steady state . . . 177

5.18 Specific bacterial species are correlating with intestinal inflammation . . . 179
5.19 Model for the mechanism behind cohousing/non-cohousing switch in phenotype 185

6.1 Model for the mechanism behind spatiotemporal infiltration of myeloid cells at the onset of Hh + aIl10R intestinal inflammation 196
6.2 Model for the microbiome-independent role of IRF5 in neutrophils at the onset of Hh + aIL10R intestinal inflammation 200
6.3 Model for the microbiome-dependent role of IRF5 in neutrophils at the onset of Hh + aIL10R intestinal inflammation 204

A.1 Expression of CX3CR1-GFP in various progenitor populations in the bone marrow 209
A.2 Sex-differences at the onset of intestinal inflammation 209
A.3 *In vitro* proposed set-up for assessing monocyte recruitment by neutrophils 210

List of Tables

2.1 Mouse strains used across DPhil project 30
2.2 Mastermix for Hh RT-qPCR 32
2.3 Mastermix for 16S RT-qPCR 32
2.4 *Helicobacter hepaticus* RT-qPCR protocol 32
2.5 16S RT-qPCR protocol 32
2.6 *Helicobacter hepaticus* primers 32
2.7 16S primers 33
2.8 Scoring system for *Helicobacter hepaticus* + aIL10R colitis 33
2.9 Extracellular flow cytometry antibodies 39
2.10 Intracellular flow cytometry antibodies 40
2.11 Mastermix for cDNA synthesis 42
2.12 cDNA PCR cycle 43
2.13 Mastermix for RT-qPCR 43
2.14 Taqman probes 43
2.15 RT-qPCR protocol 44
2.16 PLP buffer recipe for 10mL 44
2.17 Antibodies used for confocal microscopy 46
2.18 Medium used for maintenance of Hoxb8-GM-CSF cells 48
2.19 Medium used for maintenance of Hoxb8-SCF cells 48
2.20 Medium used for differentiation of Hoxb8-GM-CSF cells 49
2.21 Medium used for differentiation of Hoxb8-SCF cells 49

4.1 CD101 and CD177 for neutrophil labelling 108

List of Abbreviations

Abx . . . . . Broad-spectrum antibiotics

AHR . . . . . Aryl-hydrocarbon receptor

AIA . . . . . Antigen-induced arthritis

AMP . . . . . Antimicrobial peptides

ANOVA . . . Analysis of variance

APC . . . . . Antigen-presenting cell

BA . . . . . Bile acids

BM . . . . . Bone marrow

CCR2 . . . . C-C chemokine receptor type 2

CD . . . . . Crohn's disease

cdtB . . . . . Cytolethal distending toxin subunit B

CFU . . . . . Colony forming unit

CLP . . . . . Common Lymphoid Progenitor

CRC . . . . . Colorectal cancer

CX3CR1 . . . CX3C chemokine receptor 1

DC . . . . . Dendritic cell

DSS . . . . . Dextran sulfate sodium

ELISA . . . . Enzyme-linked immunosorbent assay

eQTL . . . . . Expression quantitative trait loci

FMO . . . . . Fluorescence minus one

FXR . . . . . Farnesoid receptor X

G-CSF . . . . Granulocyte colony-stimulating factor

GF . . . . . Germ-free

GFP . . . . . Green fluorescent protein

GI tract . . . Gastrointestinal tract

GWAS . . . . Genome-wide association study

H&E . . . . . Haematoxylin and Eosin

HFD . . . . . High fat diet

Hh . . . . . *Helicobacter hepaticus*

Hh + aIL10R *Helicobacter hepaticus* and anti-IL10R blocking antibody

IBD . . . . . Inflammatory bowel disease

ICS . . . . . Intracellular staining

IEC . . . . . Intestinal epithelial cells

IF . . . . . Immunofluorescence

IFN . . . . . Interferon

IL . . . . . Interleukin

ILC . . . . . Innate lymphoid cell

IMS . . . . . Industrial methylated spirit

IRF5 . . . . . Interferon regulatory factor 5

KO . . . . . Knock out

Lcn2 . . . . . Lipocalin 2

LF . . . . . Lactoferrin

LP . . . . . Lamina propria

MBMC . . . Mixed bone marrow chimera

MHC . . . . . Major Histocompatibility Complex

mLN . . . . . Mesenteric lymph node

MNP . . . . . Mononuclear phagocyte

MPO . . . . . Myeloid peroxidase

MPO . . . . . Myeloperoxidase

MyD88 . . . . Myeloid differentiation primary response 88

NET . . . . . Neutrophil extracellular trap

NK cells . . . Natural Killer cells

NLS . . . . . Nuclear localisation signal

OMM^{12} . . . Oligo-mouse-microbiota

p.i. . . . . . post infection

PCA . . . . . Principle component analysis

PRR . . . . . Pathogen recognition receptor

RA . . . . . Rheumatoid arthritis

Rag1 . . . . . Recombinase activating gene-1

ROS . . . . . Reactive oxygen species

RT-qPCR . . Real time quantitative polymerase chain reaction

S. Tm . . . . *Salmonella* Typhimurium

SCFA . . . . . Short-chain fatty acids

scRNA-seq . single cell RNA-sequencing

SI . . . . . Small intestine

SPF . . . . . Specific pathogen-free

SPI . . . . . *Salmonella* pathogen island

T3SS . . . . . Type III secretion system

TF . . . . . Transcription factor

TGR5 . . . . G-protein coupled BA receptor 1

THF . . . . . Tetrahydrofuran

TLR . . . . . Toll-like receptor

Treg . . . . . Regulatory T cell

tSNE . . . . . t-distributed stochastic neighbor embedding

UC . . . . . Ulcerative colitis

WT . . . . . Wild type

1 Introduction

Contents

1.1 Regional differences along the gastrointestinal tract 2
1.1.1 Architecture of the gastrointestinal tract 2
1.1.2 The intestinal tissue microenvironment 4
1.2 The intestinal immune system 12
1.2.1 Innate immune system 13
1.2.2 Adaptive immune system 17
1.3 The *Helicobacter hepaticus* model of colitis and its relation to IBD in humans 19
1.3.1 Inflammatory bowel disease 19
1.3.2 The *Helicobacter hepaticus* + anti-IL10R model of colitis 20
1.3.3 The value of experimental mouse models for studying IBD pathogenesis 21
1.4 IRF5 as a regulator of immune cell function 22
1.4.1 Signalling pathway of IRF5 22
1.4.2 The role of IRF5 in various immune cell populations 23
1.5 Hypothesis and aims 26

1.1 Regional differences along the gastrointestinal tract

1.1.1 Architecture of the gastrointestinal tract

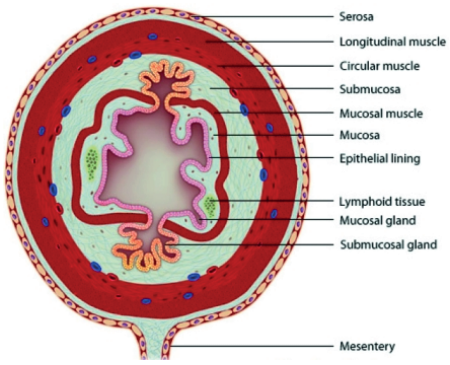


Figure 1.1: **Architecture of the gut mucosal wall.** Schematic cross-section of the gut mucosal wall, displaying the lumen in the middle, lined by epithelial cells with the underlying mucosa. The mucosa is surrounded by the submucosa and several muscle layers. The serosa is the final layer, sealing off the intestinal tube from the surrounding peritoneum. Taken from *Rao et al* [1]

The gastrointestinal (GI) tract has diverse functions mainly centering around digestion and absorption of nutrients, but it is also a major player in the immune response against pathogen infection. The mucosal surface is colonised with a large number of commensal bacteria, the so-called microbiota. Balancing tolerance against the microbiota whilst being able to mount a rapid immune response upon pathogen infection is a challenging feat. The GI tract is divided into small and large intestine, which form a continuous tube stretched from the stomach to the anus. This tube is built in several layers: the mucosa (epithelium, lamina propria (LP) and muscularis mucosae), the submucosa, the muscularis propria (inner circular muscle layer, intermuscular space and outer longitudinal muscle layer) and the serosa (Figure 1.1) [1]. Spatially, the small intestine (SI) is divided into three segments, duodenum, jejunum and ileum; whilst the colon begins at the cecum, followed by the ascending (proximal), transverse and descending (distal) colon before terminating at the anus [2]. The unique architecture of the intestine facilitates nutrient absorption by increasing the surface area by multiple levels of infolding villi in the SI. The LP harbours many innate

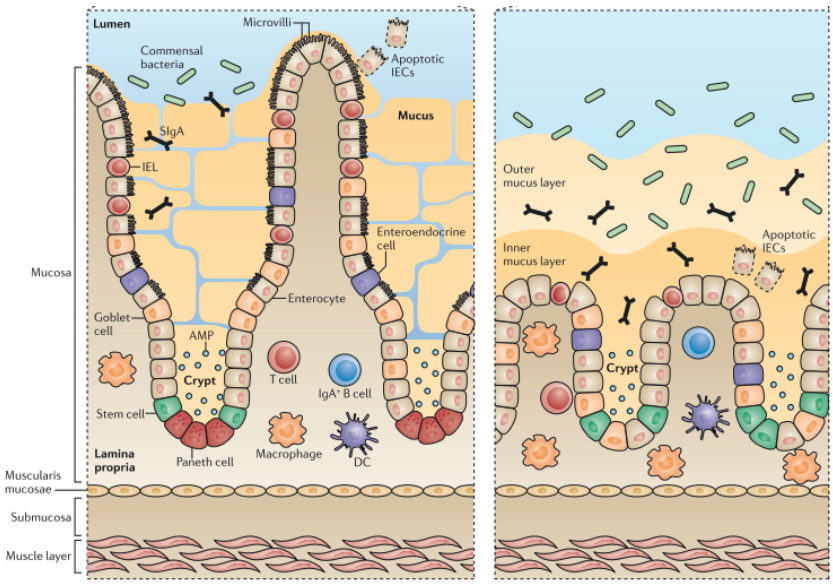


Figure 1.2: **Anatomy of the intestinal mucosa in the small intestine and colon** *Small intestine*. The mucosa is folded into villi, increasing the surface for nutrient absorption. The intestinal epithelial cells are lined with microvilli, creating the brush-border. The bacterial colonisation is lower than in the colon, kept in check by a loose mucus layer and secretion of antimicrobial peptides by Paneth cells. *Colon*: The colon is lined with two thick mucus layers as the microbial density is much greater than in the small intestine. Taken from *Mowat et al* [2]

---

and adaptive immune cells as well as blood vessels, lymphatics and nervous supply for the mucosa [2]. Despite the LP and epithelium being anatomically close, they form very distinct immunological compartments. The submucosa is important for its plexus of parasympathetic nerves and is lined by the muscularis propria, a thicker muscle layer. The serosa forms the outer layer, separating the intestine from the surrounding peritoneal cavity [2].

The SI and the colon have distinct functions, the small intestine mainly absorbs dietary factors, digested by secreted fluids like bile and pancreatic secretion. The colon harbours a vast amount of microorganisms, the microbiota, which lives in symbiosis with its host to break down indigestable nutrients. The mucus layer in the colon is much thicker than in the SI and consists of an inner, dense layer attached to the epithelial cell layer, and a looser outer layer harbouring the microbiota [3]. These distinct functions also result in vastly different

tissue structures and certain cell types are only found within one part of the GI tract (Figure 1.2). The SI has a maximized surface structure through many infolds whereas the colon is almost flat, covered with a thick mucus layer to separate the microbiota from the host tissue. To further increase the surface area, intestinal epithelial cells (IECs) on these villi are covered in microvilli, in which enzymes needed for digestion as well as nutrient transporters are embedded, creating the so-called "brush-border" [2]. In general, most immune cells are more abundantly present in the SI, with the exception of macrophages, regulatory T cells (Tregs) and IgA+ plasma cells [2]. Peyers patches, organized lymphoid structures, are only found in the SI, promoting tolerance against common food allergens [4–6]. Simultaneously, as the SI has a much looser mucus layer, Paneth cells are indispensable through their continuous secretion of antimicrobial peptides (AMPs), keeping microorganisms at bay [7]. Intraepithelial lymphocytes, acting as sentinels of the mucosal barrier, are also almost exclusively found in the SI, interspersed between IECs [8]. The colon with its thick mucus layer, high microbial load and low oxygen content provides a distinct tissue microenvironment in comparison to the SI, which likely influences the cells residing therein.

1.1.2 The intestinal tissue microenvironment

The tissue microenvironment is described as a dynamic population of cellular and non-cellular components which form a multifaceted regulatory network, helping to maintain homeostasis within a given tissue [9]. It has gained in importance mainly in the context of tumours, where the tumour and its microenvironment continuously influence each other and shape the fate of many resident cells. The tissue microenvironment has emerged as an important player in priming immune cell functions both at steady state and inflammation [10–15].

The importance of the tissue microenvironment in imprinting tissue-specific functions of immune cells was shown especially with macrophages and neutrophils [11, 12], but also with other innate immune cells like innate lymphoid cells (ILCs) [16] . Monocytes entering the SI and colon differentiate into distinct tissue-resident macrophages, highlighting the distinct tissue microenvironments found along the GI tract [14]. Understanding the

function of cells within their surroundings will therefore help us to gain more mechanistic insights in their interactions and function.

Potential differences and influences of factors on immune cells along the GI tract will be described in chapter 1.1.2.1 and 1.1.2.2.

1.1.2.1 Dietary factors

Nutritional status is closely associated with immune system function and host resistance to infection, drawing attention to the immunomodulatory function of diet [17]. The luminal concentration of diet-derived immunomodulators depends on dietary intake but is modified by the extent of in-lumen metabolic processing and absorption [10, 17]. As metabolic and absorptive processes are spatially restricted along the GI tract, local and regional bioavailability of nutrients contribute to the regional differences of the tissue microenvironments. The use of specialized diets is one of the gold-standard methods to dissect the effect of specific metabolites on various functions of the immune system [10]. A short summary of the main active dietary ingredients shown to have an impact on immune cells is provided below:

Vitamin A: Vitamin A and its degradation products retinoic acid and retinol have profound effects on the mucosal immune system, especially in the SI. Differentiation of intestinal DCs is compromised in the absence of vitamin A, but recovers rapidly following oral retinoic acid supplementation [18]. Furthermore, in mice fed on a vitamin A rich diet, SI macrophages are maintained in a quiescent state with reduced expression of pro-inflammatory mediators [19]. These macrophages however express high levels of Dectin-1, a pattern recognition receptor (PRR), triggering of which mediates a rapid switch to induce pro-inflammatory cytokine production [19]. Additionally, mice kept on a diet deficient in vitamin A had significantly lower numbers of anti-inflammatory tissue-resident macrophages, leading to a dysregulated immune response during helminth infection [20].

AHR ligands: Ligands for aryl hydrocarbon receptor (AHR), a ligand-activated transcription factor (TF) can be found in dietary compounds, microbial virulence factors,

products of tryptophan metabolism as well as in derivatives of the microbiota [10]. Based on the expression of CYP1A1, an enzyme regulating AHR signalling, ligands thereof are likely to be present at greater density in the upper murine SI compared to the colon [21]. Depletion of AHR specifically in CD11c+ cells enhanced susceptibility to murine dextran-sulfate sodium (DSS) colitis [22]. This points towards a regulation of epithelial homeostasis via AHR signalling in macrophages and DCs [22].

Amino acids: Total parenteral nutrition supplies all daily nutritional requirements administered through an intravenous administration instead of being absorbed through the GI tract and is a form of therapy for patients whose GI tract cannot fully absorb nutrients [23]. The importance of enteral nutrient provision on development of the intestinal immune system was highlighted in a study where mice receiving a total parenteral nutrition had reduced frequencies of macrophages in the SI [24]. Furthermore, these macrophages produce lower amounts of IL-10, indicating that SI macrophages were directly regulated by dietary amino acids, as a protein-free diet phenocopied this effect [24].

Bile acids: Bile acids (BAs) are secreted by the liver as the end product of cholesterol metabolism and are used for fat digestion. Additionally, BAs are a substrate for many bacterial enzymes, converting primary to secondary BAs [25, 26]. As BAs affect microbial growth, pathogen upgrowth in mice can be a result of BA-mediated microbiota perturbations [27]. The majority of BAs are reabsorbed by ileal IECs and transported back to the liver through the portal vein as part of the enterohepatic circulation [28]. An excess of BAs in the colon results in diarrheal disease, and changes in the BA pool were associated with inflammatory bowel disease (IBD) patients [28–30]. BAs can be recognised by specialized receptors like the farnesoid receptor X (FXR) and G-protein coupled BA receptor 1 (TGR5). FXR regulates the homeostatic enterohepatic circulation through sensing of BA in the liver and ileum [31]. The intestinal expression of FXR is selectively modulated by Toll-like receptor (TLR) 9 in human monocytes and its expression is required for immune-regulatory activities of TLR9 in intestinal inflammation [32]. Furthermore, depletion of FXR in mice resulted in altered colon homeostasis and exacerbated progression to intestinal inflammation

[33]. Lack of TGR5 also exacerbated DSS colitis in mice in a macrophage-dependent manner [34], highlighting the direct effects of BAs on the immune system. As BAs have effects on both the microbiota composition and direct modulation of the immune system, they provide a potent mediator of the intestinal immune system, further leading to regional differences in the tissue microenvironments along the GI tract [10].

Short-chain fatty acids: Short-chain fatty acids (SCFAs) are generated by the colonic microbiota via fermentation of indigestible dietary fiber [35]. The highest concentration of SCFAs are found in the ascending and transverse region of the human colon, measured in post-mortem individuals [36]. Low amounts of SCFAs were directly associated with several inflammatory diseases, as they are generally thought to provide protective responses [35]. Butyrate induces IL-10 production by activating GPR109a [37] as well as imprints an antimicrobial program in intestinal macrophages through inhibition of histone deacetylase 3 [38]. Depletion of SCFAs during antibiotic treatment led to hyperresponsiveness of colonic macrophages, resulting in a long-term increase in inflammatory T helper 1 (Th1) cell responses and sustained dysbiosis in mice, which was restored upon supplementation with butyrate [39]. Reduced turnover of IECs in germ-free (GF) or antibiotics (Abx)-treated mice was rescued by the addition of a SCFA-cocktail containing butyrate, acetate and propionate [40]. Furthermore, neutrophil recruitment during DSS colitis was reduced by the supplementation of acetate, highlighting the protective role of SCFAs in modulating the host immune response [41].

1.1.2.2 The microbiome and dysbiosis

The GI tract harbours several distinct niches with different microenvironments for spatial localisation of different microbiota members, allowing for spatial diversity of the microbiota along the GI tract (Figure 1.3) [42–44]. During homeostasis, the intestine is dominated by the phyla *Firmicutes* and *Bacteroidetes*, followed by *Actinobacteria, Proteobacteria*, and *Verrucomicrobia* [45], preventing pathogen invasion whilst tolerating normal gut microbiota [46, 47]. Bacterial delocalization during experimental colitis promoted macrophage activation

in genetically susceptible mice, rendering spatial reprogramming of the microbiota as an underappreciated function of IBD [48]. As oxygen availability has an impact on the microbiota composition [49], in the SI rapidly dividing and facultative anaerobes are favoured [50], whereas in the colon, strict anaerobic bacteria fermenting complex polysaccharides are more commonly found [42]. Not only the microbial load increases from the SI to the colon in the mammalian GI tract [2], but also species richness is greater in the colon [50, 51]. A preferential colonization of specific bacterial species along the length of the human colon was uncovered, alongside a region-specific transcriptional and activation profile of T and B cells [52].

The extensive interaction of the microbiota with its host directs the development of immune responses and shapes the microbiota composition [53]. Studies in GF mice show extensive defects in their development of the intestinal immune system, like gut-associated lymphoid follicles and secretory IgA+ antibody levels [54]. Furthermore, colonization of GF mice with commensal microbiota induced rapid structural and permeability functions in the mucosal barrier important for maintenance of intestinal homeostasis [55]. A tight anatomical barrier preventing bacterial translocation is formed with perivascular intestinal macrophages in the presence of the microbiota, which is severely impaired in Abx-treated and GF mice [56]. Specific macrophage subsets are also diminished in abundance in GF mice, however their numbers can be restored upon cohousing with specific-pathogen-free (SPF) mice [57]. Signalling via myeloid differentiation primary response 88 (MyD88), a universal adaptor protein through which most TLRs signal, is essential for microbiota-induced colonic expression of the AMPs RegIIIβ and RegIIIγ [58]. Furthermore, *MyD88-/-* mice as a model for loss of innate signalling revealed a shift in bacterial diversity along the GI tract, associated with a higher susceptibility to viral infections [58].

GF mice are protected from several mouse models of IBD, highlighting the crucial role of the microbiota in driving intestinal inflammation [59]. Additionally, fecal tranfer of a colitic microbiome into a healthy mouse leads to colitis development [60]. The shift in the microbiome composition during inflammation is referred to as dysbiosis and leads

to an alteration in the host immune response, causing the induction of a disease state [61]. Dysbiosis further decreases species richness, whilst favouring growth of otherwise low-abundance and harmful bacteria [62, 63]. Analysis of paired mucosal biopsies of inflamed and non-inflamed regions in IBD revealed a reduction in *Firmicutes*, together with concurrent increases in *Bacteroidetes*, as well as *Proteobacteria* in Crohn's disease (CD) specifically [63]. Simultaneously, the direct comparisons allowed for a detection of reductions in alpha diversity relating to the inflammation status within the same patient [63]. Alpha diversity is a measure for entropy and its index is used as a measure for sample richness and diversity. Despite the key role of the microbiota in IBD development, it is still part of ongoing research whether the alterations of the microbiota are a cause or consequence of IBD (Figure 1.4) [45, 64].

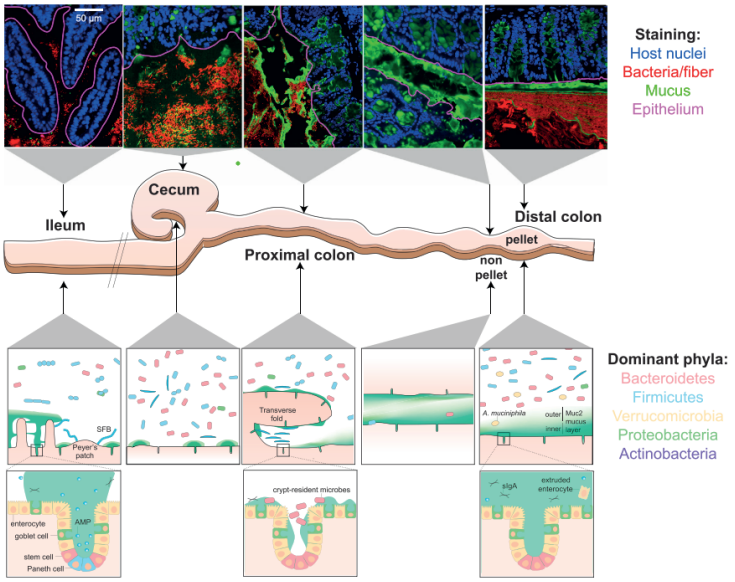


Figure 1.3: **Spatial distribution of microorganisms along the gastrointestinal tract.** Top: confocal images of intestinal sections along the gastrointestinal tract stained for host nuclei (blue), mucus (green), epithelial layer (magenta) and bacteria/fiber (red). Middle: schematic of the distal mouse GI tract. Bottom: Schematic of each section depicting dominant phyla and mucus structure heterogeneity along the longutudinal and transvere axes of the murine gastrointestinal tract. Taken from *Tropini et al* [42]

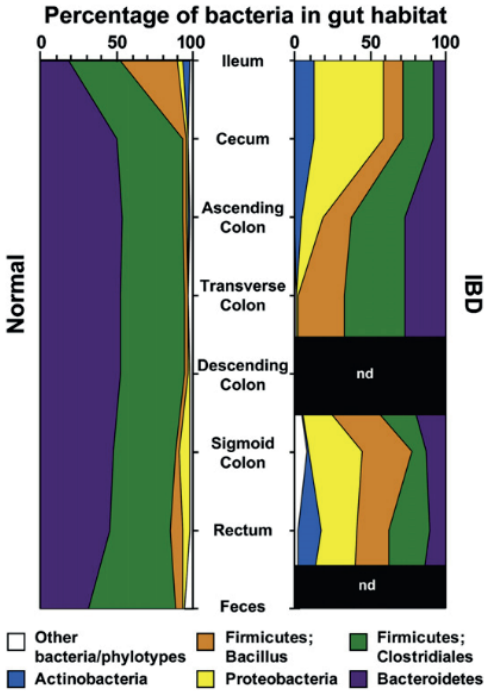


Figure 1.4: **Spatial rearrangement of main bacterial phyla in IBD.** Distribution of the main bacterial phyla along the human GI tract both in healthy (left) and in IBD patients (right). The graphs depict relative abundance. Taken from *Peterson et al* [64]

1.2 The intestinal immune system

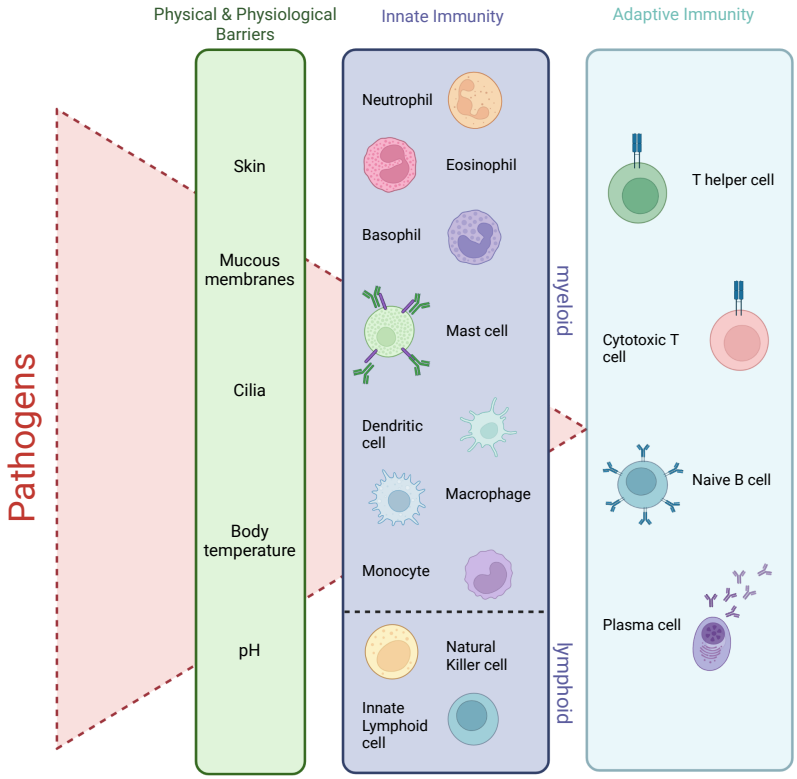


Figure 1.5: **Components of the innate and adaptive immune system.** Pathogens are faced with a multitude of host defense mechanisms: Physical and physiological barriers, followed by the innate immune system, which reacts upon triggers of pathogen - or danger-associated molecular patterns, shaping the more specific adaptive immune response. Adapted from *www.enzolifesciences.com. This figure was generated using Biorender.*

The intestinal immune system encounters the challenge of remaining unresponsive to the commensal microflora and food antigens whilst being able to mount a rapid immune response upon facing pathogens. The importance of maintaining gut homeostasis and tight control of immune response is emphasized in the context of chronic auto-inflammatory bowel diseases like CD and Ulcerative Colitis (UC) where the body is believed to mount an immune response against commensals [65]. The precise aetiology of IBD remains unclear, but genetic factors, the host immune system and the environment (diet and gut microbiota) are factors

that have been identified to play a role in its pathophysiology [66]. The immune response can be broadly divided into a rapid, unspecific innate immune response, and a slower and antigen-specific adaptive immune response. The cellular components of each system and their respective functions will be described in chapter 1.2.1 and 1.2.2 (Figure 1.5).

1.2.1 Innate immune system

The innate immune system is the first line of defense and acts swiftly upon an infection or insult, rendering its components as crucial players in setting up the inflammatory response. Based on their hematopoietic origin, innate immune cells can be broadly subdivided in myeloid and lymphoid cells.

1.2.1.1 Myeloid cells

Myeloid cells originate from a common precursor in the BM and are the major leukocyte population in the blood [67]. Generally, their main functions are phagocytosis and the secretion of cytokines. Phylogenically, they are among the oldest immune cells found even in primitive invertebrates [67]. Given their short life span at steady state, they need to be constantly replenished from hematopoietic stem cells and progenitor cells [68]. During inflammation, myeloid cells are in high demand due to their front line defense activities. In order to increase myeloid cell output from the BM, emergency hematopoiesis is switched on, launching a unique hematopoietic response program [68]. A factor regulating infection-induced emergency hematopoiesis is granulocyte colony-stimulating factor (G-CSF), exerting a key role in the differentiation of myeloid progenitors to mature granulocytes [68]. Mice lacking G-CSF have chronic neutropenia and granulocyte progenitor deficiency [69]. Direct recognition of TLR4 ligands in BM endothelial cells increased their G-CSF production, resulting in increased production of myeloid cells in the BM [70].

Macrophages and Ly6C^{hi} monocytes: Macrophages are the most abundant population of phagocytic cells in the LP [71]. They play an important role in maintenance of intestinal homeostasis by eliminating invading pathogens and secreting cytokines [71]. Due to their position directly underneath the epithelial cell layer, macrophages are ideally equipped

to capture and eliminate any microbial intruder as well as supporting barrier integrity [72, 73]. The macrophage population gets replenished through proliferation of tissue-resident macrophages and in a CCR2-dependent way by recruitment of Ly6C^{hi} blood monocytes, which differentiate locally into macrophages depending on the tissue microenvironment [74–76]. The differentiation process involves upregulation of MHCII, CD11c, CX3CR1, F4/80, CD64 and downregulation of Ly6C, along the so-called "monocyte waterfall" [77]. So far, only IL-10 and TGF-β were described to be required for the development of tissue-resident intestinal macrophages [78, 79]. Depletion of IL-10 in macrophages specifically led to a pro-inflammatory state preventing their full differentiation and eventually initiating spontaneous colitis [79]. On the other hand, depletion of TGF-β receptor on macrophages only resulted in a minor impairment on macrophage differentiation [78]. Tissue-resident macrophages were shown to be less immunoreactive, a feature which enables them to patrol tissues and remain anergic to TLR stimuli from the resident microbiota, preserving tolerance of the intestinal immune system [80, 81]. Furthermore, direct sampling of luminal antigens in a CX3CR1-dependent process and subsequent transfer to DCs is crucial for maintenance of intestinal tolerance to both food antigens and microbiota members [82].

Neutrophils: Neutrophils represent a major arm of the innate immune defence system, with a long-held view of them being transcriptionally inactive fast responders mobilised in response to microbial and tissue insults. However, this view has changed recently due to a multitude of studies highlighting neutrophils as heterogeneous and transcriptionally active cells able to adapt according to their tissue microenvironment [11, 83]. Apart from their phagocytic function, neutrophils contain different toxins, stored in distinct granules, each composed of a different set of cytotoxins and AMPs [84]. Primary granules contain high levels of myeloperoxidase (MPO), elastase, proteinase-3, cathepsins, lysozymes and others [85]. Secondary granules are filled with lactoferrin, lipocalin, collagenases, gelatinases and so on [85]. The release of these granules is termed 'degranulation' and is an important neutrophil function in host defense and inflammation [85]. Additionally, neutrophils can also form Neutrophil Extracellular Traps (NETs) though 'NETosis', releasing DNA that

binds and ensnares pathogens [86]. Furthermore, neutrophils can also generate reactive oxygen species (ROS) and produce cytokines, influencing and regulating inflammatory and adaptive immune responses [87, 88].

Immature neutrophils were shown to be associated with inflammatory diseases like giant cell arthritis in humans [89] as well as cancer progression in mice [90]. Moreover, mature and immature neutrophils display antagonistic effects on T cells, exerting opposing immunomodulatory effects [91]. Different subsets of neutrophils, discriminated by CD177, have been identified in UC patients [92]. The distribution and activation of neutrophils was further shown to correlate with endoscopic disease severity [93], however, neutrophils are critical for control of bacterial load [94]. As the antimicrobial arsenal of neutrophil can also contribute to the exacerbation of IBD, neutrophils are regarded as a double-edged sword [95].

DCs: The main function of DCs is to sample antigens, migrate to draining lymph nodes and present antigenic peptides to T cells [96]. Therefore, DCs provide a critical link between innate and adaptive immunity. It is clear from other systems, that the way in which the antigen is presented is critical to whether tolerance or immunity results. It has been shown that intestinal DCs are generally in a resting state *in situ*, but are potentially responsive to exogenous stimuli [97] Intestinal DCs also express high levels of several TLRs, upregulate costimulatory molecules and CCR7, a chemokine receptor important for migration to the mesenteric lymph node (mLN), in response to TLR stimulation [81]. Simultaneously, their expression of pro-inflammatory cytokines is inhibited by constitutive production of IL-10 [81]. Interestingly, IL-10 production increased upon TLR stimulation, suggesting that DCs actively downregulate inflammation in the intestine and are crucial for maintenance of intestinal immune homeostasis [81].

Eosinophils: Eosinophils interact with and modulate the function of other immune cells [98]. Their appearance is marked by a multi-lobed nucleus and eosinophil granules, containing many cytotoxic molecules as well as cytokines [98]. Furthermore, eosinophils can also modulate their gene expression depending on their respective tissue microenvironment, partially via AHR ligands, which shown in the context of the intestine [99].

Mast cells: Mast cells are mainly found in connective and mucosal tissues, where they release histamine- and heparin-containing granules upon IgE stimulation [100]. They are commonly associated with allergic immunity and hypersensitivity, however they also play important roles in pathogen defense [100].

Basophils: Basophils stain positive for basic dyes such as haematoxylin and play a role in defence against parasites [100]. Despite arising from separate hematopoietic progenitors to mast cells, they also have granules containing histamine and heparin, and are associated with allergic immunity [100].

1.2.1.2 Lymphoid cells

Derived from the Common Lymphoid Progenitor (CLP), but lacking T- or B-cell antigen-specific receptors are Natural Killer (NK) cells and Innate Lymphoid Cells (ILCs). NK cells can be viewed as the innate counterparts of cytotoxic CD8+ T cells, whereas the different subsets of ILCs, ILC1, ILC2 and ILC3 represent the counterparts of CD4+ Th1, Th2 and Th17 cells respectively [101].

NK cells: NK cells express high levels of cytokines, granzymes and perforin and are therefore equipped to eliminate virus-infected cells following their activation [102]. By recognizing the absence of constitutively expressed self molecules like MHC I, NK cells ensure tolerance to self while allowing toxicity toward stressed cells [102].

ILCs: Even though ILC subset differentiation is guided by the same TFs as their respective Th subsets, T-bet for ILC1, GATA-3 for ILC2 and RORγt for ILC3, they do not express antigen receptors [103]. Rather than being activated by specific antigens, ILCs get activated by stress signals, microbial compounds and the cytokine milieu of the tissue microenvironment [101]. As a result of this activation, they produce a tailored array of cytokines, directing the developing immune response into one adapted to the original insult, playing a central role in the crosstalk of the innate and adaptive immune system [101].

1.2.2 Adaptive immune system

The adaptive immune system provides a tailored antigen-specific response to pathogens and generates memory lymphocytes for immune memory. The effector cells of the adaptive immune system can be divided into T lymphocytes (T cells) and B lymphocytes (B cells), derived from CLPs and each equipped with unique T and B cell receptors, respectively for antigen recognition.

T cells: T cell precursors migrate from the BM to the thymus, where they undergo crude positive and negative selection, ensuring the elimination of self-reactive T cells [104]. To generate T cell receptors (TCR) with unique specificities, TCR gene fragments undergo V(D)J recombination with the help of specific RAG enzymes [105]. Following pathogen recognition, CD4+ and CD8+ T cells can either proliferate and become effector cells, or develop into memory T cells. Memory T cells are able to rapidly proliferate upon a secondary encounter with a specific pathogen, allowing for rapid pathogen clearance upon reinfection [106].

CD4+ Th cells interact with other immune cells, directing specific immune responses to different classes of pathogens through the production of cytokines. As they are required for almost all adaptive immune responses, their dysregulation has a major impact on the immune system. CD4+ CD8- Th cells are generated by receival of three signals in a naive T cell: 1) TCR stimulation by MHCII-bound antigen, 2) costimulation of CD28 by either CD80 or CD86 on a antigen-presenting cell (APC) and 3) cytokine receptor signalling to drive Th subset-specific TF expression [107]. Th1 cells, depending on TF T-bet, participate in the response to intracellular pathogens [108]. Th2 cells, driven by the TF GATA-3, mediate anti-parasite immunity, however dysregulation can also result in allergic responses [109]. Specialized in clearing extracellular pathogens like fungi, Th17 cells driven by RORγt, play an important role in the intestine, however they are also associated with autoimmunity [110]. An important mediator of intestinal tolerance are Tregs under the control of FOXP3 [111].

In contrast to CD4+ Th cells interacting with APCs and MHCII-molecules, CD8+ T cells recognize MHCI-bound antigens, allowing the recognition of "altered" self-peptides and targeted cytotoxicity against infected cells and tumour cells [112].

B cells: Similar to T cells, B cells also undergo developmental checkpoints to ensure the elimination of self-reactive B cells. The first checkpoint occurs in the BM, where self-reactive B cells either undergo receptor editing, get eliminated or become anergic [113]. If they pass the first checkpoint, they migrate to the spleen and undergo a second selection step [113]. Mature B cells then travel to secondary lymphoid organs, where they encounter antigens presented in B cell follicles. B cell activation occurs either thymus-dependent, following encounter with a Th cell, or thymus-independent. Activation of B cells leads to their differentiation into short-lived antibody-producing plasma cells or memory B cells within the germinal center [114]. Thymus-independent B cell activation occurs through strong PRR signalling alongside antigen ligation and leads to production of antibodies with typically lower antigen-affinities than post thymus-dependent B cell activation [115]. Following activation, B cells generally form germinal centers within the follicular region of secondary lymphoid organs. Within these specialized microenvironments, activated B cells undergo clonal expansion, class switch recombination, somatic hypermutation and affinity maturation [106]. Depending on the functional requirements of the antibody, an activated B cells changes its antibody production from IgM to either IgE, IgA or IgG [116]. IgA is the most dominant antibody class in mucosal areas, the intestine included [117]. Memory B cells undergo somatic hypermutation to generate high affinity antibodies upon secondary encounter with the pathogen. Secreted antibodies, which are a copy from their respective BCRs, bind to their ligands and lead to the neutralisation and opsonisation of pathogens.

1.3 The *Helicobacter hepaticus* model of colitis and its relation to IBD in humans

1.3.1 Inflammatory bowel disease

IBD is a chronic recurring inflammation in the GI tract and can be subdivided into CD and UC based on their pathology and location of inflammation: CD can affect the entire GI tract, is more patchy and segmental and lesions can penetrate the entire depth of the intestinal wall [118]. These transmural lesions contain large numbers of monocytes and macrophages [118]. In contrast, UC is confined to the colon, extending proximally from the rectum, featuring a significant number of neutrophils [118]. The aetiology of IBD is still largely unknown, but genetic factors, the host immune system and environmental factors like the gut microbiota each make a major contribution to disease pathogenesis [66].

Current therapeutic strategies add immunosuppressive drugs as well as biologic agents to the repertoire of classic anti-inflammatory drugs like 5-Aminosalicylates and glucocorticosteroids [119]. Despite anti-TNF biologics being the current gold-standard therapy, about 40% of patients treated are not responsive to anti-TNF therapy [120]. Since then, major efforts have been undertaken in understanding the separation between so-called responders and non-responders to TNF blockade. High expression of Oncostatin M, a cytokine expressed in stromal cells, was identified as a predictor for non-response to anti-TNF therapy [121]. Furthermore, through an unbiased untargeted approach, a recent study discovered IL-1 driven neutrophil-stromal interactions to be at the core of a subset of non-responders [122]. Targeting other cytokines like IL-6, IL-17A failed in clinical trials due to adverse effects [119, 123, 124]. The IL-23/IL-17 axis is at the heart of driving IBD pathogenesis, and trials targeting IL-23 are still currently ongoing [125]. Furthermore, a drug targeting an upstream kinase of Interferon Regulatory Factor 5 (IRF5) was shown to have promising effects in reducing inflammation both *in vivo* as well as reducing cytokine production in UC biopsies [126].

Many pathways in IBD pathogenesis have been associated with macrophage functions [79, 127–129], however recent evidence also points to a significant role of neutrophils [122, 130]. Modulating immune cell function to keep the beneficial effects whilst suppressing their detrimental side might therefore be a novel therapeutic avenue to pursue.

1.3.2 The *Helicobacter hepaticus* + anti-IL10R model of colitis

Helicobacter hepaticus (Hh), a gram-negative *Proteobacteria* colonising the murine colon, was associated with colitis development in several immunodeficient mouse strains [131, 132]. Its pathogenesis is mainly associated with IL-10 deficiency or malfunction of T cells, as well as other immunodeficiencies [133–136]. In immunocompetent hosts, it forms a symbiotic relationship, resulting in tolerogenic Treg responses, which prevent intestinal inflammation in an IL-10-dependent process [137]. Administration of anti-Interleukin 10 receptor (aIL10R) blocking antibody can induce an intestinal immune response to Hh even in wild type (WT) mice [134]. This Hh + aIL10R colitis model has been widely used to dissect the pathophysiology of colitis. The importance of the IL10-IL10R pathway in preserving intestinal homeostasis was highlighted in multiple studies, also identifying its crucial role especially in intestinal macrophages [79, 138–140].

Mechanistically, IL-23 production by CD11c+ monocyte/macrophages was found to be essential to trigger intestinal inflammation in the Hh + aIL10R colitis model [141]. A similar mechanism was identified in IBD patients, where IL-23 led to the induction of pathogenic Th1/Th17 and ILC3 responses [134, 142]. By dissecting the single elements in the inflammatory cascade, it was uncovered that infection with Hh alone does in fact induce IL-23 expression, however in absence of IL10-blockade it does not result in colitis [134]. Hh infection activates a specific anti-inflammatory program in macrophages in the absence of IL10R signalling through the secretion of an unidentified polysaccharide triggering TLR2 [143].

Furthermore, also the microbiota plays a crucial role in the induction of colitis, as germ-free *Il10-/-* mice do not develop spontaneous colitis [144]. Monitoring of NF-κB

activation with GFP in *Il10-/-* mice, revealed the critical role of TLR activation through microbiota in colitis development [145]. The signal shifted from IECs to innate and adaptive immune cells over the course of intestinal inflammation [145].

Even though colitis induced by Hh does not fully recapitulate human IBD, it captures two elements thereof, a bacterial driver and a genetic predisposition, highlighting the interplay between host and microbe for disease development [146]. It further mirrors the accumulation of pathogenic MNPs, altered cytokine milieu, Th1/Th17-driven pathology and improper Treg induction, all found in human IBD.

1.3.3 The value of experimental mouse models for studying IBD pathogenesis

Experimental models of colitis are widely used as preclinical tools for evaluation of drug efficacy and testing of biologicals prior to clinical phase trials [147]. There are a variety of different mouse models recapitulating different aspects of human disease. These models can be broadly divided into chemically induced, genetically engineered, congenic and cell transfer models [148]. Furthermore, as mice are born genetically identical and kept in a controlled pathogen-free environment, they allow the generation of more homogenous interpretable results to dissect the contribution of distinct pathways to intestinal inflammation [149]. Additionally, as animal models have a confined disease timeframe, they grant an opportunity to study disease development from the onset to established pathology [149]. Through using genetically engineered mice, contributions of each pathway to intestinal inflammation can be dissected, allowing for a deeper understanding of pathogenesis and identification of new potential therapeutic avenues [149].

1.4 IRF5 as a regulator of immune cell function

1.4.1 Signalling pathway of IRF5

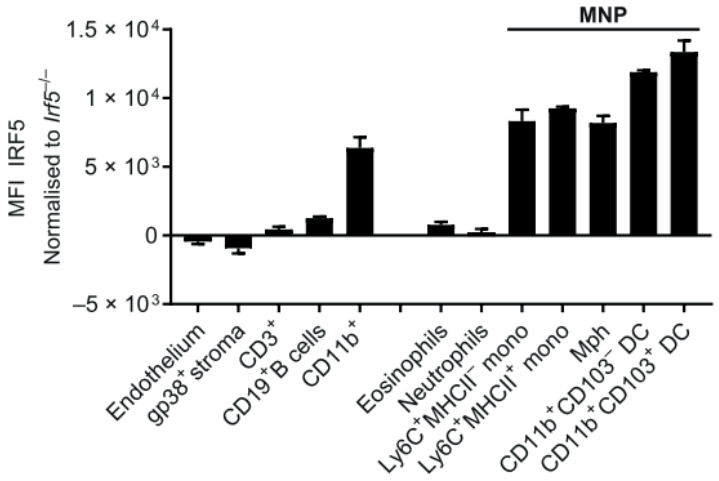


Figure 1.6: **Cells expressing IRF5 in the colonic lamina propria.** Mean Fluorescence Intensity of IRF5 normalised to *Irf5-/-* in various cell types from the colonic lamina propria at steady state. Taken from *Corbin et al* [129]

The TF IRF5 belongs to the IRF family, which are crucial regulators of immune cell differentiation and defense against pathogen infection, having been associated with the induction of type I interferon responses [150]. IRFs are multidomain-proteins, consisting of a IRF association domain, required for homo- and heterodimerization and two nuclear localisation signals (NLS): The C-terminal NLS is the DNA-binding domain and the N-terminal NLS is phosphorylation-inducible, important for IRF activation. Furthermore, IRF5 has a dominant constitutively active Nuclear Export Signal, controlling dynamic shuttling between the cytoplasm and the nucleus following activation [151]. Transcription of IRF5 has been shown to be induced by GM-CSFR, IFNγR and TLR4 signalling [152, 153]. The exact transcriptional mechanisms involved in IRF5 transcription have yet to be determined, so far Sp1 has been identified as a candidate [154]. IRF5 is then activated through several post-translational modification involving phosphorylation, ubiquitination and dimerisation prior to nuclear translocation and selective binding to its target genes

following signalling through multiple PRRs, including NOD2, TLR2, TLR4, TLR5, TLR7/9 and TLR8 [126, 150, 155, 156]. Phosphorylation of IRF5 occurs through the action of several kinases, namely TBK1, RIP2, IKKϵ, IRAK4, TAK1, IKKβ and Pyk2 [126]. IRF5 can also be negatively regulated through IKKα and Lyn [157, 158]. A cofactor of IRF5 is RelA, a factor also involved in the NF-κB signalling pathway, highlighting its crucial role in inflammatory gene transcription [159]. IRF5 is mainly expressed in myeloid cells, but also in B cells (Figure 1.6).

1.4.2 The role of IRF5 in various immune cell populations

Activation of IRF5 polarizes macrophages to differentiate into pro-inflammatory M1 macrophages [129, 152, 153]. Knockdown of IRF5 using siRNAs or full *Irf5-/-* macrophages exhibit M2 macrophage markers and gene expression. Another member of the IRF family, IRF4, has an antagonistic relationship with IRF5, occupying the IRF5 promoter and thus preventing its transcription. As IRF4 is also activated via direct interaction with MyD88, it directly competes with IRF5, and can therefore negatively regulate IRF5 signalling and promote M2 differentiation in macrophages [160]. This puts the antagonistic pair IRF4-IRF5 at the heart of macrophage polarization. By using single cell RNA (scRNA)-sequencing on mixed bone marrow chimeras (MBMCs) of WT and *Irf5-/-*, where cells reside in the same environment, the intrinsic role of IRF5 in guiding monocyte to macrophage differentiation was unravelled [129] (Figure 1.7). Furthermore, a higher proportion of Th1/Th17 cells was observed at peak of intestinal inflammation, confirming previous results generated *in vitro* [129, 153].

In addition to macrophages guiding T cell differentiation, a recent paper by *Yan et al* uncovered a direct role of IRF5 expression in CD4+ T cells in promoting Th1/Th17 cytokine expression [161]. Furthermore, IRF5 increased TCR-initiated signalling by guiding TCR complex formation and enhanced severity of T cell-transfer colitis in mice. In this model, T cells (here from both WT and *Irf5-/-* donors) are transferred into recombinase activating gene-1 (Rag1)-deficient *Rag1-/-* mice, which lack B- and T-cells, leading to severe

small bowel and colonic inflammation [162]. This model is frequently used to examine early events leading to the induction of gut inflammation as well as the role of Tregs [162]. T cells transferred from *Irf5-/-* mice led to significantly reduced inflammation, as measured by histopathology and lower lipocalin 2 (Lcn2) levels [161]. This uncovered a previously undefined role of IRF5 in mediating T cell pathology.

Furthermore, prevention of systemic lupus has been associated with IRF5 deficiency specifically in B cells [163]. In another study, an intrinsic role of IRF5 in B cell activation, proliferation and plasmablast differentiation has been defined in human primary naive B cells [164]. Stimulation of BCR and TLR9 resulted in IRF5 translocation, which was used as a measure for IRF5 activation [164]. Additionally, knockdown of IRF5 impaired B cell proliferation and activation. These results highlight an important role in IRF5 regulation of B cells, and its dysregulation leading to autoimmune diseases like systemic lupus.

In neutrophils, IRF5 has recently been highlighted to control functions like cytokine secretion and phagocytosis in activated neutrophils [165]. Their migratory capacities are not affected, which confirms observations from a previous paper [166]. However, the impact of neutrophil functions modulated by IRF5 deficiency have not yet been investigated *in vivo*.

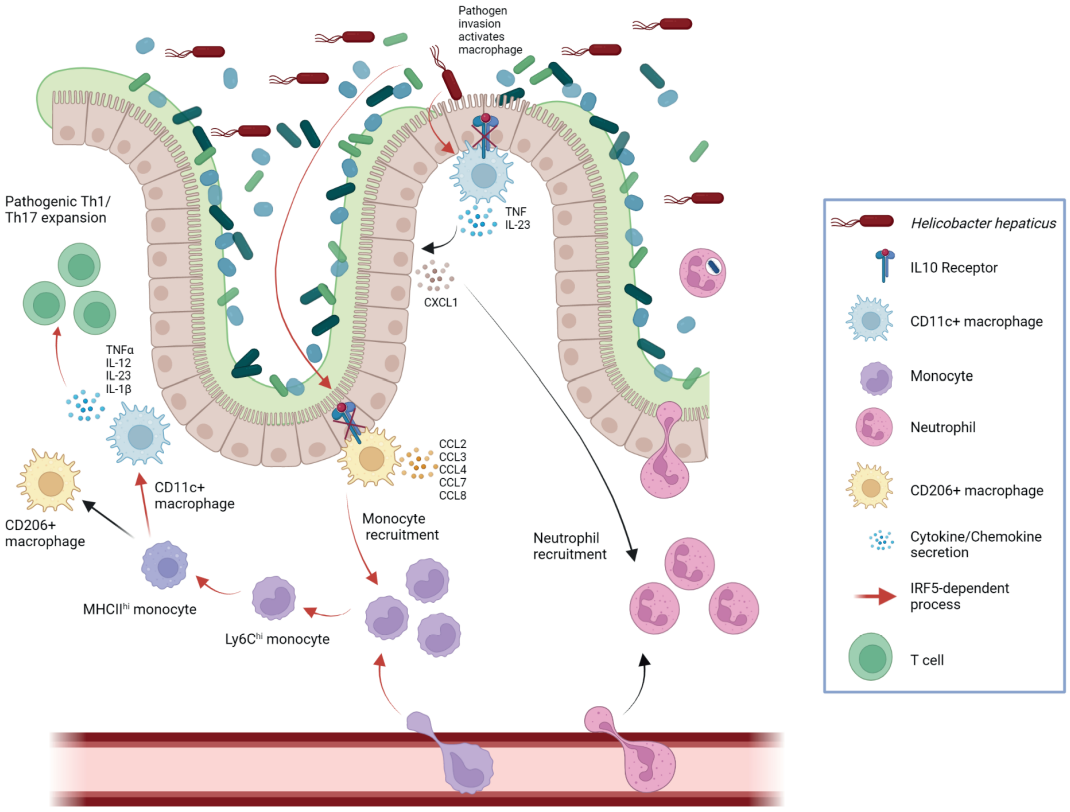


Figure 1.7: **Model of proposed role of IRF5 at peak of intestinal inflammation** Macrophages sense the breach of the intestinal barrier and respond by phagocytosing invading bacteria and secreting cytokines/chemokines. This in turn stimulates epithelial cells to secrete CXCL1, leading to neutrophil recruitment. Ly6C^{hi} monocytes are recruited along the CCL2-CCR2 axis, which is partially dependent on IRF5 expression in the monocytes. IRF5 expression is subsequently increased by PRR signalling after contact with bacterial antigens, promoting maturation to a pro-inflammatory CD11c+ macrophage. These macrophages produce high quantities of pro-inflammatory mediators such as TNFα, IL1β, IL-12 and IL-23, which support pathogenic Th1/Th17 expansion. *This figure was generated using Biorender.*

1.5 Hypothesis and aims

The importance of the tissue microenvironment in shaping the fate and function of infiltrating immune cells was demonstrated in recent studies [11, 12, 14, 167]. Furthermore, differences in the tissue microenvironment along the GI tract prime the immune system differently, setting the stage for a non-uniform immune response following an inflammatory trigger [10, 168]. However, despite this evidence, the spatiotemporal infiltration of immune cells in the context of their respective mucosal environment has not been investigated.

We therefore hypothesize that immune cells will infiltrate the colon at distinct sites and timepoints over the course of Hh + aIL10R mediated colitis, as a result of the distinct tissue microenvironments of the proximal and distal colon.

Previous work has demonstrated the crucial role of IRF5 in mediating Hh + aIL10R-driven colitis, pinpointing it back to IRF5 controlling the differentiation of infiltrating monocytes to inflammatory CD11c+ macrophages [129]. Furthermore, IRF5 was highlighted as a double-edged sword, being important for pathogen clearance but detrimental in the development of chronic intestinal inflammation [169]. Not only in monocyte/macrophages, but also in neutrophils, IRF5 was shown to control their cytokine response and phagocytosis abilities [165]. IRF5 is further mainly present in myeloid cells, which orchestrate the onset and progression of intestinal inflammation [170]. As the mechanism of this interplay has not been characterized yet, we made use of IRF5 as a tool to modulate monocyte/macrophage or neutrophil function specifically, in order to investigate their specific roles at the onset of colitis.

We further hypothesize that IRF5 plays a pivotal role in neutrophils at the onset of colitis, as a result of the unexplored effects on cytokine secretion and phagocytosis *in vivo*.

A layered approach in experimental set-up to address the different effects in IRF5-mediated neutrophil functions was employed: 1) separately housed WT and KO to assess the effect of *Irf5-/-* deletion on the general immune phenotype in their homeostatic environment, 2) cohoused WT and KO to change the microbiome, adding another layer of complexity

in order to untangle the previously uncovered effects in a comparable microbiome and 3) mixed bone marrow chimera of WT and *Irf5-/-* donors in WT recipients, rendering the microbiome and cellular environment comparable and assessing their differential gene expression to discover potential mechanisms driving the phenotypes in 1 and 2 (Figure 1.8).

Therefore, the purpose of this thesis was to:

1. Characterize the spatiotemporal pattern of myeloid cell infiltration and their respective tissuemicroenvironments over the course of Hh + aIL10R-mediated intestinal inflammation

2. Investigate the role of monocyte/macrophages and neutrophils at the onset of Hh + aIL10R colitis by the use of cell-specific IRF5-deletion

3. Examine the IRF5-dependent neutrophil-microbiota crosstalk important for setting up protective and detrimental responses at the onset of Hh + aIL10R colitis

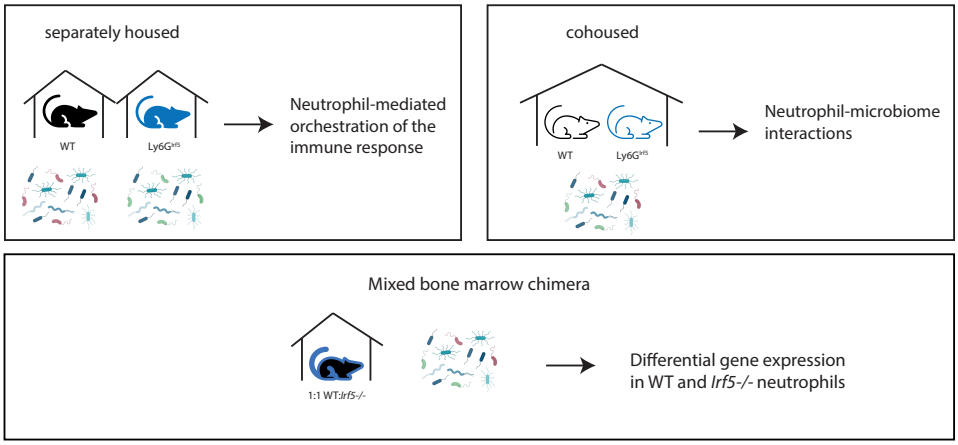


Figure 1.8: **Experimental set-up.**

2
Material and Methods

Contents

2.1 *In vivo* models 29
2.1.1 Animals 29
2.1.2 *Helicobacter hepaticus* culture 30
2.1.3 *Helicobacter hepaticus* and aIL10R model of colitis 31
2.1.4 Assessment of *Helicobacter hepaticus* colonisation 31
2.1.5 Histoscoring 34
2.1.6 *Salmonella* Typhimurium culture 34
2.1.7 *Salmonella* Typhimurium infection model 34
2.1.8 Assessment of CFU 34
2.1.9 Cecal gentamicin protection assay 35
2.2 Cell isolation protocols 35
2.2.1 Isolation of intestinal lamina propria leukocytes 35
2.2.2 Isolation of blood leukocytes 36
2.2.3 Splenocyte isolation 36
2.2.4 Bone marrow isolation 37
2.3 Flow cytometry 37
2.3.1 Extracellular labelling of cells 37
2.3.2 Intracellular labelling of cells 40
2.3.3 Flow cytometry acquisition and analysis 40
2.3.4 FACS 40
2.4 Protein and RNA analysis 41
2.4.1 CCL2, CCL3 & Lipocalin 2 ELISA 41
2.4.2 Dynabeads RNA extraction 41
2.4.3 RNA extraction with Qiagen Miniprep 42
2.4.4 cDNA generation 42
2.4.5 Taqman RT-qPCR reaction 43
2.5 Confocal microscopy 44
2.5.1 Sample preparation and embedding 44
2.5.2 Immunofluorescence labelling of colons - unfixed sections 44
2.5.3 Immunofluorescence labelling of colons - PLP fixed sections . . . 45
2.5.4 Image acquisition and processing 46
2.5.5 Image analysis and quantification 47
2.6 Cell culture and *in vitro* stimulation 48
2.6.1 Freezing and thawing of cell lines from liquid nitrogen 48

2.6.2 Maintenance and differentiation of Hoxb8 cells 48
2.6.3 *In vitro* stimulation 49
2.7 Statistical analysis 50

2.1 *In vivo* models

2.1.1 Animals

All mice were bred and maintained at a dedicated animal facility in the Kennedy Institute of Rheumatology under the establishment licence of the University of Oxford. All procedures were carried out according to the Animals in Scientific Procedures (ASPA) act of 1986 and approved by the the Kennedy Institute of Rheumatology Ethics Committee. Mice were held in individually ventilated cages and free of known intestinal pathogens, including *Helicobacter* species. Mice had access to water and food ad libitum and were kept at a constant temperature in rooms with a 12 hour day/night cycle. Mouse strains used are listed in table 2.1.

Table 2.1: Mouse strains used across DPhil project.

Mouse identifier	**Strain name**	**Source**
WT	C57Bl/6 *Ptprc*^{b}	Charles River, maintained in house
Irf5-/-	C57Bl/6.Irf5^{tm1Ttg}	Takaoka *et al.*, (2005), maintained in house
Irf5 LoxP/LoxP	C57Bl/6.Irf5^{tm1Ppr}	Jackson Laboratories (strain 017311), maintained in house
CX3CR1$^{gfp/+}$	C57Bl/6.Cx3cr1^{tmLittlJ}	Jackson Laboratories (strain 005582), maintained in house
CX3CR1^{Cre}	C57Bl/6.Cx3cr1$^{tm1.1(cre)Jung}$	Jackson Laboratories (strain 025524), maintained in house
CX3CR1^{Irf5}	C57Bl/6.Cx3cr1$^{tm1.1(cre)Jung}$.Irf5^{tm1Ppr}	crossed & maintained in house
Ly6G^{Cre}	C57Bl/6.Ly6g$^{tm2621(Cre\text{-}tdTomato)Arte}$	Hasenberg *et al.*, (2015); maintained in house
Rosa26^{Cre}	C57Bl/6 .Gt(ROSA)26Sor$^{tm14(CAG\text{-}tdTomato)Hze}$	Tal Arnon, maintained in house
Ly6G$^{tdTomato/+}$ Rosa26^{Cre}	C57Bl/6.Ly6g$^{tm2621(Cre\text{-}tdTomato)Arte}$ .Gt(ROSA)26Sor$^{tm14(CAG\text{-}tdTomato)Hze}$	crossed & maintained in house
CX3CR1$^{gfp/+}$ Ly6G$^{tdTomato/+}$ Rosa26^{Cre}	C57Bl/6.Cx3cr1$^{tm1.1(cre)Jung}$ .Ly6g$^{tm2621(Cre\text{-}tdTomato)Arte}$ .Gt(ROSA)26Sor$^{tm14(CAG\text{-}tdTomato)Hze}$	crossed & maintained in house
Ly6G^{Irf5}	C57Bl/6.Ly6g$^{tm2621(Cre\text{-}tdTomato)Arte}$ .Irf5^{tm1Ppr}	crossed & maintained in house

2.1.2 *Helicobacter hepaticus* culture

Helicobacter hepaticus (Hh) NCI-Frederick isolate 1A (Hh1a; strain 51449; American Type Culture Collection) was grown at 37°C on blood agar plates containing Campylobacter-selective supplement (skirrow), (Oxoid) under microaerophilic conditions (10% CO2, 10% H2, balance N2) in a vented CampyPak jar (Oxoid). Following two days of culture on blood agar plates, it was then transferred in liquid culture (Tryptan Soya Broth (Sigma Aldrich) dissolved in 1000 mL MilliQ H2O, and autoclaved) containing 10%

FCS + 0.4% Campylobacter-selective supplement (skirrow) (Oxoid). The culture was maintained at an OD600 of 0.05 at 37 °C shaking at 100 rpm by being split every 24 hours to prevent overgrowth.

2.1.3 *Helicobacter hepaticus* and aIL10R model of colitis

The colitis model was conducted over 4, 7 or 21 days according to the protocol described in *Arnold et al.*, 2016 [141]. Mice were gavaged twice with 1 * 10^8 colony forming units (CFU) *Helicobacter hepaticus* in 200μL sterile PBS on day 0 and 1 with a 22G curved, blunted needle (Poppers & Sons). 1mg anti-IL10R blocking antibody (clone B1.3A, 2bscientific) was injected weekly intraperitoneally, starting on day 0. Infected mice were monitored weekly for colitis symptoms and culled by a schedule 1 method on the timepoints indicated.

2.1.4 Assessment of *Helicobacter hepaticus* colonisation

Cecal content was collected in an empty eppendorf tube and flash frozen on dry ice immediately after collection for storage at -80 °C. 20ng of cecal DNA was extracted using the DNeasy PowerSoil kit (Qiagen) as per manufacturer's instructions and eluted in 70uL EB buffer. DNA concentration was measured with Nanodrop and adjusted to 5ng/μL in each sample. Hh real-time quantitative polymerase chain reaction (RT-qPCR) was performed with primers against the Hh cdtB gene (table 2.6) as described by [171]. Hh RT-qPCR and 16S RT-qPCR were set up in reaction mixes as described in tables 2.2 & 2.3. Samples were added in triplicates. Standard curves were generated from DNA extracted from Hh cultures with a DNeasy kit (Qiagen). The thermal cycling was performed on a C1000 Touch (BioRad) with the parameters described in table 2.4. Hh concentration was normalised against total 16S content by performing the 16S reaction as described in table 2.5 and with the primers found in table 2.7.

Table 2.2: Mastermix for Hh RT-qPCR (depicted is the mixing ratio for one reaction).

Reagent	**μL**
cdtB F (20 μM aliquot)	0.2
cdtB R (20 μM aliquot)	0.2
cdtB P (5 μM aliquot)	0.2
Primerdesign FAST Mastermix	5
NF H2O	2.4
DNA	2

Table 2.3: Mastermix for 16S RT-qPCR (depicted is the mixing ratio for one reaction).

Reagent	**μL**
NF H2O	3.4
SYBR Mastermix	5
515 F (10 μM aliquot)	0.3
805 R (10 μM aliquot)	0.3
DNA	1

Table 2.4: *Helicobacter hepaticus* RT-qPCR protocol

# cycles	**Time (s)**	**Temperature (°C)**
1	120	95
40	5	95
	20	60

Table 2.5: 16S RT-qPCR protocol

# cycles	**Time (s)**	**Temperature (°C)**
1	600	95
40	15	95
	60	60
1	Meltcurve	

Table 2.6: *Helicobacter hepaticus* primers

Primer	**Sequence**	**Purpose**
ctdB F	CCG CAA ATT GCA GCA ATA CTT	Forward primer Hh RT-qPCR
ctdB R	TCG TCC AAA ATG CAC AGG TG	Reverse primer Hh RT-qPCR
ctdB P	AAT ATA CGC GCA CAC CTC TCA TCT GAC CAT	ctdB Probe Hh RT-qPCR

Table 2.7: 16S primers

Primer	Sequence	Purpose
515 F	GTG CCA GCM GCC GCG GTA A	Forward primer 16S RT-qPCR
805 R	GAC TAC CAG GGT ATC TAA T	Reverse primer 16S RT-qPCR

Table 2.8: Scoring system for *Helicobacter hepaticus* + aIL10R colitis

	Epithelium	
Score	Hyperplasia and/or	Goblet Cell Depletion
0	None	None
1	Mild (1.5x)	Mild (25%)
2	Moderate (2-3x)	Marked (25-50%)
3	Severe (>3x)	Substantial (>50%)
	Inflammation of the lamina propria	
Score	Leukocyte infiltration	
0	None - few leukocytes	
1	Mild - some increase in leukocytes at tips of crypts of many lymphoid follicles	
2	Moderate - marked infiltrate (notable broadening of crypts)	
3	Severe - dense infiltrate throughout	
	Area affected	
Score	% of section	
0	None	
1	<25	
2	25-50	
3	>50	
	Markers of severe inflammation	
Score	Description	
0	None	
1	Submucosal inflammation OR few crypt abscesses (<5)	
2	Submucosal inflammation AND few crypt abscesses (<5)	
2	Many crypt abscesses (>5) OR extensive submucosal inflammation	OR crypt branching
3	Many crypt abscesses (>5) AND extensive submucosal inflammation	AND crypt branching
3	Ulceration OR extensive fibrosis	

2.1.5 Histoscoring

OCT embedded swiss rolls or paraffin embedded cross-sections were stained with Haematoxylin and Eosin (H&E) by the Kennedy Institute of Rheumatology Histology Facility (Kennedy Institute of Rheumatology, University of Oxford). The sections were acquired with Olympus BX51 microscope and scored in a blinded manner by two researches according to the scoring criteria outlined in table 2.8 [172]. The whole colon tile scans were acquired using Hamamatsu NanoZoomer S210 digital slide scanner.

2.1.6 *Salmonella* Typhimurium culture

S. Tm inoculum was grown overnight in LB broth containing 0.3M NaCl and 50μg/mL streptomycin at 37 °C shaking. On the day of infection, a 4h subculture in LB 0.3M NaCl was set up by diluting the overnight culture 1:20. 1mL of this subculture was taken and spun down for 2min at max speed. The supernatant was taken off and S.Tm was resuspended in 1mL sterile PBS, resulting in 5 * 10^7 Colony forming units (CFU) per 50μL. The inoculum was plated on McConkey agar plates to control for exact infection CFU.

2.1.7 *Salmonella* Typhimurium infection model

Infection model was performed as described by *Barthel et al* [173]. Mice were pretreated orally with 25mg/mouse streptomycin one day before infection. Their weight was recorded and feces collected daily over the course of infection. 5 * 10^7 CFU S. Tm in 50μL sterile PBS was gavaged per mouse on the day of infection. Mice were monitored daily and culled via schedule 1 method on the timepoints indicated.

2.1.8 Assessment of CFU

Feces were collected in pre-weighed eppendorfs containing 500μL PBS and homogenized for 5min at 25 Hz/s. The homogenized mixture was diluted 1/40'000 and 50μL plated on McConkey agar plates containing 50μg/mL streptomycin. The rest of the feces were immediately stored away at -20 °C for future analysis e.g. Lcn2 ELISA. On takedown

day, organs were collected in pre-weighed eppendorfs containing 500μL PBT and a sterile steelball. Homogenization occurred for 5min at 25 Hz/s, before plating on McConkey agar plates containing 50μg/mL streptomycin. All tissues were plated undiluted, and further diluted based on countability of the plates the following day. Plates were incubated o/n at 37 °C before counted. The CFU values were calculated by multiplying the number of colonies with the dilution factor and divided by the volume plated. CFUs were subsequently normalized to the weight of tissue/feces.

2.1.9 Cecal gentamicin protection assay

Cecum was opened longitudinally and washed thoroughly in cold PBS before incubation in 400μg/mL gentamicin for 30min. Following this incubation, the cecal tissue pieces were washed six times in cold PBS to remove gentamicin completely. The pieces were then transferred to pre-weighed eppendorfs containing 500μL PBT and a steel ball prior to homogenization. 50 μL were plated on McConkey plates and incubated o/n at 37 °C to determine the amount of intracellular bacteria.

2.2 Cell isolation protocols

2.2.1 Isolation of intestinal lamina propria leukocytes

Colons were excised and washed in 1x PBS 0.1% BSA (PBS/BSA) before squeezing out their content. Histology and RNA pieces were taken from proximal, mid and distal colon and transferred to the respective tubes. The rest of the colon or a 2cm piece taken from the proximal and distal end was cut open longitudinally and moved to pre-weighed eppendorf tubes containing 1x HBSS 0.1% BSA, 5mM EDTA 1% P/S (HBSS buffer). Following weighing of the tubes, the pieces were transferred to 50mL Falcon tubes containing 25mL HBSS buffer in the case of whole colon processing or 10mL for each proximal or distal piece. The tubes were shaken at 37 °C 200rpm for 20min, which was repeated following a renewal of the HBSS buffer. To remove the EDTA, the pieces were transferred into a uncoated 6-well-plate filled with 10mL PBS/BSA. The digestion media (RPMI 10% FCS

1% P/S) is prepared according to the amount of samples (15mL per whole colon, 5mL per prox/distal piece) adding 2.5 U/mL collagenase VIII (Sigma-Aldrich) and 2 U/mL DNAse I (Roche). The samples were incubated for 45min-1h shaking at 37 °C 200rpm. The supernatant was then filtered through 70μM sieves into 50mL Falcon tubes and rinsed with an equivalent volume of PBS/BSA 5mM EDTA to quench DNAse/collagenase activity. Cells were spun for 10min 4 °C at 500g before resuspension in 600-800 μL PBS for subsequent staining for flow cytometry.

2.2.2 Isolation of blood leukocytes

Tubes containing 200 IU/mL sodium heparin (Sigma Aldrich) in 100μL PBS were prepared for blood collection. Syringes with 23G needles were rinsed with PBS/BSA 10mM EDTA to prevent clogging, and blood was harvested by cardiac puncture. The blood was kept at RT until further processing. 300μL of blood was transferred into 15mL Falcon tubes containing 5mL cold ACK lysis buffer (Life Technologies) and incubated for 3-5min on ice. The samples were spun for 5min 500g at 4 °C and the supernatant was taken off by aspiration. The pellet was resuspended well in 5mL cold ACK lysis buffer and incubated on ice again. Following another centrifugation step, the pellet was washed with 5mL PBS before resuspension in 200μL PBS for extracellular staining.

2.2.3 Splenocyte isolation

Spleens were transferred into preweighed eppendorf tubes containing 500μL PBS/BSA. The samples were mashed through a 70μM sieve into 50mL Falcon tubes and washed with 10mL PBS. Following a centrifugation step 500g 5min at 4 °C, the pellet was resuspended in 5mL cold ACK lysis buffer and incubated on ice for 3-5min. This step was repeated, and the spleens were finally washed with 5mL PBS before resuspension in 600μL PBS, of which 200μL were taken for extracellular staining.

2.2.4 Bone marrow isolation

Hips were dislocated and legs are excised with bones intact, transferred into sterile bijou tubes filled with RPMI. Bones were broken apart and sterilised in a petridish with 70% Industrial Methylated Spirit (IMS). Remaining muscle was cleaned using a lint-free tissue. The ends were snipped off with scissors and the marrow was flushed with sterile PBS using a syringe with a 27G needle through 70μM cell strainer. 10mL PBS were added to flush the sieve and the cell suspension was stored on ice until further processing. After adjustment to equal volumes, the samples were spun for 10min 500g at 4 °C and resuspended in 5mL ACK buffer. Following a three-minute incubation at RT, 10mL PBS were added per sample and washed once again. The final resuspension occurred in 200μL PBS and was transferred to a 96-well plate for subsequent extracellular staining.

2.3 Flow cytometry

2.3.1 Extracellular labelling of cells

Single cell suspensions were prepared in PBS according to the appropriate cell isolation protocol. Samples were seeded on a uncoated 96-well plate in the same volume. Plates were spun at 1500rpm for 5min for each wash step. The supernatant was flicked off following centrifugation and samples were resuspended in 50μL live dead stain (ThermoFisher, 1/500 in PBS) and incubated for 10min at 4 °C. Samples were washed three times with 150μL FACS buffer (1x PBS, 0.1% BSA, 1mM EDTA, 0.01% Sodium Azide). Cells were then blocked in 30μL of Fc-block (α-CD16/32, BD) diluted 1/100 in FACS buffer for 10min at 4 °C. Primary extracellular antibodies (see table 2.9) were added at indicated concentrations in 30μL/sample and incubated for 30min at 4 °C in the dark. Labelled cells were then washed three times and fixed overnight at 4 °C or 1h at RT in 50μL Cytofix (BD) or Cytofix/Perm (BD), the latter for procession with intracellular staining. After fixation, cells were washed twice with FACS buffer and resuspended in 100μL before acquisition.

Counting beads were added to each sample before acquisition and cells were kept on ice and in the dark throughout the acquisition process.

Table 2.9: Extracellular flow cytometry antibodies

Epitope	Colour	Clone	Manufacturer	Cat #	Dilution
B220	PerCP-Cy5.5	RA3-6B2	eBio	45-0452-82	1/200
CD3	PerCP-Cy5.5	145-2C11	Biolegend	100328	1/200
CD3	APC	17A2	Biolegend	100235	1/100
CD3	PE-Cy7	145-2C11	eBioscience	25-0031-82	1/200
CD4	PerCP-Cy5.5	RM4-5	eBio	45-0042-82	1/200
CD4	PE-Cy7	RM4-5	eBioscience	25-0041-82	1/200
CD11b	BV510	M1/70	Biolegend	101245	1/100
CD11b	BV785	M1/70	Biolegend	101243	1/100
CD11b	BV605	M1/70	Biolegend	101237	1/100
CD11b	PerCP-Cy5.5	M1/70	Biolegend	101228	1/100
CD11c	BV605	N418	Biolegend	117334	1/200
CD11c	BV650	N418	Biolegend	117339	1/200
CD16/32	APC	93	eBioscience	17-0161-82	1/100
CD19	PerCP-Cy5.5	6D5	Biolegend	115533	1/200
CD19	PE-Cy7	1D3	eBioscience	25-0193-81	1/100
CD41	BV605	MWReg30	Biolegend	133921	1/100
CD45	BV650	30-F11	Biolegend	103151	1/100
CD45	BV605	30-F11	Biolegend	103139	1/100
CD45	BV785	30-F11	Biolegend	103149	1/100
CD45	BV711	30-F11	Biolegend	103147	1/100
CD48	PE/Dazzle 594	HM48-1	Biolegend	103438	1/100
CD101	PE-Cy7	Moushi101	Invitrogen	25-1011-80	1/100
CD103	PE	M290	BD	557495	1/100
CD138	PerCP-Cy5.5	281-2	Biolegend	142509	1/200
CD150	PE-Cy7	TC15-12F12.2	Biolegend	115914	1/100
CD177	AF647	1171A			1/100
CD177	FITC	1171A	eBioscience	11-1171-81	1/100
CD206	APC	C068C2	Biolegend	141707	1/100
CXCR2	PE	SA044G4	Biolegend	149303	1/100
CX3CR1	BV421	SA011F11	Biolegend	149023	1/100
CXCR4	APC	2B11	Invitrogen	17-9991-80	1/100
cKit	BV421	2B8	Biolegend	105827	1/100
EpCAM	AF488	G8.8	Biolegend	118210	1/100
F4/80	PE/Dazzle 594	BM8	Biolegend	123146	1/200
gp38	BV421	8.1.1	Biolegend	127423	1/100
Ly6C	PE-Cy7	HK1.4	Biolegend	128017	1/200
Ly6C	BV785	HK1.4	Biolegend	128041	1/200
Ly6C	PE	AL-21	BD	560592	1/200
Ly6G	BV711	1A8	Biolegend	127643	1/200
Ly6G	FITC	1A8	Biolegend	127605	1/200
Ly6G	APC	1A8	Cambridge Bioscience	20-1276-U025	1/200
Ly6G	PerCP-Cy5.5	1A8	Biolegend	127615	1/200
MHCII	AF700	M5/114.15.2	eBioscience	56-5321-80	1/200
NK1.1	PerCP-Cy5.5	PK136	eBioscience	45-5941-82	1/200
NK1.1	PE-Cy7	PK136	eBioscience	25-5941-82	1/200
Sca1	AF700	D7	eBioscience	56-5981-82	1/100
Siglec F	BV421	E50-2440	BD	562681	1/200
Ter119	PerCP-Cy5.5	TER-119	Biolegend	116227	1/200

2.3.2 Intracellular labelling of cells

Surface markers were labelled as described above. The fixation step was performed with Cytofix/Cytoperm (BD) and followed by three washes with 1x Perm/Wash buffer (BD) at 2500rpm for 5min. Intracellular antibodies (see table 2.10) were incubated in 30μL Perm/Wash at the indicated concentrations for 1h at 4 °C in the dark. Following this, samples were washed twice with Perm/Wash buffer before a final wash in FACS buffer and subsequent resuspension in 200μL FACS buffer for acquisition. Counting beads were added to each sample before acquisition and cells were kept on ice and in the dark throughout the acquisition process.

Table 2.10: Intracellular flow cytometry antibodies

Epitope	Colour	Clone	Manufacturer	Cat #	Dilution
pro-Il1b	PE-Cy7	NJTEN	ThermoFisher	25-7114-82	1/50
TNF	BV421	MP6-XT22	Biolegend	506327	1/50
live/dead	eF780	N/A	ThermoFisher	65-0865-14	1/500

2.3.3 Flow cytometry acquisition and analysis

Fluorophore compensation controls were set up by preparing single stained controls using CompBeads (BD) as per manufacturer's instructions. 10μL counting beads (BD) were added to each sample and the LOT number as well as the number of beads/50μL was noted down to calculate absolute cell numbers. Fluorescence minus one (FMO) controls were used to set gates for cell populations. Labelled cells were acquired using either an LSR II (BD), or Fortessa X20 (BD) flow cytometer using FACSDiva (BD). Data were analysed using Flowjo (Treestar, Inc.).

2.3.4 FACS

Cells were stained with extracellular cytokines as described above, except no fixation step was performed. They were filtered through a 70uM sieve into FACS buffer containing 1/1000 DNase. Cells were then sorted using a FACSAria™ III (BD) at the Kennedy Institute of Rheumatology FACS facility by Jonathan Webber (University of Oxford).

2.4 Protein and RNA analysis

2.4.1 CCL2, CCL3 & Lipocalin 2 ELISA

Levels of CCL2, CCL3 or Lcn2 were quantified using Mouse DuoSet ELISA (#DY479, #DY450 #DY1857, respectively, R & D systems). Clear 96 well plates (ThermoFisher) were coated with Capture Antibody at the required concentration in PBS and incubated at RT overnight. The next day, plates were washed three times with PBS + 0.05% Tween 20 (Sigma) (PBT). Plates were blotted onto paper towel to remove residual liquid after the final wash step. Plates were blocked with 300 µL Reagent Diluent (1 % BSA in PBS, sterile filtered) for a minimum of 1h. Following three PBT-washes, plates were incubated for 2h at RT with the duplicates of samples and standard curve. The standard curve was generated in a 1:1 dilution in blocking buffer (Reagent Diluent) in a range according to manufacturer's instructions. Plates were washed and blotted before 100μL of streptavidin-horse radish peroxidase (HRP) at working concentration was added to each well. The incubation step was performed in the dark at RT for 20min. Following another wash step, 100μL TMB substrate solution (ThermoFisher) was added to each well and incubated for another 20min in the dark at RT. Next, 50μL stop solution (#DY994, R & D) was added to each well and mixed by gentle agitation. The optical density of each well was quantified at 450nm wavelength on a SPECTROstar nano spectrophotometric Plate Reader (BMG Labtech) and corrected for plate absorption at 540nm. The data was exported by MARS Data Analysis software (BMG Labtech) and analysed in Excel.

2.4.2 Dynabeads RNA extraction

Cells were collected in 50-100μL lysis/binding buffer and efficient lysis was ensured by pipetting up and down. This mixture can be stored at -80 °C until extraction. 20 μL of vortexed oligo dT dynabeads was aliquoted in a semi-skirted 96 well plate. After placing the plate on the provided magnet, supernatant was removed and the dynabeads were washed once with 100 μL lysis/binding buffer. Samples were resuspended in beads and incubated at RT for 10min. After 5min, the samples should be mixed again. Supernatant was removed

after placing on the magnet and samples were washed twice with 150μL Wash buffer A. Following this, two washes with 50μL were performed. 13μL Elution buffer was added to the samples, prior to 2min incubation at 72 °C. The plate was immediately placed on magnet and 10μL transferred to a fresh plate or PCR tubes kept on ice. Storage of the RNA either at -80 °C or procession to cDNA generation directly as described in 2.4.4.

2.4.3 RNA extraction with Qiagen Miniprep

Sorted cells were lysed using Qiashredder columns (Qiagen). In the case of tissue RNA prep, the tissue was transferred into homogenisation tubes containing ceramic beads (Precellys) and 300uL RLT buffer (Qiagen) containing β-mercaptoethanol and homogenized for 10min at 25 Hz/s. The lysate from either sorted cells or tissue homogenisation was further processed through DNeasy Miniprep (Qiagen) according to manufacturer's instructions.

2.4.4 cDNA generation

Following normalisation of RNA concentrations by measuring with Nanodrop 1000 (ThermoFisher), cDNA master mix (n+1) was prepared as described in table 2.11. 9μL of this master mix was transferred to NO RT control, as well as 2μL NF H2O and 3*3μL random RNA samples. (n * 1μL) RT was added to the master mix, and 10μL tranferred to each reaction tube. The cDNA synthesis program was run as described in table 2.12. cDNA was stored at -20 °C and diluted 1:3 in NF H2O prior to use for RT-qPCR reaction as described in 2.4.5.

Table 2.11: Mastermix for cDNA synthesis (depicted is the mixing ratio for one reaction).

Reagent	**μL**
NF H2O	4.2
10x RT buffer	2
Random primers	2
dNTP	0.8

Table 2.12: cDNA PCR cycle

Time (min)	**Temperature (°C)**
10	25
120	37
5	85
∞	4

2.4.5 Taqman RT-qPCR reaction

A RT-qPCR master mix was prepared for each taqman probe (table 2.14) as described in table 2.13. 3.6μL/well was pipetted in a semi-skirted 384 well plate, accounting for duplicates of samples and a H_20 blank control as well as no RT sample control. 2.4μL/well cDNA was pipetted before thermal cycling was performed on a C1000 Touch (BioRad) with the parameters described in table 2.15. The relative expression of each gene was normalised to the expression of the housekeeper gene *Gapdh*.

Table 2.13: Mastermix for RT-qPCR (depicted is the mixing ratio for one reaction).

Reagent	**μL**
Fast Blue qPCR Master Mix	3
NF H2O	0.3
Taqman probe	0.3

Table 2.14: Taqman probes

Target	**Assay ID**	**Supplier**
Ccl2	Mm00441242_m1	ThermoFisher
Ccl3	Mm00441259_g1	ThermoFisher
Ccl4	Mm00443111_m1	ThermoFisher
Ccl5	Mm01302427_m1	ThermoFisher
Cxcl1	Mm00433859_m1	ThermoFisher
Cxcl2	Mm00436450_m1	ThermoFisher
Cxcl9	Mm00434946_m1	ThermoFisher
Gapdh	Mm99999915_g1	ThermoFisher
Il1a	Mm00439620_m1	ThermoFisher
Il1b	Mm00434228_m1	ThermoFisher
Il6	Mm00446190_m1	ThermoFisher
Il10	Mm00439614_m1	ThermoFisher
Il12b	Mm01288990_m1	ThermoFisher
Il22	Mm01226722_m1	ThermoFisher
Il23a	Mm00518984_m1	ThermoFisher
Irf5	Mm00496477_m1	ThermoFisher
Tnf	Mm00443258_m1	ThermoFisher

Table 2.15: RT-qPCR protocol

# cycles	Time (s)	Temperature (°C)
1	120	95
40	3	95
	30	60

2.5 Confocal microscopy

2.5.1 Sample preparation and embedding

After whole colon excision and longitudinal slicing, colon tissue was washed in PBS, rolled into swiss rolls [174], and incubated in 5mL/sample freshly prepared PLP buffer (table 2.16) for 24h rolling at 4 °C. The tissue was washed three times in PBS for 5min at 4 °C, before transfer into 30 % sucrose solution for 24h. Swiss rolls were rerolled where necessary and embedded in Optimal Cutting Temperature (OCT) medium (Tissue-Tek), before freezing on dry ice with 2-methylbutane, and stored at -80 °C. In the case of unfixed sections, the rolled swiss rolls were directly embedded in OCT medium and fixed upon staining. The section were then stained according to the protocol descriped in 2.5.2 in the case of directly embedded blocks and according to 2.5.3 for PLP-prefixed blocks.

Table 2.16: PLP buffer recipe for 10mL

Component	Amount
4 % MeOH-free PFA	2.5mL
$NaIO_4$ (Sodium periodate)	0.0212g
P-buffer	3.75mL
L-lysine	3.75mL

2.5.2 Immunofluorescence labelling of colons - unfixed sections

5 μM or 20 μM cryosections were air dried for 1h at RT. ImmEdge® Hydrophobic Barrier PAP pen (Vector Laboratories) was applied to the slides and sections were rehydrated with 100μl PBS per slide. The sections were fixed in a 1:1 mixture of methanol:acetone (Merck) and blocked with PBS containing 5% goat serum (Sigma Aldrich) and 5% mouse serum (Invitrogen) (blocking solution). Following this, the Sections were blocked with biotin/avidin (Invitrogen). Labelling with primary antibodies was performed in blocking

solution overnight at 4°C. This was followed by secondary antibody labelling, incubated in the dark for 30min at RT. Following PBS washes, the sections were stained overnight with directly labelled antibodies diluted in TBS. After PBS washes, the tissue was mounted using 5% N-propyl gallate (Merck) in glycerol, the edges sealed with nailpolish and dried overnight at RT before imaging. Primary and secondary antibodies and their working dilutions can be found in table 2.17.

2.5.3 Immunofluorescence labelling of colons - PLP fixed sections

For immunostaining, sections were allowed to air-dry for 1h at RT. ImmEdge® Hydrophobic Barrier PAP pen (Vector Laboratories) was applied to the slides and sections were rehydrated with 100μl 5% PBT per slide. The signal was enhanced by appliance of 1-2 drops of Image-iT FX Signal Enhancer™ (Life Technologies) on each of the sections and incubation for 30min at RT. Following a short 5min PBS wash, slides were then incubated with Carbo-free™ blocking solution (Vector Laboratories) supplemented with 0.05% Tx-100, 0.08% sodium azide and 0.3M glycine containing 5% goat-serum for 1h at RT. After blocking unspecific antibody binding, sections were stained with primary antibodies overnight at 4 °C. Secondary antibodies were applied following washes for 1.5h at RT. The antibodies were diluted in blocking solution and 100μL staining solution was applied per section. The antibodies and their working dilutions used for immunostaining are listed in table 2.17. Washing steps were performed in PBS (3 times for 5 min) and nuclei were counterstained with Sytox Blue (Life Technologies) diluted in 5% PBT for 10 min at RT after secondary antibody staining. Slides were briefly rinsed by immersion in dH2O and excess liquid was removed using lint free tissue. FluorSave™ (Life Technologies) mounting medium was used to place 22x50 mm coverslips while avoiding bubble formation. Slides were cured for 1h or overnight before imaging.

Table 2.17: Antibodies used for confocal microscopy

Epitope	Colour	Clone	Manufacturer	Cat #	Dilution
Ly6C	BV421	HK1.4	Biolegend	128031	1/50
E-Cadherin	AF647	36/E-Cadherin	BD	560062	1/100
gp38	BV421	8.1.1	Biolegend	127423	1/100
CD31	BV421	390	Biolegend	102423	1/100
CD31	BV421	MEC13.3	BD	562939	1/100
CD206	rat	MR5D3	BioRad	MCA2235	1/50
F4/80	rabbit	CI:A3-1	Enzo	ENZ-ABS638-0200	1/100
CD177	rabbit	1171A	R&D systems	MAB8186	1/200
CD11c	biotin	N418	Biolegend	117303	1/100
Anti-rabbit	AF488	Polyclonal	Life Technologies	A-11008	1/400
Anti-rat	AF488	Polyclonal	Life Technologies	A-11006	1/400
Anti-rabbit	AF555	Polyclonal	Life Technologies	A-21428	1/400
Anti-rabbit	AF647	Polyclonal	Life Technologies	A-27040	1/400
Streptavidin	AF647	N/A	Biolegend	405237	1/100
SytoxBlue	SytoxBlue	N/A	ThermoFisher	S34857	1/500

2.5.4 Image acquisition and processing

Images were acquired on Zeiss 880 laser scanning confocal system on an Axio Examiner upright fixed stage microscope, or Zeiss 980 laser scanning confocal inverted microscope equipped with an Airy Scan detector. Excitation of Brilliant Violet 421 was done with 405 laser line, Sytox Blue was excited with 458 laser, Alexa Fluor 488 or GFP with 488 laser, Alexa Fluor 555 or tdTomato with 561 laser, Alexa Fluor 594 with 594 laser, whereas Alexa Fluor 647 was excited using 633 laser. Fluorescence signals were acquired with sequential scans using point detection, set by observing maximum emission and minimizing fluorescence cross-over between individual fluorochromes. Tiled images were stitched and orthogonal maximum intensity projections were generated from z-stacks post acquisition in Zen Blue v2.3 software.

2.5.5 Image analysis and quantification

The images were analysed using IMARIS (Bitplane). Of each mouse, six individual colon swiss rolls sections were stained in three independent rounds of staining. Within each staining round, intensity tresholds for CD206, CD11c and F4/80 were kept constant. Surfaces were created on F4/80+ cells using the surface tool in Imaris. The size cut-off for a cell was kept at 6.5 µM constantly. Intensity means for CD11c+ and CD206+ cells were defined on single channel spot analysis and kept as a cut-off standard within one staining cycle. Using an automated Python-script, CD11c+ and CD206+ macrophages were defined within F4/80+ cells as cells that reached the intensity mean threshold for CD206 and CD11c respectively. The number of double-positive cells was counted and quantified as a percentage of total F4/80+ cells. For quantification of macrophage subsets distance to the epithelium, a region of interest within one swiss roll was selected based on tissue architecture where the different regions (epithelium, lamina propria and muscularis) across the depth of the colon were clearly visible. Using the filaments tool, the epithelium and serosal membrane were manually drawn and a channel was created using these filaments. Surfaces were created automatically on these channels, and using the distance transformation tool within the surface statistics, two channels were created that measured the distance of a selected object in relation to their surface. Again, F4/80+ cell surface statistics and defining CD206+ and CD11c+ macrophages were analysed as described above. In addition, each CD206+ and CD11c+ macrophage was set in relation to its minimal distance to the epithelium and the serosal membrane using the distance transformation channels described above. Adding the two minimal distances for each macrophage gives the total distance between the membranes for each point. Distance to membrane was calculated as a percentage of the minimal distance of the respective membrane in relation to the total membrane, allowing correction for the elongation of the epithelium in inflammation. The workflow is depicted as a schematic in Figure 3.12d.

2.6 Cell culture and *in vitro* stimulation

2.6.1 Freezing and thawing of cell lines from liquid nitrogen

Cells were collected from the corresponding box in liquid nitrogen storage and swirled in 37 °C until almost thawed. They were then transferred to 10mL pre-warmed maintenance medium (see tables 2.18 & 2.19) and spun down 5min at 1500rpm. Cells were resuspended in 10mL medium and plated in 10cm tissue culture plates. The cells were allowed to settle for two days before the first split and about five days before starting differentiation.

For freezing cell lines, earlier passages are favoured. Cells were collected and counted. $1*10^7$ cells/mL were resuspended in freezing medium (FCS + 10 % DMSO) before transfer into cryovials. Cryovials were frozen overnight at -80 °C in a MrFrosty (ThermoFisher) before transfer into liquid nitrogen storage.

2.6.2 Maintenance and differentiation of Hoxb8 cells

For splitting, cells were harvested with a cell lifter and spun down 5min 1500rpm before either splitting 1:10 in pre-warmed maintenance medium (table 2.18 for Hoxb8-GM-CSF cells and table 2.19 for Hoxb8-SCF cells) for longer term maintenance or 1:3 for growing up to start differentiation.

Table 2.18: Medium used for maintenance of Hoxb8-GM-CSF cells

Reagent	**Amount**
RPMI	500mL
10% FCS	50mL
1% P/S	5mL
30μM β-mercaptoethanol	300μL of 50mM stock
10ng/mL murine GM-CSF	1:1000 added freshly
10μM estradiol	1:1000 added freshly

Table 2.19: Medium used for maintenance of Hoxb8-SCF cells

Reagent	**Amount**
RPMI	500mL
10% FCS	50mL
1% P/S	5mL
30μM β-mercaptoethanol	300μL of 50mM stock
4% SCF	20mL
10μM estradiol	1:1000 added freshly

After reaching desired cell numbers, cells were harvested with a cell lifter and counted. $10*10^6$ Hoxb8 GM-CSF cells/condition were washed with PBS twice and resuspended in 20mL differentiation medium (table 2.20). $2.5*10^5$ Hoxb8-SCF cells were washed with 50mL PBS containing 1% FCS and resuspended in 13mL differentiation medium (table 2.21). Hoxb8-GM-CSF cells were cultured for two days to generate monocytes and seven days to generate fully differentiated macrophages. Hoxb8-SCF cells were cultured for five days to generate fully differentiated neutrophils.

Table 2.20: Medium used for differentiation of Hoxb8-GM-CSF cells

Reagent	**Amount**
DMEM	500mL
10% FCS	50mL
1% P/S	5mL
20ng/mL murine GM-CSF	1:500 added freshly

Table 2.21: Medium used for differentiation of Hoxb8-SCF cells

Reagent	**Amount**
RPMI	500mL
10% FCS	50mL
1% P/S	5mL
30μM β-mercaptoethanol	300μL of 50mM stock
4% SCF	20mL
20ng/mL G-CSF	1:5000 added freshly

2.6.3 *In vitro* stimulation

Differentiated Hoxb8 cells were scraped off and collected in a 50mL Falcon tube. Following a 5min spin at 1600rpm, cells were resuspended in 10% FCS 1% P/S RPMI media and counted. $2*10^6$ cells per well were seeded in duplicates for technical replicates in 1mL in 12-well coated tissue culture plates. For defactinib pretreatment, 10mg/mL of the stock was diluted in media to reach 0.003mM end concentration. DMSO was diluted the same way to avoid toxicity and generate comparable concentrations. The cells were incubated for 1h at 37 °C, and stimulated with Hh sIAg (10mg/mL end concentration), Zymosan (25mg/mL end concentration) or LPS (100ng/mL end concentration) for the time indicated. At the end of the incubation, the plate is spun down and the supernatant

taken off and stored at -20 °C for protein measurement. Cells are lysed by adding 200μL RLT buffer containing β-mercaptoethanol per well and incubation for 5min at RT. Lysed cells are stored at -80 °C until further processing.

2.7 Statistical analysis

All statistical analysis was performed using GraphPad Prism version 8.2.0. Statistical tests were performed as indicated in figure legends. First, it was decided whether the data was paired or unpaired, in order to determine the correct statistical test. The data was checked for normalcy and lognormalcy using Shapiro-Wilk normalty test and the normal QQ plot was consulted. Following this, ROUT testing for outliers was performed if the data is normally distributed, otherwise the data was log-transformed. Depending on the outcome of the normality test, either a parametric (normal distribution) or non-parametric t-test was performed in cases where two conditions were compared. Two way ANOVAs with Tukey's multiple comparison tests were performed to investigate significant differences across more than two experimental conditions. Mixed-effects analysis was carried out to investigate differences of the same mice over a certain time. Differences were considered statistically significant when the p-value was below or equal to 0.05.

3

Unravelling spatial differences of the tissue microenvironment and immune cell infiltration over the course of murine intestinal inflammation

Contents

3.1 Regional specialization of intestinal macrophages along the gastrointestinal tract 52
3.2 Aims 55
3.3 Results 56
3.3.1 Myeloid cells are the first responders in Hh + aIL10R-mediated inflammation 56
3.3.2 Swiss rolls as a powerful tool to investigate cellular and tissular changes during intestinal inflammation 58
3.3.3 Characterization of CX3CR1-GFP Ly6G-tdTomato double-reporter mice 60
3.3.4 Distinct infiltration of myeloid cells at specific sites over the course of intestinal inflammation 62
3.3.5 *Helicobacter hepaticus* localisation over the course of intestinal inflammation does not indicate a preferred colonisation site . . . 66
3.3.6 The tissue environment starts to differ as early as d4 Hh + aIL10R between the distinct proximal and distal microenvironments . . . 67
3.3.7 Neutrophils correlate with areas of higher inflammation at the onset of inflammation 71
3.3.8 Changes in the macrophage subset pool occur distinctly in the proximal and distal colon over the timecourse of inflammation . 73
3.3.9 Macrophage subsets occupy distinct niches in the colon at steady state 75
3.3.10 Macrophage subset markers and their localisation blur during inflammation 79
3.4 Discussion 81
3.4.1 The tissue microenvironment leads to distinct spatiotemporal immune cell infiltration in the colon 81

3.4.2 Inflammation-dependent changes of the tissue microenvironment leads to differential localisation of macrophage subsets 83
3.5 Conclusion 86
3.6 Future directions & limitations 87

3.1 Regional specialization of intestinal macrophages along the gastrointestinal tract

Intestinal macrophages represent the largest pool of resident macrophages in the body, performing crucial functions at both steady state and inflammation [71, 175]. With the majority of intestinal macrophages localised in the LP, they are ideally equipped to capture and eliminate any microbial intruder as well as supporting barrier integrity [72, 73]. Antigen sampling in a CX3CR1- and MyD88-dependent manner ensures maintenance of tolerance against commensal microbes by transferring antigens to migratory DCs as well as by conserving and expanding regulatory T cells [176–180]. Despite their bactericidal activity and expression of a full range of PRRs, phagocytosis by intestinal macrophages does not normally result in an inflammatory response, and thus are considered anergic [73, 75, 181, 182]. This anergy is generally attributed to the anti-inflammatory IL-10/IL-10R axis in both mice and humans [181, 183]. However, during infection or inflammation, intestinal macrophages initiate the innate immune response by secreting pro-inflammatory cytokines and chemokines, creating both an inflammatory tissue microenvironment and recruiting other immune cells. This microenvironment primes the high number of monocytes recruited to differentiate into inflammatory macrophages [13, 129, 184].

In contrast to many other tissues, the majority of adult intestinal macrophages arise from infiltrating Ly6C^{hi} monocytes, with only a small fraction replenished by embryonically derived macrophages at steady state [75, 76, 185]. The development of adult tolerogenic macrophages from Ly6C^{hi} monocytes is a a process that is dependent upon TGF-β [78, 186] and IL-10 [79]. Distinct gene expression profiles are being imprinted by TGF-β and IL-10, indicating complementary roles in shaping tissue-specific functions and anergy [78].

3. Unravelling spatial differences of the tissue microenvironment and immune cell infiltration over the course of murine intestinal inflammation

The importance of IL-10 signalling in the gastrointestinal tract is highlighted in the context of *Il10-/-* mice, which develop spontaneous colitis [187]. Monocytes rapidly adopt a tissue-specific gene expression profile shaped by their immediate tissue microenvironment upon extravasation [13, 14, 74, 184]. The upregulation of MHCII and downregulation of Ly6C accompanies this process, termed the "monocyte differentiation waterfall" [77].

Inflammation leads to a partial depletion of the resident macrophage population, creating a temporary niche for infiltrating monocytes, which then differentiate based on environmental cues [13, 14, 184]. This grants a high degree of plasticity in the macrophage response to infection [186]. Upon inflammation, the infiltrating monocytes no longer differentiate into anti-inflammatory macrophages, but instead develop into pro-inflammatory macrophages following as yet undefined cues within the inflammatory tissue environment [13, 75, 129, 186].

In line with other tissues, different subsets of macrophages have also been identified in the intestine based on the mutually exclusive expression of CD11c and CD206 [129].CD206+ macrophages are believed to play anergic roles in the colon, whilst CD11c+ macrophages are regarded as more inflammatory [129, 188, 189]. CD11c+ mononuclear phagocytes have previously been described to promote Hh + aIL10R intestinal inflammation, a model of chronic colitis, by secreting IL-23 [141]. One hallmark of Hh + aIL10R-induced inflammation of the LP is the accumulation of blood-borne Ly6C^{hi} monocytes which differentiate locally into inflammatory macrophages [75, 77, 190, 191]. Despite the presence of inflammatory macrophages, the resident macrophages retain their anti-inflammatory profile [75, 190].

The tissue microenvironment along the mammalian GI tract differs between the SI and the colon, but also locally, along the crypt-lumen axis [192] (see Figure 3.1, Chapter 1.1.1). In brief, the microbial load, mucus thickness, and pH increase from the SI to the colon [193]. Simultaneously, BAs, oxygen and AHR ligands decrease along the GI tract. The SI is critically important for nutrient absorption and food tolerance; It is also continuously exposed to digestive fluids such as bile, which can affect the microbiota that reside in the lower part of the mammalian SI [27, 194, 195]. The colon is heavily populated by the microbiota, which maintain a symbiotic relationship with the host and break down nutrients

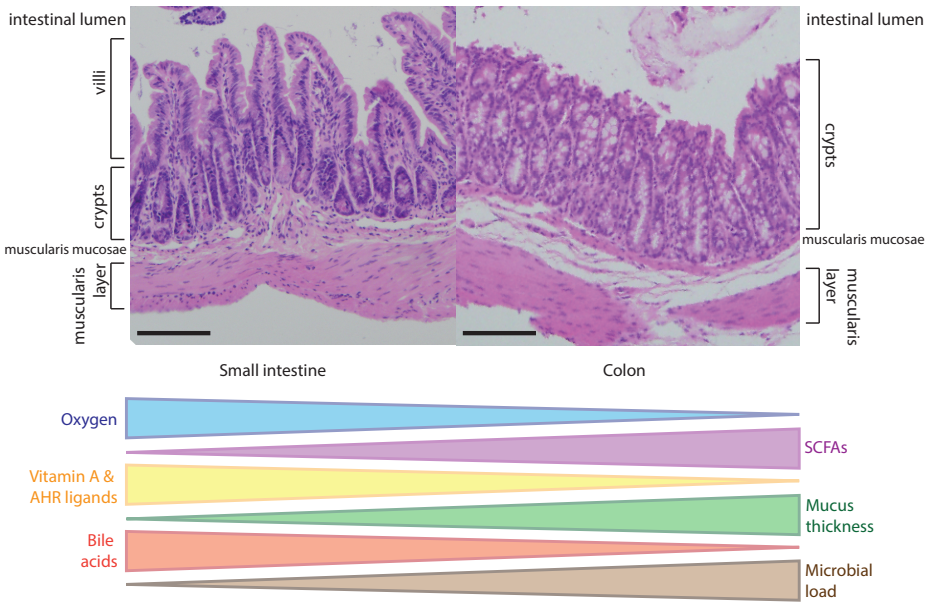


Figure 3.1: **Differences along the gastrointestinal tract include physical, chemical, dietary and microbial factors.** The main function of the SI is absorption of nutrients whereas the colon is heavily populated by microbiota breaking down nutrients that were not absorbed in the SI. These differences in function are also reflected in the structure of the SI, being composed of villi to increase surface area for nutrient absorption. Localised above the crypts in the intestinal lumen is a thick mucosal layer which separates the host tissue from the microbiota and pathogens. Oxygen, bile acids, vitamin A and aryl hydrocarbon receptor ligands are decreased along the length of the GI tract whilst microbial load, mucus thickness and SCFA availability increases from SI to colon. These changes contribute to different tissue microenvironments along the GI tract. Figure and legend from *Berthold et al* [10].

not taken up in the SI [196]. Another important function of the colon is water resorption, which happens mainly in the proximal part of the colon [197]. The clear differences in the microenvironment cues along the GI tract are likely to shape the localization, phenotype and function of the resident and recruited immune cells and lead to yet unappreciated cell heterogeneity along the tract. For instance, SCFAs and BAs are known to modulate the microbiota composition, but also to exert distinct effects on the intestinal immune system [38, 198–200]. A study comparing monocytes entering the SI and colon at steady state at different timepoints following a monocyte transfer revealed distinct transcriptomic profiles rapidly being acquired in the distinct locations [14]. Not only macrophages, but also other immune cells like neutrophils acquire tissue-specific transcriptomes [11, 12]. Also along the length of the colon, differences in microbiota colonization exist as well as variation of microbial metabolite concentration, providing distinct niches for immune cell specialization [2, 10, 52, 201]. Furthermore, the microbial diversity is significantly higher in the proximal colon than in the distal colon [202]. This highlights the importance of comparing functional differences of immune cells along the colon specifically.

3.2 Aims

Utilising confocal microscopy, flow cytometry and RT-qPCR, we aim to characterise the differences in immune cell localisation and recruitment over the timecourse of Hh + aIL10R colitis. Due to the differences along the GI tract influencing immune cell function, we hypothesize that the tissue microenvironment significantly differs between the proximal and distal colon, leading to a distinct spatiotemporal infiltration of immune cells along a course of intestinal inflammation.

3.3 Results

3.3.1 Myeloid cells are the first responders in Hh + aIL10R-mediated inflammation

Innate immune cells, especially myeloid cells, are the first responders to an infection or insult, with macrophages already present abundantly in the intestine, and neutrophils being the first immune cells recruited in high numbers. Indeed, over a time course of inflammation (SS, d4, d7, d21 Hh + aIL10R) in a Hh + aIL10R - mediated colitis, we could see that neutrophils are the highest infiltrate at d7, closely followed by monocytes (Figure 3.2a). Myeloid cell infiltration tapers off towards peak of inflammation (d21) with non-myeloid cells (CD11b- lineage+ cells; mostly B & T cells) taking over (Figure 3.2b). This renders the onset of inflammation as a highly interesting area for further studies aimed at unravelling early events in the inflammatory cascade. We therefore chose to examine the onset of inflammation in more detail and focus on myeloid cells to identify which cells orchestrate intestinal inflammation.

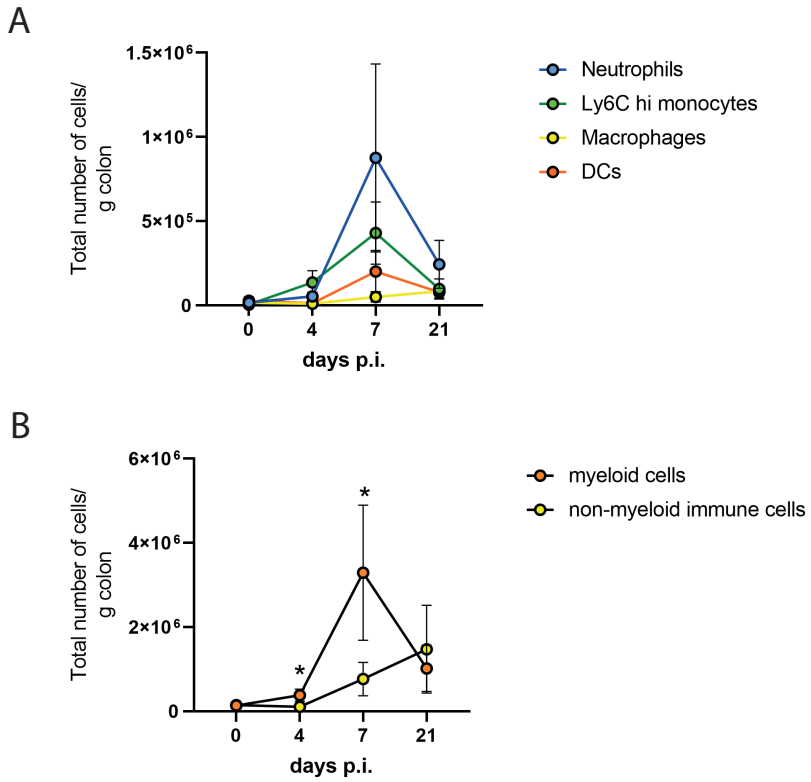


Figure 3.2: **Myeloid cells infiltrate the colon at different timepoints over the course of intestinal inflammation.** A) Infiltration of neutrophils (blue), Ly6C^{hi} monocytes (green), macrophages (yellow) and DCs (red) over the course of Hh + aIL10R colitis (day 0, 4, 7, 21), represented as total number of cells per gram, B) Myeloid cells (CD11b+, lineage-; orange) and non-myeloid cells (CD11b-, lineage+; yellow) over the course of Hh + aIL10R colitis. Data is representative of two independent experiments. Two-way analysis of variance (ANOVA) with Sidak correction. Data presented are means ±SD. ns, not significant. $^{*}P \leq 0.05$, $^{**}P \leq 0.01$, $^{***}P \leq 0.001$ and $^{****}P \leq 0.0001$

3.3.2 Swiss rolls as a powerful tool to investigate cellular and tissular changes during intestinal inflammation

Swiss rolls are an established technique for examination of longitudinal composition of intestinal tissue, where the colon is sliced longitudinally and then rolled up before embedding in a medium suitable for freezing and cryosectioning [174]. As it previously has been used to determine changes of inflammation along the entire length of the colon [169, 203], we wanted to investigate changes in our model by comparing steady state with d21 of Hh + aIL10R-mediated inflammation. Swiss rolls are a neat tool for investigating the distribution of immune cells along the colon, providing not only a small snapshot but information about differences between colon sections (proximal, mid and distal). The proximal colon can be recognized by diverticuli making it easy to distinguish from the rest of the colon.

Firstly we examined the swiss rolls for differences on a whole tissue level using Haematoxylin and Eosin (H&E) staining (Figure 3.3a). We could observe an increase in pathology score in Hh + aIL10R-induced inflammation along the entire length of the colon (Figure 3.3b), as well as an increase of the total distance between serosal membrane and epithelial border (Figure 3.3c). Furthermore, the total amount of macrophages in the colon was doubled in the inflamed colon (Figure 3.3d).

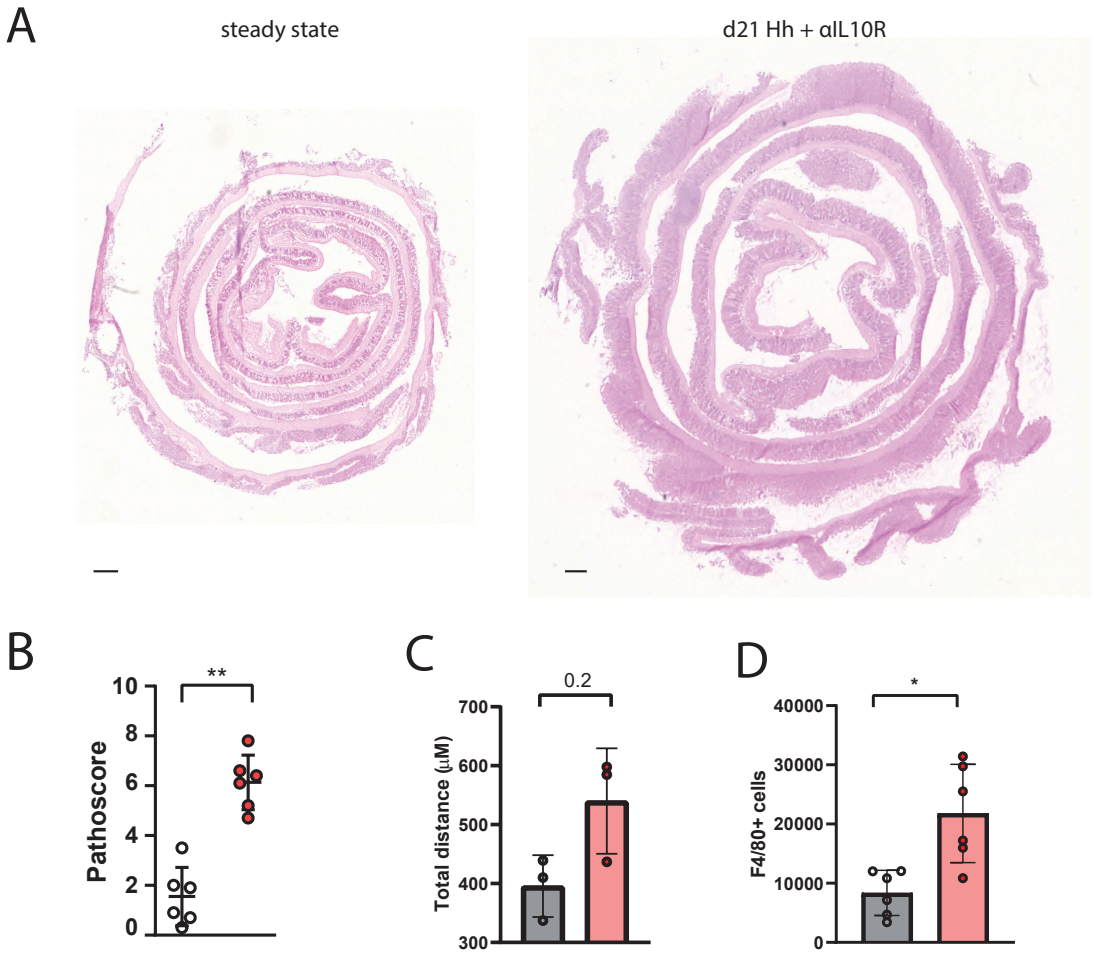


Figure 3.3: **Hh + aIL10R colitis induces severe colitis and leads to epithelial elongation and an increase in macrophage numbers.** A) Representative H&E sections of swiss rolls of steady state (left) (N = 6 from two independent experiments) and d21 Hh + aIL10R colits (right) (N = 6 from two independent experiments). Scalebars represents 500 μM. B) . B) Histopathology scoring of steady state (open white circles) and d21 Hh + aIL10R colitis (open red circles) colons. N = 6 from two independent experiments. Unpaired t-test. C) Total distance between serosal membrane and epithelium luminal barrier at steady state (grey) and d21 of Hh + aIL10R inflammation (red). (N = 3 from one experiment). Mann Whitney test. Data presented as mean ± SEM. D) Quantification of F4/80+ cells using the surface tool of IMARIS. N = 6 for each condition, from two independent experiments. Mann Whitney test. Data presented are mean ± SEM, ns, not significant. $^{*}P \leq 0.05$

3.3.3 Characterization of CX3CR1-GFP Ly6G-tdTomato double-reporter mice

Even though neutrophils and macrophages are known to play a crucial role in colitis progression, their distribution and potential interactions have not been investigated in depth. To assess potential differences in myeloid cell functions and cell-cell interactions crucial in shaping the onset of intestinal inflammation, we wanted to investigate the spatial distribution of myeloid cells during a time course of Hh + aIL10R mediated murine colitis. As described in 3.3.2, swiss rolls are a powerful tool to investigate changes along the entire length of the colon.

We made use of double-reporter mice (CX3CR1-eGFP & Ly6G-tdTomato) to visualise macrophages and neutrophils. However, colons of double-reporter mice revealed a high expression of Ly6G/reporter activity in a low number of epithelial cells (Figure 3.4a). In fact, when investigated via flow cytometry, most tdTomato+ cells at steady state were epithelial cells and not neutrophils (Figure 3.4b&c). Epithelial cells from other tissues like the cornea were also found to express Ly6G and myeloid characteristics, hinting to a similar mechanism here [204]. This may be due to a leaky Cre expression in one epithelial stem cell, giving rise to an entire tdTomato+ crypt. As the epithelial cells get replaced more swiftly during inflammation [205], the occurrence of tdTomato+ cells is more frequent during steady state, where there is less frequent turnover. Instead of using the Ly6G-tdTomato signal, we therefore resorted to labelling neutrophils with CD177. CD177 labels 90% of all neutrophils, and represents a good marker for neutrophils (Figure 3.4d). Moreover, it has also been shown to be upregulated during inflammation [92]. CX3CR1 stains mostly macrophages at steady state, but as inflammation progresses also Ly6C^{hi} and MHCII^{hi} monocytes (Figure 3.4e). We hence added Ly6C and CD177 into our myeloid panel to identify neutrophils, macrophages and monocytes reliably.

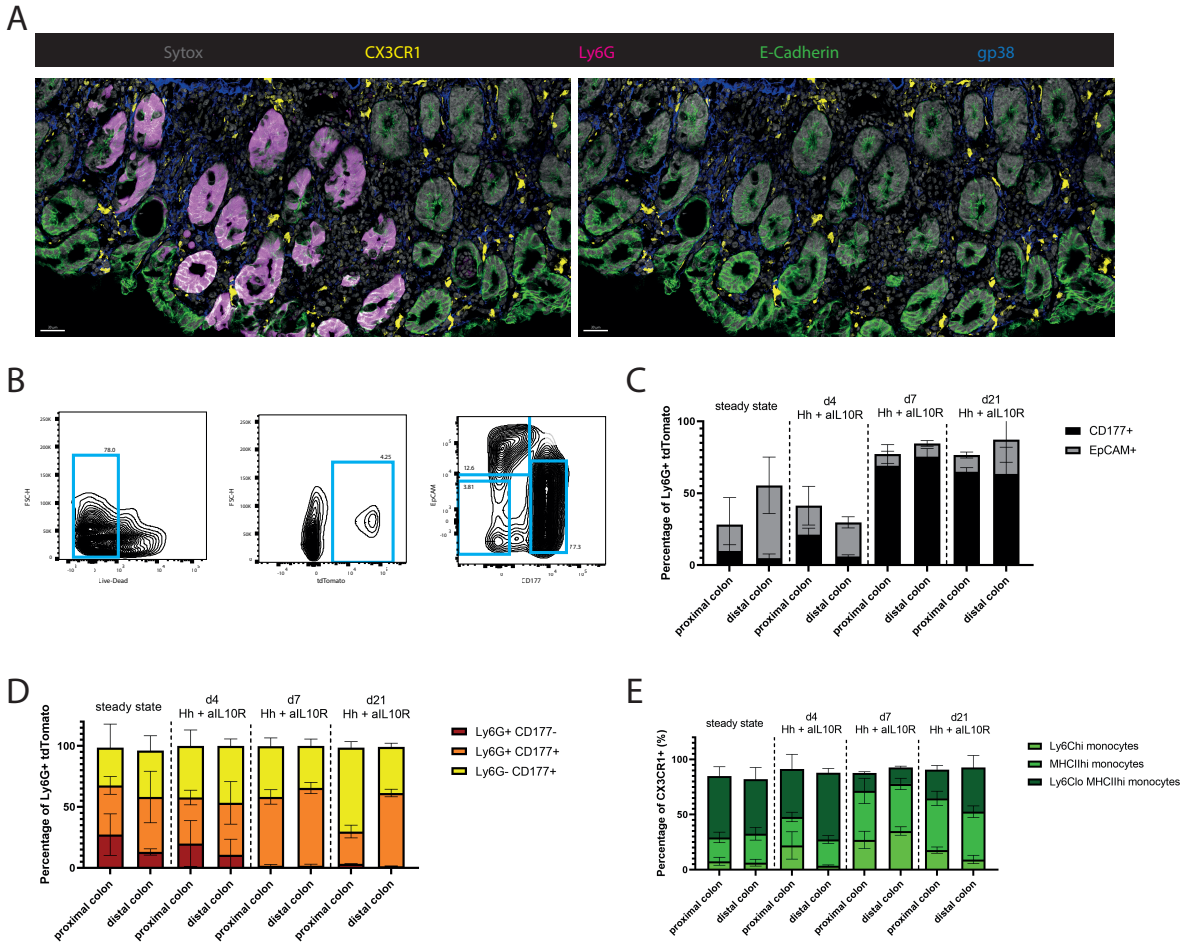


Figure 3.4: **Characterization of CX3CR1-GFP Ly6G-tdTomato double-reporter mice in intestinal inflammation.** A) Representative image of the inflamed colon staining epithelial cells (E-Cadherin, green) and fibroblasts (gp38, blue) on top of CX3CR1-GFP (yellow) and Ly6G-tdTomato (magenta). Cell nuclei are labelled with Sytoxblue (grey). Scalebar depicts 50μm B) Gating strategy for identifying epithelial cells (EpCAM+) and neutrophils (CD177+) within tdTomato+ live cells C) Quantification via flow cytometry of epithelial cells (grey) and neutrophils (black) within tdTomato+ cells over the course of Hh + aIL10R colitis D) CD177+ (yellow), CD177+ Ly6G+ (orange) and Ly6G+ (red) within neutrophils quantified via flow cytometry over the course of Hh + aIL10R colitis, identified by negative gating on other immune cells E) Percentage of Ly6C^{hi}, MHCII^{hi} monocytes and Ly6C^{lo} MHCII^{hi} monocytes within CX3CR1-GFP+ cells, quantified via flow cytometry over the course of Hh + aIL10R colitis.

3.3.4 Distinct infiltration of myeloid cells at specific sites over the course of intestinal inflammation

As there are regional factors differing along the entire GI tract (Chapter 1.1, [10]), but also along the colon, we decided to investigate differences between the proximal and distal colon in more detail. UC and colorectal cancer (CRC) both initiate in the distal colon, so it appears that the tissue microenvironment in the distal colon favours a sustenance of chronic intestinal inflammation.

Imaging the timecourse of intestinal inflammation revealed a high number of CX3CR1+ cells in the proximal colon at steady state, that also increased in the mid and distal colon at later timepoints of inflammation (Figure 3.5a). Furthermore we saw an infiltration of monocytes into the proximal colon at d4, whereas at later timepoints of inflammation, the recruitment of monocytes occurred equally into both the proximal and distal colon (Figure 3.5a). Before d7, we could barely see any neutrophils, whereas at d7 they appeared distinctly in the distal colon (Figure 3.5a). By d21 we could see an even distribution of monocytes, macrophages and neutrophils along the entire length of the colon. Despite CX3CR1 being expressed by monocytes, we could barely see any colocalisation of Ly6C and CX3CR1 (Figure 3.5b). However, when measured in flow cytometry, 5-30% of monocytes express CX3CR1-GFP depending on the timepoint chosen (Figure 3.4e). As the cells undergo a digestion process for flow cytometry, and a PLP fixation process for microscopy, antibody labelling and epitope availability may differ slightly between the techniques.

To confirm and quantify those findings, we applied a multicolour flow cytometry panel designed to capture different subsets of myeloid cells over the timecourse [206]. The proximal colon was identified during dissection by its diverticuli, and the same length of tissue was measured from the distal end of the colon to mark the two distinct environments. Flow cytometry analysis confirmed a distinct infiltration of monocytes into the proximal colon at d4, followed by infiltration into the distal colon at d7, as well as the distinct infiltration of neutrophils into the distal colon at d7 (Figure 3.6a, b). Furthermore, despite not visible by microscopy, neutrophil numbers are higher in the proximal colon at steady

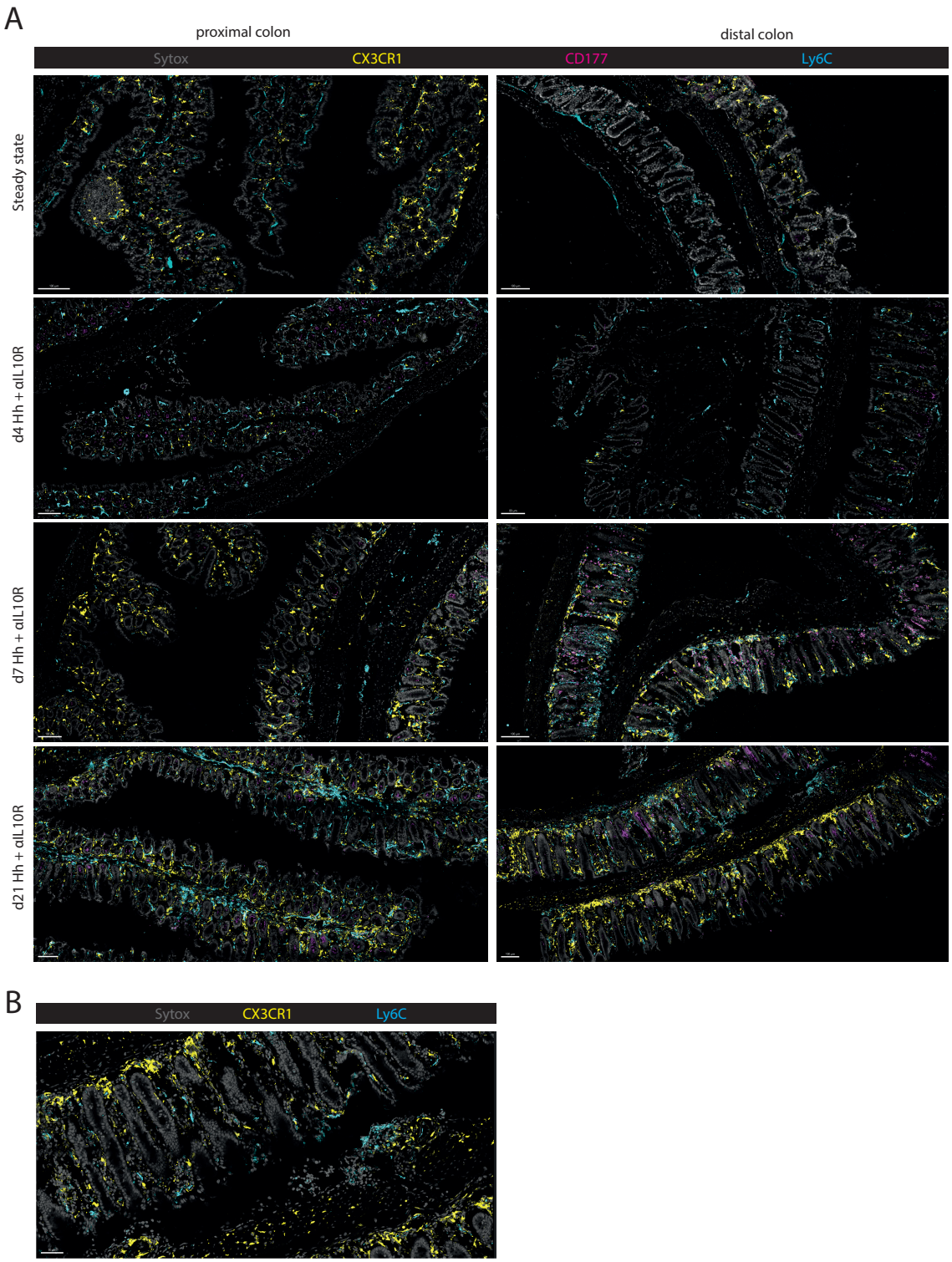


Figure 3.5: **Myeloid cells infiltrate the colon at distinct sites over the course of intestinal inflammation.** *Caption continued on the following page.*

Figure 3.5: A) Representative images of the proximal colon (left column) and distal colon (right column) labelling neutrophils (CD177, magenta), macrophages (CX3CR1, yellow) and monocytes (Ly6C, cyan) over the timecourse of Hh + aIL10R: Steady state, d4 Hh + aIL10R, d7 Hh + aIL10R and d21 Hh + aIL10R. Cell nuclei are labelled with Sytox (grey). Scalebar depicts 50 μm. B) Representative image of CX3CR1-GFP (yellow) and Ly6C (cyan) co-staining. Cell nuclei are labelled with Sytox (grey). Scalebar depicts 50 μm. All images are acquired with x20 objective on a Zeiss980 inverted confocal microscope.

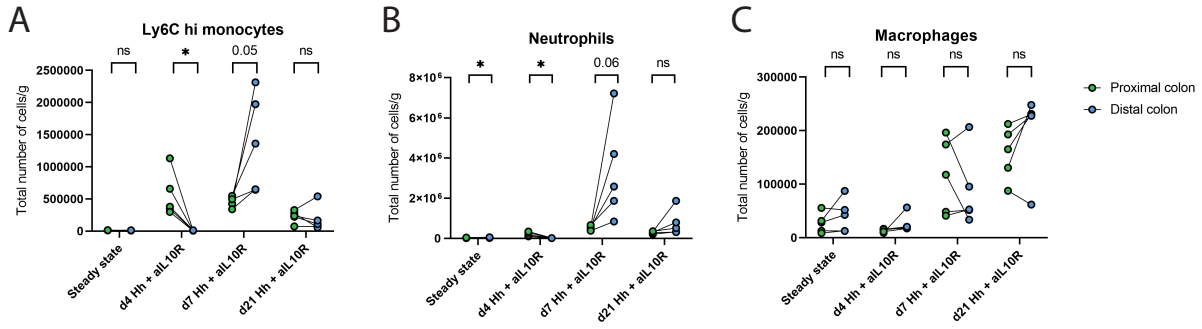


Figure 3.6: **Myeloid cells infiltrate the colon at distinct sites over the course of intestinal inflammation.** Total number per gram of Ly6C^{hi} monocytes isolated from 2cm pieces of proximal (green) and distal (blue) colon respectively (n =5) were quantified via flow cytometry over the course of intestinal inflammation. B) Total number per gram of neutrophils, C) Total number per gram of macrophages. Data is representative of two independent experiments. Paired t-test. Data presented are means ±SD. ns, not significant. $^{*}P \leq 0.05$, $^{**}P \leq 0.01$, $^{***}P \leq 0.001$ and $^{****}P \leq 0.0001$

state and d4 Hh + aIL10R, further raising the question behind mechanism of the distal recruitment of neutrophils at d7 Hh + aIL10R (Figure 3.6b). Macrophages numbers do not differ between the proximal and distal colon at any timepoint measured, however the total numbers increase as colitis progresses (Figure 3.6c).

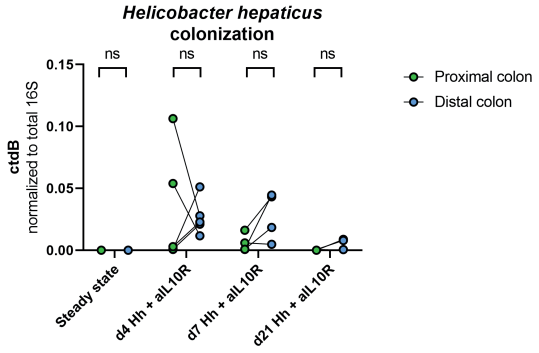


Figure 3.7: ***Helicobacter hepaticus* colonization along the timecourse of murine colitis**. *Helicobacter hepaticus* colonization was measured by quantifying the presence of Hh-specific cdtB in DNA isolated from distal (blue) and proximal (green) tissue pieces (n=5 per timepoint). The amount of cdtB was normalized to the total 16S rRNA content in the isolated DNA, which was adjusted to 5ng/uL prior to measurement via RT-qPCR. Data are representative from two independent experiments. Paired t-test. Data presented are means ±SD. ns, not significant.

3.3.5 *Helicobacter hepaticus* localisation over the course of intestinal inflammation does not indicate a preferred colonisation site

Along the length of the GI tract, distinct niches for microbiota members exist depending on their preferences for certain nutrients, oxygen levels, pH or flow rate [193]. Spatial rearrangement of microbiota members may be an underappreciated feature of intestinal inflammation, as bacterial delocalisation in genetically susceptible mice promotes macrophage activation during experimental colitis [48]. A recent study connecting 16S rRNA sequencing with 10X scRNA-seq from three different sites of human donors (post-mortem) revealed a spatial distribution of the microbiota at steady state [52]. Furthermore, it was shown that even subtle changes in diet can lead to rearrangement of the microbiota in the murine distal colon, analysed by imaging different microbiota members following high fat diet (HFD) [207]. IECs along the GI tract exhibit a spatially distinct expression of TLRs, with TLR 2 & 5 being mainly present in the proximal colon and TLR4 along the entire length of the colon [168]. As IECs are the first line of defense in the GI tract, and are among the first to come into contact with members of the microbiota, having a distinct pattern of PRRs may lead to differential recruitment of immune cells upon infection/inflammation.

The microbiome and metabolome start shifting at d6 Hh + aIL10R colitis [Powrie lab, unpublished data], indicating dysbiosis at the onset of inflammation. As Hh has been associated with driving intestinal inflammation in this model of colitis [146], and the microbiome and IEC PRR landscape differs along the length of the colon, we aimed to investigate Hh colonization between proximal and distal colon over a timecourse of colitis. For this, we extracted the DNA of proximal and distal tissue pieces from five mice per timepoint. Hh colonisation levels were determined by the presence of cdtB, a *Helicobacter*-specific enterotoxin [208]. The levels of cdtB were normalized by 16S content as a proxy for total bacterial presence. Monitoring Hh localisation over the timecourse of intestinal inflammation revealed no preferential localisation, however the levels at the onset appear to be the highest albeit variable (Figure 3.7). Nonetheless, despite no

preferential localisation of Hh, it may still drive distinct localisation of other microbiota members along the colon. Furthermore, as we undertook a qPCR-based approach of quantification, we could not account for the potential differences in the luminal niches Hh is colonising in the proximal and distal colon (closer or further away from the epithelium), which warrants further investigation.

3.3.6 The tissue environment starts to differ as early as d4 Hh + aIL10R between the distinct proximal and distal microenvironments

As we have unravelled differences in immune cell infiltration into the distal and proximal colon during the timecourse of Hh + aIL10R (chapter 3.3.4), we wanted to examine early signals responsible for the immune cell influx as well as investigating the shaping of the tissue microenvironment. Therefore, we extracted the RNA from tissue sections of the proximal and distal colon from the same mice as in 3.3.4 and analysed it via RT-qPCR for a selection of genes described in the following paragraphs.

We revealed a distinct induction of *Ccl2* in the proximal colon at d4 Hh + aIL10R, followed by *Cxcl1/Cxcl2* in the distal colon at d7 Hh + aIL10R (Figure 3.8a-c). The presence of *Cxcl1* in the distal colon during inflammation was already shown in a model of microbe-induced colon tumorigenesis [209], however the cellular source has not been investigated in depth. High-resolution staining of CXCL1 protein confirmed its distinct localisation in the distal colon at d7 Hh + aIL10R, mostly in epithelial cells (Figure 3.8d). CXCL1 has been identified to be one of the earliest signals in antigen-induced arthritis (AIA), being produced by tissue-resident macrophages [Udalova lab, unpublished data].

Furthermore, *Cxcl9* is highly expressed first in the proximal colon at d4 Hh + aIL10R followed by the distal colon at d7 Hh + aIL10R, reflecting a potential distinct T cell infiltration (Figure 3.8e). CXCL9 is a T cell chemottractant, whose secretion in epithelial cells is induced by IFN-γ [210]. Interestingly, CXCL9 has been associated with better prognosis in CRC patients [211]. Indeed, non-myeloid immune cells (CD45+ CD11b-lineage+) distinctly infiltrate into the distal colon at d7 Hh + aIL10R colitis, which is

sustained at d21 Hh + aIL10R colitis (Figure 3.8f). However, despite lineage+ cells comprising mostly T & B cells, the exact location and numbers remain to be investigated.

To further investigate the pro-inflammatory status of the tissue, we looked at a series of pro-inflammatory cytokines like *Tnf, Il-22* and *Il1b* (Figure 3.9a-c). All of the cytokines examined showed a similar pattern of being higher in the proximal colon at d4 Hh + aIL10R, followed by a continuous raise in both proximal and distal colon over the course of Hh + aIL10R. Simultaneously, *Il10*, which is mainly produced by intestinal macrophages to sustain tolerance by maintaining the Treg pool and keeping the intestinal macrophages tolerogenic [79, 81], is higher in the proximal colon at d4 Hh + aIL10R (Figure 3.9d). The receptor of IL-10, IL-10R is blocked in this model of colitis to disrupt the tolerance and permit Hh colonization.

Although this targeted analysis only uncovers a small subset of changes in the tissue microenvironment, it is apparent that there are considerable differences between the proximal and distal colon in the early onset of Hh + aIL10R, which sets the stage for recruitment and priming of immune cells.

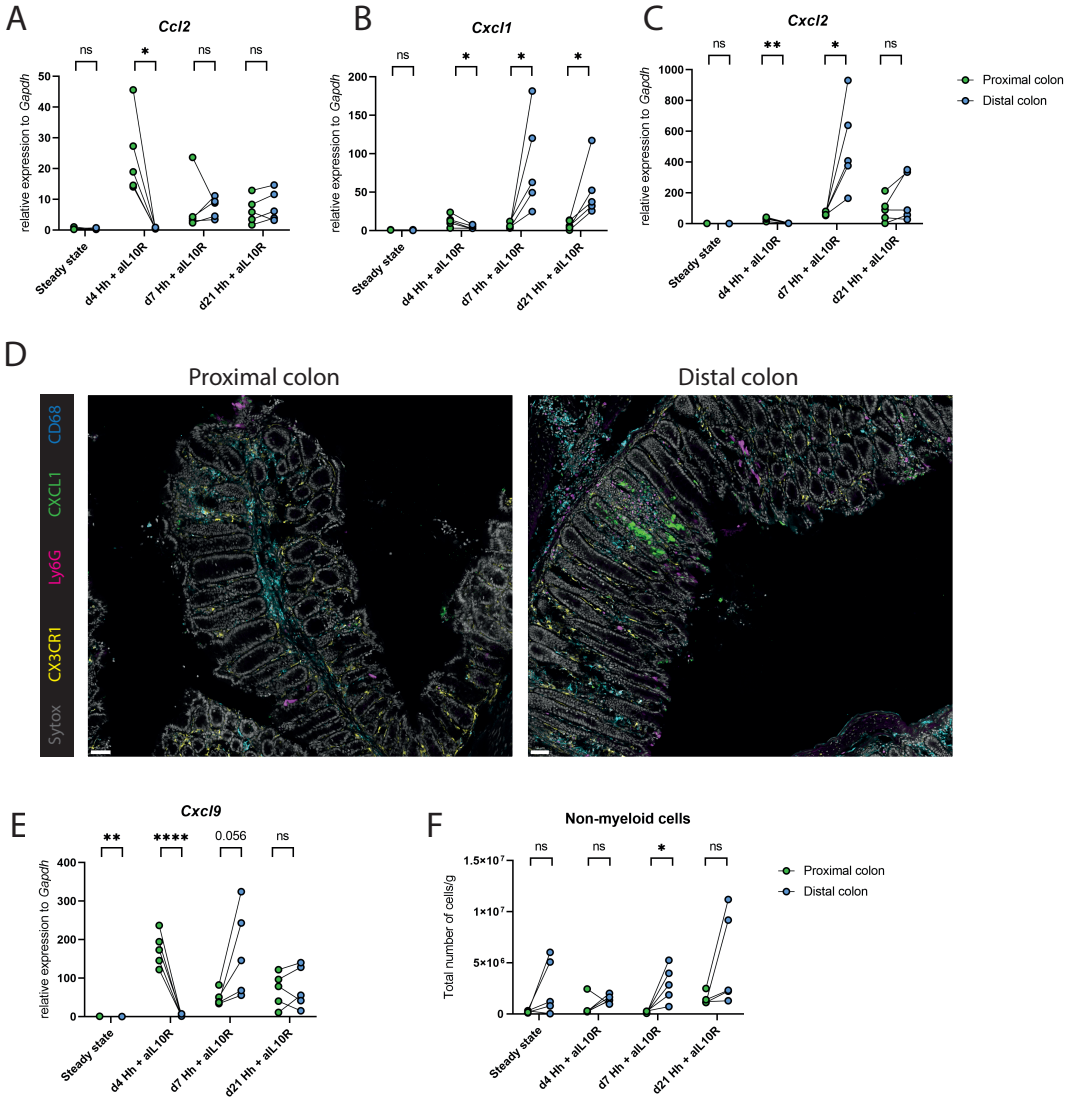


Figure 3.8: **Immune cell-recruiting chemokines are expressed distinctly in the proximal and distal colon**. The expression of selected chemokines was measured by quantifying their presence in RNA isolated from distal (blue) and proximal (green) tissue pieces (n=5 per timepoint) via RT-qPCR. The relative expression along the timecourse of Hh + aIL10R is normalised to the housekeeping gene *Gapdh*. A) *Ccl2*, B) *Cxcl1*, C) *Cxcl2* D) Representative images of CXCL1 (green) staining in the proximal and distal colon at d7 Hh + aIL10R. Neutrophils (Ly6G, magenta) and macrophages (CX3CR1, yellow and CD68, blue) are stained by tdTomato and GFP respectively. Cell nuclei are labelled with Sytoxblue (grey). Scalebar depicts 50 μm. E) *Cxcl9* relative expression F) Total number of non-myeloid cells (CD45+ CD11b- lineage+) per gram colon in the proximal and distal colon along the timecourse of Hh + aIL10R. Data are representative from two independent experiments. Paired t-test. Data presented are means ±SD. ns, not significant. $^{*}P \leq 0.05$, $^{**}P \leq 0.01$, $^{***}P \leq 0.001$ and $^{****}P \leq 0.0001$

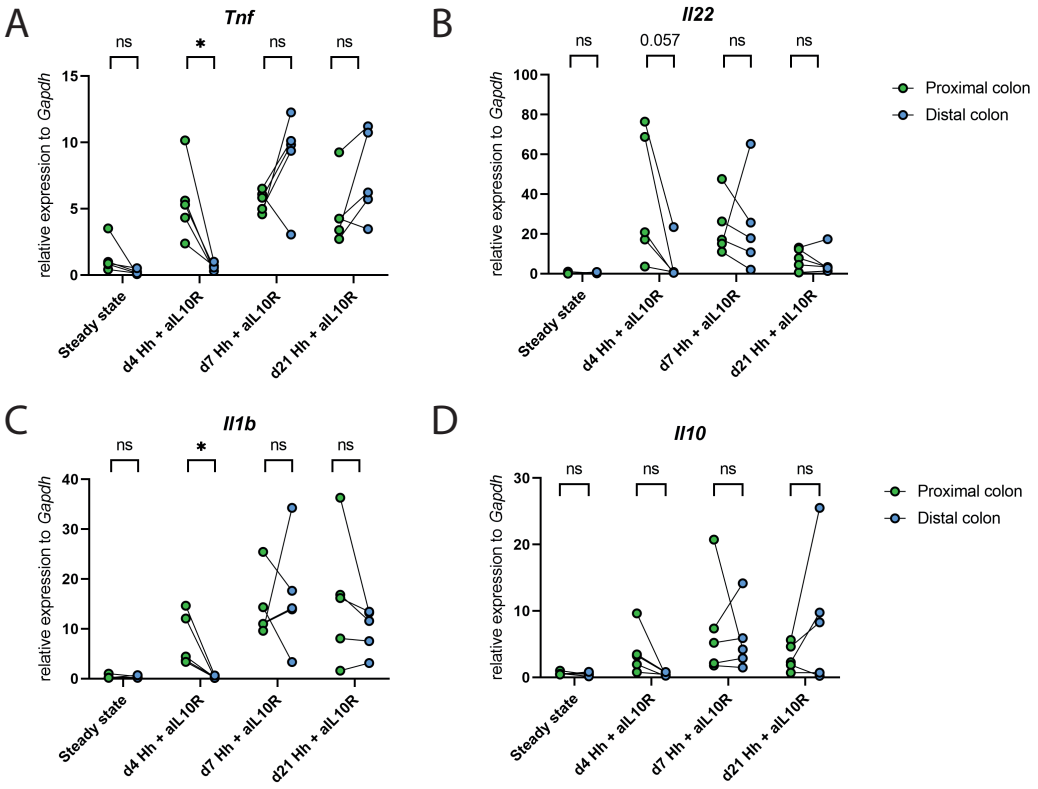


Figure 3.9: **Expression of pro-inflammatory cytokines starts in the proximal colon at d4 Hh + aIL10R**. The expression of selected cytokines was measured by quantifying their presence in RNA isolated from distal (blue) and proximal (green) tissue pieces (n=5 per timepoint) via RT-qPCR. The relative expression along the timecourse of Hh + aIL10R is normalised to the housekeeping gene *Gapdh*. A) *Tnf*, B) *Il22*, C) *Il1b*, D) *Il10*. Data are representative from two independent experiments. Paired t-testData presented are means ±SD. ns, not significant. $^{*}P \leq 0.05$ and $^{**}P \leq 0.01$

3.3.7 Neutrophils correlate with areas of higher inflammation at the onset of inflammation

Furthermore, we also wanted to investigate the inflammatory status of the tissue by the classical histopathology to visualise tissue damage and leukocyte infiltration. Histopathology assessment using Haemotoxylin and Eosin (H & E) staining is routinely used in the clinics for grading disease severity and inflammation. For IBD, different disease-associated patterns have been identified: 1) Mucosal architecture, 2) Superficial epithelial features, 3) Epithelial cellular components and 4) LP cellularity [212]. As Hh + aIL10R is a murine model recapitulating human disease (see chapter 1.3), similar patterns have been observed and are scored accordingly (Table 2.8). Since the tissue microenvironment varies along the length of the colon, we wanted to investigate whether the inflammation differs on a tissue level in the different segments. By resolving the colon in proximal, mid and distal sections, we were able to identify a significantly higher inflammation in the distal colon at d7 Hh + aIL10R, which evened out at d21 Hh + aIL10R (Figure 3.10b, c).

The higher inflammation in the distal colon strongly correlates with the neutrophil infiltration specifically in the distal colon at d7 Hh + aIL10R (Figure 3.5a, 3.6b). Part of the histoscore is taking LP infiltrate into accound (Table 2.8), which encompasses also neutrophils, making it a co-dependent relationship. However, at d7 Hh + aIL10R, the inflammation score is mainly driven by epithelial damage/elongation and the area which is affected. In other models of intestinal inflammation and CRC, distal infiltration of neutrophils has also been observed [213][Powrie lab, unpublished data]. All in all, this further highlights the importance of considering regional differences especially in the context of inflammation onset despite the codependency on neutrophil infiltration.

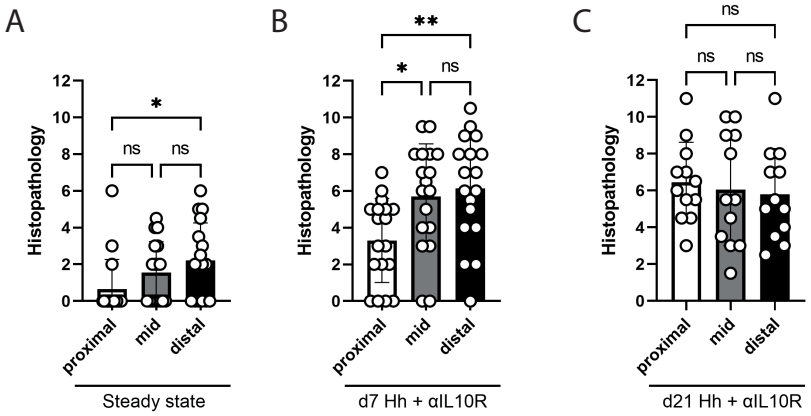


Figure 3.10: **Intestinal inflammation in Hh + aIL10R model starts in the distal colon**. Histopathology scoring from tissue sections from the proximal colon (white), mid colon (grey) and distal colon (black), embedded in paraffin and stained with H & E. A) Steady state, B) d7 Hh + aIL10R, C) d21 Hh + aIL10R. Data are pooled from two independent experiments for each timepoint separately. Ordinary one-way analysis of variance (ANOVA) with Tukey correction. Data presented are means ±SD. ns, not significant. $^{*}P \leq 0.05$ and $^{**}P \leq 0.01$

3.3.8 Changes in the macrophage subset pool occur distinctly in the proximal and distal colon over the timecourse of inflammation

The proximal colon harbors a less dense microbiota [214], and the macrophage turnover was shown to be affected by the density of the microbiota, which led us to speculating that the prevalence of macrophage subsets might be differing along the colon and during inflammation. Total macrophage numbers do not differ between proximal and distal colon at any point during the timecourse, however we can observe a slight decline at d4 followed by a massive increase in macrophage numbers at d7 and d21 of Hh + aIL10R colitis (Figure 3.11a). We decided to resolve the macrophage population roughly in two subsets marked by CD206 and CD11c. This division was based on the description in *Corbin et al*, where the authors found two major macrophage populations at both steady state and at d21 Hh + aIL10R based on scRNA-seq of CX3CR1+ cells. The CD11c+ macrophage population dominates the macrophage pool in both proximal and distal colon at d21 Hh + aIL10R (Figure 3.11a, e), whilst CD206+ macrophages are over-represented in the steady state colon. We can also see a significantly higher proportion of CD206+ macrophages in the distal colon at steady state by flow cytometry, however in the proximal colon there are no differences between the macrophage subsets (Figure 3.11b). Furthermore, upon resolving macrophage subsets at d4 and d7 in the proximal and distal colon (Figure 3.11c, d, respectively), we can detect a change in the macrophage pool in the proximal colon at d7 of Hh + aIL10R, with the expansion of CD11c+ macrophages (Figure 3.11d). This may reflect the early proximal pro-inflammatory tissue microenvironment, which was addressed in chapter 3.3.6. Expansion of CD11c+ macrophages in intestinal inflammation, which has previously been reported in both humans and mice [129, 215], was therefore confirmed, however we further expand this by showing that this change follows a particular spatiotemporal pattern. Also, since the prevalence of CD206+ macrophages is significantly higher in the distal colon at steady state and in early onset (d4 Hh + aIL10R), and this subset was associated with a chemokine-expressing signature [129], a similar mechanism

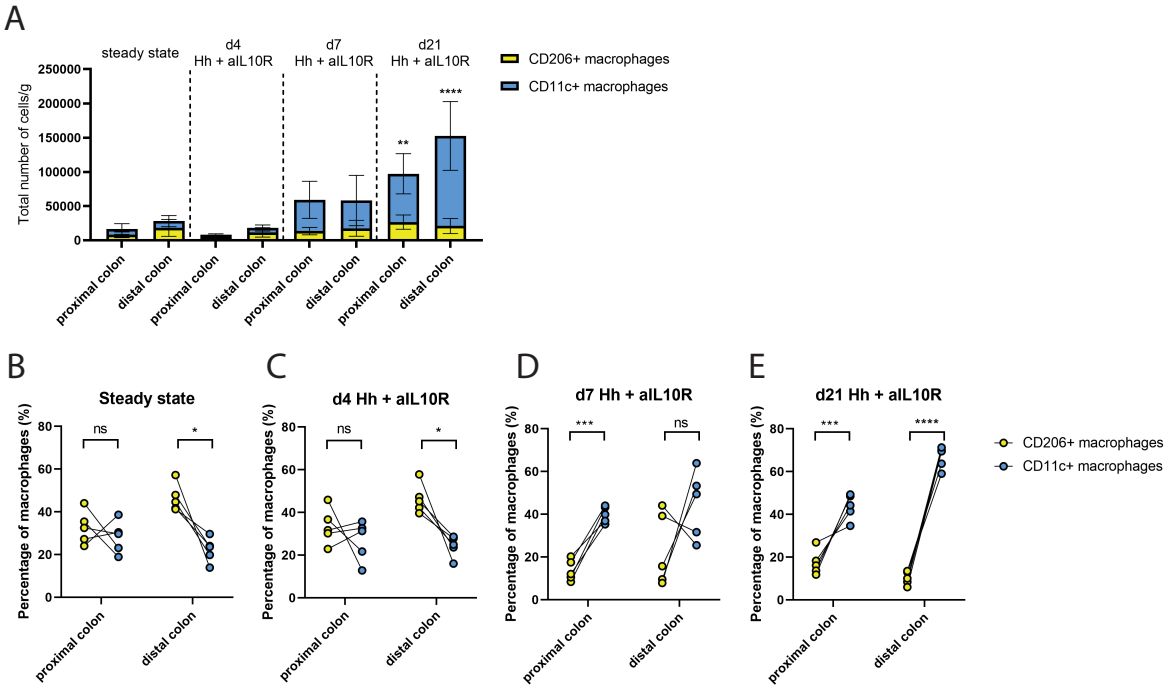


Figure 3.11: **The macrophage pool starts to differ at d7 Hh + aIL10R.** A) CD206+ macrophages (yellow) and CD11c+ macrophages (blue) as total numbers per gram colon at proximal and distal colon over the course of inflammation. Two-way analysis of variance (ANOVA) with Sidak correction. B) CD206+ macrophages (yellow) and CD11c+ macrophages (cyan) as percentages within the whole macrophage pool at steady state. C) d4 Hh + aIL10R. D) d7 Hh + aIL10R. E) d21 Hh + aIL10R. Paired t-test. Data presented are means ±SD. ns, not significant. $^{*}P \leq 0.05$, $^{**}P \leq 0.01$, $^{***}P \leq 0.001$ and $^{****}P \leq 0.0001$. Figure published as a contribution in *Corbin et al* [129].

---

might underlie neutrophil recruitment specifically in the distal colon at the onset of colitis. All in all, these observations indicate potential differences in inflammation as well as monocyte differentiation in distinct colonic niches.

3.3.9 Macrophage subsets occupy distinct niches in the colon at steady state

As the macrophage subsets were defined by *Cd206* and *Cd11c* expression on a transcriptional level, we wanted to confirm that this reflects different macrophage populations in the colon. For this, we used multi-parameter immunofluorescence analysis to map the spatial distribution of macrophage subsets along the full length of the mouse colon at both SS and peak of Hh + aIL10R-induced inflammation (d21 Hh + aIL10R), focusing on the most extreme timepoints. The macrophage subsets were determined by co-staining F4/80 with CD206 and CD11c respectively, to reflect subsets identified in previous studies [57, 129, 189]. Here, we focused on the crypt-villus axis instead of proximal-distal distribution to highlight differential distribution of the macrophage subsets within their tissular niche.

We firstly aimed to provide a quantitative assessment of their localisation along the entire length of the colon. Using IMARIS software and an automated python script, CD11c+ and CD206+ macrophages were defined within F4/80+ cells as cells that reached the intensity mean threshold for CD206 and CD11c respectively. At steady state, CD206+ F4/80+ cells (CD206+ macrophages) dominate the colonic macrophage pool and are located within the lamina propria (LP), with some residing at the base of intestinal crypts (Figure 3.12a, e). CD11c+ F4/80+ cells (CD11c+ macrophages) are sparse and mainly found at the tips of the crypts (Figure 3.12a, e).

In order to quantify the distance of the macrophage subsets in relation to the epithelium and the serosal membrane respectively, we analysed parts of the swiss roll by defining regions of interest. These were chosen in an unbiased manner along the length of the colon. The membranes were defined by manual drawing along the surfaces. By using the tool 'distance transformation' in IMARIS, the minimal distance of a macrophage to the epithelium and the serosal membrane was calculated (Figure 3.12d). At steady state, CD11c+ macrophages are significantly closer to the luminal surface than CD206+ macrophages (Figure 3.12e). The location of CD11c+ macrophages at the tips of the villi was confirmed in a recent paper, where they used a CD11c-lineage tracing model [216].

3. Unravelling spatial differences of the tissue microenvironment and immune cell infiltration over the course of murine intestinal inflammation

This study further proposed a distinct function for the CD11c+ macrophages especially in the distal colon, where they are essential for absorption of fungal toxins [216]. During Hh + aIL10R- induced inflammation both CD206+ and CD11c+ macrophages start to intersperse throughout the LP, i.e. CD11c+ macrophages can be detected at the base of the crypts (Figure 3.12b). The close proximity of CD11c+ macrophages to the epithelium, observed at steady state, is lost, with both subsets moving further away from the epithelium (Figure 3.12e). This effect is a result of the epithelial hyperplasia, a common feature of intestinal inflammation, also observed in our model (Figure 3.3b). The differences in the relative proportion of CD206+ and CD11c+ in the distal colon (Figure 3.11) were less evident by microscopy, however, we have not undertaken a specific quantification of images resolved in proximal and distal regions to address that question.

Together, the analysis of CD11c+ and CD206+ macrophage distribution in relation to epithelium, LP, crypts, submucosa, and the muscularis confirmed their distinct geographical location throughout the colon at steady state.

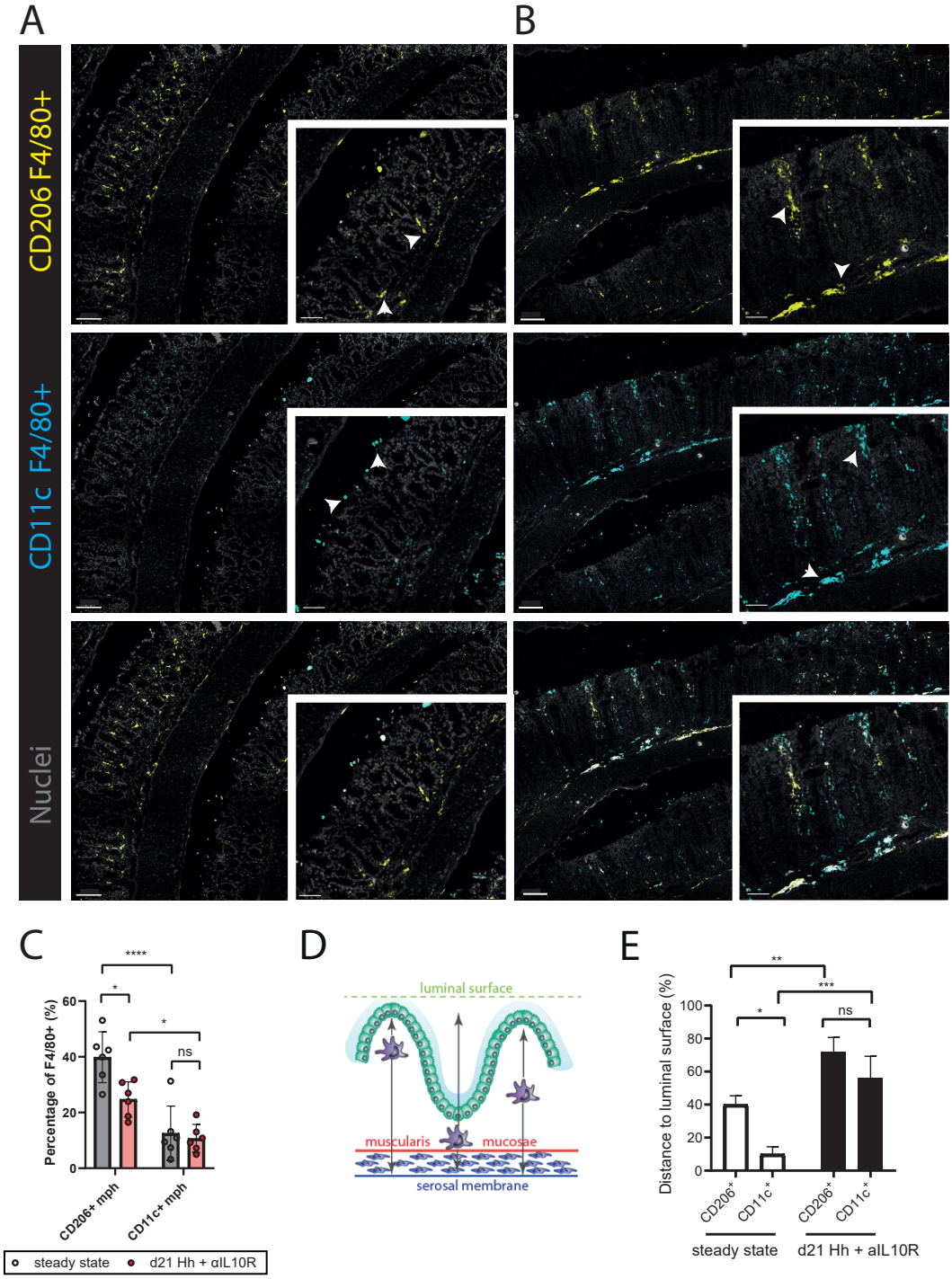


Figure 3.12: **CD206+ macrophages and CD11c+ macrophages are distinctly localised at steady state.** A) Representative images of immunofluorescent labelling in steady state swiss rolls (n = 6). Separate channels based on overlap of staining were created. Colocalised CD206+ F4/80+ labelled cells (yellow) in top right, followed by colocalised CD11c+ F4/80+ (cyan). *Caption continued on the following page.*

Figure 3.12: An overlay of CD206+ macrophages and CD11c+ macrophage in the third picture from the top. Cell nuclei were labelled with Sytoxblue (grey). Scalebars represent 100 μM in the overview images and 50μM in the enlargement. B) Representative images of immunofluorescent labelling in d21 Hh + aIL10R swiss rolls (N=6). Same pattern followed as in A). Cell nuclei were labelled with Sytoxblue (grey). Scalebars represent 100 μM in the overview im-ages and 50µM in the enlargement.C) Quantification of CD206+ F4/80+ and CD11c+ F4/80+ cells as a percentage of total number of F4/80+ cells steady state (grey) and d21 Hh + aIL10R (red). N=6 from two independent experiments, six colons per mouse, 3 staining cycles per mouse. Two-way Anova with Tukey's multiple comparisons test. Data presented as mean ± SEM, ns not significant, $^{*}P \leq 0.05$, $^{****}P \leq 0.0001$. D) Schematic depiction of quantification analysis in IMARIS. Macrophages (F4/80+, magenta) are analysed for their localisation with their minimal distance (black arrow) to the epithelium (green) and serosal membrane (blue). Exact description of the workflow can be found in the methods section under 'Image analysis and quantification'. E) Quantification of minimal distance of CD206+ F4/80+ and CD11c+ F4/80+ cells in steady state (grey) and d21 Hh + aIL10R (red) to epithelium (left) and serosal membrane (right). Minimal distance is presented as a percentage of the respective membrane to the total distance between the membranes. Two-way Anova with Tukey's multiple comparisons test. Data presented as mean ± SEM, ns not significant, $^{*}P \leq 0.05$, $^{**}P \leq 0.01$, $^{***}P \leq 0.001$

3.3.10 Macrophage subset markers and their localisation blur during inflammation

As we observed an emergence of triple positive F4/80+CD206+CD11c+ macrophages at peak of inflammation, we wanted to investigate whether this was an imaging artefact or could indeed represent an intermediate population arising during inflammation (Figure 3.12b). Counting CD206+ macrophages *in situ* reveals a decrease in proportion of the total macrophage pool (Figure 3.12c), consistent with the flow cytometry-assisted analysis of CD11c+ and CD206+ macrophage populations in the colonic LP [129]. However, the image analysis did not detect the previously observed increase in the percentage of CD11c+ macrophages during Hh + aIL10R-induced inflammation [129]. In flow cytometry analyis a neglectible amount of triple positive cells can be seen at steady state (Figure 3.13a), however they increase in inflammation (Figure 3.13b), similarly to *in situ* observations by microscopy.

Thus, intestinal inflammation changes the localization of CD206+ and CD11c+ macrophages at the base of intestinal crypts and the tips, respectively, making them ubiquitously distributed instead. As imaging only reveals a snapshot of macrophages present in time and space, it is impossible to determine if the increase in CD11c+ macrophages is mostly due to infiltration and differentiation of monocytes or due to higher replication rate of the "activated" macrophage present at steady state. Since monocytes adapt their phenotype according to the tissue microenvironment and differentiate into vastly different macrophages in an inflammatory environment [13], the former option seems more likely than the latter.

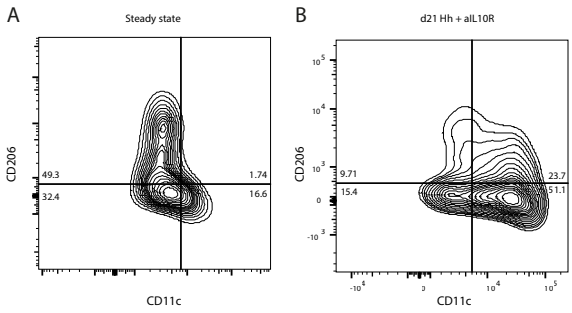


Figure 3.13: **Flow cytometry gating for CD206+ and CD11c+ macrophages reveals higher percentage of double-positive cells at d21 Hh + aIL10R.** A) Representative gating for macrophage subsets at steady state in the colon, B) Representative gating for macrophage subsets at d21 Hh + aIL10R colitis in the colon.

3.4 Discussion

3.4.1 The tissue microenvironment leads to distinct spatiotemporal immune cell infiltration in the colon

Reporter mice have been used widely for intravital imaging and other applications, rendering antibody staining redundant and allowing for tracking of cells *in vivo*. Here, we employed a newly generated double-reporter strain CX3CR1-GFP Ly6G-tdTomato, which labels monocytes/macrophages as well as neutrophils in separate colours, allowing a unique discrimination of these cell types. However, during the characterization of these mice (chapter 3.3.3), we encountered some difficulties with the Ly6G-tdTomato. Epithelial cells, especially at steady state, also express Ly6G, vastly outnumbering and outcompeting by brightness the low numbers of neutrophils present (Figure 3.4). We therefore had to resort to labelling neutrophils with CD177, on top of the already present tdTomato. This resulted in tdTomato blocking quite a few fluorescent channels, due to its wide absorption spectrum, which could have been used for other markers instead. However, the usefulness of the double-reporter mice is undebated when it comes to intravital and lightsheet imaging, circumventing the need for antibody optimization. *In situ* analysis would profit from using CX3CR1-GFP mice only, allowing for more fine cell type identification due to the availability of fluorescent channels not blocked by tdTomato.

As it is difficult to discern the tissue microenvironment in detail in humans and the onset of inflammation is hard to capture before the outbreak of symptoms, use of mouse models provides a powerful tool in studying the immune response along time and space. The distinction of proximal and distal colon as two separate sites is further emphasized in a study uncovering a distal colon-specific production of pro-inflammatory cytokines following a course of DSS colitis in mice [217]. Here, we investigated the immune cell infiltration along the entire length of the colon as well as characterized the spatial architecture and the tissue microenvironment. Myeloid cells were the focus of this investigation, as they are comprised of tissue-resident macrophages as well as the first responders neutrophils and infiltrating monocytes. Macrophages get depleted in inflammation, leading to an increased recruitment

of monocytes [218, 219]. We see a massively increased infiltration of monocytes into the proximal colon at d4 Hh + IL10R, coinciding with higher transcript levels of *Ccl2*, together with a reduction in macrophage numbers (Figure 3.2a, 3.9a, 3.11a). A second wave of monocytes is recruited into the distal colon at d7 Hh + aIL10R (Figure 3.5a & 3.2a). This corresponds to the changes in the macrophage pool first in the proximal and then in the distal colon (Figure 3.11d & e), indicating an inflammatory priming of infiltrating monocytes and the subsequent adaption to the inflammatory microenvironment. Furthermore, the differences in macrophage subsets already at steady state (Figure 3.3.8b) could lead to the distinct recruitment of immune cells into proximal and distal compartments of the colon. Blood monocytes in DSS colitis mice were found to secrete higher levels of IL-1β and TNF prior to tissue entry, implying a pro-inflammatory priming outside of the tissue niche [220]. Neutrophils are distinctly recruited to the distal colon at d7 Hh + aIL10R (Figure 3.5a & 3.2b). Infiltration of neutrophils into the distal colon was also reported in other models of murine colitis (DSS & CRC model), as well as being a feature of UC [221]. It further correlated with fibroblast activation and epithelial cell loss. Neutrophil recruitment was associated with anti-TNF therapy non-responder signatures and found to be driven through fibroblast IL-1R signalling, localising in close proximity to each other in ulcers [122]. The neutrophil receptor CD177 was recently found to associate with podoplanin, a cancer-associated fibroblast marker, further adding to a potential neutrophil-fibroblast axis in colitis onset or progression [222]. Here, we were also able to detect a correlation between influx of neutrophils in the distal colon at d7 Hh + aIL0R and higher levels of histopathology in the distal segments of the colon, however we have not assessed it in conjuction with the number and localisation of fibroblasts (Figure 3.10b). Despite the histopathology scoring being comprised in parts to infiltration of immune cells, the driving factor of the difference at d7 Hh + aIL10R is the disintegration of the epithelial barrier [data not shown].

Simultaneously, we found a high expression of *Cxcl9* first in the proximal colon at d4 Hh + aIL10R, followed by expression in the distal colon at d7 Hh + aIL10R (Figure 3.8e). Interestingly, non-myeloid cells (comprised mostly of B & T cells), can only be found elevated

in numbers in the distal colon from d7 Hh + aIL10R colitis onwards (Figure 3.8f). CXCL9 has antimicrobial functions on its own, as was shown in a *Citrobacter rodentium* colitis model [223]. Simultanously, *Tnf*, *Il22*, *Il1b* and *Il10* expression is induced in the proximal colon at d4 Hh + aIL10R (Figure 3.9). IL-22 is a potent cytokine, inducing the production of AMPs like RegIIIβ and RegIIIγ, preserving epithelial barrier and clearing off pathogens [224, 225]. However, it has also been found to have a dual role, leading to persistent chronic infections[226]. The spike of AMPs in the proximal colon at d4 Hh + aIL10R further indicates the presence and reaction to Hh in a spatiotemporally distinct manner. Furthermore, RegIIIβ and RegIIIγ are exclusively found in the proximal colon at steady state [data not shown], indicating a distinct regulation of the microbiome along the length of the colon. Delineating the exact differences in the AMP profile between the proximal and distal colon as well as consequential changes in the microbiome would help understanding the spatial rearrangement of the microbiome as a potential driver of intestinal inflammation.

3.4.2 Inflammation-dependent changes of the tissue microenvironment leads to differential localisation of macrophage subsets

Although flow cytometry analysis of the LP is a powerful tool regarding quantification of various immune cell populations, it neglects information about their spatial distribution. Here we implemented several different techniques to quantify and visualize myeloid cells along the length of the colon during a timecourse of murine colitis to understand how immune cells get recruited and interact with one another to orchestrate intestinal inflammation. We found a location- and time-specific pattern in immune cell recruitment, driven by changes in the tissue microenvironment.

Different subsets of macrophages have been discovered using a wide range of techniques in the last few years in both humans and mice [57, 129, 227, 228]. Among those are CD11c+ CD206^{int} CD121b+ and CD206^{hi} CD11c- CD121b- macrophages, two subsets highly dependent on the microbiota to develop [57]. In Abx-treated mice, the CD206+ macrophage subset decreases overall in the colon with a simultaneous increase of the CD11c+

macrophage subset [229]. The SI on the other hand does not experience such changes in the macrophage populations, highlighting the differences along the GI tract in priming the local immune cells [10]. The CD11c+ macrophage subset is greatly expanded in a murine model of colitis (Hh + aIL10R) [129] as well as in the mucosa of celiac disease patients [230] and IBD patients [215]. Furthermore, as monocytes differentiate along two major trajectories, both of which are driven by the microbiota, identifying factors determining macrophage subset localisation are crucial for resolving possible functions as well as how to manipulate the macrophage subsets in disease. Here, we identified distinct niches of CD206+ and CD11c+ macrophages at steady state (Figure 3.12a). Moreover, by developing an approach to quantify the localisation of a macrophage within the borders of lumen and serosal membrane (Figure 3.12d), we can confirm the observed distinct localisation by unbiased quantification (Figure 3.12e). CD11c+ macrophage localisation at the tip of the villi has also been confirmed in a recent study, attributing this subset with maintenance of epithelial integrity by absorption of fungal toxins in the distal colon specifically [216]. Furthermore, *Kang et al* showed that CD206+ macrophages dominate the lower crypts of the colon, and CD11c+ macrophages are largely found in the upper regions of the crypts at steady state [57], which confirms our findings (Figure 3.12) [129].

Despite many studies showing distinct macrophage subsets localisation and prevalence at steady state, their changes during inflammation remain less well understood. Here, we demonstrate that the distinct cross-sectional localisation of the macrophage subsets at steady state is lost during inflammation, as CD11c+ and CD206+ macrophages can be observed all along the crypt (Figure 3.12b, e). Their distinct transcriptional profiles imply different functions during inflammation as can be seen in a recent study comparing CD206+ and CD11c+ transcriptomes at both steady state and d21 Hh + aIL10R colitis [129]. CD11c+ macrophages express a pro-inflammatory transcriptome, coinciding with *Kang et al*, showing a higher degree of immune cell effector functions in CD11c+ macrophages. On the other hand, CD206+ macrophages are more associated with an anti-inflammatory signature, tissue regeneration and cell recruitment [57, 129]. In a perspective, the concept

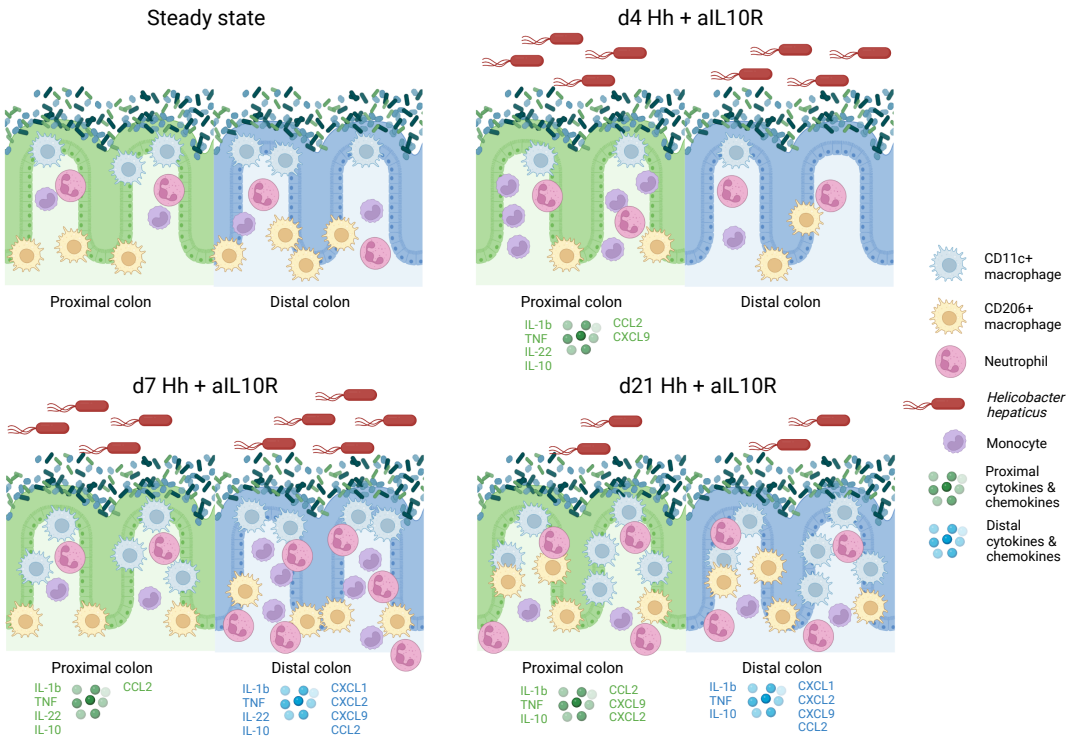


Figure 3.14: **Overview of spatiotemporal changes between the proximal and distal colon along the course of intestinal inflammation.** *This figure was generated using Biorender.*

---

of inflammatory resident macrophages was introduced [231]. These refer to tissue-resident macrophages or infiltrating monocytes during inflammation, which acquire a "memory" of the inflammation and might therefore preserve a low-key tissue inflammation. Furthermore, monocytes recruited during inflammation get dually imprinted by both the inflammation and the tissue niche, making the inflammatory memory uncoupled from the ontogeny of the respective macrophages itself [231]. Whether the emergence of the triple-positive (CD206+ CD11c+ F4/80+) macrophage subset might resemble some kind of dual-imprinted monocyte remains to be determined.

3.5 Conclusion

Here, we characterized the spatiotemporal landscape of myeloid cell infiltration and changes in the tissue microenvironment over the course of Hh + aIL10R colitis. We provide a comprehensive map of spatial cell interaction, quantification of cell infiltration as well as patterns of Hh colonization and changes in the tissue microenvironment by investigating selected cytokines and chemokines. As a mouse model offers the opportunity of unravelling early changes in the inflammatory landscape, we made use of selected timepoints to uncover mechanisms of disease onset and progression. We also identified d4 Hh + aIL10R as an early timepoint of changes in the tissue microenvironment (mainly in the proximal colon), leading up to distinct recruitment of monocytes. *Helicobacter hepaticus* does not show any preferential localisation along the colon, however that does not exclude changes in the microbial community specifically in the proximal or distal colon triggering the differential host immune response in different colon segments. Changes in the spatial distribution of the microbiota could further act as a factor priming the local immune cells in the distinct microenvironments. As the distal colon is the origin of UC and CRC, deciphering the differences in the tissue microenvironment leading to the maintenance of chronic inflammation and tumour progression is crucial to delineate future therapeutic avenues.

The data presented here highlight the importance of the proximal and distal colon as two separate tissue microenvironments already before the onset of inflammation, leading to distinct infiltration of immune cells along the length of the colon over the course of intestinal inflammation. Further research is needed to uncover the initial signals important for activation and chemokine induction in resident cells, leading to the distinct recruitment along the colon.

3.6 Future directions & limitations

Unbiased investigation of spatial differences along the colon over the course of Hh + aIl10R mediated inflammation with bulk-RNAseq will be crucial for determining mechanisms of action involved in immune cell recruitment and priming of the resident cell populations. Furthermore, deriving organoids from the proximal and the distal colon for *ex vivo* stimulation will help dissect epithelial derived mediators from immune cell signals [232].

Next steps should concentrate on connecting the differences in the proximal and distal colon to the cells that shape the distinct tissue microenvironments during the course of intestinal inflammation. Moreover, the focus should be extended to include other immune cell types like ILCs, T and B cells as well as epithelial, endothelial and stromal cells. This could be achieved by unbiased spatial transcriptomics of swiss rolls at different timepoints of Hh + aIL10R colitis.

Furthermore, deciphering the importance of different cell types in recruiting/priming other immune cells can be determined by spatial analysis as well as by modulating certain functions of immune cells by genetic modification or specific drug targeting. As it is known that the distal colon is the prime site for onset of CRC, elucidating the differences in sustenance of inflammation and resolution in the distinct tissue microenvironments is crucial in determining future therapeutic avenues.

As the microbiota is of significant importance in priming the intestinal immune system and ensuring a beneficial host-microbe relationship, investigating the spatial distribution of the microbiota and its rearrangement during intestinal inflammation might offer new insights in the aetiology of chronic intestinal inflammation and identify beneficial community members.

One of the limitations of the study is the use of a mouse model that does not fully reflect the biology of a human GI tract. However, there are clear indications of spatial differences in immune cell compositions and microbiome distributions in humans as well [52, 221, 233], implying a similar pathogenesis. Furthermore, by choosing to focus on myeloid cells, we are not capturing all changes in the tissue microenvironment important

for setting up intestinal inflammation. However, due to the crucial roles myeloid cells play as sentinels and orchestrators of intestinal inflammation, we chose to concentrate our efforts on deciphering myeloid cell function and localisation.

All in all, our data clearly highlight the importance of studying immune cells in their spatial context as well as resolving the colon into its distinct tissue microenvironments in order to understand disease mechanism.

4

The role of IRF5 in myeloid cells at the onset of colitis

Contents

4.1 Interferon regulatory factor 5 in colitis 90
4.2 Aims 92
4.3 Results 94
4.3.1 *Irf5-/-* mice display a distinctly different cellular landscape in the inflamed colon as early as d7 Hh + aIL10R 94
4.3.2 Expression of IRF5 in CX3CR1+ cells is required for the onset of intestinal inflammation and recruitment of neutrophils and monocytes 102
4.3.3 Characterization of a novel neutrophil-specific Ly6G-Cre strain . 106
4.3.4 Expression of IRF5 in neutrophils is required for the onset of intestinal inflammation 116
4.3.5 Deletion of IRF5 specifically in neutrophils is sufficient to prevent the onset of intestinal inflammation altogether 121
4.3.6 The tissue microenvironment is significantly different in Ly6G^{Irf5} mice at d7 Hh + aIL10R 125
4.3.7 CCL2 secreted from IRF5-proficient neutrophils leads to the infiltration of monocytes into the inflamed colon 127
4.3.8 The set-up of an *in vitro* system to study the effects of neutrophils and monocytes in isolation 131
4.3.9 Immature neutrophils accumulate in the colons of inflamed mice 132
4.4 Discussion 136
4.4.1 Depletion of IRF5 leads to a distinct myeloid landscape at the onset of colitis 136
4.4.2 IRF5 in neutrophils plays an indispensable role in amplifying intestinal inflammation 137
4.5 Conclusion 144
4.6 Future directions & limitations 145

4.1 Interferon regulatory factor 5 in colitis

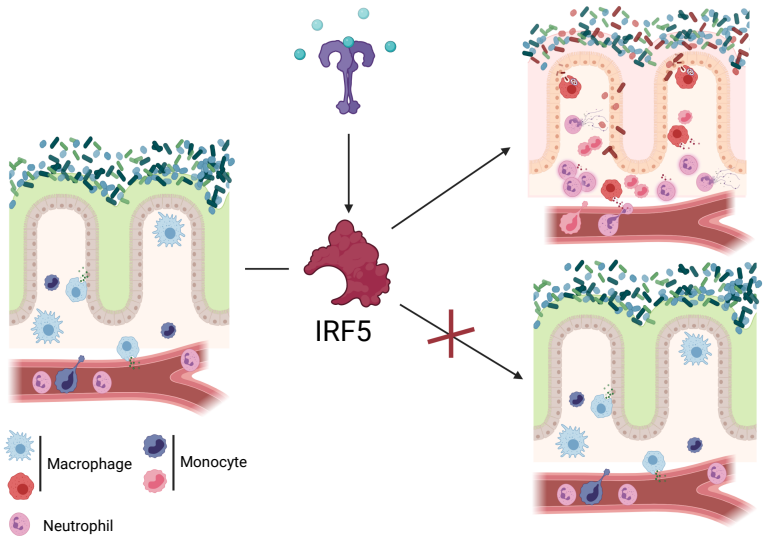


Figure 4.1: **IRF5 at the crossroad for setting up chronic intestinal inflammation.**

IRF5 is a master TF regulating the expression of several pro-inflammatory cytokines and chemokines [152, 153]. It is mainly expressed in myeloid cells and B cells, making it a immune-cell specific TF important in inflammation. Following engagement of selected receptors like TLR4 and GM-CSFR, IRF5 gets phosphorylated in cascade involving several kinases. Upon phosphorylation, IRF5 homodimerizes and translocates into the nucleus, where it regulated the expression of downstream genes [150]. Exact signalling pathways and its role in different immune cells can be found in chapter 1.4. Mutations resulting in overactivation of IRF5 are part of genome-wide association study (GWAS) risk loci identified for genetic predisposition for IBD [234]. Also in other chronic inflammatory diseases like arthritis and lupus, loss of IRF5 is beneficial for disease prevention. However, a recent paper also identified a beneficiary role of IRF5 in bacterial clearance of pathogens like S. Tm [169]. Recently, we and others have established its major role in colitis, as *Irf5-/-* mice were completely protected from colitis development in the various murine models employed [129, 169]. In order to uncover

the mechanism by which IRF5 mediates disease progression, MBMCs were created to study the WT and *Irf5-/-* immune cells in the same microenvironment. Sc-RNAseq revealed a higher proportion of CD11c+ macrophages derived from the WT counterpart, uncovering the role of IRF5 in shaping monocyte-to-macrophage differentiation into pro-inflammatory CD11c+ macrophages at peak of inflammation (d21 Hh + aIL10R) [129]. *Corbin et al* demonstrated further showed altered gene expression in WT and *Irf5-/-* MNPs at d21 Hh + aIL10R, by isolating them from a MBMC and assessing their gene expression by scRNA-seq [129]. The reduced pro-inflammatory gene expression of *Irf5-/-* monocytes and macrophages was also demonstrated at d7 Hh + aIL10R in a model where IRF5 was inhibited by defactinib, and sorted monocytes-macrophages were assessed for an array of pro-inflammatory cytokines and chemokines by RT-qPCR [126]. Deletion of IRF5 in myeloid cells specifically, using a LysM-Cre mouse, revealed its major role in myeloid cells for colitis development [169]. Furthermore, deletion of IRF5 specifically in CX3CR1-Cre (targeting monocytes, intermediates and macrophages) also led to a reduction in inflammation, albeit not as pronounced as the full knockout [129]. Uncovering the complex interplay of myeloid cells at the onset of colitis in the context of IRF5 deficiency may therefore be an useful undertaking in dissecting the mechanism by which chronic inflammation develops.

Khoyratty et al identified distinct TF-mediated networks, controlling neutrophil-driven inflammation at various stages like maturation, recruitment and activation [165]. A dual approach with *in vitro* generated Hoxb8 progenitors [235] modulated via CRISPR-Cas9 to produce TF-KOs as well as validation with a neutrophil-driven *in vivo* airpouch inflammation was used. IRF5 was identified as a crucial TF mediating cytokine production as well as having an impact on phagocytosis [165]. Furthermore, the expression of *Irf5* in neutrophils has been identified as a disease-associated trait/genome locus in an expression quantitative trait loci (eQTL) study [236]. Their migration capacities are not affected by *Irf5* deficiency, as studies both in AIA and an airpouch model of inflammation show [165, 166]. However, *Irf5-/-* mice accumulate fewer neutrophils at the site of inflammation, as chemokines important for neutrophil recruitment are reduced in their expression [166]. Comparison of

gene expression profiles of unstimulated mouse neutrophils isolated from the blood and BM with neutrophils from three disease states (serum-transfer arthritis, thioglycolate-induced peritoneitis and uric acid-induced peritoneitis) additionally highlighted the role of IRF5 in neutrophils, being implicated in both up - & downregulation of genes in all disease-associated conditions [237]. The presence of neutrophils in human colonic biopsies is used as a sign of active disease and increasingly used as a secondary endpoint in clinical trials in UC [238, 239]. Neutrophils display altered phenotype and effector functions in both peripheral blood and mucosal tissue of IBD patients [92]. High infiltration of neutrophils and their interaction with fibroblasts at sites of deep ulceration as a feature of non-response to several anti-inflammatory therapies in IBD was highlighted by a recent study [122]. In the context of mouse models of intestinal inflammation, neutrophils have been painted as both immunopathology supporting cells [240] and cells that have a beneficial role during colitis, promoting mucosal repair processes [241, 242].

4.2 Aims

We aim to investigate the role of myeloid cells at the onset of Hh + aIL10R colitis by using IRF5 as a tool for immune cell activation. Utilising a range of tailored cell-type specific mouse models, we intend to dissect the individual roles of the cell types involved in orchestrating the inflammatory cascade in the intestine. We hypothesize that IRF5 modulates neutrophils, monocytes and macrophages at different stages during the onset of inflammation, which may provide further insights into the mechanism of disease and targets for therapy. Using a bulk-RNA sequencing dataset from a mixed bone marrow chimera, we aim to investigate differential gene expression by *Irf5-/-* neutrophils to uncover potential mechanisms (Figure 4.2).

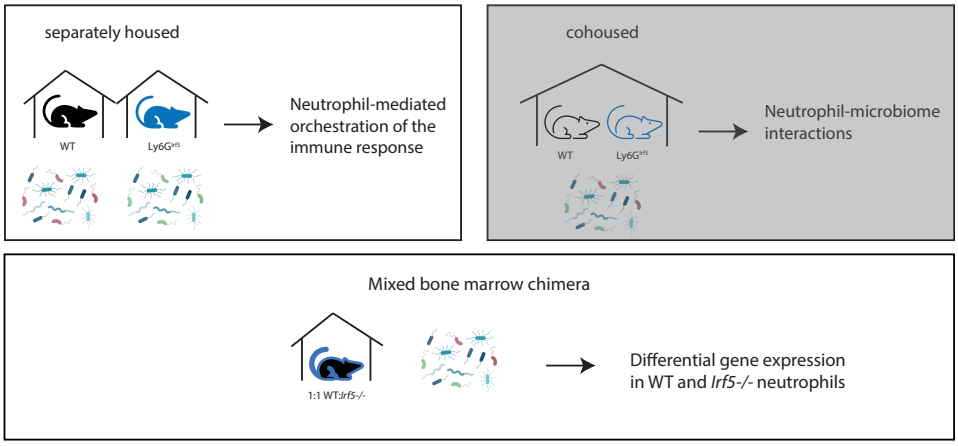


Figure 4.2: **Experimental set-up chapter 4.**

4.3 Results

4.3.1 *Irf5-/-* mice display a distinctly different cellular landscape in the inflamed colon as early as d7 Hh + aIL10R

We aimed to investigate how IRF5 sets up the inflammatory microenvironment, by analyzing the onset of inflammation (d4/d7 Hh + aIL10R). Here, we compare wild type (WT) and full IRF5 knockout (*Irf5-/-*) in order to capture the full picture of how IRF5 sets up the inflammatory stage for progression into chronic inflammation. As myelopoiesis starts in the bone marrow (BM), we also set out to investigate the progenitor landscape according to the gating scheme depicted in figure 4.3. Mature monocytes and neutrophils can be discriminated in the BM based on Ly6C expression, as neutrophils are Ly6C^{int} and monocytes Ly6C^{hi} [243]. Simultaneously, we analysed the blood, colon and spleen with a myeloid focused panel [206] by flow cytometry to capture early changes in the myeloid cell pool across organs (Figure 4.4). Furthermore, RNA and histology were collected from proximal, mid and distal colon sections to analyse tissue composition and upregulation of pro-inflammatory gene expression in the tissue. Cells from the BM are generally depicted as percentage of live cells, as we could not normalize to weight or volume taken. In tissues like the colon and spleen, total cell numbers were normalised to the weight of the respective tissue, and in the blood to the volume of blood processed (300μL in all cases).

At d4 Hh + aIL10R, no differences between WT and *Irf5-/-* mice were detectable in the intestine as the inflammation has not yet taken a hold (Figure 4.5a, b). In the BM, we can see a significant increase in WT neutrophils and a trend towards higher percentages of mature monocytes at d4 Hh + aIL10R (Figure 4.5c, d). No differences in neutrophil and monocyte numbers were observed in the blood at d4 Hh + aIL10R (Figure 4.5e, f). This indicates an early signal present that promotes myelopoiesis in the BM, ready for subsequent release.

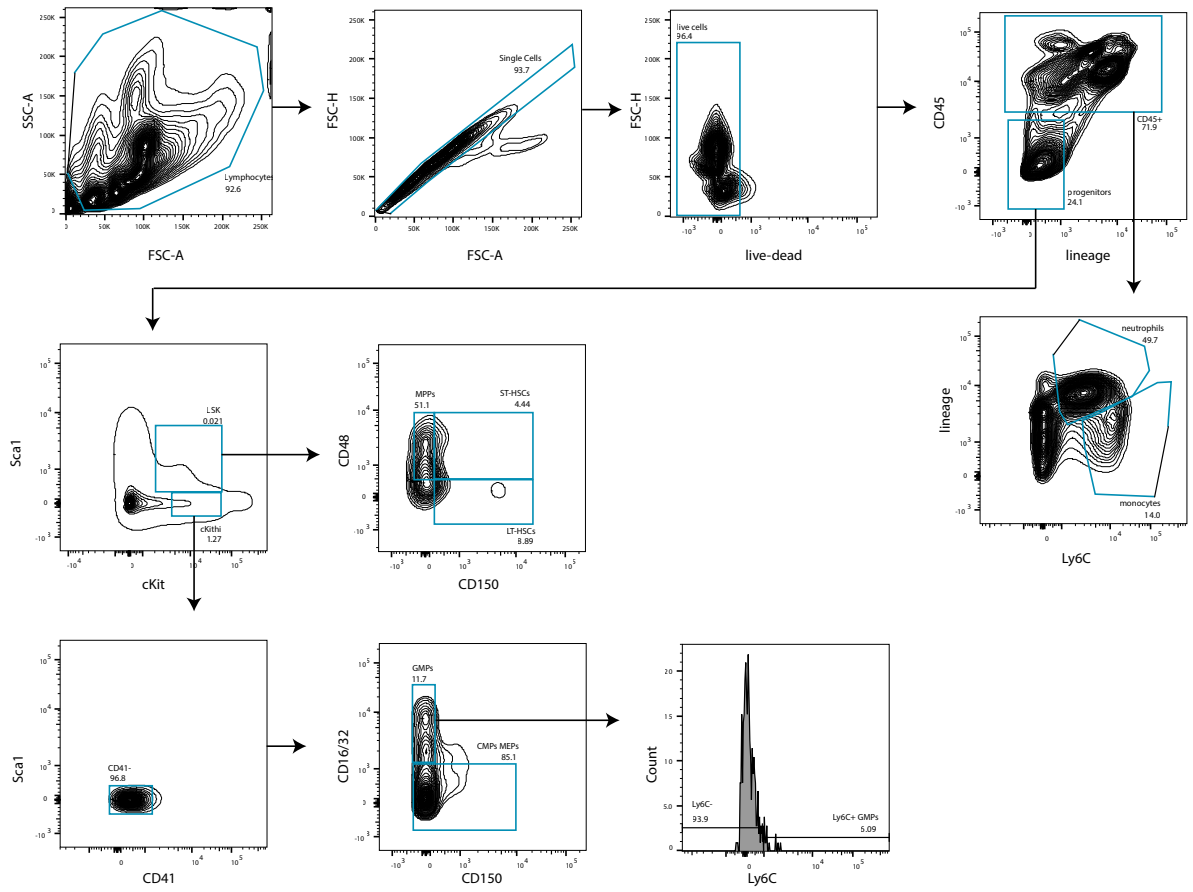


Figure 4.3: **Representative gating scheme for progenitors in the bone marrow.**

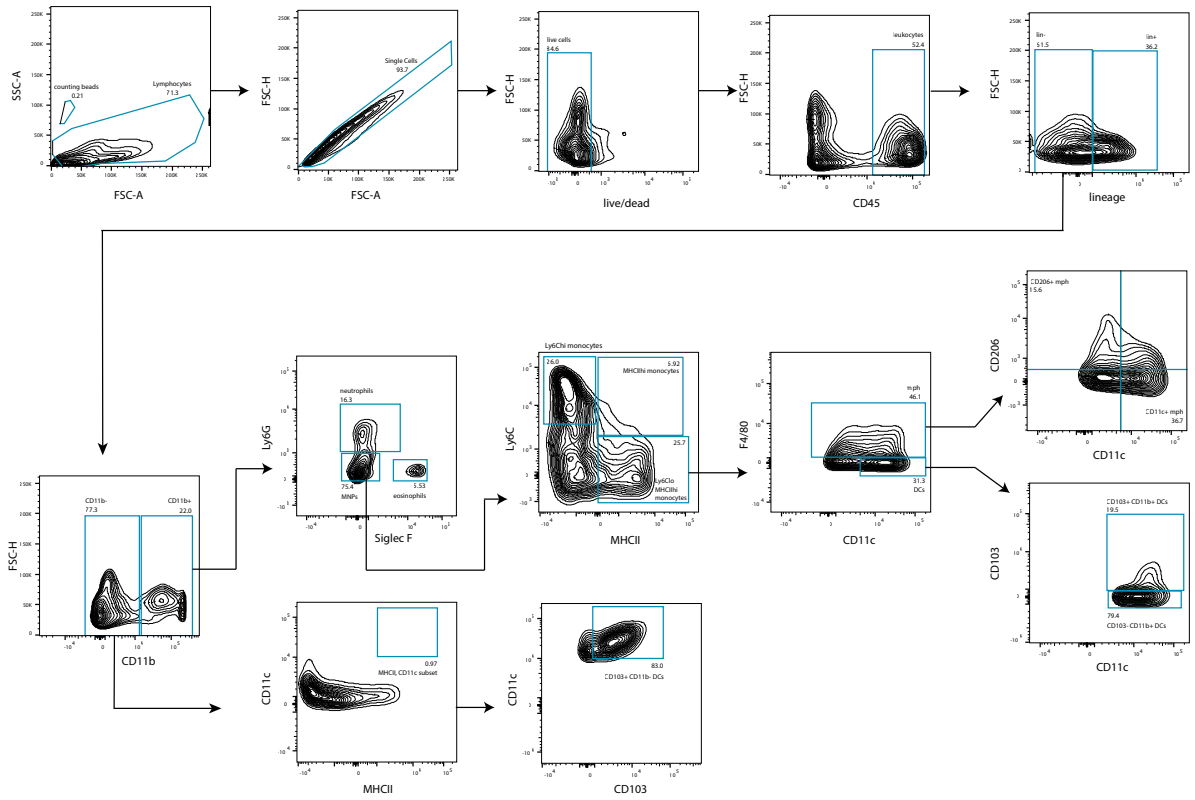


Figure 4.4: **Representative gating scheme for myeloid cells in the colon.**

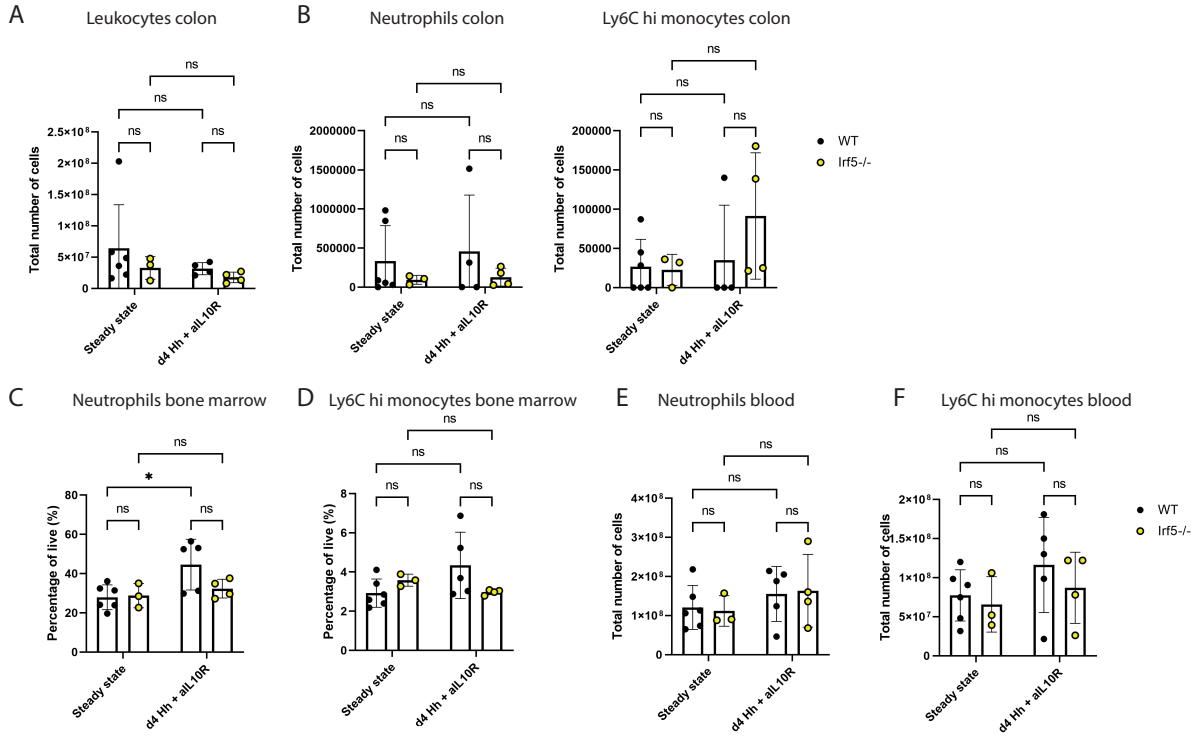


Figure 4.5: **No changes in myeloid cell pools in colon, bone marrow and blood at d4 Hh + aIL10R in *Irf5-/-*.** Flow cytometry analyis of cells isolated from tissues of uninfected (steady state, WT (n = 6, black circles), *Irf5-/-* (n = 3, yellow circles)) and d4 Hh + aIL10R mice (WT (n = 5), *Irf5-/-* (n = 4)) A) Total number of colonic leukocytes per gram tissue, B) Neutrophils and Ly6C^{hi} monocytes isolated from the colon, normalised to total number per gram tissue, C) Neutrophils in the bone marrow as percentage of live cells, D) Ly6C^{hi} monocytes in the bone marrow as percentage of live cells, E) Total number of neutrophils isolated from the blood, F) Total number of Ly6C^{hi} monocytes isolated from the blood. Data is representative from two independent experiments. Two-way analysis of variance (ANOVA) with Sidak correction. Data presented are means ±SD. ns, not significant and $^{*}P \leq 0.05$

4. The role of IRF5 in myeloid cells at the onset of colitis

A significant increase in histopathology score, as well as leukocyte infiltration numbers could be seen at d7 Hh + aIL10R, marking this as the timepoint where early changes in the myeloid cell pool could be observed in the colon (Figure 4.6a-c). *Irf5-/-* mice were already significantly less inflamed at d7 Hh + aIL10R, highlighting the early importance of IRF5 in shaping intestinal inflammation. Furthermore, significantly lower numbers of neutrophils and monocytes were present in the colon of *Irf5-/-* mice (Figure 4.6d, e). *Irf5-/-* monocytes have an impaired ability to migrate towards CCL2 than their WT counterparts [129]. This was also reflected at the onset of Hh + aIL10R-induced inflammation, as lower numbers of *Irf5-/-* monocytes were present in the blood (Figure 4.7a). In the BM, a higher proportion of mature WT monocytes was present (Figure 4.8a). Neutrophils lacking *Irf5-/-* however do not have any migration defects both *in vitro* towards CCL3 and *in vivo* in a model of airpouch inflammation [165]. Equal numbers of neutrophils in the blood of WT and *Irf5-/-* mice were present at d7 Hh + aIL10R (Figure 4.7b), however in the BM, a lower proportion of neutrophils in *Irf5-/-* mice was found (Figure 4.8b). Simultanously, Ly6C+ granulocyte/macrophage progenitors were increased in *Irf5-/-* mice at d7 Hh + aIL10R, indicating a development deficiency at the onset of inflammation starting in the BM (Figure 4.8c).

In order to dissect the importance of IRF5 at the onset of inflammation in neutrophils and monocyte/macrophages respectively, we turned to cell-specific cre-excision of IRF5; CX3CR1-Cre IRF5fl/fl (macrophages/monocytes) and Ly6G-Cre IRF5fl/fl (neutrophils). We further chose to investigate d7 Hh + aIL10R in more detail as this timepoint showed differences in the cellular compositions between WT and *Irf5-/-* mice.

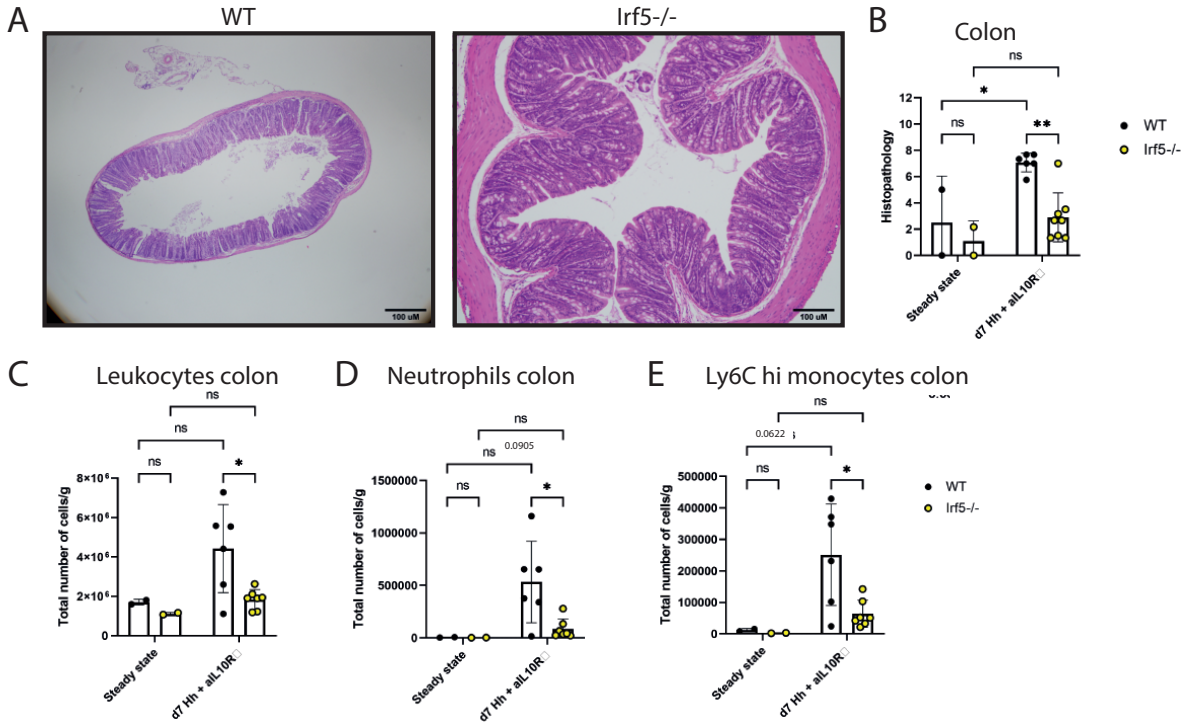


Figure 4.6: **Increased recruitment of leukocytes and myeloid cells in the colon at d7 Hh + aIL10R in *Irf5-/-*.** A) Representative hematoxylin and eosin (H &E) sections from WT (left) and *Irf5-/-* (right) mice at d7 Hh + aIL10R. Scalebars depict 100 μM, B) Histopathology scoring of steady state (WT (n = 2, black circles) and *Irf5-/-* (n = 2, yellow circles)) and d7 Hh + aIL10R (WT (n = 6) and *Irf5-/-* (n = 8)) colons, C) Total number of leukocytes, D) neutrophils, E) Ly6C^{hi} monocytes per gram tissue analysed by flow cytometry of the colonic lamina propria. Data are representative of two independent experiments. Two-way analysis of variance (ANOVA) with Sidak correction. Data presented are means ±SD. ns, not significant. $^{*}P \leq 0.05$ and $^{**}P \leq 0.01$

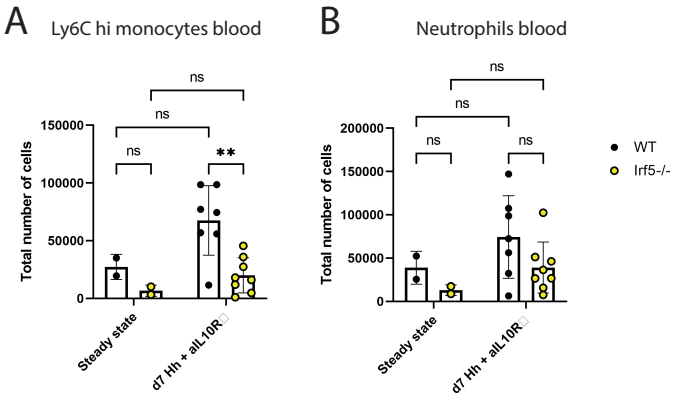


Figure 4.7: **Ly6C^{hi} monocytes are decreased in the blood of *Irf5-/-* mice at d7 Hh + aIL10R.** Flow cytometry analysis of blood and bone marrow from steady state (WT (n = 2) and *Irf5-/-* (n = 2)) and d7 Hh + aIL10R (WT (n = 6, black circles) and *Irf5-/-* (n = 8, yellow circles)) mice. A)Total number of Ly6C^{hi} monocytes in the blood, B) Total number of neutrophils in the blood. Data are representative of two independent experiments. Two-way analysis of variance (ANOVA) with Sidak correction. Data presented are means ±SD. ns, not significant. $^{*}P \leq 0.05$ and $^{**}P \leq 0.01$

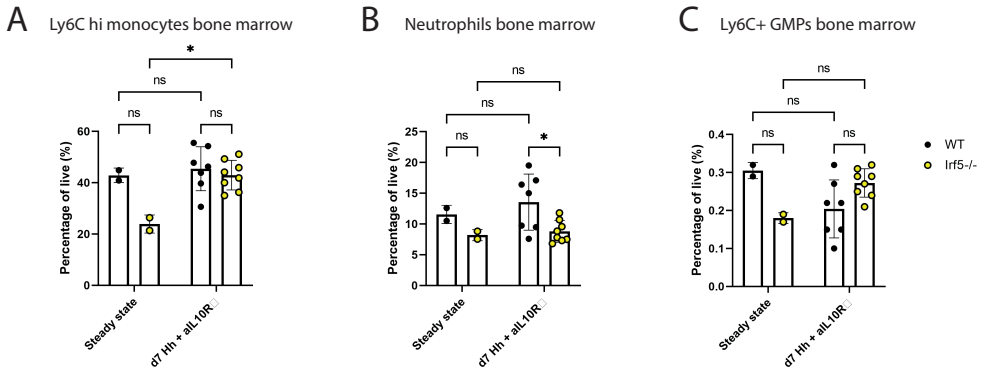


Figure 4.8: **Lower proportions of mature monocytes and neutrophils in the bone marrow of *Irf5-/-* mice at d7 Hh + aIL10R.** Flow cytometry analysis of blood and bone marrow from steady state (WT (n = 2) and *Irf5-/-* (n = 2)) and d7 Hh + aIL10R (WT (n = 6, black circles) and *Irf5-/-* (n = 8, yellow circles)) mice. A) Ly6C^{hi} monocytes, B) Neutrophils, C) Ly6C+ GMPs in the bone marrow as a percentage of live cells. Data are representative of two independent experiments. Two-way analysis of variance (ANOVA) with Sidak correction. Data presented are means ±SD. ns, not significant. $^{*}P \leq 0.05$ and $^{**}P \leq 0.01$

4.3.2 Expression of IRF5 in CX3CR1+ cells is required for the onset of intestinal inflammation and recruitment of neutrophils and monocytes

CX3CR1-Cre expression in different cell types was extensively characterized alongside CX3CR1-GFP in *Yona et al* [185]. Using a CX3CR1-GFP reporter strain as a proxy for Cre-expression, we discovered a high amount of progenitor populations expressing GFP throughout their development in the BM, which could result in Cre activity (Figure A.1). Nevertheless, it is a useful tool in targeting macrophages and monocytes more specifically than a LySM-Cre or the use of MBMCs. As we have already established the protective effect of IRF5 deletion in CX3CR1+ cells at d21 Hh + aIL10R [129], we merely wanted to confirm the importance and investigate the specific effects of CX3CR1-Cre IRF5 fl/fl ($CX3CR1^{Irf5}$) at the onset of inflammation. CX3CR1-Cre ($CX3CR1^{cre}$) mice were significantly higher inflamed than their floxed counterparts, in terms of histopathology and also leukocyte infiltration (Figure 4.9a - c). Furthermore, when we investigated cell-specific recruitment, we could see a significant lower infiltration of neutrophils and monocytes per gram tissue, as previously seen with *Irf5-/-* (Figure 4.9d, e). Despite the reported migration deficiency of monocytes, similar numbers of monocytes are found in the blood, as are neutrophils (Figure 4.10a, b). However, fully mature monocytes and neutrophils are decreased in the BM of $CX3CR1^{Irf5}$ (Figure 4.11a, b). Interestingly, a higher number of Ly6C+ GMPs are present in $CX3CR1^{Irf5}$ mice (Figure 4.11c). All in all, at d7 Hh + aIL10R $CX3CR1^{Irf5}$ mice fully recapitulates the phenotype of full *Irf5-/-* mice, apart from mature neutrophil production being unaffected in the BM of *Irf5-/-* mice (Figure 4.6b, 4.8b).

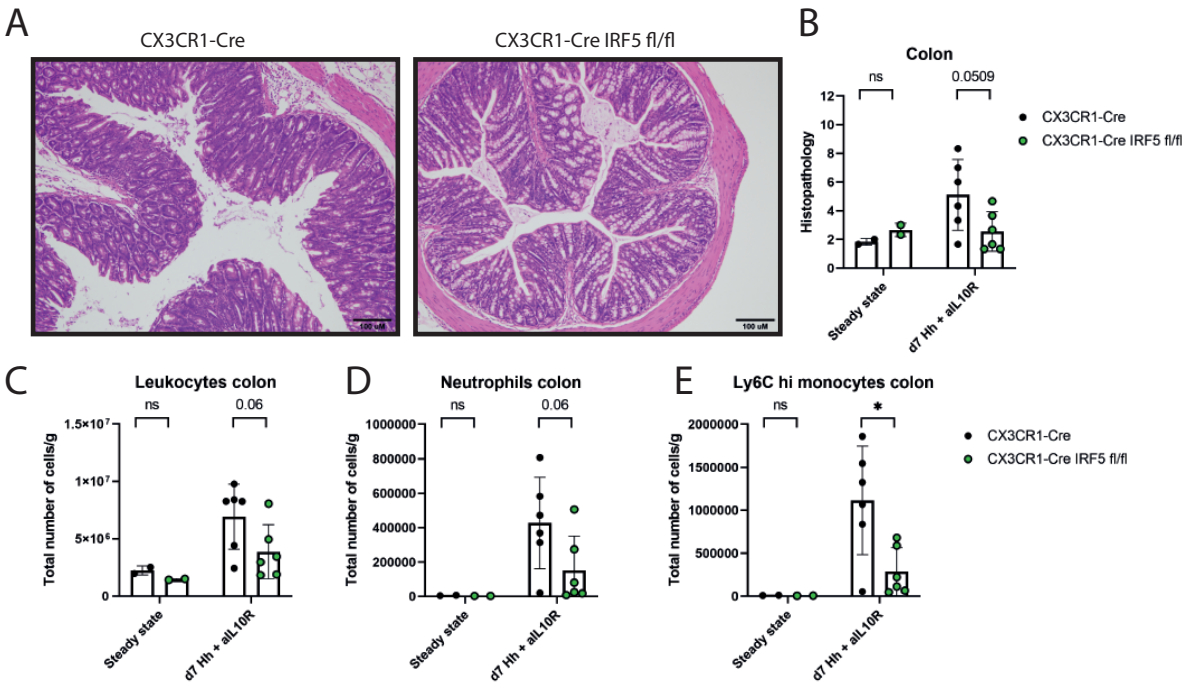


Figure 4.9: **CX3CR1^{Irf5} mice exhibit a significant reduction of pathology at the onset of inflammation.** A) Representative hematoxylin and eosin (H &E) colon sections from CX3CR1^{cre} (left) and CX3CR1^{Irf5} (right) mice at d7 Hh + aIL10R. Scalebars depict 100 μM, B) Histopathology scoring of steady state (CX3CR1^{cre} (n = 2, black circles) and CX3CR1^{Irf5} (n = 2, green circles)) and d7 Hh + aIL10R (CX3CR1^{cre}(n = 6) and CX3CR1^{Irf5} (n = 6)) colons, C) Total number of leukocytes, D) neutrophils, E) Ly6C^{hi} monocytes per gram tissue analysed by flow cytometry of the colonic lamina propria. Unpaired t-test. Data presented are means ±SD. ns, not significant and $^{*}P \leq 0.05$

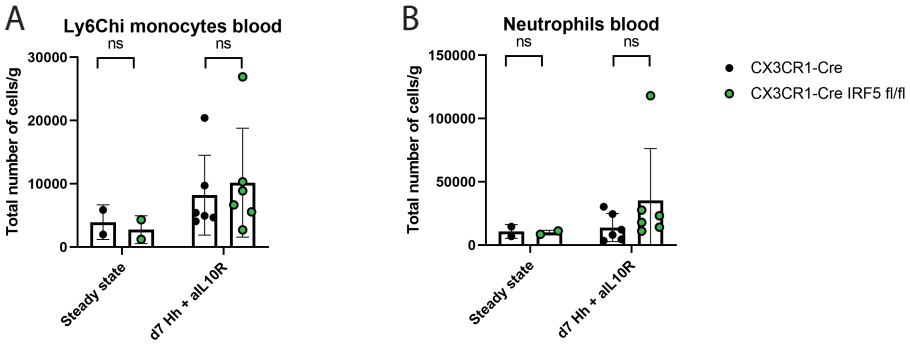


Figure 4.10: **No difference in Ly6C^{hi} monocytes and neutrophils in the blood at d7 Hh + aIL10R.** Flow cytometry analysis of blood and bone marrow from steady state (CX3CR1^{cre} (n = 2, black circles) and CX3CR1^{Irf5} (n = 2, green circles)) and d7 Hh + aIL10R (CX3CR1^{cre}(n = 6) and CX3CR1^{Irf5} (n = 6)) mice. A)Total number of Ly6C^{hi} monocytes in the blood, B) Total number of neutrophils in the blood. Unpaired t-test. Data presented are means ±SD. ns, not significant

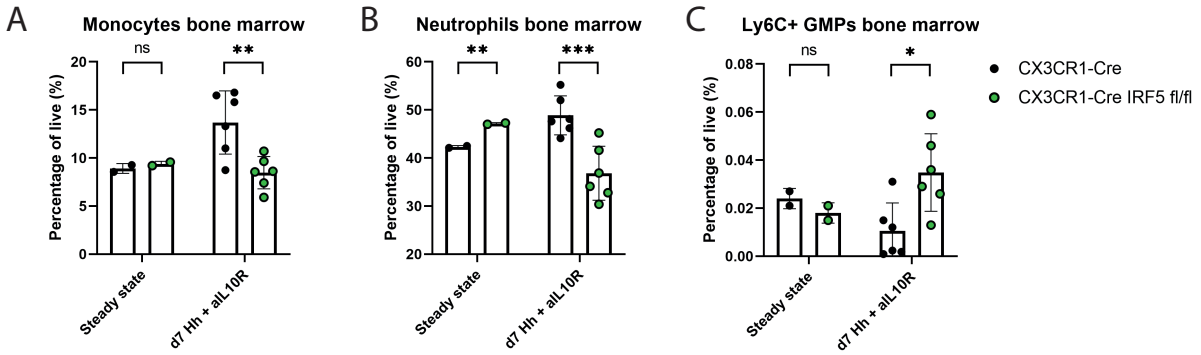


Figure 4.11: **Development deficiency of monocytes and neutrophils in the bone marrow of CX3CR1^{Irf5} during inflammation.** Flow cytometry analysis of blood and bone marrow from steady state (CX3CR1^{cre} (n = 2, black circles) and CX3CR1^{Irf5} (n = 2, green circles)) and d7 Hh + aIL10R (CX3CR1^{cre}(n = 6) and CX3CR1^{Irf5} (n = 6)) mice. A) Ly6C^{hi} monocytes in the bone marrow as a percentage of live cells, B) Neutrophils in the bone marrow as a percentage of live cells, C) Ly6C+ GMP progenitors in the bone marrow as a percentage of live cells. Unpaired t-test. Data presented are means ±SD. ns, not significant, $^{*}P \leq 0.05$, $^{**}P \leq 0.01$ and $^{***}P \leq 0.001$

4.3.3 Characterization of a novel neutrophil-specific Ly6G-Cre strain

As IRF5 was highlighted in [165] as a TF important for neutrophil activation; and its importance in colitis is undebated [129, 169, 234], we wanted to explore its effect on neutrophils. Combining a recently generated neutrophil-specific Cre strain [244] with an IRF5 LoxP cassette (Ly6G^{Irf5}) offered us a cutting-edge genomic approach to study IRF5-depletion in neutrophils specifically. The original mouse strain was generated and characterised extensively [244]. *Hasenberg et al* modulated the neutrophil-specific locus Ly6G by adding a Cre recombinase followed by a tdTomato-reporter. However, the intestine was not included in their characterization, and we wanted to certify that also during our model of inflammation, only neutrophils remain targeted by the Cre. Furthermore, due to Ly6G being coupled to the Cre-recombinase, Ly6G^{cre} mice do not express Ly6G as a surface marker, making it more challenging to reliably identify neutrophils [244].

Two additional, highly specific murine neutrophil markers exist: CD101, a neutrophil maturity marker [90] and CD177, a neutrophil activation marker [245]. We therefore first compared the labelling efficiency of CD177 and CD101 with Ly6G in a WT mouse both at steady state and at d7 Hh + aIL10R across all tissues of interest. Following gating on live CD45+ cells, we employed the strategy of first gating on Ly6C intermediate CD11b+ cells followed by gating on Ly6G+ and the respective markers. (Figure 4.12a). Ly6G+ cells that were not labelled by either CD101 (blue) nor CD177 (yellow) are marked in black, whereas double-positive cells that would be tagged by both antibodies are marked in green. Quantifying the amounts of each population present in the BM, blood and colon revealed that especially in the BM, neither CD101 nor CD177 are good markers for capturing neutrophils (Figure 4.12b). In the blood, CD101 is the most reliable marker, whereas in the colon, CD177 labels nearly 100% of Ly6G+ cells at both steady state and d7 Hh + aIL10R (Figure 4.12c, d). However, as neither marker was efficient in the blood or colon, assumingly based on maturity and activity levels of the neutrophils, a combination of markers should be used to clearly identify neutrophils in the absence of Ly6G.

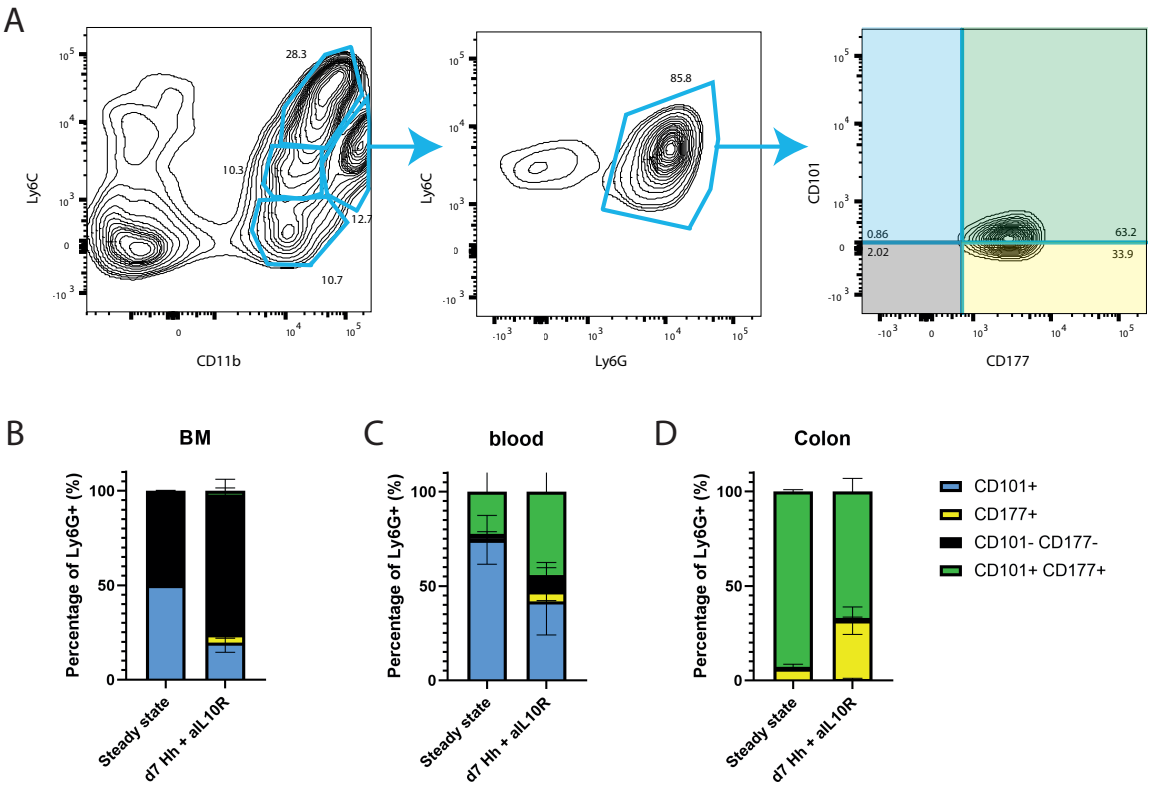


Figure 4.12: **Examining the labelling efficiency of the different neutrophil markers CD101 and CD177.** Cells were isolated from the bone marrow, blood and colon from uninfected (n = 2) and d7 Hh + aIL10R (n = 5) WT mice and subjected to flow cytometry analysis. A) gating scheme for identification of neutrophils within Ly6C^{int} CD11b+ population. B) Quantification of CD177- CD101- (black bars), CD101+ (blue), CD177+ (yellow) and CD101+ CD177+ (green) Ly6G+ neutrophils in the BM, C) blood and D) colon. Data presented are means ±SD.

We were also interested in the percentage of Ly6G+ cells labelled by either antibody in the different compartments and therefore quantified both CD101+ (including CD101+ CD177+) and CD177+ (including CD101+ CD177+) (Table 4.1). Pre-gating on Ly6C^{int} already determined about 80% of neutrophils in the BM, circumventing the need for Ly6G or any other neutrophil marker in this scenario (Figure 4.13a). Simultaneously, about 70-90 % of Ly6C^{int} cells are neutrophils in both blood and colon, making it a good pre-selection without the necessity of either neutrophil marker (Figure 4.13b, c).

Table 4.1: CD101 and CD177 95% CI ±SD for neutrophil labelling.

Tissue	**Condition**	**CD101**	**CD177**
BM	Steady state	51.08±0.19	1.46±0.16
BM	d7 Hh + aIL10R	21.53±5	6.43±2.69
blood	Steady state	96.9±2.07	23.35±11.45
blood	d7 Hh + aIL10R	86.02±8.85	49.37±16.19
colon	Steady state	92.85±0.9	99.06±1.36
colon	d7 Hh + aIL10R	67.82±5.47	97.84±0.61

ROSA26 is a locus which is continuously and ubiquitously expressed and marks a specific genetic site highly successful for inserting genetic modifications in mice [246]. By inserting fluorescently tagged sequences like GFP or tdTomato into the ROSA26 locus, flanked by *loxP* sequences, *Srinivas et al* generated so-called Cre-reporter strains, commonly used for validating the expression of a Cre in the cells of interest [247]. Here, we have used this system to amplify the tdTomato coupled to Ly6G-Cre, making it visible for flow cytometry. We employed the gating scheme depicted in Figure 4.14 [244]. Neutrophils were gated as CD177+ cells, and a WT mouse was used as a fluorescence minus one (FMO) control for td-Tomato expression.

In the colon, Ly6G was expressed in 50% of neutrophils, and about 5% of IECs, further explaining the "blotches" of Ly6G-tdTomato staining in figure 3.4a (Figure 4.15a). About 40% of Ly6C^{int} monocytes express tdTomato in the blood (Figure 4.15b). However, in the blood, CD177 only marks 49% of neutrophils definitely in inflammation, despite the Ly6C^{int} population being mainly composed of neutrophils (Figure 4.13b). *Hasenberg et al* further showed that CD115+ monocytes/macrophages in the blood expressed no tdTomato

regardless of their Ly6C expression, further proving that the Ly6C^{int} population in the blood in our case are CD177- neutrophils [244]. Simultaneously, 80% of neutrophils express tdTomato in the blood (Figure 4.15b). Upon investigation of the BM, virtually no cells except the mature neutrophils express the Ly6G-Cre, which confirms *Hasenberg et al* (Figure 4.15c), highlighting its late expression during neutrophil development as well as assuring that no other cell types express the Cre during their development [244].

To highlight differences in the colon and blood regarding identification of neutrophils on the base of Ly6C^{int} and CD177, we performed a tSNE analysis of the Ly6C^{int} population at d7 Hh + aIL10R. Clustering in the blood revealed no clear separation of CD177+ and CD177- population, as can also be seen via marker expression of CD177. Ly6G expression is found in the cluster harbouring both CD177+ and CD177- cells (Figure 4.16a). In contrast, in the colon, the clusters are clearly subdivided not only by CD177 expression, but also Ly6G and CD11b^{hi}, confirming the specificity of Ly6G-Cre within colonic neutrophils and identifying the Ly6C^{int} cluster in the blood as both CD177+ and CD177- neutrophils (Figure 4.16b). Addition of CD101 as an additional marker in the blood specifically could clarify this further as it labelled almost 90% of neutrophils in the blood (Table 4.1).

As a significant number of IECs expresses the Ly6G-Cre, seen in both microscopy and flow cytometry, we wanted to exclude any possible contribution to a phenotype. We therefore sorted IECs, fibroblasts, monocytes and neutrophils at d7 Hh + aIL10R and measured *Irf5* gene expression via RT-qPCR (Figure 4.17). Epithelial cells do not express *Irf5*, and thus would not contribute to any changes in phenotype even if expressing the Cre. By using Ly6G-Cre as WT controls we also circumvent any off-target effects of the Cre, as they would be simultaneously applied in Ly6G^{cre} and Ly6G^{Irf5} mice. To confirm knockout of IRF5 in neutrophils specifically, we sorted CD101+ neutrophils and monocytes from the colon at d7 Hh + aIL10R and measured expression of *Irf5* by RT-qPCR. This revealed a reduction in *Irf5*-expression in Ly6G^{Irf5} neutrophils whereas monocytes/macrophages express the same amounts of *Irf5* as their WT counterparts (Figure 4.18a,b).

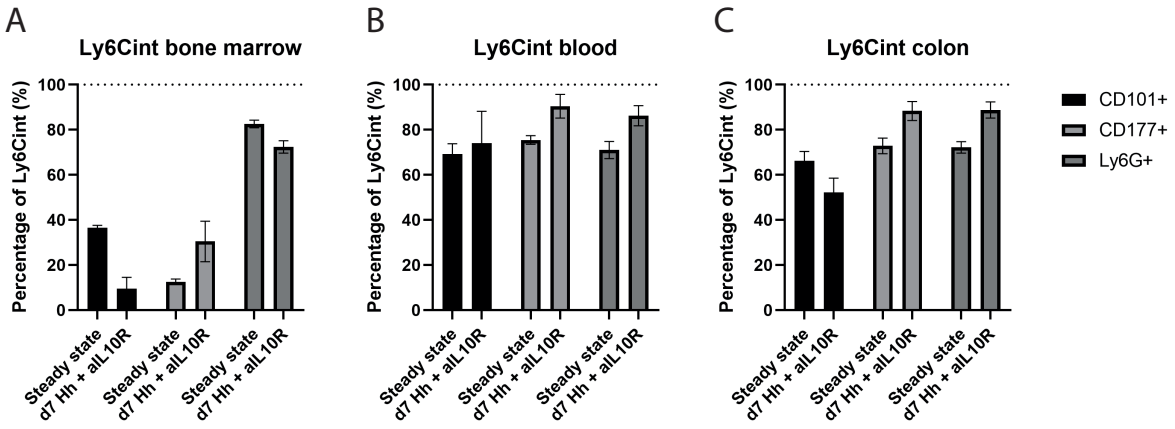


Figure 4.13: **Ly6C^{int} CD11b+ composition in bone marrow, blood and colon.** Cells were isolated from the bone marrow, blood and colon from uninfected (n = 2) and d7 Hh + aIL10R (n = 5) WT mice and subjected to flow cytometry analysis. CD101+ (black bars), CD177+ (light grey bars) and Ly6G+ (dark grey bars) cells within Ly6C^{int} CD11b+ at both steady state and d7 Hh + aIL10R were quantified in A) bone marrow, B) blood and C) colon. Data presented are means ±SD.

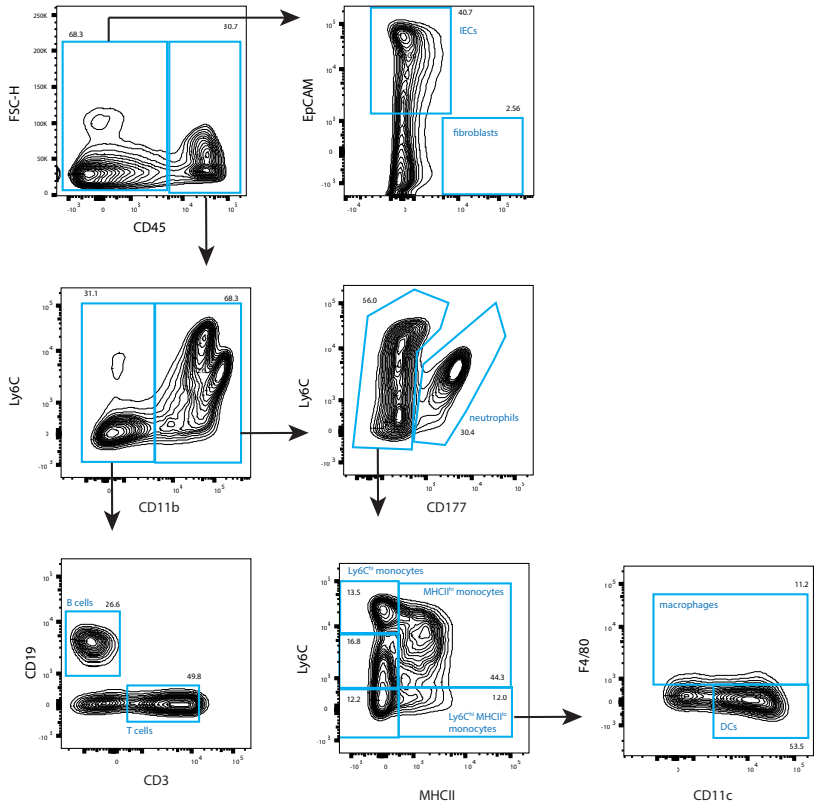


Figure 4.14: **Representative gating scheme for identification of various cell types for characterization of Ly6G-Cre tdTomato+ expressing cells.**

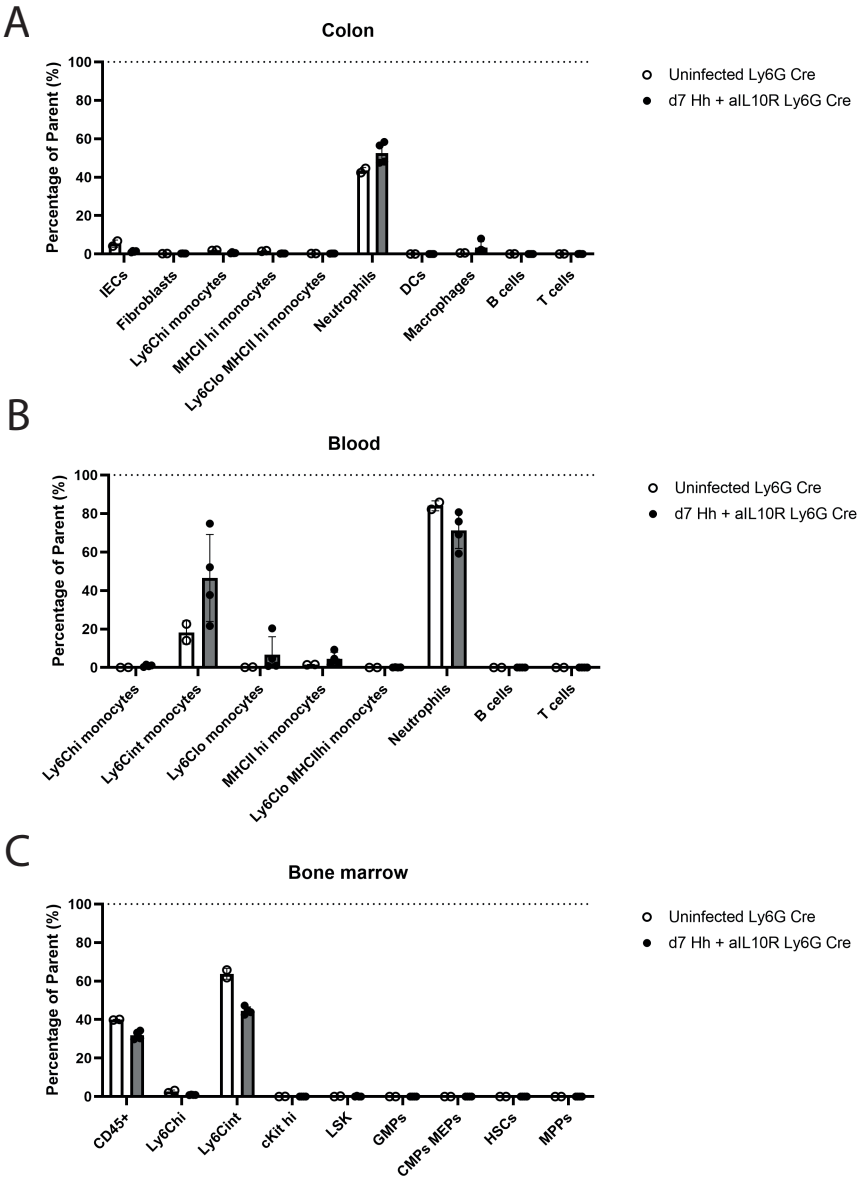


Figure 4.15: **Expression of Ly6G-driven Cre measured by td-Tomato in various cell types across different tissues.** Cells were isolated from the colon, bone marrow and blood from uninfected (n = 2, white bars) and d7 Hh + aIL10R (n = 4, grey bars) td-Tomato Rosa26-Cre mice and subjected to flow cytometry analsis. Expression of tdTomato was measured as a percentage of tdTomato+ cells within a given cell population. A) colon, B) blood, C) bone marrow. Data presented are means ±SD.

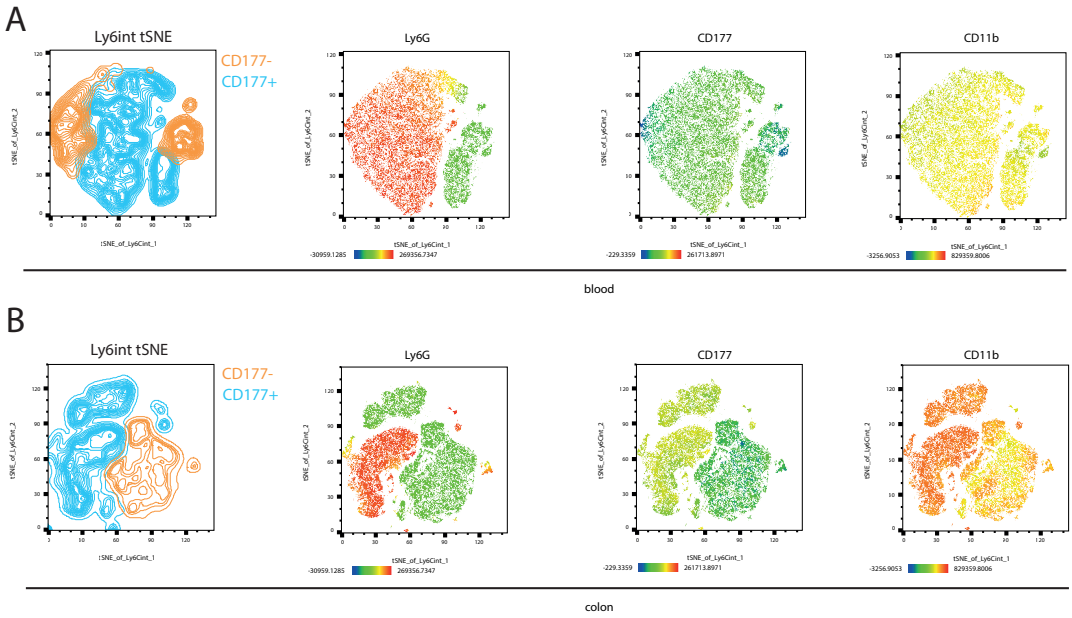


Figure 4.16: **Composition of Ly6^{int} CD11b+ using t-SNE to identify distinct cell populations.** t-distributed stochastic neighbor embedding (t-SNE) was performed on flow cytometry population of Ly6C*int* for both blood (A) and colon (B). CD177+ (blue) and CD177- (orange) populations as per flow cytometry gating are overlayed. Marker expression of Ly6G-tdTomato, CD177-AF488 and CD11b-BV510 are quantified within the different cell clusters.

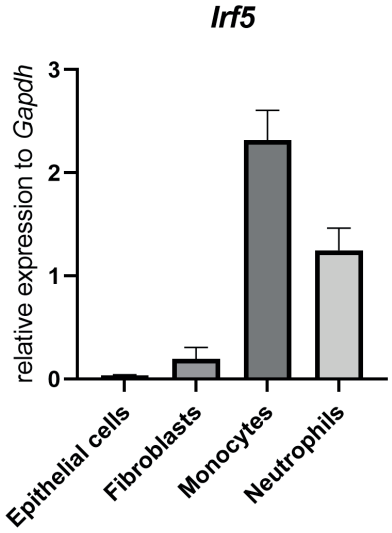


Figure 4.17: ***Irf5* is not expressed in epithelial cells and fibroblasts at d7 Hh + aIL10R** Epithelial cells, fibroblasts, Ly6C^{hi} monocytes and neutrophils were sorted from the colon of d7 Hh + aIL10R WT mice (n = 3) and subjected to RT-qPCR. Relative expression of *Irf5* was measured in relation to *Gapdh*.

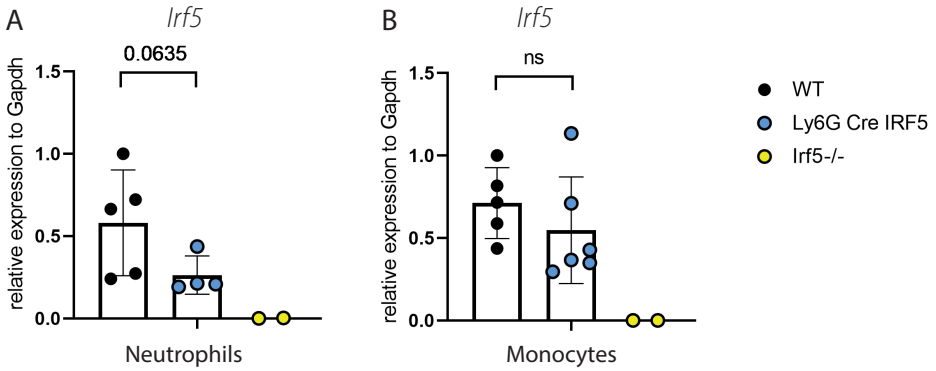


Figure 4.18: **Neutrophils exhibit a reduction in *Irf5* expression in Ly6G^{Irf5} mice** Neutrophils and Ly6C^{hi} monocytes were sorted from the colons of Ly6G^{cre} (n = 5, black circles), Ly6G^{Irf5} (n = 4, blue circles) and *Irf5-/-* (n = 2, yellow circles) mice at d7 Hh + aIL10R. The sorted cells were subjected to RT-qPCR and *Irf5* expression was measured in relation to *Gapdh*. A) Neutrophils, B) Ly6C^{hi} monocytes. Mann-Whitney test. Data presented are means ±SD. ns, non significant.

4.3.4 Expression of IRF5 in neutrophils is required for the onset of intestinal inflammation

Having confirmed the specificity of the Ly6G-Cre, we subjected Ly6G^{cre} and Ly6G^{Irf5} mice to the d7 Hh + aIL10R infection protocol. This revealed a significant reduction of histopathology and leukocyte infiltration in the Ly6G^{Irf5} mice (Figure 4.19a-c). Furthermore, the numbers of neutrophils in the colon were comparable (Figure 4.19d), however, monocytes were significantly reduced in the colon of Ly6G^{Irf5} mice (Figure 4.19e). Monocyte numbers in the blood were not affected, neither were neutrophils (Figure 4.20a, b). In the BM, a lower percentage of mature monocytes was found in Ly6G^{Irf5} mice during inflammation (Figure 4.21a). Simultaneously, a trend towards more Ly6C+ GMPs was seen at d7 Hh + aIL10R in Ly6G^{Irf5}, whilst mature neutrophil percentages were not affected (Figure 4.21b, c). Interestingly, this all mirrors the changes seen in the BM of CX3CR1^{Irf5} mice, with the exception of neutrophils remaining unaffected already in the BM (Figure 4.11). Even though the production of monocytes in the BM was affected, numbers in the blood were similar, pointing towards a lower recruitment into the inflamed colon by a mechanism yet to be determined. As neutrophils are the only IRF5-depleted cells, neutrophils seem to be involved in monocyte recruitment into the inflamed colon at the onset of Hh + aIL10R colitis either directly or indirectly.

As Hh is the driver in this model of colitis, we wanted to control that the phenotype of the Ly6G^{Irf5} mice is not due to lower colonisation of Hh in those mice. By quantifying Hh with the presence of its toxin, cdtB, we confirmed that there is no difference between Ly6G^{cre} and Ly6G^{Irf5} mice regarding their Hh colonisation (Figure 4.22).

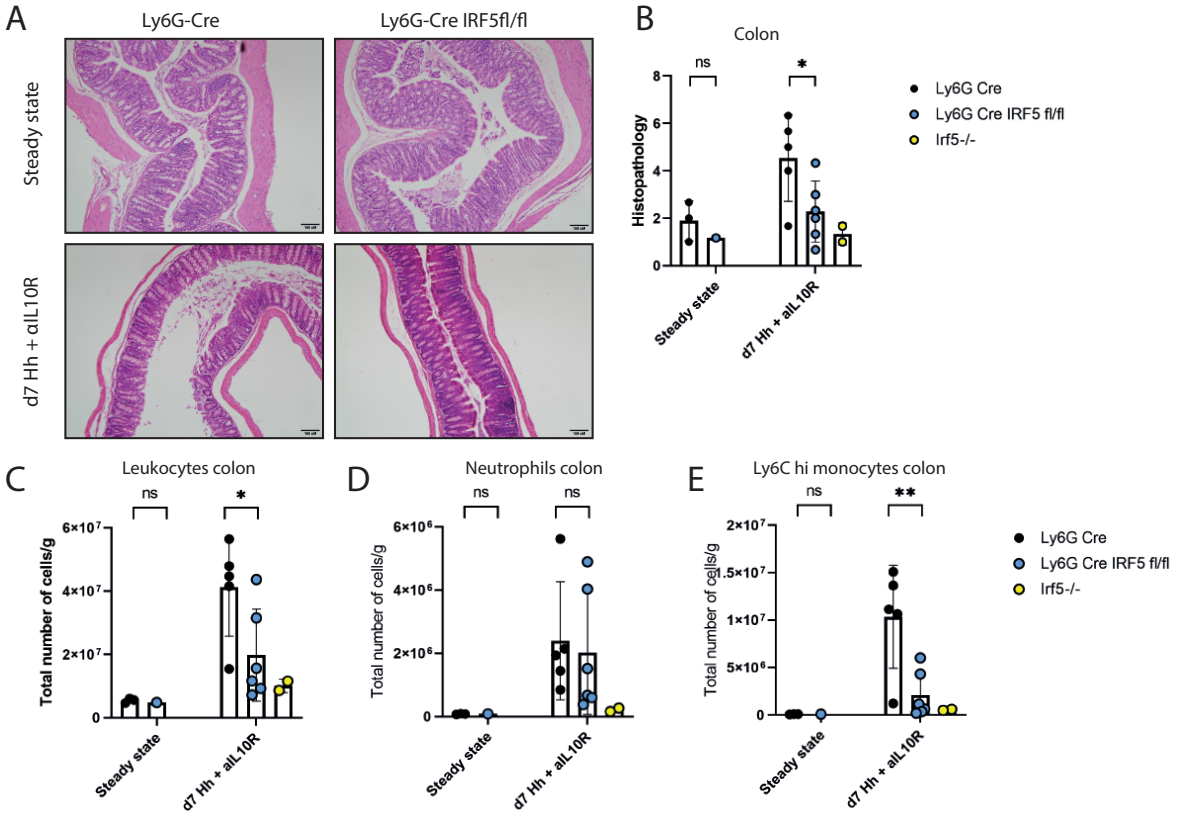


Figure 4.19: **Lower recruitment of Ly6C^{hi} monocytes into the colon of Ly6G^{Irf5} mice at the onset of inflammation.** A) Representative hematoxylin and eosin (H &E) colon sections from Ly6G^{cre} (left) and Ly6G^{Irf5} (right) mice at steady state (upper panels) and d7 Hh + aIL10R (lower panels). Scalebars depict 100 μM, B) Histopathology scoring of steady state (Ly6G^{cre} (n = 2, black circles) and Ly6G^{Irf5} (n = 2, blue circles)) and d7 Hh + aIL10R (Ly6G^{cre}(n = 5), Ly6G^{Irf5} (n = 6) and *Irf5-/-* (n = 2, yellow circles)) colons, C) Total number of leukocytes, D) neutrophils, E) Ly6C^{hi} monocytes per gram tissue analysed by flow cytometry of the colonic lamina propria. Unpaired t-test. Data presented are means ±SD. ns, not significant, *P $\leq$ 0.05 and **P $\leq$ 0.01

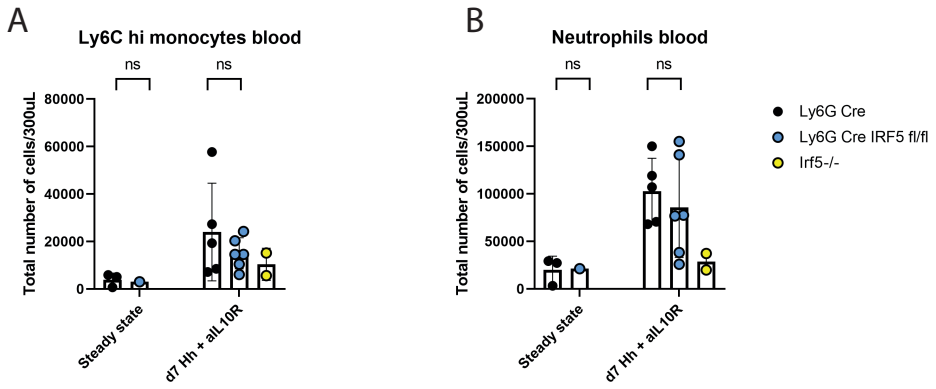


Figure 4.20: **No differences in Ly6C^{hi} monocytes numbers in the blood.** A) Total number of Ly6C^{hi} monocytes in the blood, B) Total number of neutrophils in the blood. Unpaired t-test. Data presented are means ±SD. ns, not significant

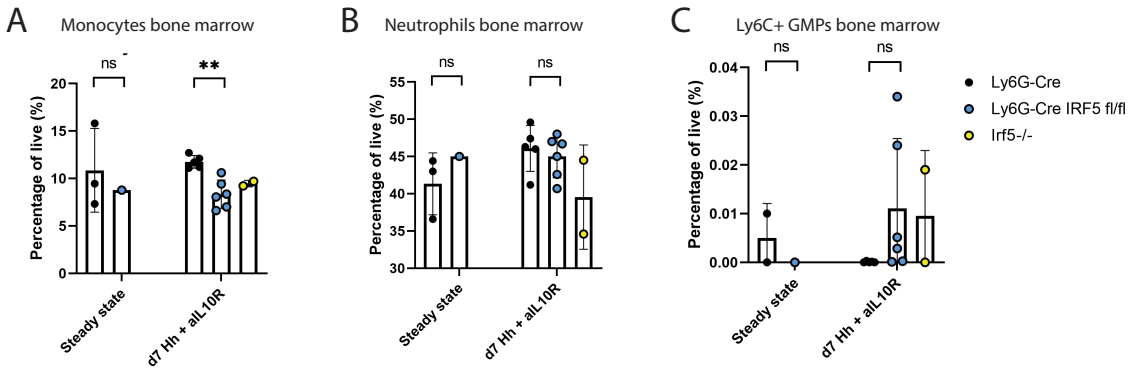


Figure 4.21: **Lower production of mature monocytes in the bone marrow of Ly6G^{Irf5} mice.** A) Monocytes, B) neutrophils C) Ly6C+ GMPsls in the bone marrow as a percentage of live cells. Unpaired t-test. Data presented are means ±SD. ns, not significant, $^{*}P \leq 0.05$ and $^{**}P \leq 0.01$

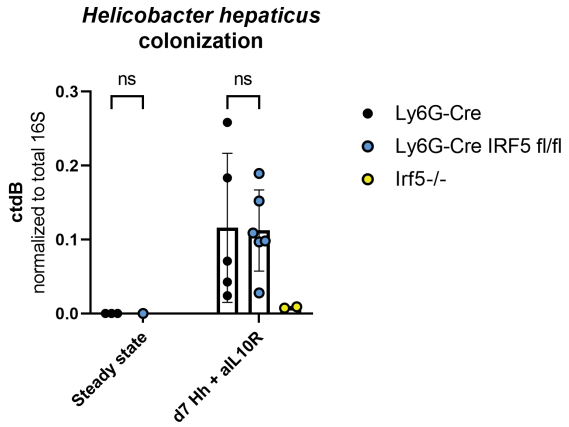


Figure 4.22: ***Helicobacter hepaticus* colonization is not different at d7 Hh + aIL10R between Ly6G^{cre} and Ly6G^{Irf5} mice.** *Helicobacter hepaticus* colonisation measured with the presence of its toxin cdtB, normalised to total 16S content in 5ng/uL cecal content. Unpaired t-test. Data presented are means ±SD. ns, not significant

4.3.5 Deletion of IRF5 specifically in neutrophils is sufficient to prevent the onset of intestinal inflammation altogether

We wanted to investigate whether deletion of IRF5 specifically in neutrophils would be enough to hold up the entire cascade of inflammation or if it gets overthrown by a redundant mechanism. Ly6G^{cre} and Ly6G^{Irf5} mice were therefore subjected to a full course of Hh + aIL10R colitis (d21 Hh + aIL10R) and their pathology as well as the myeloid cell pool in the colon, blood, BM and spleen was analysed. Surprisingly, Ly6G^{Irf5} were completely protected from Hh + aIL10R-mediated colitis, with a significantly reduced histopathology as well as leukocyte numbers in the colon (Figure 4.23a-c). Furthermore, neutrophils and monocytes were completely cleared out of the colon, with numbers resembling the colons of uninfected mice (Figure 4.23d, e). Interestingly, by investigating CD11c+ and CD206+ macrophages, we could see higher percentages of CD11c+ macrophages in the Ly6G^{cre} and simultaneous higher levels of CD206+ macrophages in Ly6G^{Irf5} mice at d21 Hh + aIL10R (Figure 4.23f). As the tissue microenvironment is fundamental in shaping macrophage function [12], differences in the tissue microenvironment as well as potential direct priming of infiltrating monocytes by *Irf5-/-* neutrophils could be underlying factors in the altered macrophage differentiation.

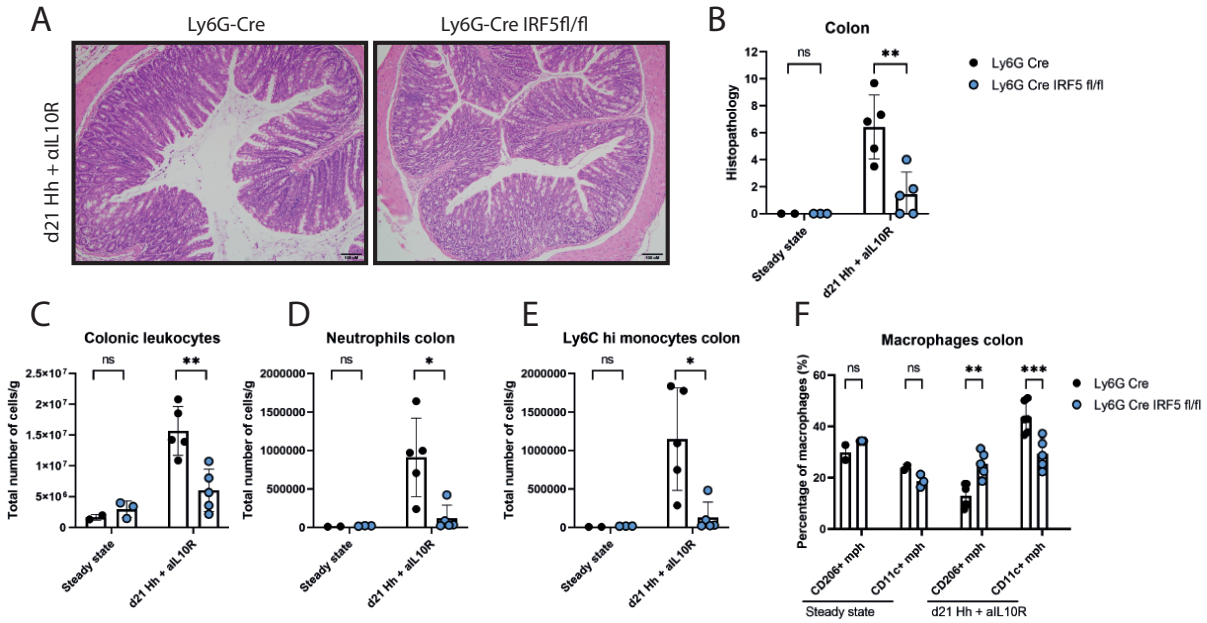


Figure 4.23: ***Irf5*-deficient neutrophils prevent intestinal inflammation.** A) Representative hematoxylin and eosin (H &E) colon sections from Ly6G^{cre} (left) and Ly6G^{Irf5} (right) mice d21 Hh + aIL10R. Scalebars depict 100 μM, B) Histopathology scoring of steady state (Ly6G^{cre} (n = 2, black circles) and Ly6G^{Irf5} (n = 2, blue circles)) and d21 Hh + aIL10R (Ly6G^{cre}(n = 5) and Ly6G^{Irf5} (n = 5) colons, C) Total number of leukocytes, D) neutrophils, E) Ly6C^{hi} monocytes per gram tissue analysed by flow cytometry of the colonic lamina propria, E) CD206+ and CD11c+ macrophages in the colons of steady state and d21 Hh + aIL10R mice, depicted as percentage of macrophages. Unpaired t-test. Data presented are means ±SD. ns, not significant, $^{*}P \leq 0.05$, $^{**}P \leq 0.01$ and $^{***}P \leq 0.001$

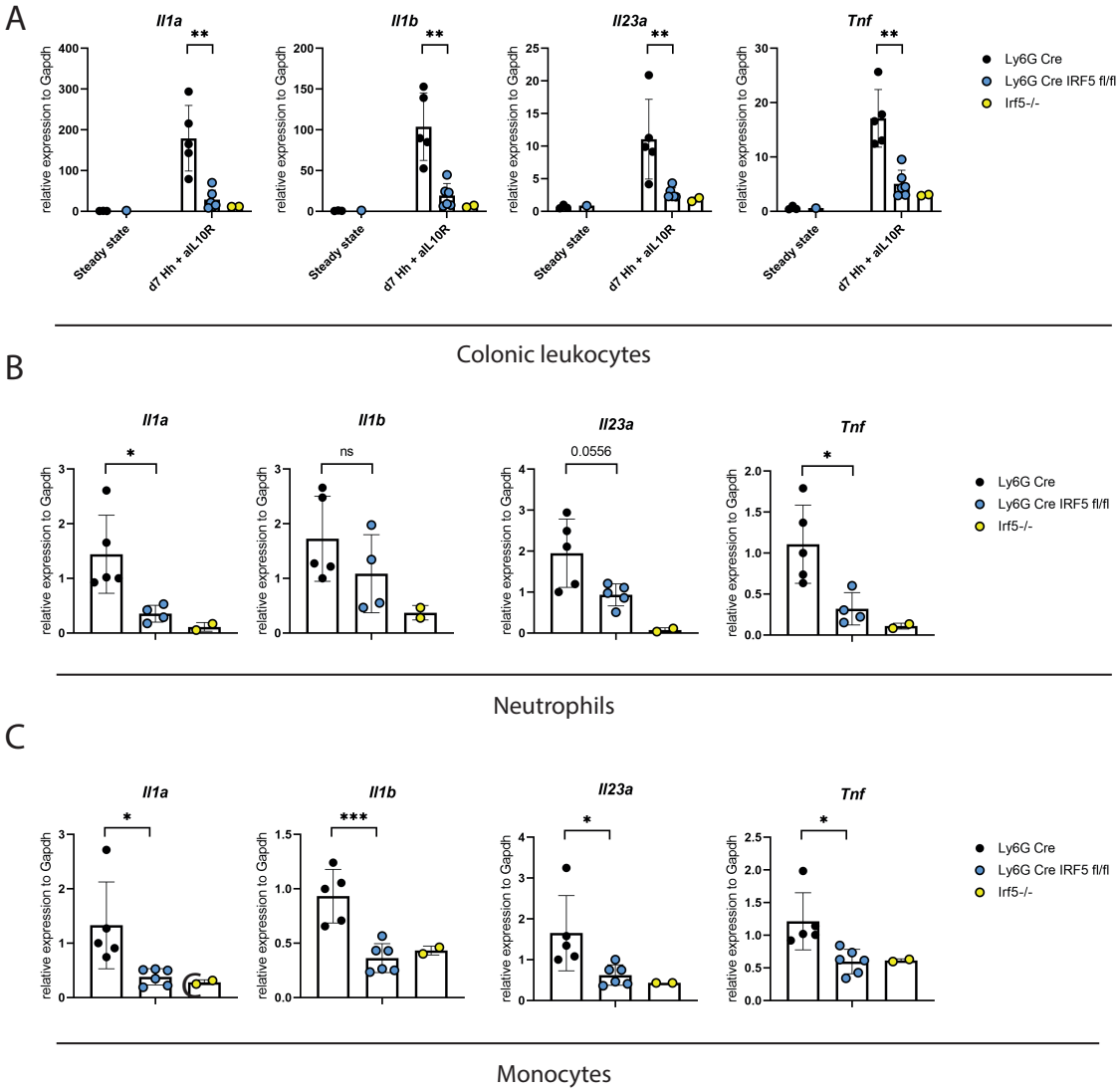


Figure 4.24: **The cytokine landscape is distinctly set up at d7 Hh + aIL10R in Ly6G^{Irf5} mice.** Relative expression of *Il1a*, *Il1b*. *Il23a*, *Tnf* in relation to *Gapdh* was measured via RT-qPCR in A) colonic leukocytes isolated from steady state (Ly6G^{cre} (n = 2, black circles) and Ly6G^{Irf5} (n = 2, blue circles)) and d7 Hh + aIL10R (Ly6G^{cre}(n = 5), Ly6G^{Irf5} (n = 6) and *Irf5-/-* (n = 2, yellow circles)) colons, B) sorted neutrophils C) sorted Ly6C^{hi} monocytes from Ly6G^{cre} (n = 5, black circles), Ly6G^{Irf5} (n = 4, blue circles) and *Irf5-/-* (n = 2, yellow circles) mice at d7 Hh + aIL10R. Mann-Whitney test. Data presented are means ±SD. ns, non significant, $^{*}P \leq 0.05$, $^{**}P \leq 0.01$ and $^{***}P \leq 0.001$

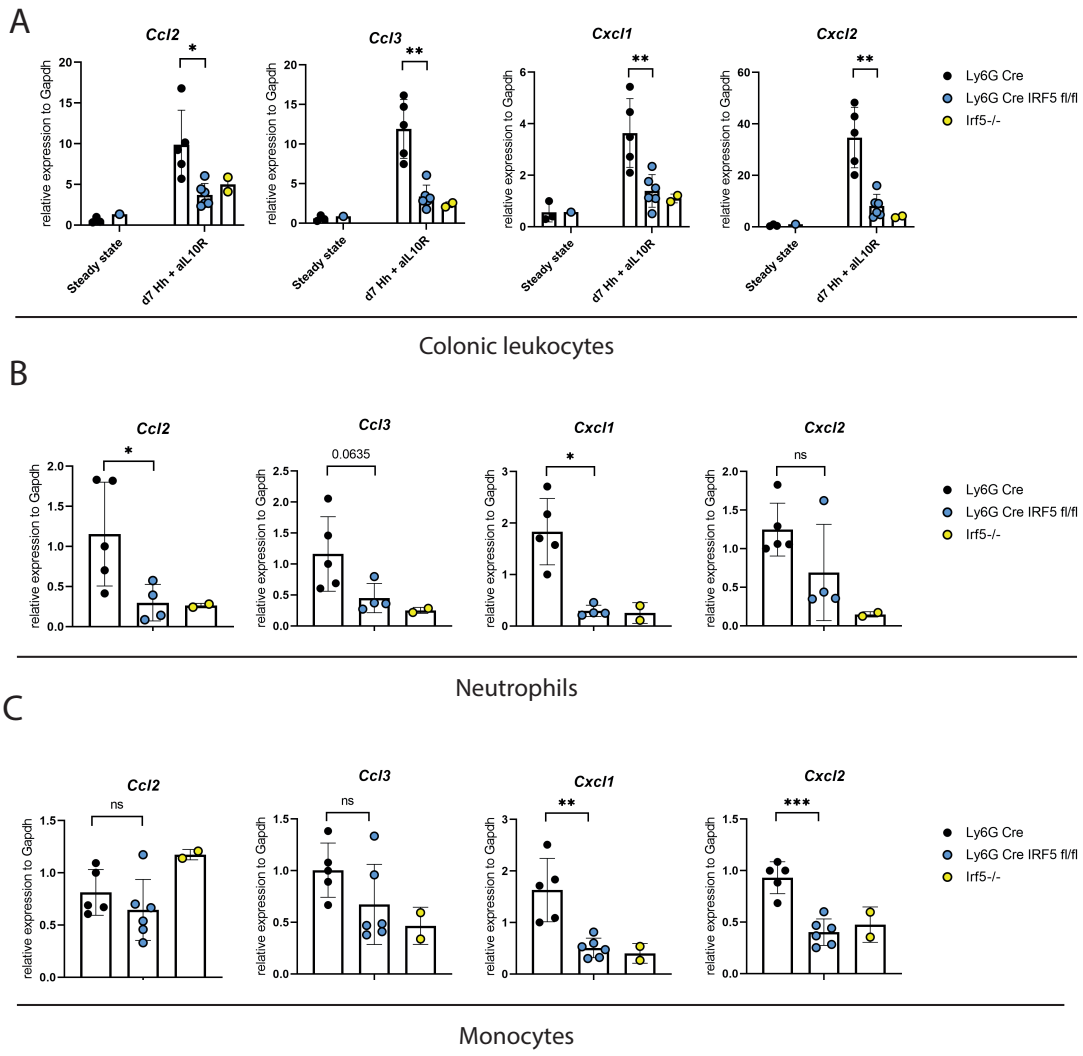


Figure 4.25: **The chemokine landscape is distinctly set up at d7 Hh + aIL10R in Ly6G^{Irf5} mice.** Relative expression of *Ccl2*, *Ccl3*, *Cxcl1*, *Cxcl2* in relation to *Gapdh* was measured via RT-qPCR in A) colonic leukocytes isolated from steady state (Ly6G^{cre} (n = 2, black circles) and Ly6G^{Irf5} (n = 2, blue circles)) and d7 Hh + aIL10R (Ly6G^{cre}(n = 5), Ly6G^{Irf5} (n = 6) and *Irf5-/-* (n = 2, yellow circles)) colons, B) sorted neutrophils C) sorted Ly6C^{hi} monocytes from Ly6G^{cre} (n = 5, black circles), Ly6G^{Irf5} (n = 4, blue circles) and *Irf5-/-* (n = 2, yellow circles) mice at d7 Hh + aIL10R. Mann-Whitney test. Data presented are means ±SD. ns, non significant, $^{*}P \leq 0.05$, $^{**}P \leq 0.01$ and $^{***}P \leq 0.001$

4.3.6 The tissue microenvironment is significantly different in Ly6G^{Irf5} mice at d7 Hh + aIL10R

Having uncovered the differences in macrophage subset generation in Ly6G^{Irf5} mice at d21 Hh + aIL10R (Figure 4.23f), we aimed to characterize the tissue environment at the onset of inflammation to uncover mediators potentially shaping monocyte-to macrophage differentiation. Analysing the tissue-microenvironment at d7 Hh + aIL10R in both Ly6G^{cre} and Ly6G^{Irf5} mice via RT-qPCR to identify potential mediators of this neutrophil-mediated protection, we found a significant downregulation of most pro-inflammatory cytokines (*Il1a, Il1b, Il12a, Il6, Tnf, Il12b*) and chemokines (*Ccl2, Ccl3, Ccl4, Ccl5, Cxcl1, Cxcl2*) in colonic leukocytes (Figure 4.24a & 4.25a). Neutrophils and monocytes were analysed separately, by examining their gene expressions from sorted cells. The neutrophils were sorted on the basis of CD101 expression, meaning that only the expression in mature neutrophils was assessed, as well as only about 70% of total neutrophils were analysed (table 4.1). Surprisingly, despite *Irf5* only being downregulated in neutrophils (Figure 4.18a, b), monocytes express significantly lower levels of pro-inflammatory cytokines and chemokines, mirroring the expression in neutrophils (Figure 4.24b, c & 4.25b, c).

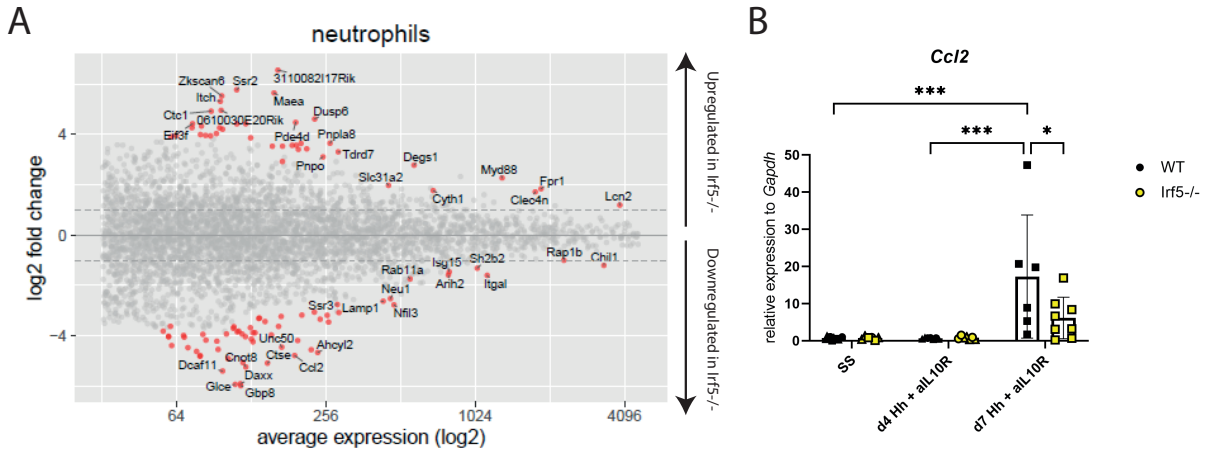


Figure 4.26: ***Ccl2* expression is lower in *Irf5-/-* tissue and *Irf5-/-* neutrophils during inflammation.** A) Neutrophils sorted from mixed bone marrow chimeras (n = 3) at d21 Hh + aIL10R and subjected to bulk RNA-seq analysis. Top differentially expressed genes marked in red. B) *Ccl2* expression in relation to *Gapdh* at steady state (WT (n = 11, black symbols), *Irf5-/-* (n = 6, yellow symbols)), d4 Hh + aIL10R (WT (n = 7), *Irf5-/-* (n = 7)) and d7 Hh + aIL10R (WT (n = 6), *Irf5-/-* (n = 8)). Data pooled from three independent experiments, marked with different symbols. Two-way analysis of variance (ANOVA) with Sidak correction. Data presented are means ±SD. $^{*}P \leq 0.05$ and $^{***}P \leq 0.001$

4.3.7 CCL2 secreted from IRF5-proficient neutrophils leads to the infiltration of monocytes into the inflamed colon

As almost all genes investigated were significantly downregulated in Ly6G^{Irf5} mice at d7 Hh + aIL10R, we were unable to decipher direct and indirect effects of the tissue microenvironment on gene expression. We therefore turned to analysis of a mixed bone marrow chimera (MBMC), where *Irf5-/-* and WT immune cells are exposed to the same environment, and sorted neutrophils at d21 Hh + aIL10R for analysis via bulk RNA-seq. *Ccl2* was among the top 10 genes downregulated in *Irf5-/-* neutrophils (Figure 4.26b), indicating a potential role for neutrophils and their CCL2 production in monocyte recruitment to the inflamed colon. CCL2 is one of the major chemokines involved in monocyte recruitment [248]. To confirm its potential importance at the onset of inflammation, we investigated its expression in the inflamed tissue of WT/*Irf5-/-* mice at the onset of Hh + aIL10R-mediated intestinal inflammation (chapter 4.3.1). We saw a significant reduction in *Ccl2* expression in the colonic tissue of *Irf5-/-* mice at d7 Hh + aIL10R (Figure 4.26a). This is in concordance with the reduction of monocytes in the inflamed colon at d7 Hh + aIL10R in all *Irf5-/-*, CX3CR1^{Irf5} and Ly6G^{Irf5} mice compared to their respective WT counterparts (Figure 4.6e, 4.9e, 4.19e). By focusing on *Ccl2* specifically, we saw the reduction at d7 Hh + aIL10R to be due to expression within CD101+ neutrophils specifically, whereas its levels remained the same between Ly6G^{cre} and Ly6G^{Irf5} mice in monocytes (Figure 4.25a-c).

The use of Hoxb8 neutrophils in an *in vitro* setting was employed to study the ability of neutrophils to directly produce CCL2 following a stimulus. *Irf5-/-* neutrophils produced lower amounts of CCL2 protein after zymosan stimulation (Figure 4.27a). Defactinib is an inhibitor of Pyk2, an upstream phosphorylating kinase of IRF5 [126]. It was applied to WT and *Irf5-/-* Hoxb8 neutrophils prior to stimulation with Hh sIAg or zymosan. Defactinib significantly reduced CCL2 production in WT neutrophils, whereas it had limited effect on *Irf5-/-* neutrophils (Figure 4.27b). This renders IRF5-mediated CCL2 production in neutrophils as a novel mechanism mediating intestinal inflammation and puts neutrophils at the crossroad for orchestrating downstream inflammation.

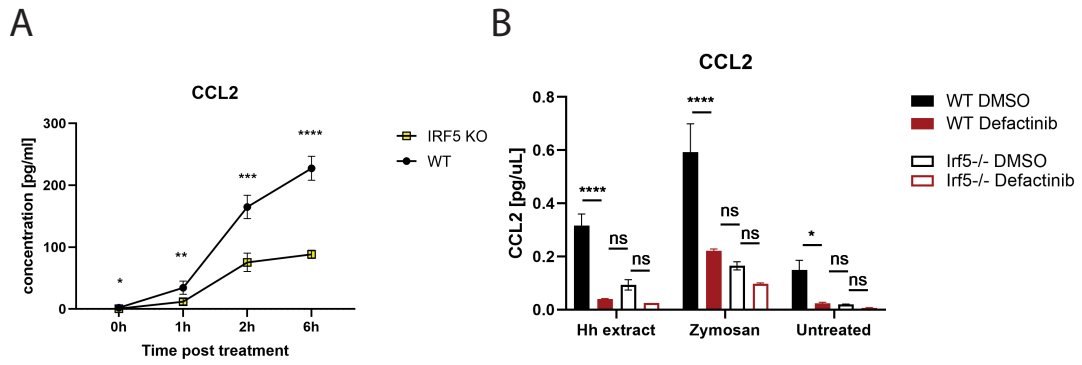


Figure 4.27: **IRF5-deficient neutrophils produce lower levels of CCL2 *in vitro*.** A) CCL2 concentration measured by ELISA from the supernatant of WT (n = 4) and IRF5 KO (n = 4) Hoxb8 neutrophils stimulated with 50 pg/uL zymosam at 0, 1, 2 and 6h post stimulation. Unpaired t-test. B) CCL2 concentration measured by ELISA from the supernatant of WT (n = 2 technical replicates) and IRF5 KO (n = 2 technical replicates) Hoxb8 neutrophils. The neutrophils were pretreated with 0.003mM defactinib or DMSO and then stimulated with 10mg/mL Hh sIAg or 25mg/mL zymosan. The supernatant was collected after 2h of stimulation. Two-way analysis of variance (ANOVA) with Sidak correction. Data presented are means ±SD. ns, non significant, $^{*}P \leq 0.05$, $^{**}P \leq 0.01$, $^{***}P \leq 0.001$ and $^{****}P \leq 0.0001$

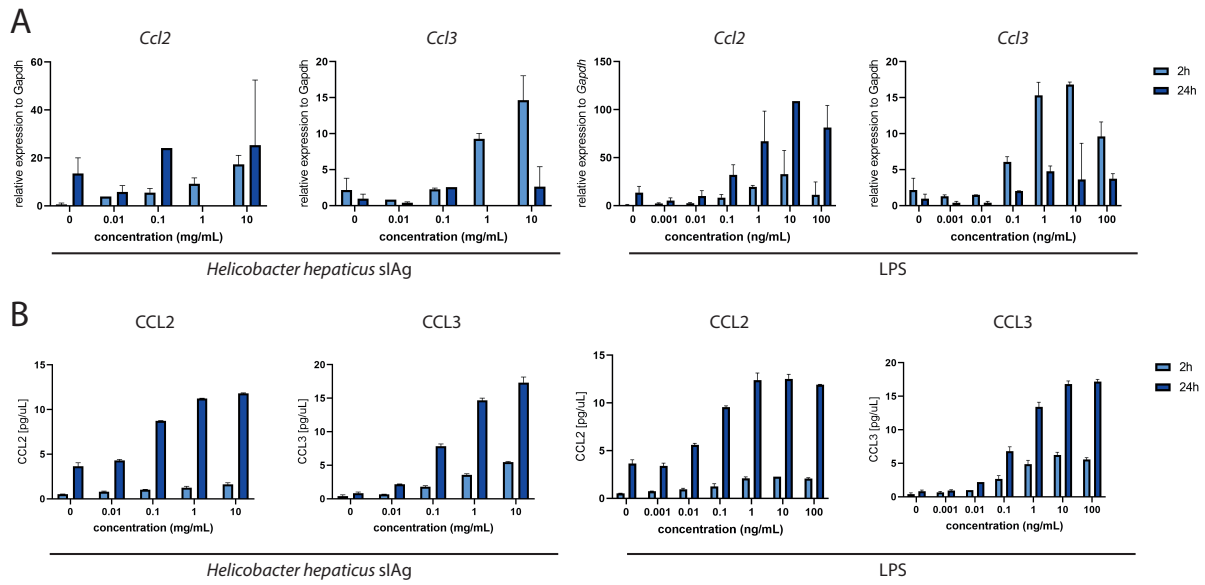


Figure 4.28: **Titration of *Helicobacter hepaticus* sIAg and LPS on Hoxb8 neutrophils.** Hoxb8 neutrophils (n = 2 technical replicates) were stimulated with various concentrations of *Helicobacter hepaticus* sIAg and LPS for 2h (light blue bars) and 24h (dark blue bars) respectively. CCL2 and CCL3 expression/production was assessed via A) RT-qPCR, B) ELISA. Data presented are means ±SD.

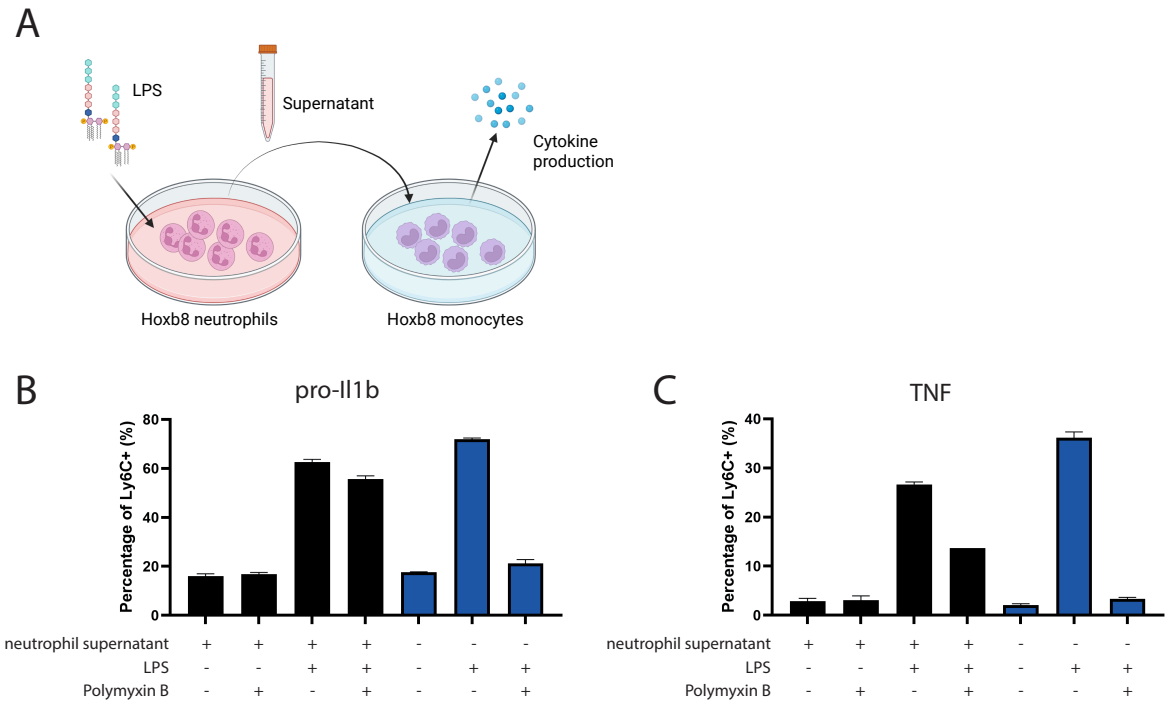


Figure 4.29: **Neutrophils secrete a soluble factor stimulating monocyte pro-inflammatory cytokine secretion.** Hoxb8 neutrophils were stimulated with 1ng/mL LPS for 24h. The supernatant was collected and quenched with polymyxin B where indicated. Hoxb8 monocytes (n = 2 technical replicates) were stimulated with neutrophil supernatant (black bars) or LPS directly (blue bars) for 4h. Cytokine production was assessed with intracellular cytokine staining by flow cytometry. A) Schematic of experimental set-up, B) pro-IL1b production by monocytes, C) TNF production by monocytes. Data presented are means ±SD.

4.3.8 The set-up of an *in vitro* system to study the effects of neutrophils and monocytes in isolation

Monocytes exhibit a significantly altered gene expression landscape in the colon of Ly6G^{Irf5} mice at d7 Hh + aIL10R, despite only neutrophils harbouring an IRF5 deficiency (Figure 4.24c & 4.25c). This raises the question whether in our model, neutrophils are able to prime the monocytes directly or via other cell types/tissue microenvironment. In order to address this, we set out to assess the production of various chemokines and cytokines by neutrophils in a isolated Hoxb8 *in vitro* setting. By titrating a range of LPS and Hh sIAg concentration and assessing the gene expression of *Ccl2, Ccl3, Tnf & Il1b* as well as protein secretion of CCL2 and CCL3 both 2h and 24h post stimulation, we were able to determine a minimum concentration for effective neutrophil stimulation (Figure 4.28a). Interestingly, *Ccl2* was highest induced 24h post stimulation in both LPS and Hh sIAg, whereas *Ccl3* reached its peak expression 2h post stimulation, subsiding at the later timepoint. Protein expression peaked at 24h post stimulation in both CCL2 and CCL3, highlighting time differences in transcription and translation (Figure 4.28b). From this titration, we determined 1ng/mL LPS and 10ng/mL Hh sIAg as the minimum concentration required for effective neutrophil stimulation after 24h. Conveniently, polymyxin B can quench up to 1ng/mL LPS effectively in an *in vitro* setting [249]. As we wanted to investigate the effect of neutrophil stimulation on monocytes without compounding effects of LPS or Hh sIAg, we therefore collected supernatant of 1ng/mL LPS-stimulated neutrophils and quenched it with polymyxin B. This supernatant was put on d2 differentiated Hoxb8 macrophages (timepoint for monocyte-resembling cells in the Hoxb8 macrophage differentiation timeline [Udalova lab, unpublished data]) and compared with directly LPS-stimulated monocytes (Figure 4.29a). Assessing pro-Il1b, TNF, IL6 and IL12p40 via intracellular staining (ICS) in stimulated monocytes, we were able to detect a significant expression of pro-Il1b and TNF in neutrophil-supernatant stimulated monocytes, which was absent in the polymyxin B + LPS direct stimulation (Figure 4.29b, c). This indicates a soluble factor secreted by neutrophils, which is directly

able to alter monocyte protein production. The nature of this factor as well as its relevance *in vivo* will be part of future studies.

4.3.9 Immature neutrophils accumulate in the colons of inflamed mice

To zoom into the heterogeneity of neutrophils present in the inflamed gut, we characterized their maturity both at d7 and d21 Hh + aIL10R colitis. We found a significant accumulation of immature neutrophils in the blood and colon at d7 Hh + aIL10R, mirroring an accumulation of immature neutrophil in the BM (Figure 4.30a-c). Investigation of the differences between Ly6G^{cre} and Ly6G^{Irf5} at d7 Hh + aIL10R revealed the same rise in immature neutrophils in the colon of Ly6G^{cre} mice, whereas Ly6G^{Irf5} mice harboured more mature neutrophils in comparison (Figure 4.31). At d21 Hh + aIL10R, this is even more skewed towards significantly more immature neutrophils in the colon of Ly6G^{cre} mice, despite a similar distribution of neutrophils in the blood (Figure 4.32a, b). Simultaneously, there are no differences between Ly6G^{cre} and Ly6G^{Irf5} at steady state in neither blood nor colon (Figure 4.32a, b). All of these data put neutrophils and their activation/maturation status as crucial players at the onset of inflammation, determining the course of intestinal inflammation.

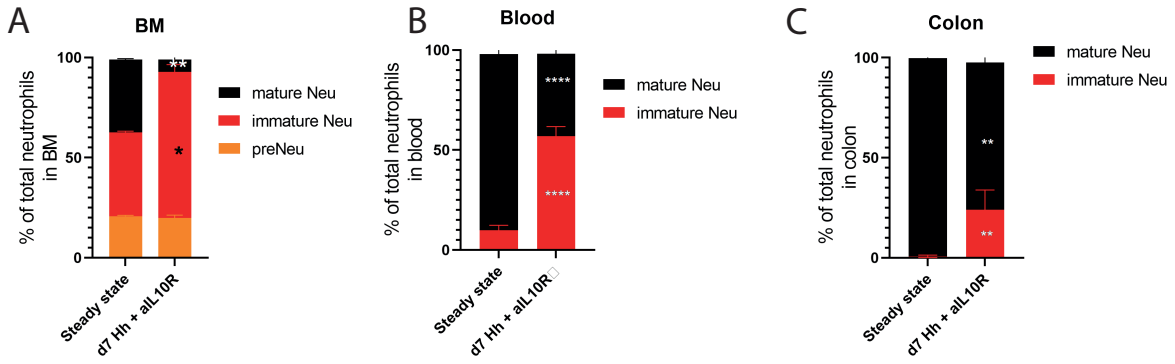


Figure 4.30: **Change in the proportion of neutrophil populations in the inflamed colons of WT mice.** Pre-neutrophils (orange bars), immature neutrophils (red bars) and mature neutrophils (black bars) as percentage of total neutrophils within given tissue at both steady state (n = 3) and d7 Hh + aIL10R (n = 3) in A) bone marrow, B) blood and C) colon. Unpaired t-test. Data presented are means ±SD. *P ≤ 0.05, **P ≤ 0.01, ***P ≤ 0.001 and ****P ≤ 0.0001

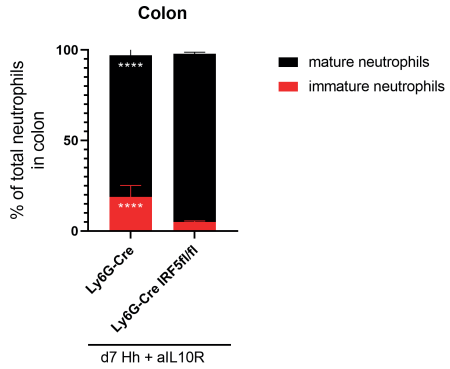


Figure 4.31: **Ly6G^{cre} mice have higher percentages of immature neutrophils in the colon at d7 Hh + aIL10R.** Immature neutrophils (red bars) and mature neutrophils (black bars) as percentage of total neutrophils within the colon in both Ly6G^{cre} (n = 3) and Ly6G^{Irf5} (n = 3) mice at d7 Hh + aIL10R. Two-way analysis of variance with Tukey's corrections. Data presented are means ±SD. ****P $\leq$ 0.0001

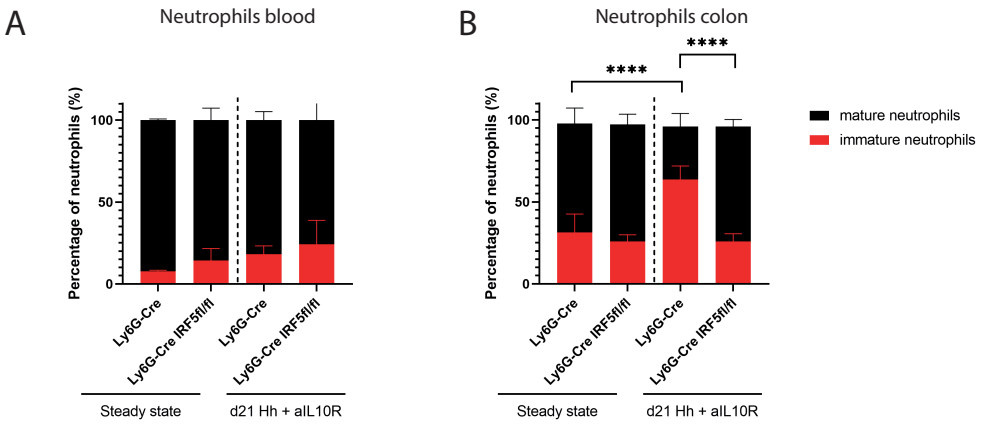


Figure 4.32: **Ly6G^{cre} mice have higher percentages of immature neutrophils in the colon at d21 Hh + aIL10R with unchanged levels in the blood.** Immature neutrophils (red bars) and mature neutrophils (black bars) as percentage of total neutrophils in both Ly6G^{cre} and Ly6G^{Irf5} mice at steady state (n = 2, 3) and d21 Hh + aIL10R (n = 6, 5). A) blood, B) colon. Two-way analysis of variance with Tukey's corrections. Data presented are means ±SD. ****P $\leq$ 0.0001

4.4 Discussion

4.4.1 Depletion of IRF5 leads to a distinct myeloid landscape at the onset of colitis

We found IRF5 to alter the myeloid landscape in the colon already as early as d7 Hh + aIL10R (Figure 4.6). Interestingly, despite no changes detectable in the colon (Figure 4.5a, b), at d4 Hh + aIL10R we were able to detect increases in the production of neutrophils and Ly6C^{hi} monocytes in the BM (Figure 4.5c, d). Differences in Ly6C^{hi} monocytes, neutrophils and Ly6C+ GMPs were found in the BM of all *Irf5-/-*, CX3CR1^{Irf5} and Ly6G^{Irf5} mice with various degrees of expression at d7 Hh + aIL10R (Figure 4.8, 4.11 & 4.21). In *Irf5-/-* and CX3CR1^{Irf5} mice, neutrophils and monocytes were present at lower proportions whilst Ly6C+ GMPs were elevated in the KOs (Figure 4.8 & 4.11). However, in Ly6G^{Irf5} mice, only the proportion of monocytes is signficicantly affected (Figure 4.21). In MBMCs, no differences in reconstitution of hematopoietic stem cells, myeloid progenitors, or Ly6C^{hi} mature monocyte population in the bone marrow was found [129]. *Corbin et al* also found no reconstitution deficiencies of Ly6C^{hi} monocytes in the blood of the MBMC at d21 Hh + aIL10R, and almost no differentially regulated genes between WT and *Irf5-/-* monocytes in a scRNA-seq analysis [129]. In contrast to this, we could see a significantly higher proportion of WT Ly6C^{hi} monocytes at d7 Hh + aIL10R in the blood (Figure 4.7a). This discrepancy may be due to the timepoint analysed, as well as the inflammatory environment being highly skewed in *Irf5-/-* mice early on, whereas MBMCs have the same environment for both WT and *Irf5-/-* mice. Analysing MBMCs at d7 Hh + aIL10R might therefore answer whether the environment or the timepoint is crucial for recruitment of monocytes into the blood and colon of WT mice.

As CX3CR1^{Irf5} mice were already shown to have significant amelioration of colitis at d21 Hh + aIL10R [129], we merely wanted to confirm its protective effect at the onset. Investigation of the early timepoint d7 Hh + aIL10R revealed significant protection by histopathology as well as reduced infiltration of neutrophils and monocytes respectively in CX3CR1^{Irf5} mice (Figure 4.9). However, as CX3CR1 is expressed in many progenitor

populations in the BM (Figure A.1), cell types other than monocyte/macrophages may have IRF5 excised early during their development, leading to a more general knockout of IRF5. *Irf5-/-* monocytes exhibit a development deficiency at the onset of inflammation, with fewer mature monocytes being present in the BM of CX3CR1^{Irf5} mice, in contrast to the heightened production in CX3CR1^{cre} mice (Figure 4.11a). As tissue-resident macrophages in

Irf5-/- mice lack IRF5 expression, their initial signal to recruit neutrophils is likely to be impaired, as reflected in a reduced secretion of chemokines and cytokines [126]. Together, our data on the importance of IRF5 in CX3CR1+ cells at the onset of colitis nicely confirms pre-existing results and further emphasizes the crucial role of macrophages and monocytes in shaping intestinal inflammation.

4.4.2 IRF5 in neutrophils plays an indispensable role in amplifying intestinal inflammation

Using IRF5 as a tool for immune cell activation, we were able to modulate neutrophil and monocyte/macrophage function selectively, without compromising other crucial functions in controlling inflammation. In addition to previous results, we zoomed in on the role of IRF5 in neutrophils specifically, making use of the Ly6G-Cre Flox system [244]. Characterization of the Ly6G-Cre mice revealed Ly6C^{int} CD177- cells in the blood to express high levels of td-Tomato, which was used as a proxy for Cre excision (Figure 4.15b). However, neutrophils were labelled with CD177 in this experiment, and in the blood only about 50% of neutrophils are reliably labelled with this marker at both steady state and inflammation (table 4.1). Together with the analysis of the composition of Ly6C^{int} cells in WT mice using all three neutrophil markers (Figure 4.13b) and using tSNE plots of blood and colon in inflamed Ly6G-Cre ROSA26-tdTomato mice (Figure 4.16), revealed that the Ly6C^{int} population is mainly composed of neutrophils in the blood, and CD177 is not sufficient to separate neutrophils reliably in the blood, whereas it is a superb marker in the colon.

Despite IECs having about 5% Cre-expression, which was also visible in Figure 3.4a, they do not express *Irf5*, which renders their Cre-expression insignificant (Figure 4.17). All in all, Ly6G^{Cre} mice are a highly specific genomic tool for specific modulation of neutrophils also in Hh + aIL10R-mediated colitis.

By dissecting the mechanism through which IRF5 mediates intestinal inflammation, we have uncovered a novel role of neutrophils in recruiting monocytes to the inflamed colon at the onset of murine colitis in a IRF5-controlled manner (Figure 4.19). Also in other models of inflammation, neutrophils have been reported to recruit monocytes. In an airpouch model as well as in cremaster muscle inflammation, neutrophil secretion products were determined as mediators of monocyte recruitment due to significantly reduced numbers of inflammatory monocytes in the inflamed areas of neutrophil-depleted mice [250]. They further showed, alongside other studies, that neutrophil recruitment precedes monocyte recruitment [170, 250–254]. The infiltrating neutrophils adapt their phenotype to suit the changing environment in order to efficiently regulate the subsequent release of chemoattractants [170, 255]. At d4 and d7 Hh + aIL10R, the timepoints at the onset of colitis we investigated, we have not seen a staggered infiltration of neutrophils and monocytes in WT mice (Figure 4.5, 4.6). However, as shown in chapter 3, the distal colon has a distinct infiltration of neutrophils, followed by monocytes. By analysing the colon as a whole, especially at the onset of inflammation, we might lose such fine effects. Additionally, the timescales in the studies mentioned was mere hours, whereas we investigated different days. Nevertheless, as we have shown neutrophils to infiltrate the colon in equal numbers in both Ly6G^{Cre} and Ly6G^{Irf5} mice, whilst monocyte numbers are significantly reduced in Ly6G^{Irf5} mice, we indirectly show that neutrophils precede and even regulate monocyte recruitment (Figure 4.19d, e).

Previous data hinted towards a potential role for *Ccl2* in neutrophils as it was down-regulated in *Irf5-/-* neutrophils both *in vitro* and *in vivo* (Figure 4.26b, 4.25b). The CCL2-CCR2 axis for monocyte recruitment was shown to be even more exclusive during inflammation in a model for sterile SI inflammation [13]. Here, we demonstrate a significant

downregulation of *Ccl2* expression in the LP enriched fraction of Ly6G^{Irf5} mice at d7 Hh + aIL10R, which is due to its lower expression in neutrophils specifically (Figure 4.25b, c). However, at d7 Hh + aIL10R, immature CD101- neutrophils are present in much higher proportions in the colon than their mature CD101+ counterparts (Figure 4.30c). Whether the levels of *Ccl2* in immature neutrophils is higher or lower than their mature counterparts therefore remains to be addressed, as their contribution to the overall *Ccl2* levels will be significant. Human neutrophils isolated from the blood or synovial fluid of RA patients stimulated with both LPS and IFN-γ produce CCL2 [256]. However, in a study where neutrophils were isolated from the blood with F4/80- and bright Gr-1, *Irf5-/-* neutrophils secreted less CCL2 than their WT counterparts only in response to TLR9, whereas TLR2 and TLR4 stimulation produced comparable levels [237]. This is in contrast with our results showing *Irf5-/-* neutrophils stimulated both with zymosan (TLR2) and Hh extract (TLR2/TLR4) producing significantly less CCL2 (Figure 4.27a, b). This discrepancy could be due to different sources of neutrophils used, as blood isolated neutrophils and Hoxb8-stimulated neutrophils may react slightly differently to stimuli. In previous studies, IRF5-mediated inflammatory cytokine production following TLR stimulation has varied widely with the cell types studied [156, 257]. Therefore, studying the effect *in vivo*, where multiple stimuli might interact and activate IRF5, may be the only way to untangle the complex TLR-IRF5 interactions. In another model of inflammation, HFD-induced vascular inflammation, neutrophils were found to be the mediators of monocyte recruitment to the artery via their CCL2 production [251]. They identified the complement component C5a as a crucial regulator of vascular inflammation, as its addition alone induced leukocyte recruitment via stimulation of neutrophils to produce CCL2 [251]. A similar mechanism could be at play in the intestine, as complement components have recently gained significant attention due to their various functions in regulating gut motility and tuning inflammatory responses of epithelial cells [258, 259].

A distinct change in the colonic tissue microenvironment, reflected both in neutrophils and monocytes was found in Ly6G^{Irf5} mice at d7 Hh + aIL10R (Figure 4.24 & 4.25). Despite

Irf5 only being downregulated in neutrophils (Figure 4.18), the gene expression landscape in monocytes is dramatically altered in in Ly6G^{Irf5} mice (Figure 4.24c & 4.25c). Monocytes are highly plastic cells, acquiring a tissue-specific gene expression profile upon extravasation from the blood [14]. Investigation of direct priming on monocytes by neutrophils in a sophisticated *in vitro* system revealed the presence of a soluble factor, secreted by activated neutrophils, that is capable of altering monocyte gene expression. The nature of this factor, and whether cell-cell direct contact could trigger a distinct set of receptors, remains to be investigated in future experiments. The altered tissue microenvironment and/or direct priming by neutrophils leads to a distinct macrophage landscape at d21 Hh + aIL10R colitis (Figure 4.23f). Neutrophil-derived azurodicin was shown to attract and polarise monocytes towards M1 macrophages (CD11c+ macrophages) *in vivo* [250, 260]. Whether or not this priming is directly IRF5-mediated needs to be further investigated, as well as if it is one factor mediating these changes in monocyte gene expression or several.

Using a panel separating mature and immature neutrophils on the basis of CD101+ and CD101-, we were able to detect a massive increase in immature neutrophils already at d7 Hh + aIL10R in the BM, which runs like a red thread through the blood to the inflamed colon (Figure 4.30a-c). Here, we showed neutrophil numbers were unaffected in the colon of Ly6G^{Irf5} mice at d7 Hh + aIL10R (Figure 4.19d); however the IRF5 deletion most likely still affects their phenotype, since we know neutrophil populations to be heterogeneous in disease settings [89, 92, 261]. Different subsets of neutrophils have been identified in human IBD patients, which were could be discriminated on the basis of CD177 expression, which is uniquely expressed in neutrophils and upregulated during inflammation [92]. By analysing CD177+ and CD177- neutrophils isolated from the blood of IBD patients, they were able to determine significantly lower pro-inflammatory gene expression in CD177+ neutrophils [92]. In a model of DSS colitis, *Cd177-/-* mice had more severe colitis and a compromised epithelial barrier, which they led back to a beneficial increased IL-22 secretion by CD177+ neutrophils [92]. An expansion in CD77+ neutrophils in both blood and mucosa was detected in IBD patients, similar to our data

showing a significant increase in CD177+ immature neutrophils at d21 Hh + aIL10R in the colon (Figure 4.32b). Interestingly, we were not able to detect any changes in neutrophil populations in the blood (Figure 4.32a), indicating a change in their markers and potentially gene expression upon transmigration into the inflamed tissue. Furthermore, in the colon of Ly6G^{Irf5} mice, more mature and less immature neutrophils were detectable at d21 Hh + aIL10R, hinting towards distinct functions of mature and immature neutrophils in intestinal inflammation (Figure 4.32b). As there are already significant differences in immature neutrophil populations at d7 Hh + aIL10R between the genotypes (Figure 4.31), shaping of the recruited neutrophil populations by the tissue microenvironment could be a further mechanism of disease [255]. The function of the different neutrophil subsets over the course of intestinal inflammation, as well as differences of said subpopulations between Ly6G^{cre} and Ly6G^{Irf5} mice remain to be determined. Investigation of the gene expression changes in the neutrophil (subsets) upon extravasation into the inflammatory intestinal environment could also point towards novel targets for modulation of neutrophil function.

Not many genes are differentially expressed in male and female immune cells, yet males have more frequent and severe infectious diseases and females are more prone to develop autoimmune diseases [262]. Characterization of sex differences by both ATAC-seq and RNA-seq revealed few differentially expressed genes, except in macrophages. This transcriptional sexual dimorphism in macrophages is mediated by genes of innate immune pathways, and increases after interferon stimulation [262]. Differences in *Irf5* expression levels have been reported between male and females [263, 264], therefore we extended our studies to compare the effect between sexes. Furthermore, IRF5 levels were shown to be higher in females of both mice and humans [263, 264]. The partial protection of female mice in DSS colitis was shown to be mediated by estradiol [265]. IRF5 was found to be induced by estradiol receptor α stimulation, leading to its translocation into the nucleus and subsequent transcription of pro-inflammatory cytokines [263]. This is further supported by the notion that deletion of the estrogen receptor reduces *Irf5* in pDCs [264]. Investigation of a potential confounding effect of sex on the onset of colitis led to the discovery of profound sex differences between

males and females at d7 Hh + aIL10R colitis. Females exhibited significantly higher levels of neutrophils and monocytes, making it also impossible to see differences between WT and Ly6G^{Irf5} (Figure A.2a, b). At d21 Hh + aIL10R however, sex differences between males and females were not visible anymore (Figure A.2c). This is supported by the fact that experiments with WT and *Irf5-/-* were repeated with both males and females in *Pandey et al* without seeing any noticeable effect [169]. We have not investigated the interplay between the genotypes and sexes at d21 Hh + aIL10R in Ly6G^{cre} and Ly6G^{Irf5} mice, however as there were no differences visible at d21 Hh + aIL10R in WT mice, redundant responses over the course of inflammation might mask the early sex difference seen in this experiment.

Neutrophils and monocyte/macrophages are fundamental in shaping the subsequent adaptive immune response by generating a corresponding tissue microenvironment, recruiting other immune cells and presentation of antigens to adaptive immune cells [170]. At d7 Hh + aIL10R, the myeloid compartment is highly expanded, whereas non-myeloid (lineage+ CD11b+) cells begin to expland later during the infection (Figure 3.2b). As IRF5-deficient macrophages have a distinct transcriptomic profile, their antigen presentation might differ from their WT counterparts, resulting in a altered adaptive immune response. Given the differences in macrophage subsets at d21 Hh + aIL10R in Ly6G^{Irf5} mice, it is tempting to speculate that different Th1/Th17 to Treg ratios might be present compared to Ly6G^{cre} mice. The effect of IRF5 depletion in neutrophils and/or monocyte/macrophages on the adaptive immune response remains to be further explored, but is bound to have a significant effect.

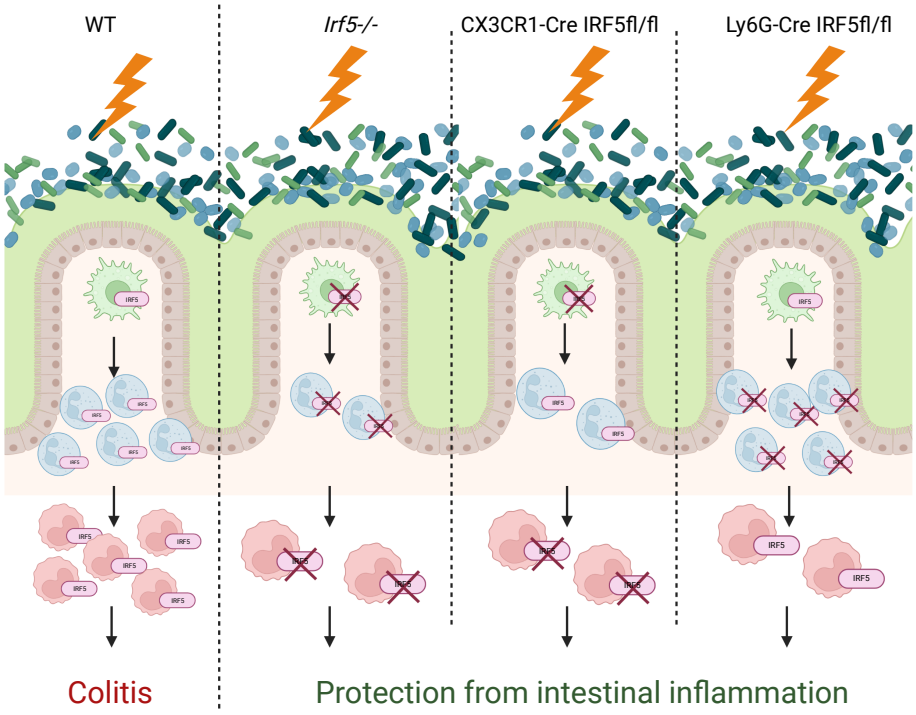


Figure 4.33: **Model for the onset of colitis in WT, *Irf5-/-*, CX3CR1^{Irf5}, Ly6G^{Irf5} mice.** *This figure was generated using Biorender.*

4.5 Conclusion

Here, we characterized the roles of neutrophils and monocytes/macrophages in orchestrating the onset of intestinal inflammation in light of the master TF IRF5. By using cutting-edge genomic mouse models, we were able to dissect the mechanism by which IRF5 sets up the inflammatory microenvironment, leading to chronic inflammation in the case of IBD. A novel role for IRF5-proficient neutrophils in recruiting monocytes via secretion of CCL2 has been identified, which is a "stop or go" signal at the onset of colitis. Furthermore, by characterizing the onset of colitis across BM, blood, spleen and colon, we provide a comprehensive overview of the changes within progenitor populations as well as migration and recruitment of myeloid cells via the blood to the colon and systemic sites like the spleen. By comparing the effects of IRF5 at the onset of colitis on neutrophils and monocytes/macrophages separately, we were able to discern the inflammatory cascade in more detail, allowing for selective targeting of individual cell types (Figure 4.33). Using CX3CR1^{Irf5} mice, we uncovered tissue-resident macrophages at the top of the hierarchy, their initial signal being responsible for recruitment of the first wave of neutrophils at d7 Hh + aIL10R. Neutrophils are second in the inflammatory cascade, as Ly6G^{Irf5} neutrophils are recruited in a similar manner, but fail to recruit the second wave of inflammatory Ly6C^{hi} monocytes.

The data presented here highlight the importance of neutrophils in intestinal inflammation and their capability to orchestrate the host response in concert with other myeloid cells like monocytes and macrophages. By modulating their activation instead of crude deletion of neutrophils, we conserve their essential functions in controlling the infection whilst preventing augmentation of the inflammation through monocyte recruitment. Further research into the exact mechanism by which neutrophils modulate monocyte gene expression might offer further insight into the aetiology of IBD. Targeted modulation of neutrophil activity may lead to the development of a new class of therapeutic strategies, based on selective modulation of neutrophil biology, to combat pathological inflammation and associated inflammatory disorders like IBD.

4.6 Future directions & limitations

Next steps should focus on proving a clear neutrophil-CCL2 causality, we aim to develop a sophisticated *in vitro* system assessing monocyte recruitment in absence of additional cell types other than WT and IRF5 KO Hoxb8 neutrophils. This system will incorporate migration of Hoxb8 monocytes towards neutrophil stimulated media in transwell plates, in the presence and absence of a CCL2 inhibitor (Figure A.3). Additionally, *in situ* staining of CCL2 could confirm its presence in neutrophils as well as intracellular staining of CCL2 using flow cytometry. Potential further neutrophil mediators in shaping monocyte responses, identified in abovementioned scRNA-seq could also be tested in this *in vitro* system. The most potent mediators would be confirmed *in vivo* and could provide novel targets in preventing or altering the onset of intestinal inflammation in IBD patients.

As uncovered in chapter 3, neutrophils and monocytes have distinct infiltration patterns at the onset of Hh + aIL10R colitis in WT mice. Further research should therefore also investigate if and how the spatial recruitment changes in CX3CR1^{Irf5} and Ly6G^{Irf5} mice in comparison to WT mice, offering the potential for additional differences masked by analysis of the colon as a whole. Further analysis of spatial interactions could be done using spatial transcriptomics on colonic swiss rolls in order to capture changes along the entire length of the colon.

One of the limitations of this study is the lack of comparative data in this model in regards to the importance of neutrophils for overall pathogenesis in Hh + aIL10R colitis. The pathology of Ly6G^{Irf5} mice should be compared to mice depleted of neutrophils in order to investigate onset and progression of intestinal inflammation. So far, neutrophils have been painted both as immunopathology-supporting cells [240] as well as having a beneficial role during colitis, promoting mucosal repair processes [241, 242]. Depletion of neutrophils might therefore have a more wide-ranging effect, making it difficult to dissect the exact mechanism by which neutrophils mediate the onset of disease. Nevertheless, depletion of neutrophils with a combination of α-Ly6G and α-rat antibodies [266] or in

a DTR model using diphteria toxin [267] would provide a baseline on which to put the effects of IRF5-regulated effects of neutrophil biology.

Further limitations are the previously mentioned sex-effect at the onset of Hh + aIL10R-mediated colitis, leading us to the use of males only for our studies. The mice were age-matched as closely as possible to not confound experiments due to differently developed immune systems. As the mice were not littermates, they were not cohoused, offering the possibility of a potential microbiome effect. To address this, the mice were cohoused in the subsequent chapter and colitis outcome assessed.

A study comparing the importance of neutrophils in three different models of colitis has found beneficial and detrimental effects of neutrophil depletion depending on the model (and therefore the trigger for intestinal inflammation) [268]. This highlights the importance of testing the role of IRF5 in neutrophils also in other models in order to determine its potential for therapeutic targeting.

All in all, our data highlight the importance of the interplay between neutrophils and monocytes/macrophages at the onset of intestinal inflammation, setting the stage for either resolution of inflammation or progression to chronic intestinal inflammation. Understanding the mechanism thereof will provide useful and novel therapeutic targets for IBD therapy.

5

IRF5-dependent neutrophil-microbiota crosstalk at the onset of intestinal inflammation

Contents

5.1 Crosstalk between neutrophils and the microbiota 148
5.1.1 Regulation of neutrophils by the microbiome 150
5.1.2 Neutrophil responses toward the microbiota and gut infection . . 151
5.2 Aims 154
5.3 Results 156
5.3.1 IRF5-deficient neutrophils are not deficient in clearing SPI-2 deficient *Salmonella in vivo* 156
5.3.2 IRF5-deficient neutrophils produce more lipocalin 2 161
5.3.3 IRF5-deficiency in neutrophils leads to inflammation in cohoused mice 164
5.3.4 Higher Lcn2 levels in the cecum of cohoused Ly6G^{Irf5} mice . . . 167
5.3.5 Hh colonisation does not account for the differences between genotypes 167
5.3.6 Metagenomic microbiome sequencing reveals differences in overall microbiota composition 170
5.3.7 Dysbiosis ratios not altered between inflamed and protected conditions 173
5.3.8 Differences at steady state between cohoused and separately housed mice 175
5.3.9 Specific microbiota species are associated with inflammation status independently of the genotype of the mice 178
5.4 Discussion 180
5.4.1 The ability of *Irf5-/-* neutrophils in controlling pathogen infection 180
5.4.2 The effect of microbiome composition on IRF5 function in neutrophils 181
5.5 Conclusion 186
5.6 Future directions & limitations 186

5.1 Crosstalk between neutrophils and the microbiota

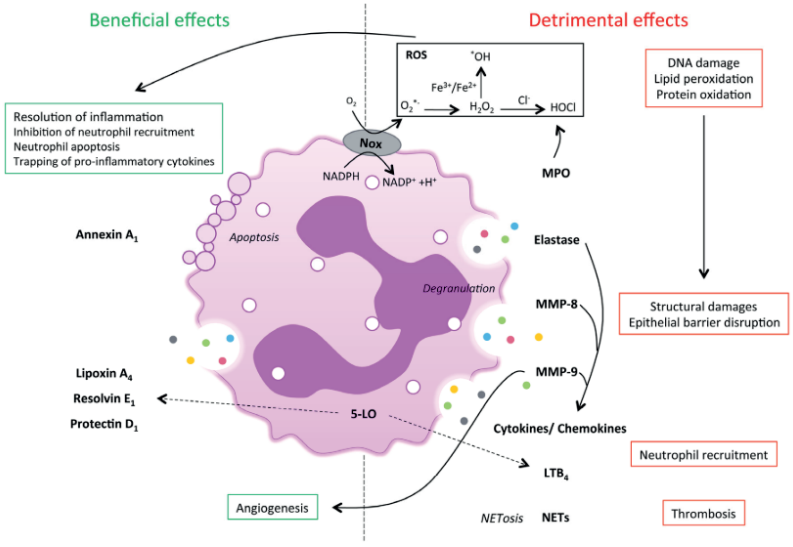


Figure 5.1: **The double-edged sword of neutrophils.** Figure taken from *Wera et al* [149]

Host-microbiome interactions educate the intestinal immune system and shapes microbiota composition. The microbiome has emerged as an important regulator of the host immunity by priming and functionally modulating local and systemic immune responses [269–271]. Translocation and fine tuning of the composition and distribution of the microbiota is in turn regulated by the intestinal immune system [272]. The depletion of the mucosal barrier in UC and CD leads to an elevated mucosa-bacterial interaction, which can either be cause or consequence of intestinal inflammation [273]. Alterations in the microbiome contribute among other factors to the development of intestinal inflammation [274]. As described in chapter 1.1.2.2, several changes in the microbiome composition have been associated with inflammation and dysbiosis. By comparing different microbiomes in their ability to trigger DSS-mediated colitis, it was found that different inflammatory responses were

raised depending on the respective microbiota composition [275]. Specific host-microbiome interactions therefore drive colitis development via different mechanisms, rendering colitis an even more heterogeneous disease than previously thought. Despite the higher complexity of host-microbiome interactions in humans, in part underlied by their genetic variability, studying microbial interactions in rodents might inform us on disease-driving relations and how to circumvent them. The importance in defining a immunologically relevant microbiome is therefore crucial in identifying mucosal responses critical for maintaining homeostasis and disruption thereof in IBD [276].

Neutrophils are the first immune cells to be recruited to the site of inflammation and are essential in limiting invasion by microorganisms [149]. A dysregulation in the fine-tuned neutrophil function can therefore be detrimental for disease progression into chronic inflammation, rendering neutrophils a double-edged sword [95] (Figure 5.1). The microbiota is a major driver in IBD pathogenesis, highlighting the delicate balance between microbes and host defensive responses at the mucosal interface [118]. The crosstalk between neutrophils and the microbiota is a crucial mediator in adjusting the magnitude of neutrophil-mediated inflammation whilst preventing their activity against commensals [269]. Indication of the importance of neutrophils also lies in the pathogenesis of UC and CD, which are marked by two extremes in neutrophil function: UC features a massive accumulation of neutrophils, whose presence in the stool correlates with active disease [277], and is used as a marker for severity in UC trials [239]. On the other hand, CD exhibits defects in neutrophil recruitment [278–281], however the neutrophils themselves are competent [281].The oxidative burst of neutrophils during inflammation leads to a decrease in tissue oxygenation, further resulting in a change in microbiota by favouring strictly anaerobic species [282]. Indeed, the microbiota is less diverse in both UC and CD, with disease- and site-specific changes in compositions [283]. Neutrophil-derived mediators as well as neutrophils themselves therefore are crucial in modulating the microbiota and ensuring homeostasis.

5.1.1 Regulation of neutrophils by the microbiome

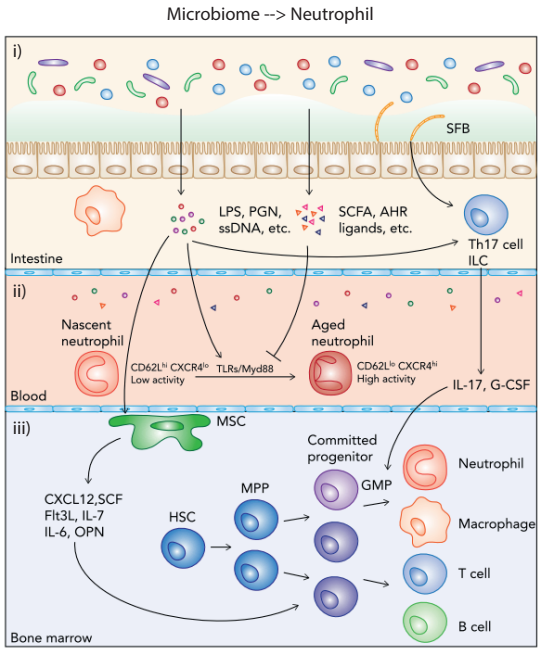


Figure 5.2: **Microbiome-mediated modulation of neutrophil recruitment and function.** i) microbial components as well as direct contact of specific species induce IL-17 and G-CSF, a master regulator of neutrophil production in the BM. ii) microbial products and metabolites diffused in the blood directly regulate functions of circulating neutrophils. iii) microbial products sensed by mesenchymal stem cells (MSC) stimulates production of cytokines supporting neutrophil lineage differentiation from HSCs. Figure taken from *Zhang et al* [269].

Reduction or absence of the microbiota has a profound effect on neutrophil numbers and renders mice susceptible to subsequent infections [284–287]. Direct priming of the BM niche by the microbiota via NOD1 ligands was shown to affect neutrophil numbers [288]. Furthermore, low doses of intravenously administered LPS are sensed in the BM, leading to a rapid mobilization of the resident neutrophils and monocytes [289]. Upon challenge, GF mice secrete higher amounts of IL-10, which results in a reduced neutrophil recruitment [290, 291]. This effect can be reversed by pre-priming the mice with low doses of LPS, restoring neutrophil recruitment to the level of SPF mice [291]. Furthermore, neutrophils

isolated from GF mice have impaired function, like reduced MPO levels and chemotaxis, as well as a reduction in phagocytic killing of pathogens, which was also reversible by pre-priming with LPS [292–294]. Additionally, fewer aged neutrophils can be found in GF mice, leading to a less robust response against an infection [295].

Microbiota-derived metabolites influence a broad range of cells and are relevant for host physiology and disease [270, 271]. In macrophages, especially SCFAs and bile acids were highlighted as modulators of their functions in the colon [10]. SCFAs have contradictory effects in neutrophils, on one hand SCFA-mediated HDAC inhibition downregulates NF-kB signalling in neutrophils, also inducing apoptosis [296–298], on the other hand, signalling via GPR43 promotes ROS production and enhances phagocytosis [299, 300]. In multiple models of colitis, *Gpr43-/-* mice exhibited exacerbated inflammation, partly due to high neutrophil infiltration [301]. In WT mice, neutrophil migration could be dampened via addition of acetate, which highlighted the signalling of SCFA through GPR43 in neutrophils, directly modulating their recruitment [299]. No direct effect of bile acids on neutrophils has been shown so far, however bile acids were shown to mediate an anti-inflammatory environment via MNPs and other cells, which suppresses neutrophil recruitment and activation [302, 303]. Host-derived AHR ligands suppress chemotaxis in neutrophils during inflammation [304, 305]. Whether microbe-derived AHR ligands also directly communicate with neutrophils remains unknown.

These findings highlight the important role of the microbiota in modulating and tailoring neutrophil recruitment and functions (Figure 5.2).

5.1.2 Neutrophil responses toward the microbiota and gut infection

Neutrophils are implicated in the containment of pathobionts by transluminal migration. They can also generate so-called "luminal casts", organized structures which prevent direct contact with the epithelium and produce high amounts of ROS [306]. Discrimination of commensals and pathogens was proposed to occur via the NLRC4 inflammasome, cleaving

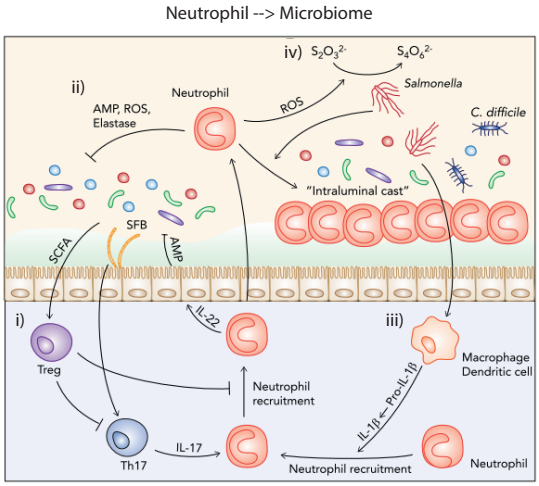


Figure 5.3: **Neutrophil-mediated modulation of the microbiome.** i) regulatory network induced by the microbiota suppresses neutrophil recruitment at steady state. ii) IL-22 production by neutrophils lead to the release of AMPs by IECs as well as by neutrophils. iii) pro-IL1b secreted by macrophages get cleaved into their active form through triggering of the NLRC4 inflammasome by pathogens, resulting in neutrophil recruitment. iv) neutrophils produce ROS and siderophores to limit pathogen growth, however certain pathogens have evolved to take advantage of netrophil-mediated defense mechanisms. Figure taken from *Zhang et al* [269].

---

the high amounts of pro-IL1β secreted by resident cells upon pathogen encounter, leading to a rapid recruitment of neutrophils [307]. Recruitment of neutrophils depends on their chemokine receptor CXCR2, which was shown by use of *Cxcr2-/-* mice [308, 309]. These mice further displayed significant shifts in the microbiome [310, 311], as well as a higher susceptibility to infections [308, 309], highlighting the role of neutrophils in modulating the microbiome as well as fighting off pathogens. Upon early recruitment of neutrophils, IL-23 is thought to stimulate IL-22 production by neutrophils [213]. This leads to the release of RegIIIβ and RegIIIγ in IECs, which in turn regulates the microbiota by selectively killing susceptible members [213, 312]. Despite the similarities in expression, regulation and structure of the homologues RegIIIβ and RegIIIγ, they appear to have distinct bactericidal activity [313]. By binding to lipid A, RegIIIβ is specialized for killing gram-negative bacteria, whereas RegIIIγ recognizes peptidoglycan on gram-positive bacteria [314, 315]. Furthermore,

neutrophils store large quantities of AMPs in granules, which are quickly released upon pathogen encounter, leading to a fine regulation of the microbiome composition [269]. Examples of such granule-containing proteins are azurodicin, MPO, neutrophil elastase, lipocalin 2 (Lcn2) and lactoferrin (LF) [316] (Figure 5.3).

In IBD patients, there is an increased ratio of lactoferrin to MPO, as well as an imbalance between ROS and antioxidants, hinting towards a dysfunction of neutrophils [317, 318]. LF and Lcn2, two neutrophil-derived siderophores, which limit the growth of iron-dependent bacteria, are elevated in IBD patients [317, 319]. Whilst LF was shown to restore dysbiosis induced by antibiotics [320], Lcn2 is used as a disease activity marker in UC [319].

The neutrophil response towards inflammation is tightly regulated, and either beneficial or detrimental depending on the context. Depletion of neutrophils therefore will not be protective against intestinal inflammation as the antimicrobial action of neutrophils is required to clear the infection. In fact, depletion of neutrophils with a Ly6G-depleting antibody in different microbiota compositions did not have an impact on colitis outcome, highlighting the importance of their antimicrobial activities on the resolution of inflammation [275]. Modulation of neutrophil function rather than crude depletion might be a tool to shape microbiota composition in a way that might prevent or resolve intestinal inflammation. Understanding how to modulate neutrophil function to tease out the protective effects without any drawbacks might therefore be a novel therapeutic avenue, hinged on understanding the exact molecular mechanisms of the neutrophil-microbiota crosstalk.

IRF5 is a TF being activated by signalling through different PRRs, via MyD88, and is therefore right at the beginning of the inflammatory cascade, having a similar activation pathway as NF-κB [150]. In chapter 4, we have uncovered the protective role of IRF5-deletion specifically in neutrophils as the bottleneck of intestinal inflammation. Mechanistically, it was led back to the altered cytokine profile secreted by *Irf5-/-* neutrophils, leading to a reduced recruitment of inflammatory monocytes. However, IRF5 also has an impact on phagocytosis in neutrophils, as was uncovered by studying the effects of different TFs in neutrophils specifically [165]. Neutrophils isolated from *Irf5-/-* mice were defective

in their ability to clear intracellular bacteria *ex vivo*, as well as production of ROS and RNS production following TLR4 stimulation [169]. In contrast to this, IRF5 KO Hoxb8 neutrophils were not impaired in their ability to produce ROS or phagocytose gram-negative pathogens *in vitro* [165]. In order to clear up this discrepancy, we aimed to compare the effects of neutrophils and their respective modulation of the microbiota directly *in vivo* following an inflammatory stimuli. Furthermore, as IRF5 provides a small modulation of the neutrophil function, it may be a potential avenue for targeting, rendering the neutrophils mostly functional.

5.2 Aims

We aim to investigate the effect of the microbiome on neutrophil-function and *vice versa* by focusing on a small modulation of neutrophil function; depletion of IRF5. As GF and Abx mice do not develop colitis, we cohoused Ly6G^{cre} and Ly6G^{Irf5} mice to generate a hybridised changed microbiome and studied the effects of IRF5-deletion in neutrophils at the onset of intestinal inflammation. Simultaneously, we assessed the phagocytosis ability of Ly6G^{Irf5} mice in a pathogen-driven acute infection model. We hypothesize that due to the effect of IRF5 on phagocytosis in neutrophils, the microbiome will be altered in Ly6G^{Irf5} mice, potentially exacerbating or limiting the protective effect of IRF5-deletion in neutrophils in an inflammatory setting. Using a bulk-RNA sequencing dataset from a mixed bone marrow chimera, we aim to investigate differential gene expression by *Irf5-/-* neutrophils to uncover potential mechanisms (Figure 5.4).

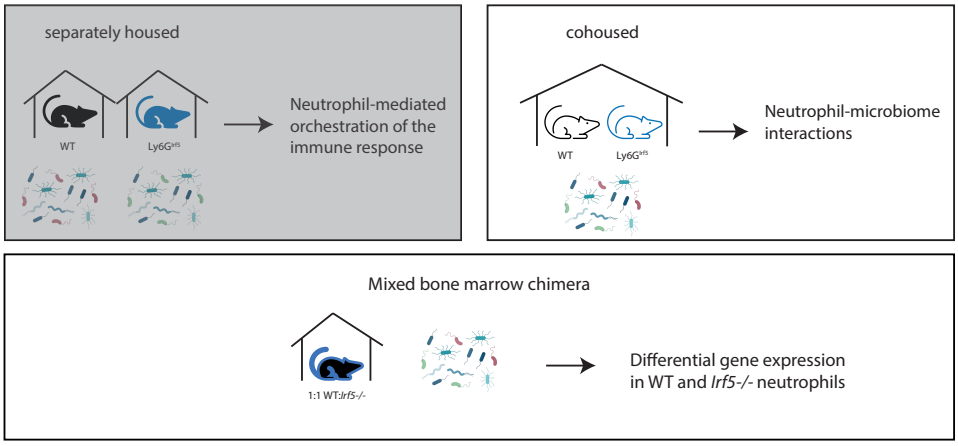


Figure 5.4: **Experimental set-up chapter 5.**

5.3 Results

5.3.1 IRF5-deficient neutrophils are not deficient in clearing SPI-2 deficient *Salmonella in vivo*

As *Irf5-/-* neutrophils exhibit a deficiency in phagocytosis [165, 169], we wanted to investigate their ability to clear the upgrowth of a pathogen. The S. Tm model of disease is a well-established host-pathogen model, used by both microbiologists and immunologists to study different aspects in bacterial and host responses to mucosal infection [173]. The resident microbiota provides protection against S. Tm infection, by a mechanism termed 'colonisation resistance' [46]. This colonisation resistance is broken by pretreatment with the antibiotic streptomycin [173]. S. Tm then rapidly grows up to high bacterial loads, spreading systemically from the intestine, leading to the death of its immunocompromised host. S. Tm has two pathogenicity islands (*Salmonella* pathogen island, SPI) and type III secretion systems (T3SS), SPI-1 and SPI-2. SPI-1 encodes genes important for the invasion of IECs and triggering of pro-inflammatory immune responses, whereas SPI-2 is crucial for hijacking and intracellular survival within IECs and phagocytes. Phagocytes are being used by S. Tm as trojan horses for spreading to the mLN and further systemic sites [176].

Previously, IRF5 has been reported to be important for *in vivo* clearance of S. Tm, in both *Irf5-/-* and LysM-Cre IRF5fl/fl, the latter of which targets both neutrophils and macrophages. Furthermore, neutrophils isolated from *Irf5-/-* mice showed impaired bacterial killing and phagocytosis *in vitro* [169]. Since *Pandey et al* saw differences in bacterial clearance only from day 4 onwards, we wanted to find a model which allowed us to monitor the mice over a longer period of time. SPI-2 deficient S. Tm trigger the gastrointestinal disease as seen with WT S. Tm, however their ability to survive intracellularly is impaired, leading to a contained gastrointestinal disease rather than a systemic one [176].

WT and Ly6G^{Irf5} mice were pretreated with streptomycin and then infected with SPI-2 deficient mutant S. Tm ΔssaD. Feces and weights were collected daily and the colony forming units (CFU) values in the mLN, spleen and liver were analyzed at d5 post infection (p.i.). By assessing the CFU values of the feces over the course of the infection, we were

able to detect significantly lower CFUs in the feces of Ly6G^{Irf5} mice (Figure 5.5a, b). Simultaneously, *Irf5-/-* mice, which were included as a control for differences to *Pandey et al*, showed no differences in fecal CFU counts to the WT (Figure 5.5a, b) [169]. Interestingly, the lower fecal CFU values were associated with a weight loss in Ly6G^{Irf5} mice, which was not recovered over the course of the infection (Figure 5.5c, d).

No significant differences in the CFU counts in mLN, spleen and liver were found between WT and Ly6G^{Irf5} mice at d5 p.i, although there was a trend towards lower CFU counts in Ly6G^{Irf5} mice in mLN and spleen (Figure 5.6a-c).

To assess the number of intracellular bacteria taken up by either IECs or phagocytes within the cecal tissue, we performed a gentamicin protection assay, which kills off all extracellular bacteria. There seemed to be a trend towards higher CFU values in the cecum of Ly6G^{Irf5} mice, however it was not statistically significant due to the low numbers of usable samples (Figure 5.6d). Furthermore, the cecal tissue was analysed via flow cytometry to assess the presence of different immune cell populations during infection, however no significant differences were detectable (Figure 5.7a-f). The lower CFU counts in Ly6G^{Irf5} mice as well as no differences in any organs or immune cells investigated led to the conclusion that *Irf5-/-* neutrophils are not deficient in killing SPI-2 deficient S. Tm *in vivo*. However, it was uncovered that SPI-2 deficient and WT *Salmonella* Typhimurium have distinct infection profiles [Hardt lab, unpublished data], which may explain the differences seen in regards to *Pandey et al*. It also further questions whether IRF5-deficient neutrophils might in fact have a deficiency in clearing a pathogen nevertheless, which may be masked by the SPI-2 deficiency of S. Tm in this experiment.

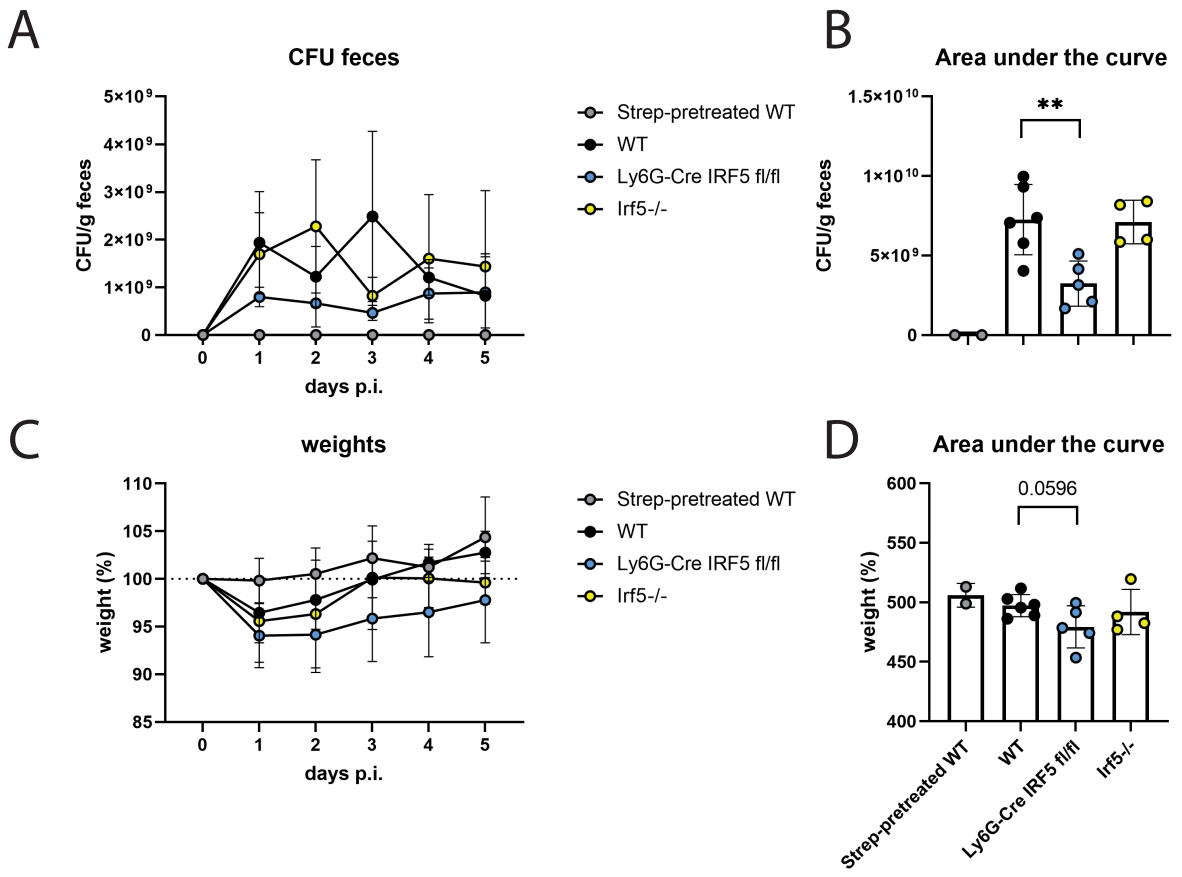


Figure 5.5: **Ly6G^{Irf5} mice have lower CFU values over the course of *Salmonella* Typhimurium infection.** A) Pathogen loads as colony forming units (CFU) of mice infected with 5*10^7 CFU S. Tm by gavage (n = 2, 6, 5, 4) over the course of a 5 day infection. Mixed-effects analysis. B) Area under the curve for CFU/g feces. Unpaired t-test. C) Weight as % of original weight over the course of a 5 day infection. Mixed-effects analysis. D) Area under the curve for weights. Unpaired t-test. Data presented are means ±SD. $^{**}P \leq 0.01$ and $^{***}P \leq 0.001$

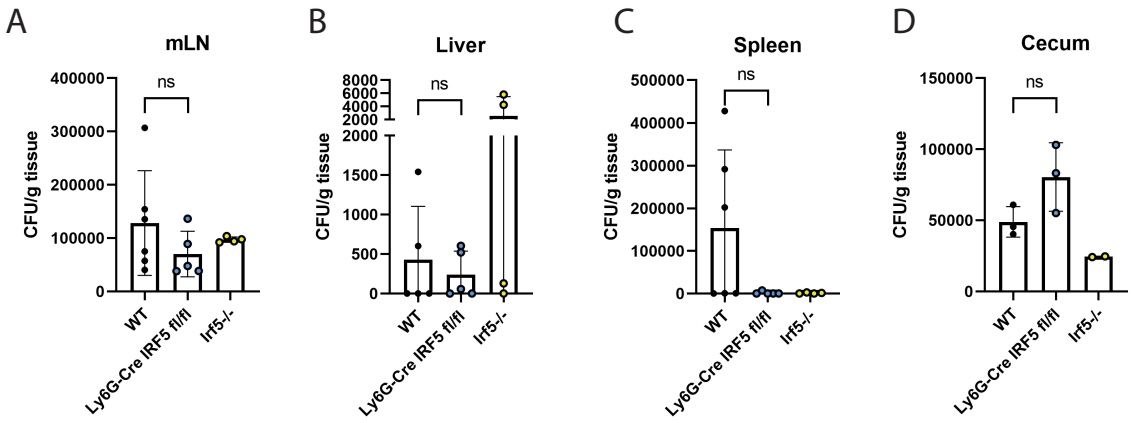


Figure 5.6: **No differences in bacterial loads of systemic organs and the cecum at d5 p.i.** Tissue of WT (n =6), Ly6G^{Irf5} (n = 5) and *Irf5-/-* (n = 4) was assessed for pathogen load via colony forming units (CFU) at d5 p.i. with 5*10^7 CFU S. Tm A) mLN, B) Liver, C) Spleen, D) Gentamicin-treated cecum. Unpaired t-test. Data presented are means ±SD. ns, not significant.

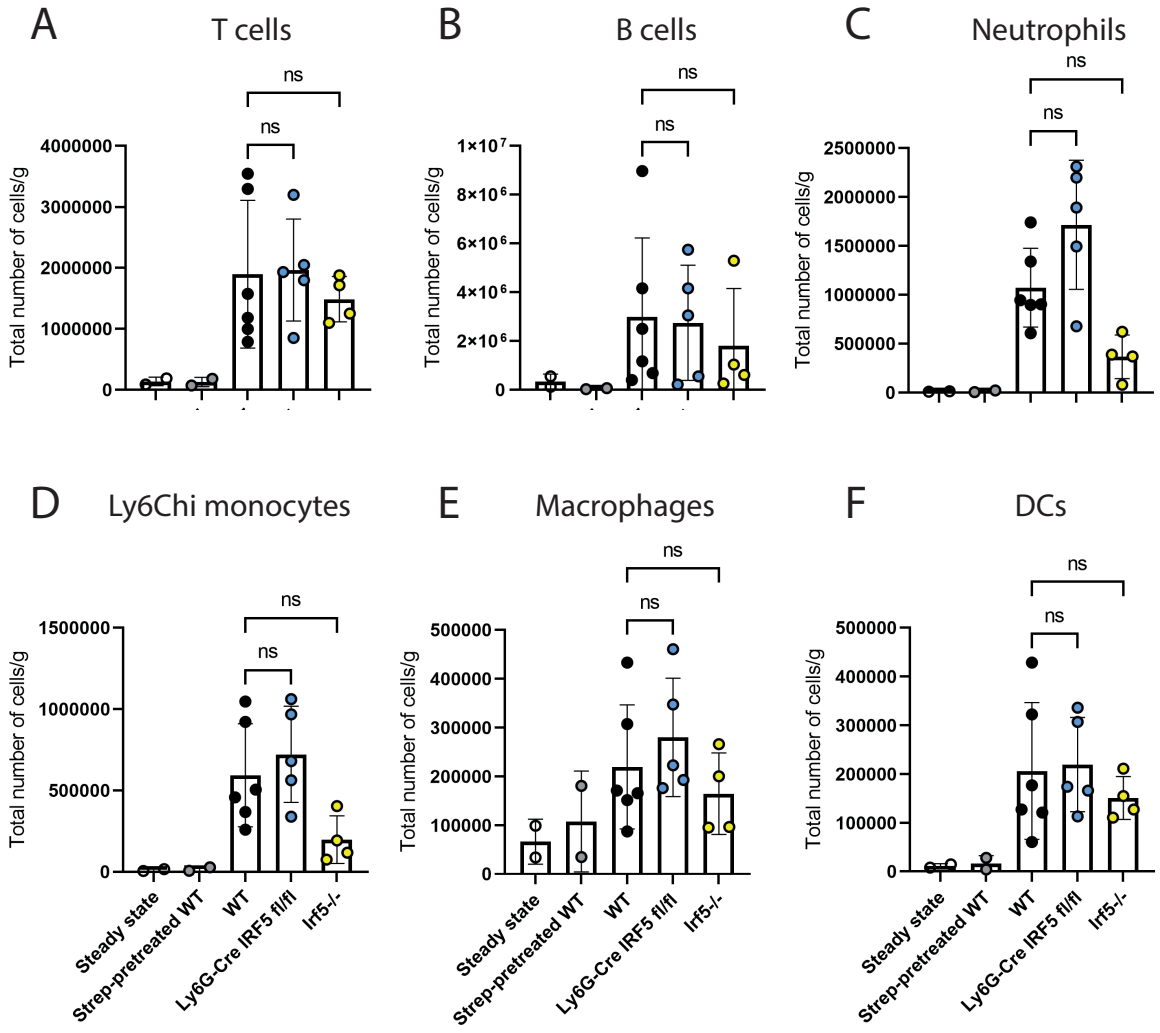


Figure 5.7: **No differences in immune cell populations of the cecal tissue at d5 p.i.** Cecal tissue of steady state (n = 2), streptomycin-pretreated WT (n = 2), WT (n =6), Ly6G^{Irf5} (n = 5) and *Irf5-/-* (n = 4) were analysed by flow cytometry and its immune cell populations depicted as total number of cells per gram tissue. A) T cells, B) B cells, C) Neutrophils, D) Ly6C^{hi} monocytes, E) Macrophages and F) DCs. One-way ANOVA. Data presented are means ±SD. ns, not significant.

5.3.2 IRF5-deficient neutrophils produce more lipocalin 2

Lipocalin 2 is used as a measure of inflammation in S. Tm experiments, as its the infection is marked by a massive infiltration of neutrophils (Figure 5.7c) [173]. It is a siderophore produced in high quantities by neutrophils and is also used as a biomarker for UC [316, 319]. Lcn2 is an iron-sequestering AMP, inhibiting growth of bacteria depending on iron. However, Lcn2 also can only inhibit the growth of bacteria whose siderophores (iron-binding proteins) bind Lcn2 [321]. We therefore measured Lcn2 concentration in the feces by ELISA. This resulted in higher quantities of Lcn2 in the feces of Ly6G^{Irf5} mice, albeit not significant at any point nor over the course of the infection (Figure 5.8a, b). Additionally, Lcn2 was amongst the top genes upregulated in *Irf5-/-* neutrophils (Figure 4.26b). To measure Lcn2 production in a controlled setting, we set out to stimulate WT and *Irf5-/-* Hoxb8 neutrophils with 1ng/mL LPS and measured Lcn2 concentration in their supernatants. This revealed that *Irf5-/-* Hoxb8 neutrophils do in fact secrete almost triple the amount of Lcn2 in comparison to WT neutrophils (Figure 5.9). Recently, it was shown that Lcn2 deficiency had a strong effect in shaping the host microbiome [322, 323]. We therefore set out to investigate whether overproduction of Lcn2 might have similar effects and whether this shapes the outcome of Hh + aIL10R colitis.

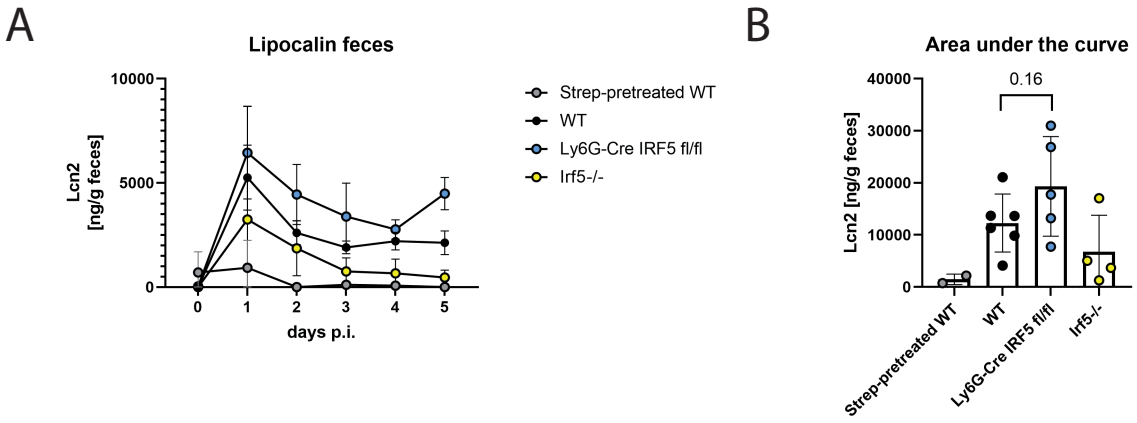


Figure 5.8: **Trend towards higher Lcn2 production in Ly6G^{Irf5} mice approaching chronic infection of S. Tm.** Lipocalin 2 (Lcn2) concentration was measured by ELISA in the feces of streptomycin-pretreated WT (n = 2), infected WT (n = 6), Ly6G^{Irf5} (n = 5) and *Irf5-/-* (n = 4). A) Lcn2 concentration per gram feces over the course of infection. Mixed-effects analysis. B) Area under the curve for Lcn2 concentration. Unpaired t-test. Data presented are means ±SD.

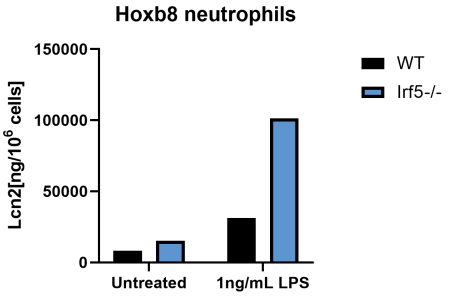


Figure 5.9: ***Irf5-/-* neutrophils produce higher quantities of Lcn2 after stimulation.** Lipocalin 2 (Lcn2) concentration was measured by ELISA in the supernatant of untreated and LPS-stimulated WT and *Irf5-/-* Hoxb8 neutrophils.

5.3.3 IRF5-deficiency in neutrophils leads to inflammation in cohoused mice

To determine the effect of the microbiome on IRF5-mediated protection from intestinal inflammation and *vice versa*, we generated a setting where the microbiome is comparable in both Ly6G^{cre} and Ly6G^{Irf5} mice. For this, we cohoused Ly6G^{cre} and Ly6G^{Irf5} mice for six weeks post weaning (Figure 5.4). Cohousing mice from different backgrounds/genotypes results in a near-comparable microbiome composition after four weeks of co-housing [324]. These mice were compared to their littermates or age- & sex-matched controls residing in separate cages at both steady state and d7 Hh + aIL10R (Figure 5.10). As demonstrated previously, Ly6G^{cre} mice were inflamed, and Ly6G^{Irf5} mice protected in the separately housed cages at d7 Hh + aIL10R (Figure 4.19, 5.10). Surprisingly, in the cohoused setting, IRF5-deletion in neutrophils seems to be detrimental, as cohoused Ly6G^{Irf5} mice were inflamed, whilst their cohoused Ly6G^{cre} were protected from colitis development (Figure 5.10). This was manifested in higher percentages of neutrophils as well as Ly6C^{hi} monocytes in cohoused Ly6G^{Irf5} mice (Figure 5.10). Macrophages were depleted in a similar manner during inflammation in separately housed Ly6G^{cre} and Ly6G^{Irf5} mice, whilst in the cohoused setting, they were proportionally lower in Ly6G^{Irf5} mice, possibly compensating for the influx of Ly6C^{hi} mono (Figure 5.10). These results point towards an indispensable role of the microbiome and IRF5-mediated crosstalk with neutrophils in orchestrating intestinal inflammation.

Additionally, Ly6G^{cre} mice have no modulation of their neutrophil function and nevertheless exhibit protection against intestinal inflammation in the cohoused setting (Figure 5.10c). So the microbiome of Ly6G^{Irf5} mice seems to contain a certain flora, which upon transfer to Ly6G^{cre} mice leads to protection against Hh + aIL10R-mediated intestinal inflammation, potentially via niche competition with Hh. Unravelling the underlying changes in the microbiome composition and a potential mechanism by which IRF5-deficient neutrophils mediate either protection or inflammation depending on their environment will be part of the future directions of this project.

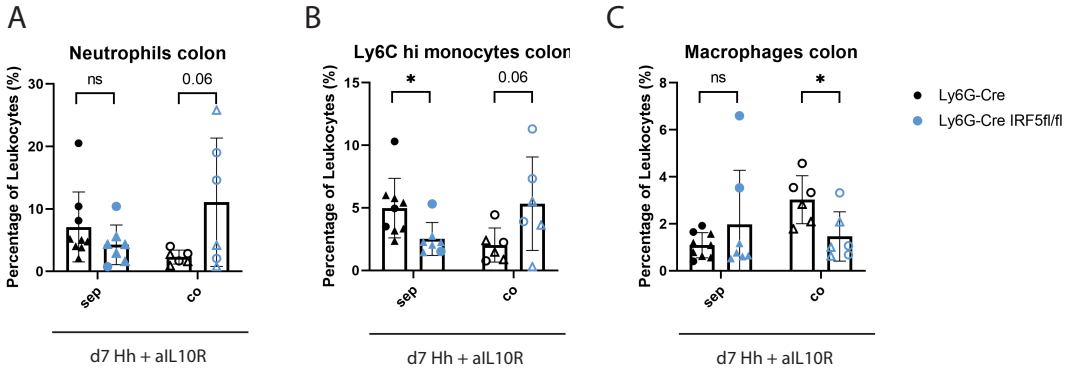


Figure 5.10: **The effect of Ly6G^{Irf5}-mediated protection is dependent on the microbiome.** Cells were isolated from the colon of d7 Hh + aIL10R (Ly6G^{cre}(n = 9, 6), Ly6G^{Irf5} (n = 7, 6) separately-housed mice (closed symbols) and cohoused mice (open symbols). A) Neutrophils, B) Ly6C^{hi} monocytes and C) macrophages, presented as percentage of leukocytes. Data is pooled from two independent experiments, marked with different symbols (circle and triangle). Unpaired t-test. Data presented are means ±SD. ns, not significant and $^{*}P \leq 0.05$. Sep: separately housed, co: cohoused

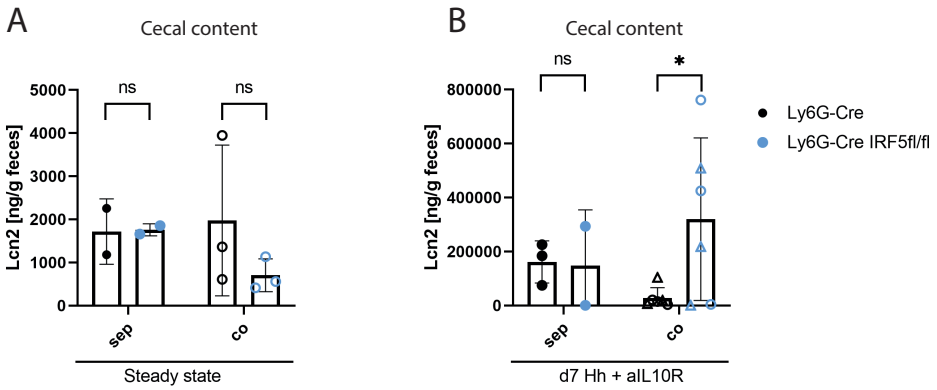


Figure 5.11: **Higher levels of Lcn2 are found in the cecum of cohoused Ly6G^{Irf5} mice at d7 Hh + aIL10R.** Lipocalin 2 (Lcn2) concentration was measured by ELISA in the cecal content of separately housed and cohoused Ly6G^{cre} and Ly6G^{Irf5} mice at steady state and d7 Hh + aIL10R. Data presented are means ±SD. Unpaired t-test. ns, not significant and $^{*}P \leq 0.05$. Sep: separately housed, co: cohoused

5.3.4 Higher Lcn2 levels in the cecum of cohoused Ly6G^{Irf5} mice

As we have observed the higher Lcn2 production by *Irf5-/-* neutrophils both *in vivo* and *in vitro* (Figure 5.8 & 5.9), we aimed to compare the concentration of Lcn2 in the Hh + aIL10R colitis model. For this, we took cecal content at both steady state and d7 Hh + aIL10R from cohoused and separately housed Ly6G^{cre} and Ly6G^{Irf5} mice and measured Lcn2 concentration in the homogenised supernatant via ELISA. We saw no differences at steady state (Figure 5.11a), however there are significantly higher levels of Lcn2 present in the cecum of cohoused Ly6G^{Irf5} mice at d7 Hh + aIL10R (Figure 5.11b). This indicates that at least partly, Lcn2 overproduction by *Irf5-/-* neutrophils could account for the differences seen upon cohousing Ly6G^{cre} and Ly6G^{Irf5} mice (Figure 5.10). However, what effect this has on the microbiota composition and what might trigger the higher Lcn2 production still remains to be determined.

5.3.5 Hh colonisation does not account for the differences between genotypes

The pathobiont *Helicobacter hepaticus* has been associated with colitis development in several immunodeficient mouse strains [146]. Together with the tolerance blocking anti IL10R antibody, it is half of the equation as the bacterial driver in the Hh + aIL10R model of colitis (chapter 1.3). We therefore wanted to investigate whether differences in Hh colonisation could account for the effects seen in the distinct settings (Figure 5.10). Cohoused Ly6G^{cre} mice are protected from Hh + aIL10R, which hints toward a potential microbiome-exclusive role in preventing Hh colonisation.

We quantified Hh colonisation by measuring *ctdB*, a Hh toxin gene, in the cecal content from two independent experiments, and normalising to the presence of eubacteria by 16S quantification. In line with previous observations (Figure 4.22), there was no difference between separately housed Ly6G^{cre} and Ly6G^{Irf5} mice in regards to their colonisation with Hh at d7 (Figure 5.12a). In contrast to this, cohoused Ly6G^{cre} mice have significantly lower levels of Hh in comparison to their Ly6G^{Irf5} cagemates (Figure 5.12b).

5. IRF5-dependent neutrophil-microbiota crosstalk at the onset of intestinal inflammation

By comparing the Hh colonisation between the two genotypes in regards to their housing situation, we revealed a significantly lower Hh colonisation in cohoused Ly6G^{cre} mice compared to separately housed mice of the same genotype (Figure 5.12c). Simultaneously, Ly6G^{Irf5} mice are colonised with Hh to the same level regardless if they are housed separately or together with Ly6G^{cre} mice (Figure 5.12d). However, there is a trend towards higher colonisation in cohoused Ly6G^{Irf5} mice, which may be significant in a more powered experiment. As cohoused Ly6G^{cre} and Ly6G^{Irf5} mice should have a similar microbiome, the prevention of Hh colonisation in Ly6G^{cre} mice may be due to regulation of the altered mixed microbiome by IRF5-proficient neutrophils during inflammation.

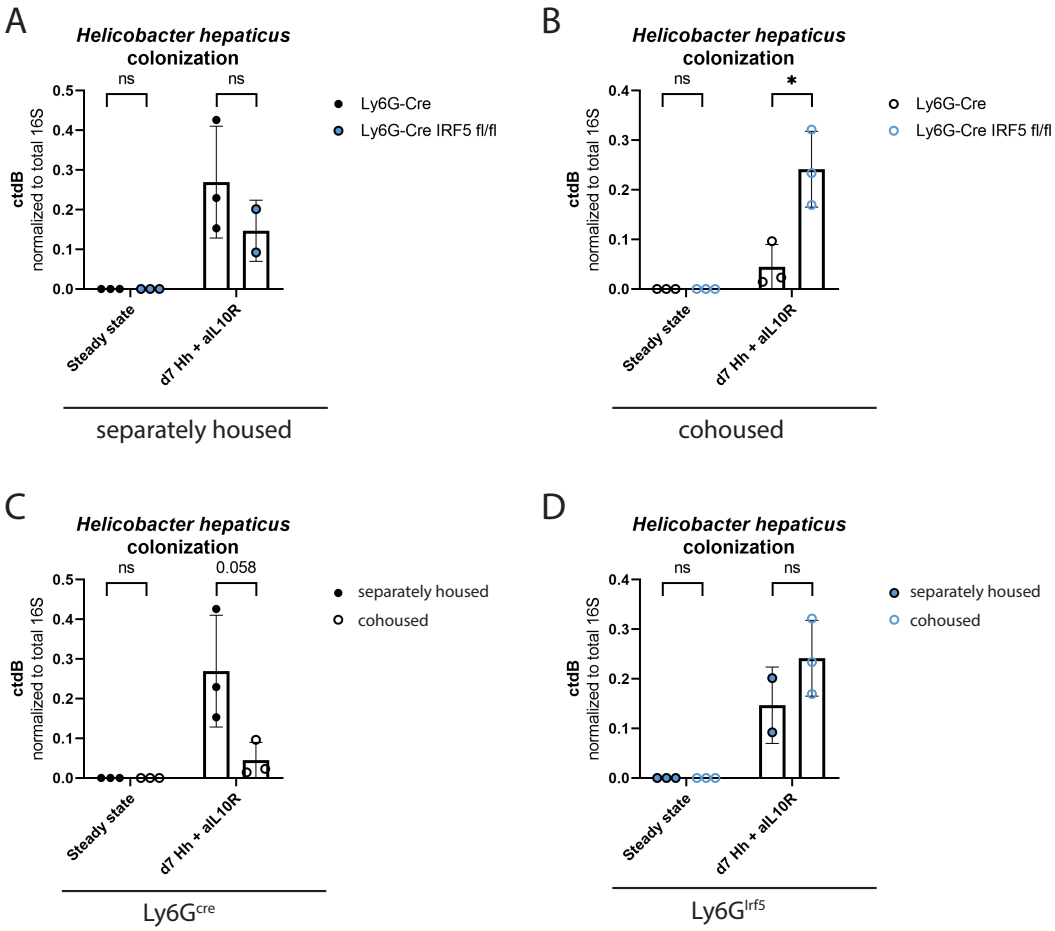


Figure 5.12: ***Helicobacter hepaticus* colonisation is significantly lower in cohoused Ly6G^{cre} mice.** Hh colonisation was quantified by measuring cdtB, a toxin gene specific for Hh, in cecal content. Its abundance was normalised to the total 16S content as well as to 5ng/uL DNA content, measured with nanodrop. A) separately housed Ly6G^{cre} and Ly6G^{Irf5} mice at steady state (n = 3, each) and d7 Hh + aIL10R (Ly6G^{cre} (n = 3) and Ly6G^{Irf5} (n = 2)). B) Cohoused Ly6G^{cre} and Ly6G^{Irf5} mice at steady state (n = 3, each) and d7 Hh + aIL10R (Ly6G^{cre} (n = 3) and Ly6G^{Irf5} (n = 3)). C) Ly6G^{cre} cohoused (open black circles) and separately housed (closed black circles) at steady state and d7 Hh + aIL10R. D) Ly6G^{Irf5} cohoused (open blue circles) and separately housed (closed blue circles) at steady state and d7 Hh + aIL10R. Data is representative from two independent experiments. Unpaired t-test. Data presented are means ±SD. ns, not significant and $^{*}P \leq 0.05$

5.3.6 Metagenomic microbiome sequencing reveals differences in overall microbiota composition

To further unravel microbiome-mediated changes and link those to our observations, we performed shallow shot-gun metagenomic sequencing on the colon content of the mice in chapter 5.3.3. The complexity of this dataset is further enhanced due to the fact that the microbiomes at steady state and d7 Hh + aIL10R are not derived from the same mice. First, we checked whether the species diversity was comparable between the different conditions, as reduced microbial diversity is a feature of inflammation in IBD [283]. Alpha diversity between the cohorts was compared, showing equal diversity across samples (Figure 5.13). In inflammation, the alpha diversity normally is significantly lower in comparison to their steady state counterparts, however as d7 Hh + aIl10R represents the onset of Hh + aIL10R-mediated colitis, the changes in the microbiome occurring from day 6 onwards may not yet have resulted in a loss of microbial diversity. In a study comparing Hh + aIL10R with Hh infection alone as well as anti-IL10R treatment separately also found no changes in alpha diversity even at a later stage during Hh + aIL10R-mediated intestinal inflammation [325].

Principal component analysis (PCA) was used to look at the degree of similarity between the different microbiome samples. Comparing all Ly6G^{cre} mice in one PCA plot, only the inflamed separately housed Ly6G^{cre} samples cluster away from the rest, with minimal changes to the microbiome in the cohoused Ly6G^{cre} mice at d7 Hh + aIL10R (Figure 5.14a). In Ly6G^{Irf5} mice, the microbiome clustering is determined both by housing condition and Hh infection (Figure 5.14b). This highlights the importance of microbiome-IRF5-neutrophil crosstalk in shaping the microbiome composition. One cohoused Ly6G^{Irf5} mouse is clustering separately to their cagemates. However, its Hh levels were in the normal range (Figure 5.12d), whilst its neutrophil/monocyte percentages were ranging at the lower end of the spectrum. This indicates that the slightly different microbiome in this mouse might have resulted in the protective phenotype of Ly6G^{Irf5} mice.

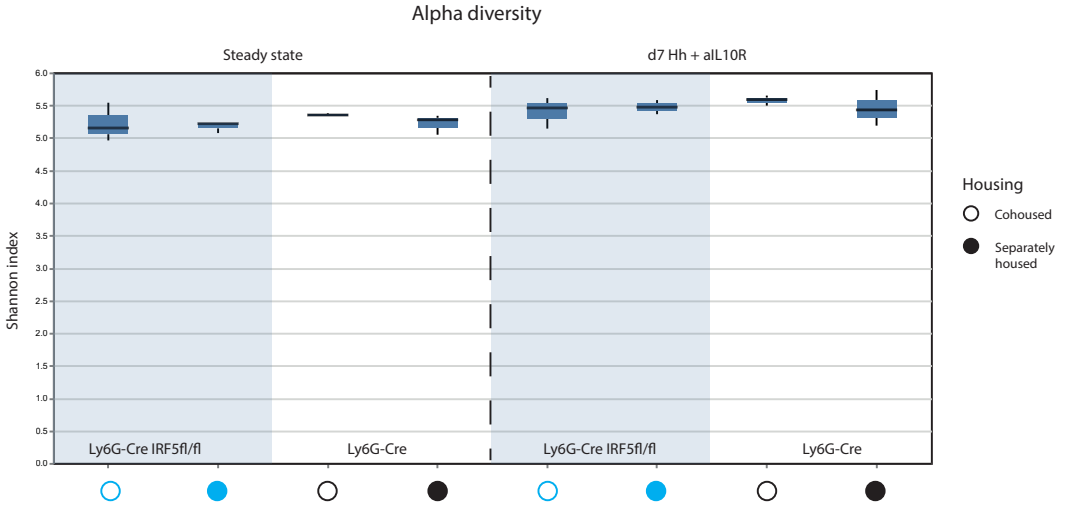


Figure 5.13: **Alpha diversity is comparable across samples.** Alpha diversity was measured using the shannon index. Data are presented as means ±SD.

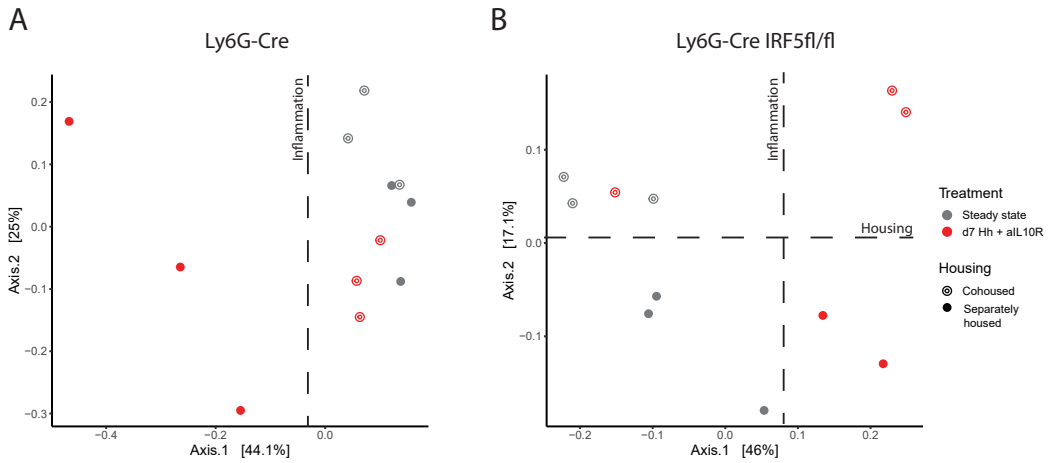


Figure 5.14: **Microbiome analysis reveals specific clustering based on inflammation status.** Shallow metagenomic sequencing was performed on the colon content of steady state (grey) and d7 Hh + aIL10R (red), cohoused (open circles) and separately housed (closed circles). Principle component analysis (PCA) was performed on a species level. A) Ly6G^{cre} mice, B) Ly6G^{Irf5} mice

5.3.7 Dysbiosis ratios not altered between inflamed and protected conditions

A depletion of commensal bacteria, notably of the phylum of *Firmicutes* and *Bacteroidetes* has been associated with IBD [326]. Simultaneously, a massive increase in *Proteobacteria* was noted, a fact which *Roy et al* used to mark dysbiosis in ratios of relative abundances to each other [275, 326]. They showed that a decrease in the ratio of *Firmicutes/Bacteroidetes* and *Firmicutes/Proteobacteria* was a measure for dysbiosis in their model of DSS colitis [275].

Here, we compared the same ratios in our microbiome samples on the phyla level. Notably, there were no changes in the ratio of *Firmicutes/Bacteroidetes* relative abundances (Figure 5.15a), however a massive increase in *Proteobacteria* in relation to *Firmicutes* could be observed in all d7 Hh + aIL10R samples (Figure 5.15b). *Helicobacter hepaticus* belongs to the phylum of *Proteobacteria*, skewing the results in regards to their relative abundance. Nevertheless, other *Proteobacteria* might profit from Hh upgrowth and removal of tolerance mechanisms and hitchhike on the beneficial conditions, perhaps also exploiting the IRF5-deficiency of neutrophils. Together with the absence of changes in alpha diversity observed previously (Figure 5.13), this indicates that changes in the microbiota composition, but not dysbiosis or reduction in species diversity are the drivers of the altered phenotype in cohoused mice.

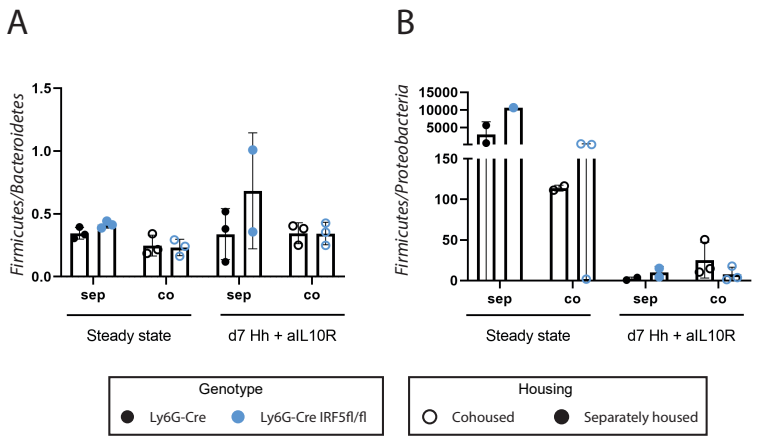


Figure 5.15: **Dysbiosis ratios are comparable between the different conditions at d7 Hh + aIL10R** Cohoused (empty circles) and separately housed (full circles) Ly6G^{cre} (black), Ly6G^{Irf5} (blue) and *Irf5-/-* (yellow) mice are compared in their relative abundances of bacterial phyla. A) *Firmicutes/Bacteroidetes* ratio, B) *Firmicutes/Proteobacteria* ratio. Data presented are means ±SD.

5.3.8 Differences at steady state between cohoused and separately housed mice

To identify specific species associated with the phenotype change, we performed a series of Kruskal-Wallis tests on the species level on all microbiome samples to pinpoint bacteria that were significantly different in one condition in regards to the others. By investigating species composition at steady state and d7 Hh + aIL10R separately, we aim to identify species important for immune priming prior to infection as well as driving immunopathology. For simplicity reasons, we call separately housed Ly6G^{cre} and cohoused Ly6G^{Irf5} "inflamed conditions" and cohoused Ly6G^{cre} and separately housed Ly6G^{Irf5} "protected conditions" from here onwards.

5.3.8.1 Ly6G^{cre} mice at steady state

As cohoused Ly6G^{cre} mice had much lower Hh colonisation levels, we set out to investigate bacterial species that were different between cohoused and separately housed Ly6G^{cre} mice, potentially preventing Hh colonization. Three bacterial species, all belonging to the phyla of *Bacteroidetes* were significantly elevated in cohoused Ly6G^{cre} in comparison to separately housed Ly6G^{cre} mice (Figure 5.16).

5.3.8.2 Ly6G^{Irf5} mice at steady state

To identify a potential detrimental species present already at steady state, we compared differences between cohoused and separately housed Ly6G^{Irf5} mice. Three distinct bacteria, all belonging to the phyla of *Bacteroidetes* were significantly higher in cohoused Ly6G^{Irf5} mice at steady state: *Prevotellaceae bacterium, Parabacteroides goldsteinii* and *Alistipes sp UBA3409* (Figure 5.17). The effects of their metabolic products on *Irf5-/-* neutrophils remain to be determined, as well as potential indirect effects via tissue-resident macrophages e.g.

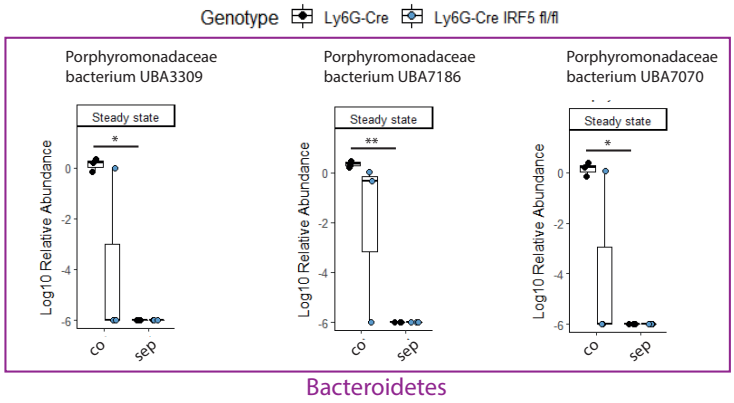


Figure 5.16: ***Porphyromonadaceae* are significantly higher in cohoused Ly6G^{cre} mice.** Log10 of relative abundances in steady state in cohoused and separately housed Ly6G^{cre} (black circles) & Ly6G^{Irf5} (blue circles) mice. *Porphyromonadaceae bacterium UBA7186*, *Porphyromonadaceae bacterium UBA3309* and *Porphyromonadaceae bacterium UBA7070* with significant differences at steady state. *Bacteroidetes* are marked with violet. Kruskal-Wallis test. Data presented are means ±SD. $^{*}P \leq 0.05$. Co: cohoused, sep: separately housed

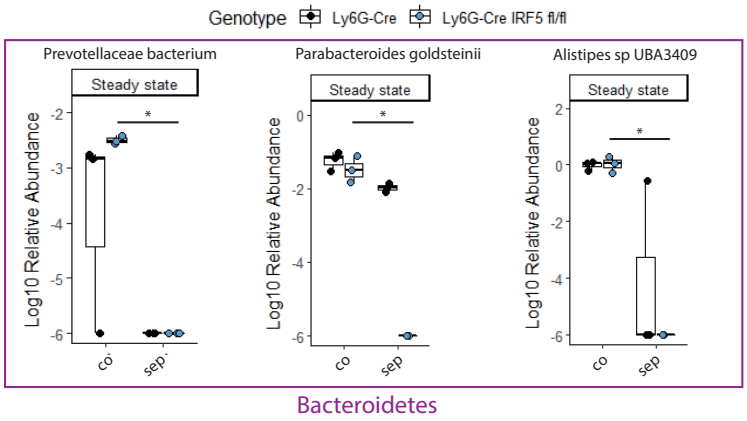


Figure 5.17: **Several distinct bacterial species are elevated in cohoused Ly6G^{Irf5} mice at steady state.** Log10 of relative abundances in steady state (left) and at d7 Hh + aIL10R (right) in cohoused and separately housed Ly6G^{cre} (black circles) & Ly6G^{Irf5} (blue circles) mice. *Prevotellaceae bacterium*, *Parabacteroides goldsteinii* and *Alistipes sp UBA3409* with significant differences at steady state. Kruskal-Wallis test. *Bacteroidetes* are marked with violet. Data presented are means ±SD. $^{*}P \leq 0.05$. Co: cohoused, sep: separately housed

5.3.9 Specific microbiota species are associated with inflammation status independently of the genotype of the mice

Additionally, we wanted to compare cohoused and separately housed Ly6G^{cre} and Ly6G^{Irf5} mice at d7 Hh + aIL10R to determine species that were associated with inflammation independently of the genotype of the mice. We identified one species "dropping" in relative abundance in all the inflamed settings whilst remaining elevated in the protected settings and four species significantly higher in their relative abundance in the inflamed settings. Interestingly, *Lactobacillus intestinalis*, associated with the protective settings, belonged to the phylum of *Firmicutes*, whilst all "inflamed" species (*Parabacteroides goldsteinii, Bacteroides ovatus, Bacteroides vulgatus* and *Alistipes sp UBA3409*) are in the phylum of *Bacteroidetes*. Both of those phyla were associated with a loss in relative abundances in IBD patients [326]. Interestingly, both *Parabacteroides goldsteinii* and *Alistipes sp UBA3409* were already present exclusively in cohoused Ly6G^{Irf5} mice at steady state (Figure 5.17), indicating a potential immune priming role before onset of intestinal inflammation. How exactly those bacterial species contribute to intestinal inflammation or protection thereof and how they interact with neutrophils specifically remains part of future studies.

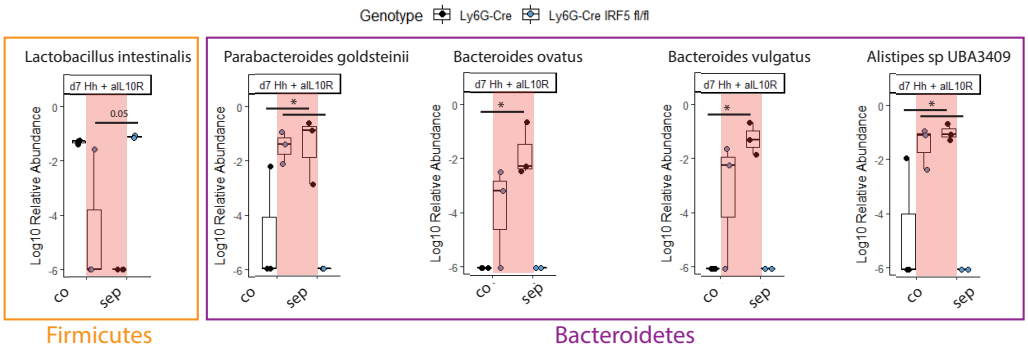


Figure 5.18: **Specific bacterial species are correlating with intestinal inflammation.** Log10 of relative abundances at d7 Hh + aIL10R in cohoused and separately housed Ly6G^{cre} (black circles) & Ly6G^{Irf5} (blue circles) mice. *Lactobacillus intestinalis, Parabacteroides goldsteinii, Bacteroides ovatus, Bacteroides vulgatus* and *Alistipes sp UBA3409* with significant differences at d7 Hh + aIL10R. The inflamed settings are highlighted with a red square. *Firmicutes* are marked in orange, whilst *Bacteroidetes* are marked with violet. Kruskal-Wallis test. Data presented are means ±SD. $^{*}P \leq 0.05$. Co: cohoused, sep: separately housed

5.4 Discussion

5.4.1 The ability of *Irf5-/-* neutrophils in controlling pathogen infection

Previously, a deficiency in phagocytosis was observed in *Irf5-/-* neutrophils *in vitro* [165, 169]. Furthermore, *Gbp4*, a gene significantly downregulated in *Irf5-/-* neutrophils *in vivo* (Figure 4.26b) during intestinal inflammation was shown to be crucial for *Salmonella* clearance in zebrafish [327]. We found no differences in the CFU loads in any organs or immune cells investigated (Figure 5.6, 5.7), albeit there were lower luminal CFU in Ly6G^{Irf5} mice over the course of infection (Figure 5.5a, b). CFU levels in the feces and weights of *Irf5-/-* however were comparable to WT (Figure 5.5), in contrast to *Pandey et al* [169]. This led us to the conclusion that *Irf5-/-* neutrophils are not deficient in killing SPI-2 deficient S. Tm *in vivo*. However, the recruitment of neutrophils might occur earlier, as well as differences in other cell populations, which we might miss due to the late timepoint chosen in this experiment. Furthermore, recent data uncovered that the *Salmonella* infection profile of a SPI-2 mutant differs signficiantly to that of WT S. Tm [Hardt lab, unpublished data]. Transluminal migration of neutrophils was less observed in this infection routine, potentially explaining the reason behind the discrepancies of our results in regards to *Pandey et al* [169]. A repeat of this experiment using WT *Salmonella*, investigating an acute timepoint might therefore be more informative in regards to neutrophils and their ÎRF5-dependent ability to clear intestinal pathogens. As neutrophil depletion itself has no effect on the progression of streptomycin-pretreated S. Tm infection [Hardt lab, unpublished data], a more refined break of colonisation resistance, like HFD [27], might be beneficial in order to study the effect of neutrophils in particular rather than triggering broad inflammation. Including *Irf5-/-* as a control is necessary to dissect neutrophil-specific defects in controlling S. Tm infection in contrast to effects by neutrophils and monocyte/macrophages combined.

Lcn2 levels in the feces of Ly6G^{Irf5} mice were constantly higher over the course of S. Tm infection, albeit not significantly (Figure 5.8). By investigating the concentration of Lcn2 *in vitro*, we uncovered a massively increased secretion in *Irf5-/-* Hoxb8 neutrophils

upon LPS stimulation (Figure 5.9). This confirmed previous observations in MBMCs, where Lcn2 was identified as one of the top-upregulated genes in *Irf5-/-* neutrophils (Figure 4.26b). The lower CFU values of S. Tm in Ly6G^{Irf5} mice throughout the infection further highlights the protective effects mediated via Lcn2 [328], and also serves as an indirect measure of Lcn2 overproduction by *Irf5-/-* neutrophils. The origin of Lcn2 levels in feces cannot be distinguished between dead neutrophils containing high amounts of Lcn2 and secreted Lcn2. However, as S. Tm is sensitive to Lcn2, the lower levels of CFU throughout might correspond to higher levels secreted *in vivo*. Also, the accompanied weight loss infers a potentially dysregulated microbiota in Ly6G^{Irf5} mice, indicating the loss of beneficial microbiota members needed for nutrient conversion and uptake (Figure 5.5c, d). Whether or not the dysregulation precedes or accompanies *Irf5-/-* neutrophil accumulation remains to be determined, possibly via microbiome sequencing. Furthermore, investigation of Lcn2 concentration in cohoused and separately housed Ly6G^{Irf5} mice revealed higher Lcn2 amounts in the cecum of cohoused Ly6G^{Irf5} mice (Figure 5.11), offering a partial mechanism in which *Irf5-/-* neutrophils might alter the microbiome detrimentally. *Vice versa*, the altered microbiome might also stimulate the higher Lcn2 production in *Irf5-/-* neutrophils.

5.4.2 The effect of microbiome composition on IRF5 function in neutrophils

Cohousing completely reversed the protective phenotype of Ly6G^{Irf5} mice at the onset of colitis, which was confirmed in a subsequent experiment (Figure 5.10b, c). *Irf5-/-* mice were cohoused with WT mice in earlier experiments (Figure 4.6), however no such effect was seen there, either due to the lack of initial neutrophil recruitment signal or different microbiota in *Irf5-/-* mice. IRF5-depletion in Hoxb8 neutrophils not only showed a reduction in their cytokine response but also impaired phagocytosis, whilst bacterial killing was not affected [165]. Furthermore, ROS production and NET formation was not affected by IRF5 deletion *in vitro*. In contrast to this, *Pandey et al* showed impairment of ROS and reactive nitrogen species (RNS) production in addition to defects in phagocytosis and bacterial clearance in

neutrophils isolated from *Irf5-/-* mice [169]. The effects of IRF5 on neutrophil function might therefore be dependent on microbial products and/or cell-cell contact within the tissue microenvironment. In both studies, neutrophil function was assessed *in vitro* with artificial stimuli like lipid A or PMA. Here, we have not investigated neutrophil function in the different settings, however this will be key in unravelling the mechanism behind microbiota-tissue microenvironment-neutrophil crosstalk and its detrimental and protective results. Given that WT and *Irf5-/-* only have a few differentially regulated genes (Figure 4.26), a combination of those might be important in the different settings, tipping the balance of protective versus detrimental functions.

The low levels of Hh colonisation in cohoused Ly6G^{cre} mice point towards a role of the microbiota in preventing Hh colonisation, even though cohoused Ly6G^{Irf5} are not protected from colitis. This could be due to immune priming at steady state, affecting WT and *Irf5-/-* neutrophils differently. By investigating the differences of the microbiome of cohoused and separately housed Ly6G^{cre} mice, we were able to identify three *Porphyromonadaceae*, which were only present in the cohoused Ly6G^{cre} mice at steady state (Figure 5.16). Interestingly, those bacteria were not present in separately housed Ly6G^{Irf5} mice, which are also protected from developing colitis. A higher prevalence of *Porphyromonadaceae* was found in a subpopulation of patients with low risk for development of gastric cancer, a cancer whose high risk factor is *Helicobacter pylori* infection [329]. However, *Porphyromonadaceae* are also found in high abundance in CD patients, questioning whether their presence exacerbates or prevents intestinal inflammation [330]. Analysis of the respective niche requirements of *Porphyromonadaceae* and *Helicobacter* might offer insight as to whether these species compete for nutrients during intestinal inflammation. Furthermore, bacterial toxins produced by either of the species might lead to the reduction or depletion of the other.

Characterization of the microbiota composition of isogenic mouse lines with different susceptibilities to streptomycin-pretreated S. Tm infection led to the identification of microbial species linked with increased resistance against *Salmonella* infection [331]. Ampicillin-treated mice, targeting a different range of bacteria than streptomycin, developed

a similar microbiota composition post treatment. However, the distinct responses to S. Tm infection were conserved, highlighting the role of immune priming prior to S. Tm infection as the underlying cause for susceptibility [331]. The protective phenotype of the microbiota composition in this model was transferrable by cohousing [331], whereas in our model, cohousing had distinct effects depending on the underlying genotype of the mice (Figure 5.10). Differences at steady state in Ly6G^{Irf5} mice in bacterial composition might therefore point towards important immune-priming bacterial species. Here, we identified three species significantly elevated in cohoused Ly6G^{Irf5} mice at steady state (Figure 5.17). Interestingly, both *Parabacteroides goldsteinii* and *Alistipes sp. UBA3409* are also associated with the inflamed settings independently of the genotype of the mice (Figure 5.18). Further analysis of the microbial products produced by those two species could inform about potential immune-microbe interactions detrimental for colitis development.

By focusing on the differences in bacterial species composition at d7 Hh + aIL10R, we identified four species significantly elevated in the inflamed settings (Figure 5.18). Three of those species belong to *Bacteroides*, a family within the phyla of *Bacteroidetes*, whose ability to evade the host immune response and high expression of multidrug resistance efflux pumps makes them highly resistant members of the gut microbiota [332]. Interestingly, *Bloom et al* identified several bacterial species able to induce colitis in IBD-susceptible mice, all belonging to the family of *Bacteroides* [333]. Simultaneously, whilst *Enterobacteriaceae*, a family within *Proteobacteria*, are over 100-fold enriched in colitis, they were unable to induce colitis on their own [333]. Furthermore, several *Bacteroidetes* species correlated with disease activity in UC patients [334]. Interestingly, certain *Bacteroidetes*, among others also *Parabacteroides goldsteinii*, were much higher in healthy controls compared to UC patients [334], highlighting the dual role of *Bacteroidetes* in pathology. Also, *Parabacteroides goldsteinii* was higher in the inflamed settings in our experiment, highlighting differences between human IBD and murine models of colitis (Figure 5.18). Additionally, *Bacteroides vulgatus* was elevated in the inflamed settings (Figure 5.18), concurring with a recent study, where its proteases were linked to disease severity in UC [335]. A broad-spectrum

protease-inhibitor prevented colitis in *Il-10-/- Bacteroides vulgatus* monocolonised mice [335]. Whether or not the *Bacteroidetes* are driving the immunopathology in our model or are merely survivors of the higher inflammation triggered by an unknown mechanism remains to be investigated in future studies.

Furthermore, *Alistipes sp UBA3409* was also associated with the inflamed settings (Figure 5.18). *Alistipes* were found to have the highest number of putrefaction pathways among all commensal bacteria [336]. The fermentation and decomposition of undigested proteins, typically leading to harmful metabolites, is termed putrefaction. *Alistipes* produce high amounts of indole, phenole and tetrahydrofuran (THF), the latter as a histidine degradation product, as well as sulfonolipids [337]. Breakdown of histidine via THF releases a vast amount of excess ammonia, shown to damage IECs upon absorption [338]. *Alistipes* was recently associated with gut inflammation and development of CRC, however controversially, it also had immune-attenuating features [337]. The interplay between distinct bacterial metabolites and *Irf5-/-* deficient neutrophils both at steady state and inflammation might be the underlying mechanisms inducing intestinal inflammation. Identification of those pathways will not only deepen our understanding for host-microbial interactions, but also offer new therapeutic avenues through modulation of immune cell function.

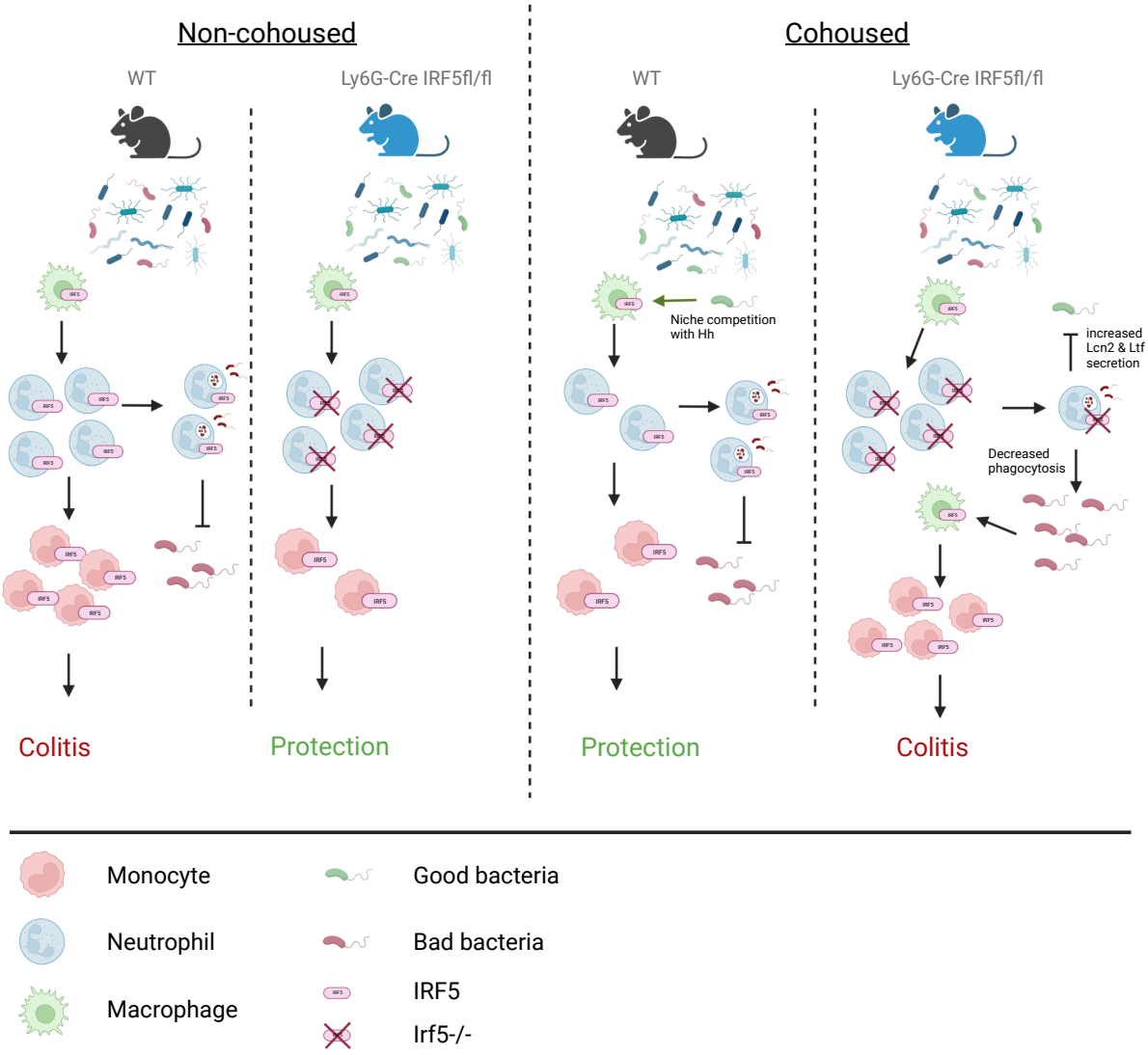


Figure 5.19: **Model for the mechanism behind cohousing/non-cohousing switch in phenotype.** *This figure was generated using Biorender.*

5.5 Conclusion

Here, we investigated the effect of the microbiome on the IRF5-mediated protection of neutrophils in intestinal inflammation. By using the S. Tm infection model, we aimed to investigate the ability of *Irf5-/-* neutrophils clearing upgrowing pathogens. Due to differences in infection course of a SPI-2 deficient S. Tm, we are unable to draw any concrete conclusions, but it remains a potential and important mechanism to investigate further. We used cohousing as a means to create a hybridised microbiome between Ly6G^{cre} and Ly6G^{Irf5} mice, observing a complete reversal of the protective phenotype previously reported in Ly6G^{Irf5} mice (chapter 4). By metagenome sequencing, we aimed to uncover changes in the microbiome and associate specific bacterial species with inflammation. This revealed a number of species that correlated with inflammation or protection independent of genotype and housing, providing an angle to uncover the specific mediators of IRF5-dependent neutrophil-microbiota crosstalk and shaping of the microbiome composition.

The data presented here highlight the importance of taking the microbiota into consideration especially in regards to different genetically modified mice and their respective phenotypes. Further research is needed to uncover the microbial-derived mediators of neutrophil function and what effects the modulated microbiota may have on other immune cells. Potential spatial differences in microbiota distribution and changes thereof could further be of importance in defining colitis outcome.

5.6 Future directions & limitations

Next steps should concentrate on deciphering whether the microbiome or the genetically modified neutrophils mediate the protective or detrimental phenotype in the respective settings. For this, a fecal microbiome transfer of the cecal content from cohoused Ly6G^{cre} (1), cohoused Ly6G^{Irf5} (2), separately housed Ly6G^{cre} (3) and separately housed Ly6G^{Irf5} (4) into GF breeding pairs is planned. The litters from those breeding pairs will have a similar microbiome, and having been colonized from birth, their immune system will

develop normally. The mice will then simultaneously be infected with Hh + aIL10R and their inflammation measured by profiling the myeloid cells, histology and their microbiome. As the microbiome is being transferred into genetically identical mice, the result will solely depend on how the microbiome modulate the immune system and not the other way around. We expect the two Ly6G^{cre} conditions (1 & 3) to result in the same phenotype as observed in the BSU. On the other hand, separately housed Ly6G^{Irf5} (4) is an important control as to whether the protective phenotype observed previously is really due to IRF5-deficient neutrophils or if the mice were protected due to their microbiome. Cohoused Ly6G^{Irf5} (2) has two possible outcomes: if they are inflamed in GF mice, the microbiome was driving the inflammation rather than the neutrophils, and if they are protected in GF mice, the deficiency in neutrophils somehow leads to the inflammation, possibly as a result of the slightly altered microbiome.

Furthermore, in order to tease out effects mediated by Hh alone in terms of microbiota composition changes, we could compare Hh infected mice with Hh + aIL10R infected mice. Imaging of mice infected with Hh only could also investigate whether neutrophils are recruited on the base of Hh colonisation alone or only in combination with breakage of tolerance with anti-IL10R.

Also, investigation of *Irf5-/-* neutrophils in their ability to clear pathogens remains to be further investigated as novel findings revealed a distinct infection course of SPI-2 S. Tm mutants, skewing our results and making it difficult to form conclusions. There are some indications that *Irf5-/-* neutrophils may overreact by Lcn2 overproduction and lower extent of intracellular killing in the cecal tissue, however this needs to be confirmed in a subsequent experiment.

One of the limitations of this study is the use of a single mouse model to investigate microbiota-neutrophil crosstalk. Different triggers of colitis might mediate distinct microbiota compositions leading to different outcomes in terms of colitis progression. However, as we have extensively characterized the neutrophil response at the onset of Hh + aIL10R colitis and not to further complicate matters, we have chosen to limit ourselves to one mouse model.

Moreover, we have compared the microbiomes of exclusively female mice at steady state and male mice at d7 Hh + aIL10R colitis, which could add further differences not crucial for modulating disease outcome. Whether female mice exhibit a similar phenotype switch was also not investigated. Furthermore, changes in the microbiome over time have also not been assessed, as the samples at steady state and d7 Hh + aIL10R are derived from different mice.

All in all, our data clearly highlight the importance of neutrophil-microbiome crosstalk in shaping the outcome of intestinal inflammation. Also, by limiting the differences to a slight modulation in neutrophil function, we confine the number of possible mediators, paving the road to uncover crucial mediators and possible treatment avenues.

6
General Discussion

Contents

6.1 Summary of results 189
6.2 Intrinsic and extrinsic regulation of the BM niche during inflammation 190
6.3 The tissue microenvironment as a scaffold for intestinal inflammation 192
6.4 New insights in neutrophil-monocyte interactions during intestinal inflammation 197
6.5 Deciphering the priming of immune cells by the microbiota . 201
6.6 Future directions 205
6.7 Conclusion 206

IBD is one of the most prevalent chronic inflammatory disorders, however the underlying cause and aetiology still remain largely unknown. The environment, genetic factors and immune system are all factors with a crucial role in driving IBD development. In this thesis, we take a holistic approach in deciphering underlying mechanisms by firstly focusing on the tissue microenvironment and the recruitment cascade of inflammatory cells. Secondly, we dissect the contributions of individual cell types to the onset of intestinal inflammation by modulating their activation with IRF5 deletion. Thirdly, we investigate the immune-microbe crosstalk at the mucosal interface as another factor in mediating intestinal inflammation.

6.1 Summary of results

The tissue microenvironment has been established as a major factor in shaping immune cell function and tissue-specificity [11, 12]. The differences along the GI tract are exemplified by macrophages localised in the SI and colon exhibiting distinct tissue-specific transcriptomes

[14]. We hypothesized that the tissue microenvironment plays a crucial role in imprinting immune cell function, acting as a driving factor for intestinal inflammation. Here, we provide an atlas of cellular and molecular changes along the entire length of the murine colon over the course of Hh + aIL10R mediated colitis. By focusing on myeloid cells, we were able to observe a distinct spatiotemporal infiltration pattern preceded by molecular changes and linked to immunopathology (chapter 3).

IRF5 was identified as a crucial driver of intestinal inflammation, mainly via its polarization of monocytes to differentiate into pro-inflammatory macrophages [129]. We aimed to unravel the early events by which IRF5 initiates the inflammatory cascade by using cutting-edge genomic models. We discovered a novel function of IRF5 in neutrophils at the onset of Hh + aIL10R, mediating the recruitment of monocytes into the inflamed colon via CCL2 secretion (chapter 4).

The interplay between microbiota and the intestinal immune system is crucial in shaping immune responses and the microbiota composition respectively [270, 271]. Neutrophils are right at the heart of these interactions, selectively killing susceptible members whilst their function is being finetuned by the microbiota [269]. As IRF5 reportedly had a indispensable role in clearing bacterial infection [169], we wanted to address the function of *Irf5-/-* neutrophils in phagocytosing pathogens *in vivo*, as well as investigate the role of the microbiome on the IRF5-mediated protection from intestinal inflammation. Here, we addressed the role of IRF5 in neutrophils both in acute and chronic inflammation in the context of the host microbiome composition and immunopathology. We found an indispensable role of the microbiome in modulating neutrophil function via IRF5, which remains to be further investigated (chapter 5).

6.2 Intrinsic and extrinsic regulation of the BM niche during inflammation

The BM serves as a "buffet à discrétion" with its many progenitor populations, and their plasticity allows for tailoring to specific needs of the host depending on the signals

received [339, 340]. For example, direct regulation of myelopoiesis in the BM by IFNγ has been proposed as a mechanism for control of infections [341]. We found higher proportions of mature monocytes and neutrophils in the BM of WT mice as early as d4 Hh + aIL10R (Figure 4.5c, d). By comparing the effects of cell-specific IRF5 deletion, we aimed to uncover intrinsic modulators of BM development of monocytes and neutrophils. Previously, *Irf5-/-* was found to affect monocyte maturation in the BM [129], whereas *Irf5-/-* neutrophil development was unaffected [165]. Both neutrophil and monocyte production were impaired in the BM of CX3CR^{Irf5} mice (Figure 4.11), whereas IRF5 deletion in neutrophils only affected maturation of monocytes (Figure 4.21). This could be due to the remote regulation of granulopoiesis by neutrophils in the intestine [342]. The authors proposed a mechanism through which intestinal macrophages suppress IL-23 production following neutrophil infiltration, which regulates systemic G-CSF levels via IL-17 and BM activity [342]. Furthermore, interactions between intramedullary macrophages and neutrophils are required for modulation of the BM niche [343], providing a direct link whereby *Irf5-/-* neutrophils potentially affect monocyte development already in the BM. The equal proportions of neutrophils in Ly6G^{cre} and Ly6G^{Irf5} mice, both at steady state and d7 Hh + aIL10R, confirms previously observed maturation proficiency of *Irf5-/-* neutrophils [165] (Figure 4.21b).

The microbiome plays a crucial role in regulating the BM niche via NOD1 ligands, stimulating myelopoiesis both at steady state and during bacterial infection [285, 287, 288, 294]. In fact, GF mice exhibit reduced amounts and differential potential in BM-derived populations, which was reversible upon administration of TLR ligands [291]. Low-doses of intravenously delivered LPS are sensed in the BM, leading to a rapid mobilization of resident neutrophils and monocytes [289].

Deciphering intrinsic and extrinsic factors regulating myelopoiesis is almost impossible in a setting where WT and KO cells are not exposed to the same environment. MBMCs offer the unique ability to untangle cell-intrinsic deficiencies from alterations in initial inflammatory triggers and microbiome stimulations. No differences in the reconsititution

of BM cells were found in a WT/*Irf5-/-* MBMC at steady state and d21 Hh + aIL10R [129], however early events could have been masked in this study.

6.3 The tissue microenvironment as a scaffold for intestinal inflammation

Macrophage turnover is affected by the microbiota density, which increases along the colon [344, 345]. As such, commmensal microbiota are a major player in macrophage subset differentiation [57], highlighting the crucial role of the microbiota in priming the host immune system. In the intestine, a persistent "controlled" inflammation has been attributed to the high monocyte-macrophage turnover [346]. This is further supported by the observation that mice lacking CCR2 or depleted of monocytes have significantly reduced numbers of LP macrophages [73, 347], as well as slower replenishment of the macrophage niche following injury [56]. Here, we expand the distinct location of macrophage subsets along the crypt-lumen axis, observed both by us and *Kang et al* [57], by quantifying them in the proximal and distal colon over the course of Hh + aIl10R mediated colitis (Figure 3.11). CD206+ macrophages are dominating the macrophage pool in the distal colon at steady state, whereas equal proportions of CD206+ and CD11c+ macrophages are found in the proximal colon, indicating a potential for different reaction to inflammatory stimuli in the proximal and the distal colon (Figure 3.11b). *Chikina et al* found more CD11c+ macrophages in the distal colon at steady state, which are important for maintenance of epithelial integrity through fungal toxin absorption [216]. This is in contrast to our data, however it could be due to the different microbiome and fungal composition between facilities, generating a distinct distal colonic microenvironment. As the inflammation takes hold in the colon, we observed a "switch" to predominantly CD11c+ macrophages in the proximal colon at d7 Hh + aIL10R, followed by CD11c+ macrophages dominating the macrophage pool in both the proximal and distal colon segments at d21 Hh + aIL10R (Figure 3.11d &e).

Tissue-resident macrophages die at the onset of bacterial infection, initiating a cascade of tightly regulated events ensuring pathogen clearance and return to tissue homeostasis

[219, 348]. Here, we see a reduction of macrophage numbers at d4 Hh + aIL10R (Figure 3.3.8a), which confirmed the visual absence of CX3CR1 in both proximal and distal colon (Figure 3.5a). Furthermore, the death of tissue-resident macrophages leads to secretion of chemoattractants, leading to the recruitment of monocytes [348]. In fact, we observed an induction of *Ccl2* and distinct infiltration of monocytes into the proximal colon at d4 Hh + aIL10R (Figure 3.8a, 3.6a, 3.5), supporting this hypothesis. Interestingly, *Ccl2* is subsequently upregulated in the distal colon at d7 Hh + aIl10R, probably following the neutrophil recruitment to the distal colon (Figure 3.8). This indicates that monocyte recruitment into the inflamed colon is regulated by two distinct events; in the proximal colon by the death of tissue-resident macrophages, followed by neutrophil-mediated monocyte recruitment into the distal colon.

Hh produces a large polysaccharide, which, via TLR2 ligation, activates resident macrophages to produce IL-10 [143]. Higher levels of *Il10* were found in the proximal colon (Figure 3.9d), accompanied by a loss of macrophage numbers at d4 Hh + aIL10R (Figure 3.6c). Hh was found to primarily colonise the cecum, rendering the proximal colon as a neighbouring site for polysaccharide-mediated macrophage activation. The TLR expression landscape further differs significantly along the length of the GI tract, setting the stage for further diversion in immune cell response to infection along the colon [168]. In this study, they analyzed TLR expression specifically in epithelial cells under homeostatic conditions, making use of newly generated TLR reporter mice. TLR2 is mainly expressed in the proximal colon as reported in [168] by epithelial cells, which could explain the spatiotemporal activation and recruitment of monocytes we observed. Interestingly, *Tlr2* expression is highest in the proximal colon at steady state, and then gets subsequently upregulated in the distal colon during Hh-driven intestinal inflammation [Powrie lab, unpublished data]. Investigating Hh colonisation along the timecourse of colitis revealed no preferential localisation of Hh during the course of inflammation, however levels of Hh were highest at the onset of inflammation (Figure 3.7). *Helicobacter hepaticus* manages to colonize GF mice lacking IL10R but fails to induce colitis, indicating that immune cell priming by

other microbes or Hh-microbe interactions are required for Hh to trigger a host response [349]. It would therefore be interesting to study potential patterns of community shifts in the distinct sites of the colon during the course of inflammation, as microbial and metabolite changes occur at d6 Hh + aIL10R colitis [Powrie lab, unpublished data], and community rearrangement was identified as an underappreciated feature of IBD pathogenesis [48, 64].

High neutrophil recruitment occurred distinctly into the distal colon at d7 Hh + aIL10R (Figure 3.6b, 3.5), which was accompanied by immunopathology (Figure 3.10b). UC initiates in the descending (distal) colon, and is associated with high neutrophil infiltration, mirroring the observations in our timecourse [118, 221]. We have identified higher CXCL1 transcript and protein levels in the distal colon at d7 Hh + aIL10R (Figure 3.8b, d), confirming a previous study using a microbe-induced tumour model [209]. The upstream cellular source of CXCL1 as well as its initial trigger especially in the distal colon remains to be identified. Preliminary data using high-resolution confocal microscopy suggests epithelial cells to be the primary source in the distal colon [data not shown], which was also proposed by *Chung et al.* They further linked STAT3 signalling and NF-κB activation in epithelial cells to their *Cxcl1* expression [209]. A recent paper highlighted that NF-κB signalling in murine IECs is not directly responsive to extracellular TLR4 stimulation but rather regulated by TNF-producing intercrypt macrophages [258]. The localisation and function of this intercrypt macrophage population was proposed to be similar to that of CD11c+ CD121b+ macrophages identified in [57]. We also observed a change in *Tnf* production from proximal colon at d4 Hh +aIl10R to the distal colon at d7 Hh + aIl10R (Figure 3.9a). The importance of IEC-macrophage crosstalk is further highlighted by IL-23 producing macrophages inducing the secretion of IL-22 by ILC3 and Th17 cells [226]. IL-22 in turn stimulates IECs to release AMPs as well as production of neutrophil chemoattractants, leading to neutrophil recruitment [226]. Interestingly, IL-22 also mediates neutrophil influx into the middle and distal colon at the onset of DSS colitis [213], providing a potential mechanism to be further investigated.

Previously, the SI and colon have been highlighted as distinct tissue microenvironments, modulating their resident macrophage population to express tissue-specific transcriptomes [10, 14]. Remodelling of the mesenchyme and epithelial cell diversity changes are associated with IBD, further emphasizing the role of the tissue microenvironment in shaping cell function [350, 351]. Here, we expand this view by showing distinct spatiotemporal immune cell infiltration along the length of the colon over a timecourse of murine intestinal inflammation, marking the proximal and distal colon as distinct tissue microenvironments (Figure 3.6, 3.5). We also show molecular changes in the tissue microenvironment, which are initiated in the proximal colon at d4 Hh + aIL10R, preceding immune cell infiltration (Figure 3.8, 3.9). A recent study similarly revealed compartmentalization of immune cells as well as microbial species along the human steady state colon, showing preferred microbiota colonization in certain areas of the colon and distinct patterns of immune cell prevalence in the three distinct sites assessed [52]. Thus, it is possible a similar microbial-related compartmentalization is influencing the distinct molecular and cellular changes in the Hh + aIL10R mediated intestinal inflammation.

Taken together, we propose a model of spatiotemporal immune cell activation, leading to the distinct expression of pro-inflammatory chemokines and cytokines, resulting in differential immune cell recruitment along the colon. Following Hh colonisation in the cecum, tissue-resident macrophages in the proximal colon get exposed to higher quantities of the Hh-polysaccharide, resulting in their cell death and consequential expression of *Ccl2*. The presence of high quantities of antimicrobial peptides through expression of *Il22* and *Cxcl9* at d4 Hh + aIl10R suggests a more antimicrobial rather than pro-inflammatory tissue microenvironment in the proximal colon. The higher prevalence of *Ccl2* subsequently leads to a distinct infiltration of monocytes into the proximal colon at d4 Hh + aIL10R. By community rearrangement or another unknown mechanism, tissue-resident macrophages get triggered in the distal colon at d7 Hh + aIL10R, leading to their production of TNF and other mediators like IL-23. This results in epithelial-derived CXCL1 specifically in the distal colon, recruiting neutrophils and driving further immunopathology (Figure 6.1).

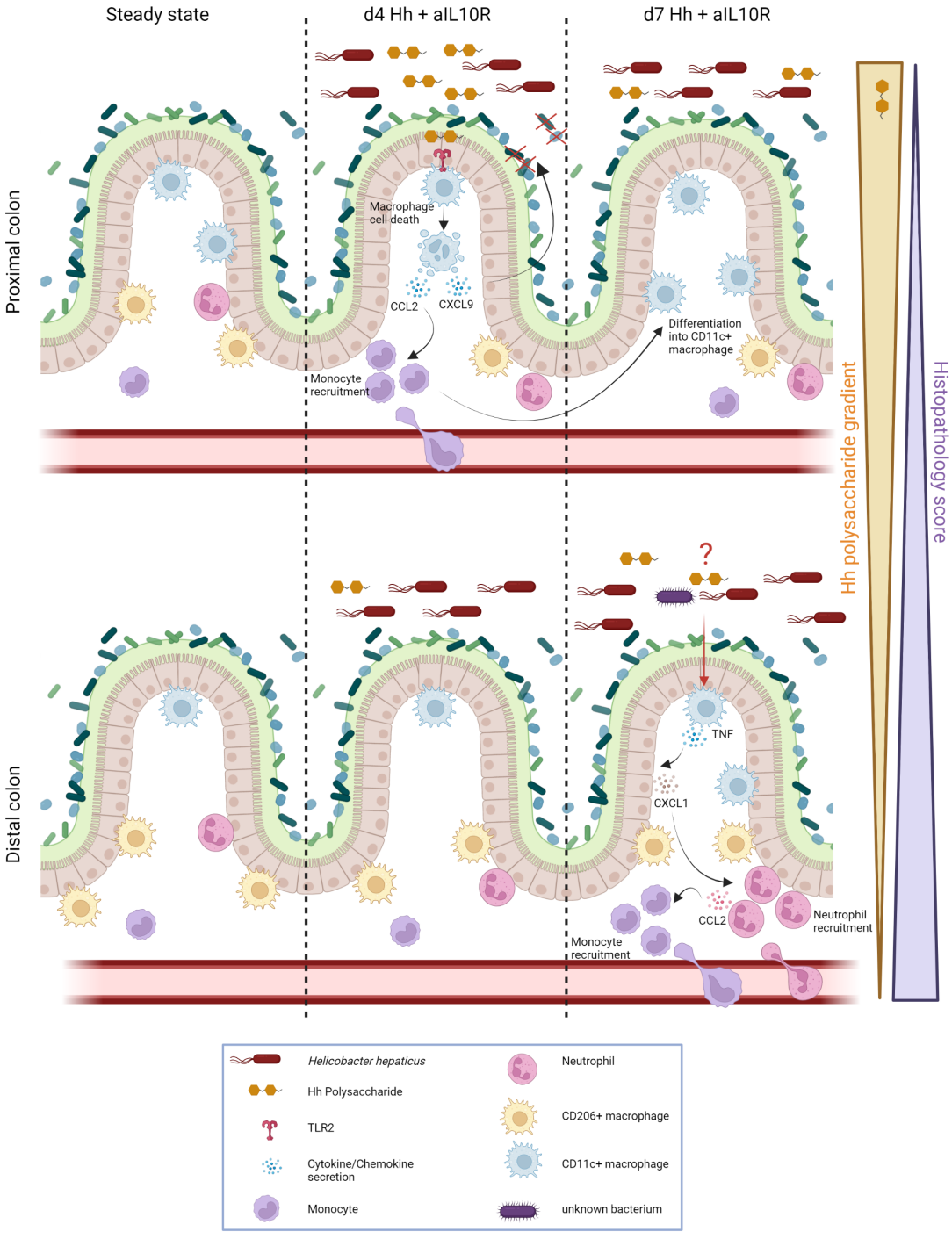


Figure 6.1: **Model for the mechanism behind spatiotemporal infiltration of myeloid cells at the onset of Hh + aIl10R intestinal inflammation.** *Caption continued on the following page.*

Figure 6.1: Upper panel: proximal colon, lower panel: distal colon. At steady state, there is normal macrophage turnover, being replaced by infiltrating monocytes, as well as a low number of neutrophils being present. As *Helicobacter hepaticus* colonizes primarily in the cecum, the proximal colon is exposed to higher quantities of the Hh polysaccharide, which activates macrophages via TLR2 (see Hh polysaccharide gradient). This activation leads to macrophage cell death, releasing CCL2 and recruiting monocytes as their replacement. Simultaneously, high levels of CXCL9 are released, acting as an antimicrobial. At d7 Hh + aIl10R, monocytes in the proximal colon have differentiated into CD11c+ macrophages, as a result of the antimicrobial environment of the proximal colon at d4 Hh + aIl10R. In the distal colon, macrophages get activated via an unknown mechanism, producing TNF, which leads to a release of CXCL1 by epithelial cells. This in turn results in great numbers of neutrophils being recruited to the distal colon specifically. Among their other antimicrobial functions, neutrophils release high quantities of CCL2, leading to a second wave of monocyte recruitment and the establishment of an inflammatory distal colon niche (see histopathology gradient). *This figure was generated using Biorender.*

6.4 New insights in neutrophil-monocyte interactions during intestinal inflammation

The prevalence of neutrophils in the blood differs significantly between mice (10-25 %) and humans (50-70 %) [352]. This, together with the omission of neutrophils in many studies should be taken into account when studying the importance and functions of neutrophils in inflammation. Furthermore, the roles of neutrophils and macrophages differ significantly between CD and UC, highlighting the importance of understanding their role in the initiation of chronic intestinal inflammation [170]. Intestinal inflammation changes the composition of the macrophage compartment by infiltrating Ly6C^{hi} monocytes rapidly differentiating into inflammatory macrophages [74]. Ly6C^{hi} monocytes and neutrophils are present in low numbers in the periphery during homeostasis, but get swiftly mobilized from the BM early during infection [352, 353]. Neutrophils and monocytes were highlighted as "partners in crime", orchestrating the innate immune response and regulating other cell types respectively [170, 255].

It was further shown that neutrophils are able to modulate the phenotype of inflammatory monocytes by their secretion of azurodicin [250]. We show that the tissue microenvironment

and monocyte gene expression is significantly affected in Ly6G^{Irf5} mice (Figure 4.25, 4.24), despite IRF5 only being deleted in neutrophils (Figure 4.18). By using an *in vitro* model, we further demonstrate that Hoxb8 neutrophils were able to induce pro-inflammatory gene expression in Hoxb8 monocytes (Figure 4.29. The nature of the soluble factor capable of stimulating monocytes is currently unknown. We also have not yet investigated the differences in stimulation capacities between WT and *Irf5-/-* neutrophils. This will be addressed in future studies both *in vitro* and *in vivo*, using co-cultures and scRNA-sequencing.

Ly6C^{hi} monocytes and neutrophils produce overlapping repertoires of inflammatory cytokines [354]. *Casson et al* aimed to dissect the contributions of cytokines produced by neutrophils and Ly6C^{hi} monocytes in a model of pneumonary bacterial infection by depletion of neutrophils and monocytes respectively. They found an importance of neutrophils in controlling bacterial burden as well as a significant cooperation in shaping the optimal cytokine response [354]. Various studies have shown neutrophils to produce significantly lower amounts of cytokine on a *per cell* basis compared to monocytes, however neutrophils vastly outnumber monocytes at the onset of inflammation, rendering their contribution to the inflammatory tissue microenvironment fundamental [355]. Depletion of mononuclear phagocytes (MNPs), which are comprised of monocytes, macrophages and DCs, has been reported to increase neutrophil infiltration and severity in a DSS-colitis model, whilst depletion of both neutrophils and MNPs did not worsen colitis [356]. This indicates that neutrophils are detrimental in the absence of MNPs during intestinal inflammation, highlighting the complex interplay of myeloid cells at the onset of inflammation.

The ability of neutrophils to recruit monocytes was shown in multiple studies using various models of inflammation [250, 251, 253]. To our knowledge, we are the first to demonstrate this occurring in a spatiotemporal manner over the course of intestinal inflammation (Figure 3.5) and linking it to *Irf5* expression in neutrophils (Figure 4.19 & 6.2). *Ccl2* expression differs significantly in WT and *Irf5-/-* neutrophils both *in vitro* and *in vivo* (Figure 4.25, 4.27, 4.26a). We aim to prove the IRF5-CCL2 link as a crucial link in

mediating intestinal inflammation by studying neutrophil and monocyte interaction in an isolated *in vitro* setting, as well as *in vivo* by intracellular cytokine staining (Figure A.3).

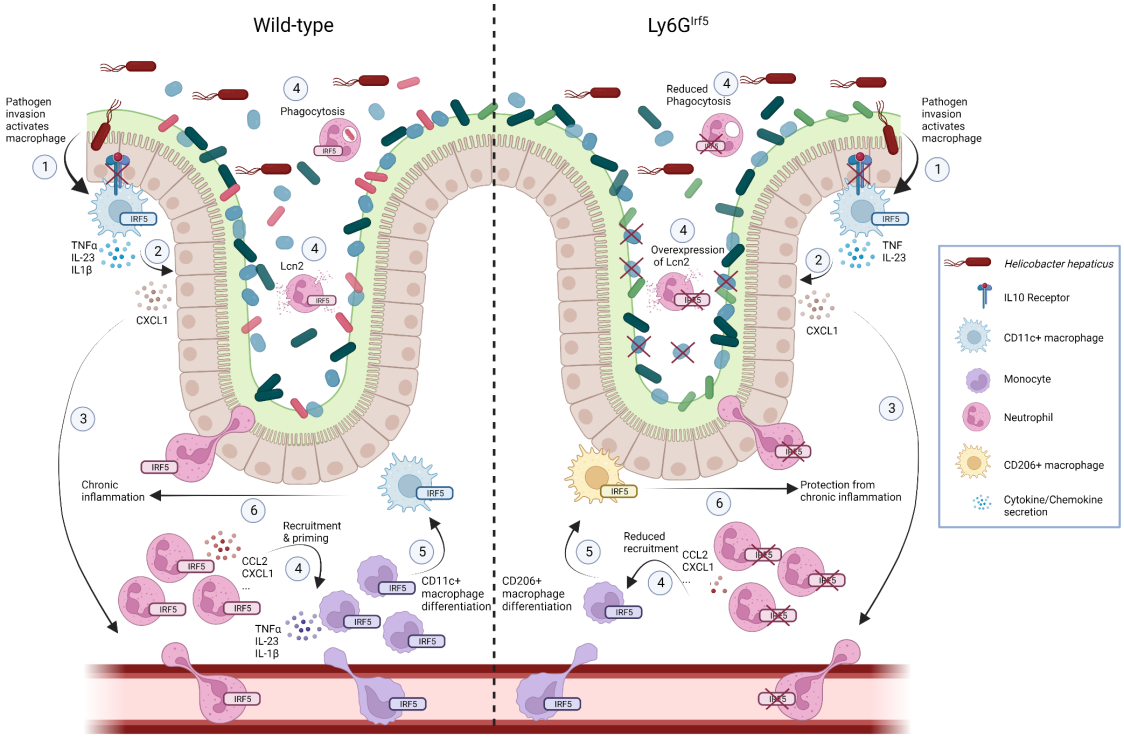


Figure 6.2: **Model for the microbiome-independent role of IRF5 in neutrophils at the onset of Hh + aIL10R intestinal inflammation.** Macrophages sense the breach of the intestinal barrier and respond by phagocytosing invading bacteria and secreting cytokines/chemokines (1). These in turn stimulate IECs to secrete CXCL1 (2), recruiting neutrophils as primary responders (3). Incoming WT neutrophils secrete high levels of CCL2 and other chemoattractants, phagocytose bacteria in the lumen and degranulate, releasing AMPs and ROS (4). Monocytes are recruited in great numbers, and are primed by the tissue microenvironment and neutrophil factors, polarizing them to differentiate into CD11c+ macrophages and secrete pro-inflammatory cytokines (5). The macrophages amplify the intestinal inflammation present, leading to the establishment of chronic inflammation in WT mice (6). *Irf5-/-* neutrophils secrete lower levels of CCL2, recruiting fewer monocytes (4). Simultaneously, they overexpress Lcn2 and have a reduced ability to phagocytose (4). The infiltrating monocytes in Ly6G^{Irf5} mice differentiate into CD206+ macrophages due to the less pro-inflammatory microenvironment and neutrophils (5). The lower numbers of monocytes as well as their differentiation into CD206+ macropahges establishes a homeostatic tissue microenvironment, protecting Ly6G^{Irf5} mice from intestinal inflammation (6). *This figure was generated using Biorender.*

6.5 Deciphering the priming of immune cells by the microbiota

The microbiota plays an indispensable role in shaping the intestinal immune system by providing both pro- and anti-inflammatory stimuli important for establishment of a mutually beneficial host-microbe relationship [357]. Decreased numbers of macrophages have been detected in GF mice, further proof of the crucial function of the microbiota in shaping the macrophage pool [57, 76]. Not only the presence, but also the location of macrophages is dependent on the microbiota, as the distribution of perivascular macrophages was severely altered in GF and Abx-treated mice [56]. Broad-spectrum Abx-treated mice have a reduced induction of monocyte-recruiting CCL2 in DSS colitis compared to their untreated WT counterparts [56]. This was linked to microbiota-induced TLR4 activation in epithelial cells, resulting in increased *Ccl2* expression [358]. Also, GF mice are ineffective in refilling the macrophage niche post depletion with DSS [344]. Together, this highlights the role of the microbiota in inducing monocyte recruitment and macrophage replenishment following injury and during inflammation [56, 344, 358]. We have highlighted the role of neutrophils and their IRF5-dependent CCL2-secretion during Hh + aIL10R driven intestinal inflammation (chapter 4). The contribution of various cell types to the total amount of CCL2 needs to be assessed carefully in future experiments, which might vary dependent on the timepoint and location within the colon.

Metabolic functions of macrophages are also influenced by the presence of microbiota. A recent study comparing colon and SI macrophages in control and Abx-treated mice, has shown that SI macrophages are microbiota-independent and metabolically less active than their colonic counterparts [229]. Uncovering mechanisms through which the microbiota contributes to regulating macrophage phenotype and function is crucial in determining signalling pathways prone to being manipulated in health and disease. Direct effects of the microbiome on neutrophil function was shown in multiple studies, where neutrophils isolated from GF mice have impaired functions, such as phagocytosis, chemotaxis and reduced MPO

levels, among others [292–294]. Upon treatment with LPS, the impaired functions were restored, highlighting the role of the microbiome in priming neutrophil function.

Cohoused Ly6G^{cre} mice also displayed a reduced neutrophil recruitment, alongside significantly lower Hh levels (Figure 5.10 & 5.12b, c). The lower Hh levels indicate that not only a modulated microbiota, but also the intensity of the inflammatory trigger (in this case Hh), regulates the extent to which neutrophils are recruited to the site of inflammation. Neutrophil infiltration is regulated by the microbiota, as was demonstrated in a study where microbiota ablation significantly reduced neutrophil infiltration in a HFD setting [359]. In a model of DSS colitis, where mice were either fed normal chow or non-fiber diet (NF), neutrophil recruitment was exacerbated without the presence of fiber [41]. This effect could be reversed by addition of acetate to the drinking water, indicating a role of SCFA in mediating neutrophil recruitment to the colon [41]. SCFA-producing bacteria mostly belong to the phyla of *Firmicutes* (butyrate) and *Bacteroidetes* (acetate and propionate) [360]. Here, we did not see a skewing of the microbiota in either the direction of *Firmicutes* nor *Bacteroidetes* at d7 Hh + aIL10R in any of the mice (Figure 5.15a). However, whether SCFA levels change as a result of certain bacterial species diminishing or increasing within the respective phyla was not examined. *Lactobacillus intestinalis*, a species highly abundant at steady state and in the protected settings (Figure 5.18), has high SCFA-producing potential, potentially modulating neutrophil recruitment and/or neutrophil function in the various settings. *Lactobacillus intestinalis* was further shown to restore gut permeability and microbiota composition in ovariectomized rats, highlighting its potential as a probiotic [361]. The direct effect of SCFA on neutrophils is debated, some studies hint at an involvement of GPR43 signalling being involved in their ROS production and phagocytosis abilities [299, 300]. Indeed, neutrophil infiltration is exacerbated in *Gpr43-/-* mice in multiple models of colitis [301]. Within a microbial community, a lot of redundancy exists, which could show a changes in bacterial species, however they might exert the same functions as the bacteria it 'replaced'. Functional analysis of the microbiome sequencing data would therefore reveal a shift in the genomic potential of the microbial

community, independently of the assignment to different species. This might be indicative of the pathways involved in neutrophil modulation.

Degranulation is a key neutrophil effector function in response to bacterial infection [85]. By measuring the concentration of the anti-microbial proteins contained within a certain granule, e.g. MPO or Lcn2, the specific degranulation process occuring can be quantified [85]. During S. Tm infection, *Irf5-/-* mice have significantly lower levels of MPO, indicating a deficiency in neutrophil primary degranulation [169]. The amounts of Lcn2 were not measured, so there is no indication as to whether *Irf5-/-* neutrophils are also deficient in secondary granule release. In our data, we found higher expression of *Lcn2* within *Irf5-/-* neutrophils during intestinal inflammation in MBMC (Figure 4.26a). Indeed, LPS stimulation *in vitro* revealed an almost triple amount of Lcn2 released by *Irf5-/-* Hoxb8 neutropils (Figure 5.9). *In vivo*, secretion of lipocalin 2 is hard to distinguish from the accumulation of dead neutrophils in the lumen. However, as S. Tm is sensitive to Lcn2, its lower CFUs in Ly6G^{Irf5} throughout the infection indicate higher amounts of Lcn2 secreted, despite the same amounts of neutrophils present in both Ly6G^{cre} and Ly6G^{Irf5} mice (Figure 5.5a,b & 5.7c). In the lung, high levels of Lcn2 were associated with deactivated macrophages, impairing bacterial clearance upon infection [362]. In another study, authors identified the effect of Lcn2 on the function of CD103+ DCs in the lung [322]. Taken together, Lcn2 does not only exert profound effects on the microbiome through its anti-microbial properties [322], but also affects immune cell function. Analysing the crosstalk of neutrophils with other myeloid cells together with spatial microbiome changes will therefore be crucial in identifying potential mediators skewing the immune reponse in one way or the other.

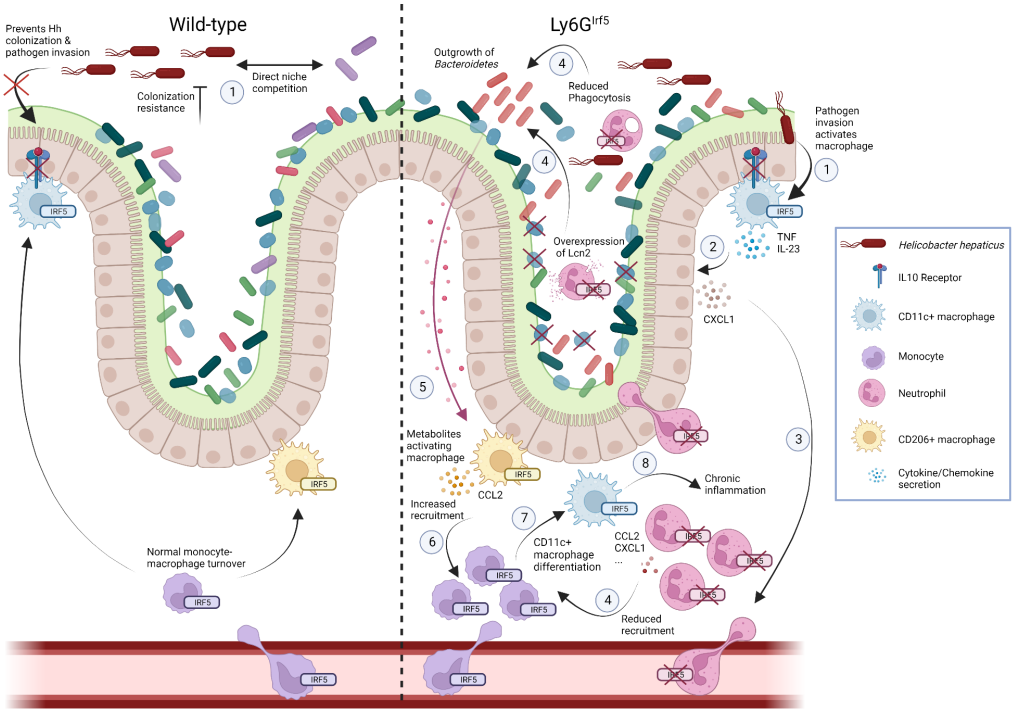


Figure 6.3: **Model for the microbiome-dependent role of IRF5 in neutrophils at the onset of Hh + aIL10R intestinal inflammation.** In WT mice, the changed microbiome leads to a prevention of Hh colonization either due to direct niche competition by an unknown bacteria or through combined colonization resistance of the altered microbiome (1). This prevents the inital trigger of macrophages, preventing onset of inflammation altogether. In Ly6G^{Irf5} mice, macrophages sense the breach of the intestinal barrier and respond by phagocytosing invading bacteria and secreting cytokines/chemokines (1). These in turn stimulate IECs to secrete CXCL1 (2), recruiting neutrophils as primary responders (3). *Irf5-/-* neutrophils secrete lower levels of CCL2, recruiting fewer monocytes (4). The altered microbiome and the reduced ability of *Irf5-/-* neutrophils to phagocytose as well as the overexpression of Lcn2 by *Irf5-/-* neutrophils leads to a shift in the microbiome, resulting in a *Bacteroidetes* outgrowth (4). Metabolites of *Bacteroidetes* activate CD206+ macrophages residing in the crypt to produced chemokines, among others also CCL2 (5). This results in an increased monocyte recruitment (6), and due to the pro-inflammatory microenvironment, these monocytes differentiate into CD11c+ macrophages (7), resulting in chronic inflammation (8). *This figure was generated using Biorender.*

6.6 Future directions

Next steps should concentrate on investigating the functionality of WT and *Irf5-/-* neutrophils at the onset of inflammation as well as potential cell-cell interactions with other myeloid cells. To get a snapshot of the functions of a cell at a given cell type, transcriptomics is a fantastic tool, as it reveals the genes being expressed at collection. As *ex vivo* functional approaches will not recapitulate the local microenvironment important for cell function as well as the low gene expression in neutrophils, scRNA-seq of the colon and blood of Ly6G^{Cre} and Ly6G^{Irf5} mice at d7 Hh + aIL10R will offer insights in the differences between the genotypes on a single-cell resolution. In order to include other myeloid cells as well as resolve spatial differences along the colon, CD11b+ from the proximal and distal colon will be sorted and compared to their blood counterparts for gene acquisition upon extravasation. Analysis of cell-cell interactions using algorithms like NicheNet or CellPhone DB [167, 363], which investigate receptor-ligand pairs and downstream gene activation/downregulation will further explore neutrophil mediators shaping the influx and phenotype of monocytes. Furthermore, comparing the transcriptome of neutrophils in separately housed versus cohoused Ly6G^{Irf5} mice at d7 Hh + aIL10R might inform us about priming of the neutrophils by the microbiome, offering novel pathways to target and modulate neutrophil function.

Apart from analysing the differences between the species via microbiome sequencing, sorting out IgA-coated bacteria might be another means to identify and quantify pathobionts [364, 365]. Furthermore, a novel method using imaging of commensals and labelling of their metabolites to track host-microbiota interactions *in vivo* might be informative of the crosstalk shaping the distinct responses to Hh + aIL10R-mediated colitis [366]. Oligo-mouse-microbiota (OMM^{12}), a gnotobiotic mouse model harboring the presence of twelve sequenced bacterial strains, representing five bacterial phyla that are naturally abundant in the murine GI tract [367, 368]. Rederivation of the Ly6G^{Irf5} strain into GF could provide a useful tool to study individual microbe-neutrophil interactions, once colonised with the OMM^{12} flora. Finally, spatial host-microbiome sequencing might be the ultimate

experiment to connect spatial differences along the colon with neutrophil function and the microbiome at both steady state and d7 Hh + aIL0R [369].

6.7 Conclusion

This thesis highlights the importance of the tissue microenvironment, encompassing both the immediate cell environment as well as the microbiome, in priming and shaping the intestinal immune response. Neutrophils were uncovered to be pivotal players at the onset of intestinal inflammation, providing a "stop or go" signal for establishment of colitis. We also demonstrate the importance of the microbiome in shaping the innate immune response and identify potential bacterial species involved in immune priming both at steady state and during intestinal inflammation. By using a precise modulation of neutrophil function via IRF5, whereby only a few genes are differentially regulated, we offer means through which to dissect crucial mediators of neutrophil functions.

Appendices

A
Appendix 1

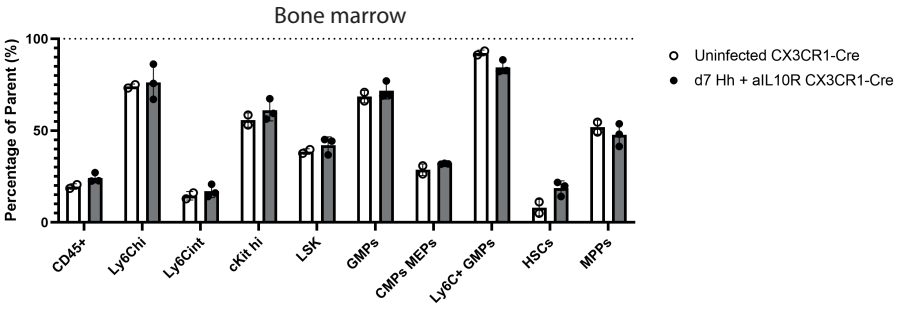


Figure A.1: **Expression of CX3CR1-GFP in various progenitor populations in the bone marrow.** Cells were isolated from the bone marrow from uninfected (n = 2, white bars) and d7 Hh + aIL10R (n = 3, grey bars) CX3CR1-GFP mice and subjected to flow cytometry analsis. Expression of GFP was measured as a percentage of GFP+ cells within a given cell population in the bone marrow. Data presented are means ±SD.

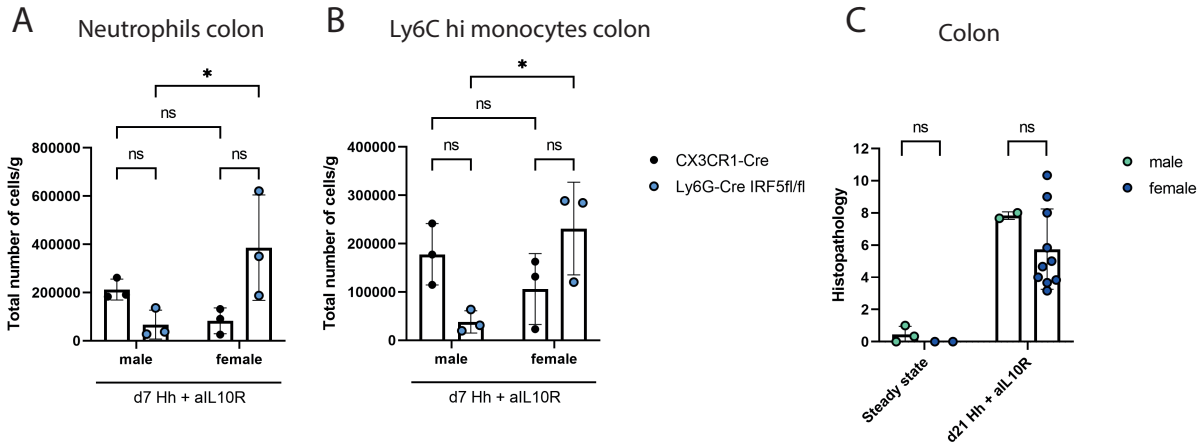


Figure A.2: **Sex-differences at the onset of intestinal inflammation.** A) Neutrophils and B) Ly6C^{hi} monocytes in the colon of d7 Hh + aIL10R Ly6G^{cre} (male (n = 3), female (n = 3)) and Ly6G^{Irf5} (male (n = 3), female (n = 3)) mice. Two-way analysis of variance (ANOVA) with Sidak correction. Data from one independent experiment. C) Histopathology scoring of male and female mice at steady state (males (n = 3), females (n = 2)) and d21 Hh + aIL10R (males (n = 2), females (n = 10)). Data pooled from two independent experiments. Unpaired t-test. Data presented are means ±SD. ns, non significant and *P $\leq$ 0.05

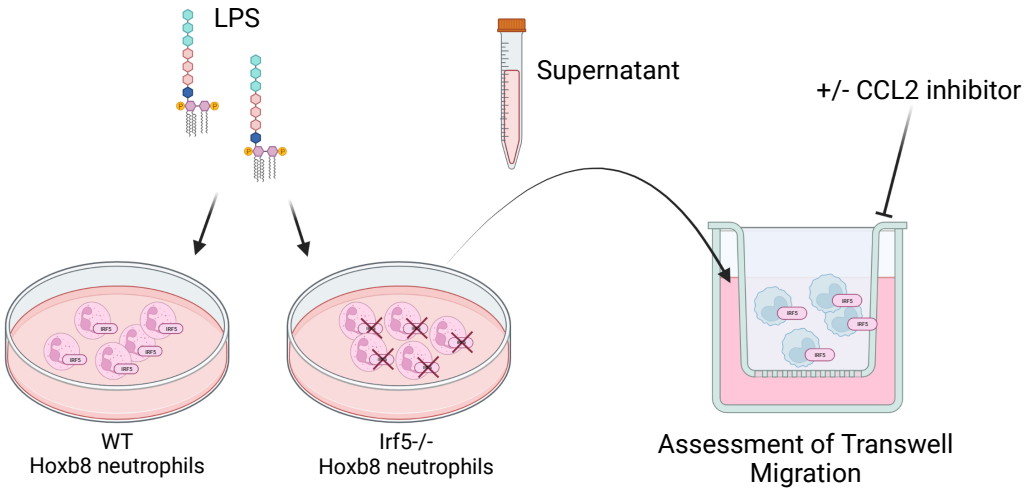


Figure A.3: ***In vitro* proposed set-up for assessing monocyte recruitment by neutrophils.** *This figure was generated using Biorender.*

References

[1] Jaladanki N. Rao and Jian-Ying Wang. "Regulation of Gastrointestinal Mucosal Growth". In: (2011).

[2] Allan M. Mowat and William W. Agace. "Regional specialization within the intestinal immune system". In: *Nature Reviews Immunology* 14.10 (2014), pp. 667–685.

[3] Malin E. V. Johansson, Jessica M. Holmén Larsson, and Gunnar C. Hansson. "The two mucus layers of colon are organized by the MUC2 mucin, whereas the outer layer is a legislator of host–microbial interactions". In: *Proceedings of the National Academy of Sciences* 108.Supplement 1 (Mar. 2011), pp. 4659–4665.

[4] J. S. Cornes. "Number, size, and distribution of Peyer's patches in the human small intestine: Part I The development of Peyer's patches". In: *Gut* 6.3 (June 1965), p. 225.

[5] Kohtaro Fujihashi et al. "Peyer's patches are required for oral tolerance to proteins". In: *PNAS* 98.6 (Mar. 2001), p. 3310.

[6] Christophe P. Frossard et al. "Lymphocytes in Peyer patches regulate clinical tolerance in a murine model of food allergy". In: *Journal of Allergy and Clinical Immunology* 113.5 (May 2004), pp. 958–964.

[7] Hans C. Clevers and Charles L. Bevins. "Paneth Cells: Maestros of the Small Intestinal Crypts". In: *Annual Review of Physiology* 75 (Feb. 2013), pp. 289–311.

[8] Danyvid Olivares-Villagómez and Luc Van Kaer. "Intestinal Intraepithelial Lymphocytes: Sentinels of the Mucosal Barrier". In: *Trends in Immunology* 39.4 (Apr. 2018), pp. 264–275.

[9] Bhavna Rani et al. "Role of the tissue microenvironment as a therapeutic target in hepatocellular carcinoma". In: *World Journal of Gastroenterology* 20.15 (Apr. 2014), p. 4128.

[10] Dorothée L Berthold, Kelsey D J Jones, and Irina A Udalova. "Regional specialization of macrophages along the gastrointestinal tract". In: *Trends in Immunology* (2021).

[11] Iván Ballesteros et al. "Co-option of Neutrophil Fates by Tissue Environments". In: *Cell* 183.5 (Nov. 2020), pp. 1282–1297.

[12] Yonit Lavin et al. "Tissue-Resident Macrophage Enhancer Landscapes Are Shaped by the Local Microenvironment". In: *Cell* 159.6 (Dec. 2014), pp. 1312–1326.

[13] Girmay Desalegn, Oliver Pabst, and Oliver Pabst Girmay Desalegn. "Inflammation triggers immediate rather than progressive changes in monocyte differentiation in the small intestine". In: *Nature Communications* 10.1 (2019), pp. 1–14.

[14] Mor Gross-Vered et al. "Defining murine monocyte differentiation into colonic and ileal macrophages". In: *eLife* 9 (2020), pp. 1–19.

[15] Daisuke Kurotaki, Haruka Sasaki, and Tomohiko Tamura. "Transcriptional control of monocyte and macrophage development". In: *International immunology* (2017).

[16] Geraldine M. Jowett et al. "Organoids capture tissue-specific innate lymphoid cell development in mice and humans". In: *Cell Reports* 40.9 (Aug. 2022), p. 111281.

[17] Dayong Wu et al. "Nutritional Modulation of Immune Function: Analysis of Evidence, Mechanisms, and Clinical Relevance". In: *Frontiers in Immunology* 9.JAN (Jan. 2019), p. 3160.

[18] R. Zeng et al. "Generation and transcriptional programming of intestinal dendritic cells: Essential role of retinoic acid". In: *Mucosal Immunology* 9.1 (Jan. 2016), pp. 183–193.

[19] Martje N. Erkelens et al. "Intestinal Macrophages Balance Inflammatory Expression Profiles via Vitamin A and Dectin-1-Mediated Signaling". In: *Frontiers in Immunology* 11.March (Mar. 2020), p. 551.

[20] Uma Mahesh Gundra et al. "Vitamin A mediates conversion of monocyte-derived macrophages into tissue-resident macrophages during alternative activation". In: *Nature Immunology* 18.6 (2017), pp. 642–653.

[21] Chris Schiering et al. "Feedback control of AHR signalling regulates intestinal immunity". In: *Nature* 542 (2017).

[22] Song Hui Chng et al. "Ablating the aryl hydrocarbon receptor (AhR) in CD11c+ cells perturbs intestinal epithelium development and intestinal immunity". In: *Scientific Reports* (2016).

[23] M. Braga et al. "ESPEN Guidelines on Parenteral Nutrition: Surgery". In: *Clinical Nutrition* 28.4 (Aug. 2009), pp. 378–386.

[24] Takanori Ochi et al. "Diet-dependent, microbiota-independent regulation of IL-10-producing lamina propria macrophages in the small intestine". In: *Scientific Reports* 6.June (2016), pp. 1–12.

[25] Sarah Just et al. "The gut microbiota drives the impact of bile acids and fat source in diet on mouse metabolism". In: *Microbiome* 6.1 (Aug. 2018), pp. 1–18.

[26] Jenessa A. Winston and Casey M. Theriot. "Diversification of host bile acids by members of the gut microbiota". In: *Gut Microbes* 11.2 (Mar. 2020), p. 158.

[27] Sandra Y Wotzka et al. "Escherichia coli limits Salmonella Typhimurium infections after diet shifts and fat-mediated microbiota perturbation in mice". In: *Nature Microbiology* 4 (2019), pp. 2164–2174.

[28] John Y.L. Chiang. "Bile acids: Regulation of synthesis". In: *Journal of Lipid Research* 50.10 (2009), pp. 1955–1966.

[29] G Vantrappen et al. "Bile acid studies in uncomplicated Crohn's disease". In: *Gut* 18 (1977), pp. 730–735.

[30] Eric A. Franzosa et al. "Gut microbiome structure and metabolic activity in inflammatory bowel disease". In: *Nature Microbiology* 4.2 (Feb. 2019), pp. 293–305.

[31] Jacqueline R. M. Plass et al. "Farnesoid X receptor and bile salts are involved in transcriptional regulation of the gene encoding the human bile salt export pump". In: *Hepatology* 35.3 (Mar. 2002), pp. 589–596.

[32] Barbara Renga et al. "The Bile Acid Sensor FXR Is Required for Immune-Regulatory Activities of TLR-9 in Intestinal Inflammation". In: *PLoS ONE* 8.1 (Jan. 2013).

[33] Piero Vavassori et al. "The Bile Acid Receptor FXR Is a Modulator of Intestinal Innate Immunity". In: *The Journal of Immunology* 183.10 (Nov. 2009), pp. 6251–6261.

[34] Michele Biagioli et al. “The Bile Acid Receptor GPBAR1 Regulates the M1/M2 Phenotype of Intestinal Macrophages and Activation of GPBAR1 Rescues Mice from Murine Colitis”. In: *The Journal of Immunology* 199.2 (July 2017), pp. 718–733.

[35] Alison N. Thorburn, Laurence Macia, and Charles R. Mackay. “Diet, Metabolites, and "Western-Lifestyle" Inflammatory Diseases”. In: *Immunity* 40.6 (2014), pp. 833–842.

[36] J. H. Cummings et al. “Short chain fatty acids in human large intestine, portal, hepatic and venous blood.” In: *Gut* 28.10 (Oct. 1987), pp. 1221–1227.

[37] Nagendra Singh et al. “Activation of Gpr109a, Receptor for Niacin and the Commensal Metabolite Butyrate, Suppresses Colonic Inflammation and Carcinogenesis”. In: *Immunity* 40 (2014), pp. 128–139.

[38] Julie Schulthess, Sumeet Pandey, and Melania Capitani. “The Short Chain Fatty Acid Butyrate Imprints an Antimicrobial Program in Macrophages”. In: *Immunity* 50 (2019), pp. 432–445.

[39] Nicholas A. Scott et al. “Antibiotics induce sustained dysregulation of intestinal T cell immunity by perturbing macrophage homeostasis”. In: *Science Translational Medicine* 10.464 (Oct. 2018).

[40] Jung Ha Park et al. “Promotion of Intestinal Epithelial Cell Turnover by Commensal Bacteria: Role of Short-Chain Fatty Acids”. In: *PLOS ONE* 11.5 (May 2016), e0156334.

[41] Sj Shen et al. “Deficiency of Dietary Fiber Modulates Gut Microbiota Composition, Neutrophil Recruitment and Worsens Experimental Colitis”. In: *Frontiers in Immunology* 12 (Feb. 2021), p. 1.

[42] Carolina Tropini et al. “The Gut Microbiome: Connecting Spatial Organization to Function”. In: *Cell Host & Microbe* 21 (2017).

[43] Henning Seedorf et al. “Bacteria from Diverse Habitats Colonize and Compete in the Mouse Gut”. In: *Cell* 159 (2014), pp. 253–266.

[44] Jeremiah J. Faith et al. “The Long-Term Stability of the Human Gut Microbiota”. In: *Science* 341.6141 (July 2013), p. 1237439.

[45] Christoph Becker, Markus F. Neurath, and Stefan Wirtz. “The intestinal microbiota in inflammatory bowel disease”. In: *ILAR Journal* 56.2 (2015), pp. 192–204.

[46] Sandra Y. Wotzka, Bidong D. Nguyen, and Wolf Dietrich Hardt. *Salmonella Typhimurium Diarrhea Reveals Basic Principles of Enteropathogen Infection and Disease-Promoted DNA Exchange*. Apr. 2017.

[47] Stefani Lobionda et al. “The Role of Gut Microbiota in Intestinal Inflammation with Respect to Diet and Extrinsic Stressors”. In: *Microorganisms* 7.8 (Aug. 2019).

[48] Christina A. Hickey et al. “Colitogenic Bacteroides thetaiotaomicron antigens access host immune cells in a sulfatase-dependent manner via outer membrane vesicles”. In: *Cell Host and Microbe* 17.5 (2015), pp. 672–680.

[49] Lindsey Albenberg et al. “Correlation between intraluminal oxygen gradient and radial partitioning of intestinal microbiota”. In: *Gastroenterology* 147.5 (Nov. 2014), pp. 1055–1063.

[50] S Gu et al. “Bacterial Community Mapping of the Mouse Gastrointestinal Tract”. In: *PLoS ONE* 8.10 (2013), p. 74957.

[51] Daniel Crespo-Piazuelo et al. “Characterization of bacterial microbiota compositions along the intestinal tract in pigs and their interactions and functions”. In: *Scientific Reports* 8.1 (Dec. 2018), p. 12727.

[52] Kylie R. James et al. “Distinct microbial and immune niches of the human colon”. In: *Nature Immunology* 21.3 (Feb. 2020), pp. 343–353.

[53] June L. Round and Sarkis K. Mazmanian. “The gut microbiome shapes intestinal immune responses during health and disease”. In: *Nature Reviews Immunology* 9.5 (May 2009), p. 313.

[54] Andrew J Macpherson and Nicola L Harris. “Interactions between commensal intestinal bacteria and the immune system”. In: 4.June (2004), pp. 1626–1632.

[55] Christina L. Hayes et al. “Commensal microbiota induces colonic barrier structure and functions that contribute to homeostasis”. In: *Scientific Reports* 8.1 (Dec. 2018), p. 14184.

[56] Masaki Honda et al. “Perivascular localization of macrophages in the intestinal mucosa is regulated by Nr4a1 and the microbiome”. In: *Nature Communications* (2020).

[57] Byunghyun Kang et al. “Commensal microbiota drive the functional diversification of colon macrophages”. In: *Mucosal Immunology* 13.2 (Mar. 2020), pp. 216–229.

[58] Erik Larsson et al. “Analysis of gut microbial regulation of host gene expression along the length of the gut and regulation of gut microbial ecology through MyD88”. In: *Gut* (2012).

[59] Stefan Wirtz and Markus F. Neurath. “Mouse models of inflammatory bowel disease”. In: *Advanced Drug Delivery Reviews* 59.11 (2007), pp. 1073–1083.

[60] Wendy S. Garrett et al. “Communicable Ulcerative Colitis Induced by T-bet Deficiency in the Innate Immune System”. In: *Cell* 131.1 (Oct. 2007), pp. 33–45.

[61] Yu Jie Zhang et al. “Impacts of Gut Bacteria on Human Health and Diseases”. In: *International Journal of Molecular Sciences* 16.4 (Apr. 2015), pp. 7493–7519.

[62] M. Y. Zeng, N. Inohara, and G. Nuñez. “Mechanisms of inflammation-driven bacterial dysbiosis in the gut”. In: *Mucosal Immunology* 10.1 (Aug. 2016), pp. 18–26.

[63] Alan W. Walker et al. “High-throughput clone library analysis of the mucosa-associated microbiota reveals dysbiosis and differences between inflamed and non-inflamed regions of the intestine in inflammatory bowel disease”. In: *BMC Microbiology* 11.1 (Jan. 2011), pp. 1–12.

[64] Daniel A. Peterson et al. “Metagenomic Approaches for Defining the Pathogenesis of Inflammatory Bowel Diseases”. In: *Cell Host & Microbe* 3.6 (June 2008), pp. 417–427.

[65] Maya Saleh and Giorgio Trinchieri. “Innate immune mechanisms of colitis and colitis-associated colorectal cancer”. In: *Nature Reviews Immunology* 11.1 (Jan. 2011), pp. 9–20.

[66] Kevin J. Maloy and Fiona Powrie. “Intestinal homeostasis and its breakdown in inflammatory bowel disease”. In: *Nature* 474.7351 (2011), pp. 298–306.

[67] Hiroshi Kawamoto and Nagahiro Minato. "Myeloid cells". In: *The International Journal of Biochemistry & Cell Biology* 36.8 (Aug. 2004), pp. 1374–1379.

[68] Steffen Boettcher and Markus G. Manz. "Regulation of Inflammation- and Infection-Driven Hematopoiesis". In: *Trends in Immunology* 38.5 (May 2017), pp. 345–357.

[69] Graham J. Lieschke et al. "Mice lacking granulocyte colony-stimulating factor have chronic neutropenia, granulocyte and macrophage progenitor cell deficiency, and impaired neutrophil mobilization". In: *Blood* 84.6 (Sept. 1994), pp. 1737–1746.

[70] Steffen Boettcher et al. "Endothelial cells translate pathogen signals into G-CSF–driven emergency granulopoiesis". In: *Blood* 124.9 (Aug. 2014), pp. 1393–1403.

[71] Szu-Lee Lee, Phyllis M. Starkey, and Siamon Gordon. "Quantitative analysis of total macrophage content in adult mouse tissues. Immunochemical studies with monoclonal antibody F4/80". In: *Journal of Experimental Medicine* (1985).

[72] Sarah L Pull et al. "Activated macrophages are an adaptive element of the colonic epithelial progenitor niche necessary for regenerative responses to injury". In: *PNAS* 102 (2004), pp. 99–104.

[73] Lesley E. Smythies et al. "Human intestinal macrophages display profound inflammatory anergy despite avid phagocytic and bacteriocidal activity". In: *Journal of Clinical Investigation* 115.1 (Jan. 2005), pp. 66–75.

[74] C. C. Bain et al. "Resident and pro-inflammatory macrophages in the colon represent alternative context-dependent fates of the same Ly6Chi monocyte precursors". In: *Mucosal Immunology* 6.3 (May 2013), pp. 498–510.

[75] Calum C Bain et al. "Constant replenishment from circulating monocytes maintains the macrophage pool in the intestine of adult mice". In: *Nat Immunol* 15.10 (Aug. 2014), pp. 929–937.

[76] Tovah N Shaw et al. "Tissue-resident macrophages in the intestine are long lived and defined by Tim-4 and CD4 expression". In: *The Journal of Experimental Medicine* (2018).

[77] Samira Tamoutounour et al. "CD64 distinguishes macrophages from dendritic cells in the gut and reveals the Th1-inducing role of mesenteric lymph node macrophages during colitis". In: *European Journal of Immunology* 42.12 (Dec. 2012), pp. 3150–3166.

[78] A Schridde et al. "Tissue-specific differentiation of colonic macrophages requires TGFβ receptor-mediated signaling". In: *Mucosal Immunology 2017 10:6* 10.6 (Feb. 2017), pp. 1387–1399.

[79] Ehud Zigmond et al. "Macrophage-restricted interleukin-10 receptor deficiency, but not IL-10 deficiency, causes severe spontaneous colitis". In: *Immunity* 40.5 (2014), pp. 720–733.

[80] Luke C. Davies and Philip R. Taylor. "Tissue-resident macrophages: then and now". In: *Immunology* 144.4 (Apr. 2015), pp. 541–548.

[81] Ivan Monteleone et al. "IL-10-dependent partial refractoriness to Toll-like receptor stimulation modulates gut mucosal dendritic cell function". In: *European Journal of Immunology* 38.6 (June 2008), pp. 1533–1547.

[82] Siegfried Hapfelmeier et al. “Microbe sampling by mucosal dendritic cells is a discrete, MyD88-independent step in ΔinvG S. Typhimurium colitis”. In: *Journal of Experimental Medicine* 205.2 (2008), pp. 437–450.

[83] Xuemei Xie et al. “Single-cell transcriptome profiling reveals neutrophil heterogeneity in homeostasis and infection”. In: *Nature Immunology* 21.9 (July 2020), pp. 1119–1133.

[84] Mikkel Faurschou and Niels Borregaard. “Neutrophil granules and secretory vesicles in inflammation”. In: *Microbes and Infection* 5.14 (2003), pp. 1317–1327.

[85] Samia Bedouhène et al. “Neutrophil Degranulation of Azurophil and Specific Granules”. In: *Methods in Molecular Biology* 2087 (2020), pp. 215–222.

[86] Volker Brinkmann et al. “Neutrophil Extracellular Traps Kill Bacteria”. In: *Science* 303.5663 (2004), pp. 1532–1535.

[87] Patrizia Scapini and Marco A. Cassatella. “Social networking of human neutrophils within the immune system”. In: *Blood* 124.5 (July 2014), pp. 710–719.

[88] William M. Nauseef and Niels Borregaard. “Neutrophils at work”. In: *Nature Immunology* 15.7 (June 2014), pp. 602–611.

[89] Lihui Wang et al. “ROS-producing immature neutrophils in giant cell arteritis are linked to vascular pathologies”. In: *JCI Insight* 5.20 (Oct. 2020).

[90] Maximilien Evrard et al. “Developmental Analysis of Bone Marrow Neutrophils Reveals Populations Specialized in Expansion, Trafficking, and Effector Functions”. In: *Immunity* 48.2 (Feb. 2018), pp. 364–379.

[91] Olivia Marini et al. “Mature CD10+ and immature CD10 neutrophils present in G-CSF–treated donors display opposite effects on T cells”. In: *Blood* 129.10 (Mar. 2017), pp. 1343–1356.

[92] Guangxi Zhou et al. “CD177 + neutrophils as functionally activated neutrophils negatively regulate IBD”. In: *Gut* (2018).

[93] A. Therrien et al. “Recruitment of activated neutrophils correlates with disease severity in adult Crohn’s disease”. In: *Clinical and Experimental Immunology* 195.2 (Feb. 2019), p. 251.

[94] Yongmei Li et al. “Determination of the Critical Concentration of Neutrophils Required to Block Bacterial Growth in Tissues The Journal of Experimental Medicine”. In: 200.5 (2004).

[95] B. M. Fournier and C. A. Parkos. “The role of neutrophils during intestinal inflammation”. In: *Mucosal Immunology 2012 5:4* 5.4 (Apr. 2012), pp. 354–366.

[96] Emma K Persson et al. “IRF4 Transcription-Factor-Dependent CD103⁺CD11b⁺ Dendritic Cells Drive Mucosal T Helper 17 Cell Differentiation”. In: *Immunity* 38.5 (2013), pp. 958–969.

[97] Fernando G Chirdo et al. “Immunomodulatory dendritic cells in intestinal lamina propria.” In: *European journal of immunology* 35.6 (June 2005), pp. 1831–40.

[98] Helene F. Rosenberg, Kimberly D. Dyer, and Paul S. Foster. "Eosinophils: changing perspectives in health and disease". In: *Nature Reviews Immunology* 13.1 (Nov. 2012), pp. 9–22.

[99] Nicola Laura Diny et al. "The aryl hydrocarbon receptor contributes to tissue adaptation of intestinal eosinophils in mice". In: (2022).

[100] Kelly D. Stone, Calman Prussin, and Dean D. Metcalfe. "IgE, mast cells, basophils, and eosinophils". In: *Journal of Allergy and Clinical Immunology* 125.2 (Feb. 2010), S73–S80.

[101] Gérard Eberl et al. "Innate lymphoid cells: A new paradigm in immunology". In: *Science* 348.6237 (May 2015).

[102] Eric Vivier et al. "Functions of natural killer cells". In: *Nature Immunology* 9.5 (Apr. 2008), pp. 503–510.

[103] Nicolas Serafini, Christian A.J. Vosshenrich, and James P. Di Santo. "Transcriptional regulation of innate lymphoid cell fate". In: *Nature Reviews Immunology* 15.7 (June 2015), pp. 415–428.

[104] Hiroyuki Takaba and Hiroshi Takayanagi. "The Mechanisms of T Cell Selection in the Thymus". In: *Trends in Immunology* 38.11 (Nov. 2017), pp. 805–816.

[105] Martin Gellert. "V(D)J Recombination: RAG Proteins, Repair Factors, and Regulation*". In: *Annual Review of Biochemistry* 71 (Nov. 2003), pp. 101–132.

[106] Donna L. Farber, Naomi A. Yudanin, and Nicholas P. Restifo. "Human memory T cells: generation, compartmentalization and homeostasis". In: *Nature Reviews Immunology* 14.1 (Dec. 2013), pp. 24–35.

[107] Dirk H. Busch and Eric G. Pamer. "T cell affinity maturation by selective expansion during infection". In: *Journal of Experimental Medicine* 189.4 (1999), pp. 701–709.

[108] K. Matsuoka et al. "T-bet upregulation and subsequent interleukin 12 stimulation are essential for induction of Th1 mediated immunopathology in Crohn's disease". In: *Gut* 53.9 (Sept. 2004), pp. 1303–1308.

[109] Rajamanickam Anuradha et al. "Parasite-Antigen Driven Expansion of IL-5 and IL-5+ Th2 Human Subpopulations in Lymphatic Filariasis and Their Differential Dependence on IL-10 and TGFβ". In: *PLOS Neglected Tropical Diseases* 8.1 (2014), e2658.

[110] Laurie E. Harrington et al. "Interleukin 17–producing CD4+ effector T cells develop via a lineage distinct from the T helper type 1 and 2 lineages". In: *Nature Immunology* 6.11 (Oct. 2005), pp. 1123–1132.

[111] Shimon Sakaguchi et al. "Regulatory T Cells and Immune Tolerance". In: *Cell* 133.5 (May 2008), pp. 775–787.

[112] Mads Hald Andersen et al. "Cytotoxic T Cells". In: *Journal of Investigative Dermatology* 126.1 (Jan. 2006), pp. 32–41.

[113] Santiago F. Gonzalez et al. "Trafficking of B Cell Antigen in Lymph Nodes". In: *Annual Review of Immunology* 29 (Mar. 2011), pp. 215–233.

[114] Stephen L. Nutt et al. "The generation of antibody-secreting plasma cells". In: *Nature Reviews Immunology* 15.3 (Feb. 2015), pp. 160–171.

[115] Alexandra Bortnick and David Allman. "What Is and What Should Always Have Been: Long-Lived Plasma Cells Induced by T Cell–Independent Antigens". In: *The Journal of Immunology* 190.12 (June 2013), pp. 5913–5918.

[116] Janet Stavnezer, Jeroen E.J. Guikema, and Carol E. Schrader. "Mechanism and Regulation of Class Switch Recombination". In: *Annual Review of Immunology* 26 (Mar. 2008), pp. 261–292.

[117] Oliver Pabst and Emma Slack. "IgA and the intestinal microbiota: the importance of being specific". In: *Mucosal Immunology* 13.1 (Nov. 2019), pp. 12–21.

[118] R. J. Xavier and D. K. Podolsky. "Unravelling the pathogenesis of inflammatory bowel disease". In: *Nature* 448.7152 (July 2007), pp. 427–434.

[119] Markus F. Neurath. "Current and emerging therapeutic targets for IBD". In: *Nature Reviews Gastroenterology & Hepatology* 14.5 (Feb. 2017), pp. 269–278.

[120] Benjamin L. Cohen and David B. Sachar. "Update on anti-tumor necrosis factor agents and other new drugs for inflammatory bowel disease". In: *BMJ* 357 (June 2017).

[121] Nathaniel R. West et al. "Oncostatin M drives intestinal inflammation and predicts response to tumor necrosis factor–neutralizing therapy in patients with inflammatory bowel disease". In: *Nature Medicine* 23.5 (Apr. 2017), pp. 579–589.

[122] Matthias Friedrich et al. "IL-1-driven stromal–neutrophil interactions define a subset of patients with inflammatory bowel disease that does not respond to therapies". In: *Nature Medicine* (Oct. 2021), pp. 1–12.

[123] Wolfgang Hueber et al. "Secukinumab, a human anti-IL-17A monoclonal antibody, for moderate to severe Crohn's disease: unexpected results of a randomised, double-blind placebo-controlled trial". In: *Gut* 61.12 (Dec. 2012), pp. 1693–1700.

[124] Gerhard Rogler. "Where are we heading to in pharmacological IBD therapy?" In: *Pharmacological Research* 100 (Oct. 2015), pp. 220–227.

[125] Daniele Noviello et al. "The IL23-IL17 Immune Axis in the Treatment of Ulcerative Colitis: Successes, Defeats, and Ongoing Challenges". In: *Frontiers in Immunology* 12 (May 2021), p. 1735.

[126] Grigory Ryzhakov et al. "Defactinib inhibits PYK2 phosphorylation of IRF5 and reduces intestinal inflammation". In: *Nature Communications* 12.1 (Nov. 2021), pp. 1–15.

[127] J Rugtveit et al. "Cytokine profiles differ in newly recruited and resident subsets of mucosal macrophages from inflammatory bowel disease." In: *Gastroenterology* 112.5 (May 1997), pp. 1493–505.

[128] A. S. Mee, J. Berney, and D. P. Jewellt. "Monocytes in inflammatory bowel disease: absolute monocyte counts." In: *Journal of Clinical Pathology* 33.10 (Oct. 1980), pp. 917–920.

[129] Alastair L Corbin et al. "IRF5 guides monocytes toward an inflammatory CD11c + macrophage phenotype and promotes intestinal inflammation". In: *Science Immunology* 6085 (2020), pp. 1–16.

[130] Anthony W. Segal. "The role of neutrophils in the pathogenesis of Crohn's disease". In: *European Journal of Clinical Investigation* 48 (Nov. 2018), e12983.

[131] Jerrold M. Ward et al. "Inflammatory large bowel disease in immunodeficient mice naturally infected with Helicobacter hepaticus." In: *Laboratory Animal Science* 46.1 (Feb. 1996), pp. 15–20.

[132] Charmaine J. Foltz et al. "Spontaneous Inflammatory Bowel Disease in Multiple Mutant Mouse Lines: Association with Colonization by Helicobacter hepaticus". In: *Helicobacter* 3.2 (June 1998), pp. 69–78.

[133] Marika C Kullberg et al. "Helicobacter hepaticus Triggers Colitis in Specific-Pathogen-Free Interleukin-10 (IL-10)-Deficient Mice through an IL-12- and Gamma Interferon-Dependent Mechanism". In: *Infection and Immunity* 66.11 (1998), pp. 5157–5166.

[134] Marika C Kullberg et al. "IL-23 plays a key role in Helicobacter hepaticus-induced T cell-dependent colitis". In: *The Journal of Experimental Medicine ARTICLE* 203.11 (2006).

[135] Sofia Buonocore et al. "Innate lymphoid cells drive interleukin-23-dependent innate intestinal pathology". In: *Nature* 464.7293 (Apr. 2010), pp. 1371–1375.

[136] P. J. Morrison et al. "Th17-cell plasticity in Helicobacter hepaticus–induced intestinal inflammation". In: *Mucosal Immunology* 6.6 (Mar. 2013), pp. 1143–1156.

[137] Marika C Kullberg et al. "Bacteria-triggered CD4(+) T Regulatory Cells Suppress Helicobacter hepaticus–induced Colitis". In: *The Journal of Experimental Medicine* 196.4 (2002), pp. 505–515.

[138] Bernadette Begue et al. "Defective IL10 signaling defining a subgroup of patients with inflammatory bowel disease". In: *American Journal of Gastroenterology* 106.8 (2011), pp. 1544–1555.

[139] D. K. Amre et al. "Interleukin 10 (IL-10) gene variants and susceptibility for paediatric onset Crohn's disease". In: *Alimentary Pharmacology and Therapeutics* 29.9 (2009), pp. 1025–1031.

[140] Andre Franke et al. "Sequence variants in IL10, ARPC2 and multiple other loci contribute to ulcerative colitis susceptibility". In: *Nature Genetics* 40.11 (Oct. 2008), pp. 1319–1323.

[141] I. C. Arnold et al. "CD11c+monocyte/macrophages promote chronic Helicobacter hepaticus-induced intestinal inflammation through the production of IL-23". In: *Mucosal Immunology* 9.2 (2016), pp. 352–363.

[142] Claire Pearson et al. "ILC3 GM-CSF production and mobilisation orchestrate acute intestinal inflammation". In: *eLife* 5.JANUARY2016 (Jan. 2016).

[143] Camille Danne et al. "A Large Polysaccharide Produced by Helicobacter hepaticus Induces an Anti-inflammatory Gene Signature in Macrophages". In: *Cell Host and Microbe* 22.6 (Dec. 2017), pp. 733–745.

[144] Rance K Sellon et al. "Resident Enteric Bacteria Are Necessary for Development of Spontaneous Colitis and Immune System Activation in Interleukin-10-Deficient Mice". In: *Infection and Immunity* 66.11 (1998), pp. 5224–5231.

[145] Thomas Karrasch et al. "Gnotobiotic IL-10/;NF-κBEGFP Mice Reveal the Critical Role of TLR/NF-κB Signaling in Commensal Bacteria-Induced Colitis". In: *The Journal of Immunology* 178.10 (May 2007), pp. 6522–6532.

[146] Rebecca Jeffery, Nicholas E Ilott, and Fiona Powrie. "Genetic and environmental factors shape the host response to Helicobacter hepaticus: insights into IBD pathogenesis". In: *Current Opinion in Microbiology* 65 (Feb. 2022), pp. 145–155.

[147] Vassilis Valatas, Michael Vakas, and George Kolios. "The value of experimental models of colitis in predicting efficacy of biological therapies for inflammatory bowel diseases". In: *American Journal of Physiology - Gastrointestinal and Liver Physiology* 305.11 (2013).

[148] Atsushi Mizoguchi. "Animal Models of Inflammatory Bowel Disease". In: *Progress in Molecular Biology and Translational Science* 105 (Jan. 2012), pp. 263–320.

[149] Odile Wéra et al. "The Dual Role of Neutrophils in Inflammatory Bowel Diseases". In: *Journal of Experimental Medicine* (2016).

[150] Grigory Ryzhakov, Hayley L. Eames, and Irina A. Udalova. "Activation and Function of Interferon Regulatory Factor 5". In: *Journal of Interferon & Cytokine Research* 35.2 (2015), pp. 71–78.

[151] Rongtuan Lin et al. "A CRM1-dependent Nuclear Export Pathway Is Involved in the Regulation of IRF-5 Subcellular Localization". In: *Journal of Biological Chemistry* 280.4 (Jan. 2005), pp. 3088–3095.

[152] Miriam Weiss et al. "IRF5 Is a Specific Marker of Inflammatory Macrophages In Vivo". In: *Mediators of Inflammation* 2013 (2013).

[153] Thomas Krausgruber et al. "IRF5 promotes inflammatory macrophage polarization and TH1-TH17 responses". In: *Nat Immunol* 12.3 (2011), pp. 231–238.

[154] Jin Shu et al. "Expression of interferon regulatory factor 5 is regulated by the Sp1 transcription factor". In: *Molecular Medicine Reports* 14.3 (Sept. 2016), pp. 2815–2822.

[155] Bjarte Bergstrøm et al. "TLR8 Senses Staphylococcus aureus RNA in Human Primary Monocytes and Macrophages and Induces IFN-β Production via a TAK1–IKKβ–IRF5 Signaling Pathway". In: *The Journal of Immunology* 195.3 (Aug. 2015), pp. 1100–1111.

[156] Akinori Takaoka et al. "Integral role of IRF5 in the gene induction programme activated by Toll-like receptors". In: *Nature* 434.7030 (Jan. 2005), pp. 243–249.

[157] Mumtaz Yaseen Balkhi, Katherine A. Fitzgerald, and Paula M. Pitha. "IKKα negatively regulates IRF-5 function in a MyD88–TRAF6 pathway". In: *Cellular Signalling* 22.1 (Jan. 2010), pp. 117–127.

[158] Tatsuma Ban et al. "Lyn Kinase Suppresses the Transcriptional Activity of IRF5 in the TLR-MyD88 Pathway to Restrain the Development of Autoimmunity". In: *Immunity* 45.2 (Aug. 2016), pp. 319–332.

[159] David G Saliba et al. "IRF5:RelA Interaction Targets Inflammatory Genes in Macrophages". In: *Cell Reports* 8.5 (2014), pp. 1308–1317.

[160] Dongsheng Xu et al. "Interferon Regulatory Factor 4 (IRF-4) targets IRF-5 to regulate Epstein-Barr virus transformation". In: *Journal of Biological Chemistry* 286.20 (2011), pp. 18261–18267.

[161] Jie Yan et al. "T Cell-Intrinsic IRF5 Regulates T Cell Signaling, Migration, and Differentiation and Promotes Intestinal Inflammation". In: *Cell Reports* 31.13 (June 2020).

[162] Dmitry V. Ostanin et al. "T cell transfer model of chronic colitis: Concepts, considerations, and tricks of the trade". In: *American Journal of Physiology - Gastrointestinal and Liver Physiology* 296.2 (Feb. 2009), pp. 135–146.

[163] Alex Pellerin et al. "Monoallelic IRF5 deficiency in B cells prevents murine lupus". In: *JCI Insight* 6.15 (Aug. 2021).

[164] Saurav De et al. "B cell-intrinsic role for IRF5 in TLR9/BCR-induced human B cell activation, proliferation, and plasmablast differentiation". In: *Frontiers in Immunology* 8.JAN (2018), pp. 1–18.

[165] Tariq E Khoyratty et al. "Distinct transcription factor networks control neutrophil-driven inflammation". In: *Nature Immunology* (2021).

[166] Miriam Weiss et al. "IRF5 controls both acute and chronic inflammation". In: *PNAS* 112.35 (Sept. 2015), pp. 11001–11006.

[167] Johnny Bonnardel et al. "Stellate Cells, Hepatocytes, and Endothelial Cells Imprint the Kupffer Cell Identity on Monocytes Colonizing the Liver Macrophage Niche". In: *Immunity* (Sept. 2019).

[168] April E Price et al. "A Map of Toll-like Receptor Expression in the Intestinal Epithelium Reveals Distinct Spatial, Cell Type-Specific, and Temporal Patterns". In: *Immunity* 49 (2018), pp. 560–575.

[169] Surya P Pandey et al. "Reducing IRF5 expression attenuates colitis in mice, but impairs the clearance of intestinal pathogens". In: *Mucosal Immunology* (2019).

[170] Kathryn Prame Kumar, Alyce J Nicholls, and Connie H Y Wong. "Partners in crime: neutrophils and monocytes/macrophages in inflammation and disease". In: *Cell and Tissue Research* (2018).

[171] Kevin J Maloy et al. "CD4(+)CD25(+) T(R) Cells Suppress Innate Immune Pathology Through Cytokine-dependent Mechanisms". In: *The Journal of Experimental Medicine* 197.1 (2003), pp. 111–119.

[172] Ana Izcue et al. "Interleukin-23 Restrains Regulatory T Cell Activity to Drive T Cell-Dependent Colitis". In: *Immunity* 28.4 (2008), pp. 559–570.

[173] Manja Barthel et al. "Pretreatment of mice with streptomycin provides a Salmonella enterica serovar Typhimurium colitis model that allows analysis of both pathogen and host". In: *Infection and Immunity* 71.5 (May 2003), pp. 2839–2858.

[174] Agnieszka B. Bialkowska et al. "Improved Swiss-rolling Technique for Intestinal Tissue Preparation for Immunohistochemical and Immunofluorescent Analyses". In: *Journal of Visualized Experiments* 113 (July 2016), e54161.

[175] David A. Hume, V. Hugh Perry, and Siamon Gordon. "The mononuclear phagocyte system of the mouse defined by immunohistochemical localisation of antigen F4/80: Macrophages associated with epithelia". In: *The Anatomical Record* 210.3 (1984), pp. 503–512.

[176] Siegfried Hapfelmeier et al. "The Salmonella Pathogenicity Island (SPI)-2 and SPI-1 Type III Secretion Systems Allow Salmonella Serovar typhimurium to Trigger Colitis via MyD88-Dependent and MyD88-Independent Mechanisms". In: *The Journal of Immunology* 174.3 (Feb. 2008), pp. 1675–1685.

[177] Jan Hendrik Niess et al. "CX3CR1-Mediated Dendritic Cell Access to the Intestinal Lumen and Bacterial Clearance". In: *Science* 307.5707 (2005), pp. 254–258.

[178] Ryan J. Cummings et al. "Different tissue phagocytes sample apoptotic cells to direct distinct homeostasis programs". In: *Nature* 539.7630 (Nov. 2016), pp. 565–569.

[179] Myunghoo Kim et al. "Critical Role for the Microbiota in CX3CR1+ Intestinal Mononuclear Phagocyte Regulation of Intestinal T Cell Responses". In: *Immunity* 49.1 (July 2018), pp. 151–163.

[180] Elisa Mazzini et al. "Oral Tolerance Can Be Established via Gap Junction Transfer of Fed Antigens from CX3CR1+ Macrophages to CD103+ Dendritic Cells". In: *Immunity* 40.2 (Feb. 2014), pp. 248–261.

[181] Calum C. Bain and Anika Schridde. "Origin, Differentiation, and Function of Intestinal Macrophages". In: *Frontiers in Immunology* 9.November (2018), pp. 1–15.

[182] Lesley E. Smythies et al. "Inflammation anergy in human intestinal macrophages is due to Smad-induced IκBα expression and NF-κB inactivation". In: *Journal of Biological Chemistry* 285.25 (June 2010), pp. 19593–19604.

[183] Timothy L. Denning et al. "Lamina propria macrophages and dendritic cells differentially induce regulatory and interleukin 17-producing T cell responses". In: *Nature Immunology* 8.10 (2007), pp. 1086–1094.

[184] Aymeric Rivollier et al. "Inflammation switches the differentiation program of Ly6C hi monocytes from antiinflammatory macrophages to inflammatory dendritic cells in the colon". In: *The Journal of Experimental Medicine* 209.1 (2012), pp. 139–155.

[185] Simon Yona et al. "Fate Mapping Reveals Origins and Dynamics of Monocytes and Tissue Macrophages under Homeostasis". In: *Immunity* 38.1 (Jan. 2013), pp. 79–91.

[186] Martin Guilliams and Charlotte L Scott. *Does niche competition determine the origin of tissue-resident macrophages?* Tech. rep. 2017.

[187] Ralf Kühn et al. "Interleukin-10-deficient mice develop chronic enterocolitis". In: *Cell* 75.2 (Oct. 1993), pp. 263–274.

[188] Carey N Lumeng et al. "Phenotypic Switching of Adipose Tissue Macrophages With Obesity Is Generated by Spatiotemporal Differences in Macrophage Subtypes". In: *Diabetes* 57 (2008), pp. 3239–3246.

[189] Yanij Zhu and Ling Zhang and Qing Lu and Yushuo Gao and Yujuan Cai and Ailing Sui and Ting Su and Xi Shen and Bing Xie. "Identification of different macrophage subpopulations with distinct activities in a mouse model of oxygen-induced retinopathy". In: *International Journal of Molecular Medicine* (2017).

[190] Ehud Zigmond et al. "Ly6Chi Monocytes in the Inflamed Colon Give Rise to Proinflammatory Effector Cells and Migratory Antigen-Presenting Cells". In: *Immunity* 37.6 (Dec. 2012), pp. 1076–1090.

[191] John R. Grainger et al. “Macrophages in gastrointestinal homeostasis and inflammation”. In: *Pflugers Archiv European Journal of Physiology* 469.3-4 (2017), pp. 527–539.

[192] David A. Hume, Katharine M. Irvine, and Clare Pridans. “The Mononuclear Phagocyte System: The Relationship between Monocytes and Macrophages”. In: *Trends in Immunology* 0.0 (Feb. 2018), pp. 98–112.

[193] Gregory P Donaldson, S Melanie Lee, and Sarkis K Mazmanian. “Gut biogeography of the bacterial microbiota.” In: *Nature reviews. Microbiology* 14.1 (Jan. 2016), pp. 20–32.

[194] Genta Kakiyama et al. “Modulation of the fecal bile acid profile by gut microbiota in cirrhosis”. In: *Journal of Hepatology* 58.5 (2013), pp. 949–955.

[195] K B M Saiful Islam et al. “Bile Acid Is a Host Factor That Regulates the Composition of the Cecal Microbiota in Rats”. In: *Gastroenterology* 141.5 (2011).

[196] Mantas Kazimieras Malys, Laura Campbell, and Naglis Malys. “Symbiotic and antibiotic interactions between gut commensal microbiota and host immune system”. In: *Medicina* 51.2 (Jan. 2015), pp. 69–75.

[197] Ghislain J. Devroede et al. “Regional Differences in Rates of Insorption of Sodium and Water from the Human Large Intestine”. In: *Canadian Journal of Physiology and Pharmacology* 49.12 (1971), pp. 1023–1029.

[198] Mariana X. Byndloss et al. “Microbiota-activated PPAR-γ signaling inhibits dysbiotic Enterobacteriaceae expansion”. In: *Science* 357.6351 (2017), pp. 570–575.

[199] Renan Corrêa-Oliveira et al. “Regulation of immune cell function by short-chain fatty acids.” In: *Clinical & translational immunology* 5.4 (Apr. 2016), e73.

[200] Pedro Gonçalves, João Ricardo Araújo, and James P Di Santo. “A Cross-Talk Between Microbiota-Derived Short-Chain Fatty Acids and the Host Mucosal Immune System Regulates Intestinal Homeostasis and Inflammatory Bowel Disease”. In: *Inflammatory Bowel Diseases* 24.3 (Feb. 2018), pp. 558–572.

[201] Jessica L Mark Welch et al. “Spatial organization of a model 15-member human gut microbiota established in gnotobiotic mice”. In: *PNAS* (2017).

[202] Fer Vuik et al. “Composition of the mucosa-associated microbiota along the entire gastrointestinal tract of human individuals.” In: *United European Gastroenterology Journal* 7.7 (May 2019), pp. 897–907.

[203] Sara M. Parigi et al. “The spatial transcriptomic landscape of the healing mouse intestine following damage”. In: *Nature Communications* 13.1 (Feb. 2022), pp. 1–16.

[204] Derek J. Royer et al. “Corneal Epithelial Cells Exhibit Myeloid Characteristics and Present Antigen via MHC Class II”. In: *Investigative Ophthalmology & Visual Science* 59.3 (2018), p. 1512.

[205] Thomas T. Macdonald. “Epithelial Proliferation in Response to Gastrointestinal Inflammation”. In: *Annals of the New York Academy of Sciences* 664.1 (Oct. 1992), pp. 202–209.

[206] Sara A. Mathie et al. “Multiparametric analysis of myeloid populations by flow cytometry”. In: *Methods in Molecular Biology* 1745 (2018), pp. 113–124.

[207] Kristen A Earle et al. "Quantitative Imaging of Gut Microbiota Spatial Organization In Brief Resource Quantitative Imaging of Gut Microbiota Spatial Organization". In: *Cell Host & Microbe* 18 (2015), pp. 478–488.

[208] Jason S. Pratt et al. "Modulation of host immune responses by the cytolethal distending toxin of Helicobacter hepaticus". In: *Infection and Immunity* 74.8 (2006), pp. 4496–4504.

[209] Liam Chung et al. "Bacteroides fragilis Toxin Coordinates a Pro-carcinogenic Inflammatory Cascade via Targeting of Colonic Epithelial Cells". In: *Cell Host & Microbe* 23 (2018), pp. 203–214.

[210] G. Elia and G. Guglielmi. "CXCL9 chemokine in ulcerative colitis". In: *Clinica Terapeutica* 169.5 (2018), E235–E241.

[211] Zhenqian Wu et al. "The chemokine CXCL9 expression is associated with better prognosis for colorectal carcinoma patients". In: *Biomedicine and Pharmacotherapy* 78 (2016), pp. 8–13.

[212] Vincenzo Villanacci et al. "Histopathology of IBD colitis. A practical approach from the pathologists of the Italian group for the study of the gastrointestinal tract (GIPAD)". In: *Pathologica* 113.1 (2021), pp. 39–53.

[213] Carlene L. Zindl et al. "IL-22-producing neutrophils contribute to antimicrobial defense and restitution of colonic epithelial integrity during colitis". In: *Proceedings of the National Academy of Sciences of the United States of America* 110.31 (July 2013), pp. 12768–12773.

[214] Qi Chen, Sajith Nair, and Christiane Ruedl. "Microbiota regulates the turnover kinetics of gut macrophages in health and inflammation". In: (2021).

[215] D Bernardo et al. "Human intestinal pro-inflammatory CD11c high CCR2 + CX3CR1 + macrophages, but not their tolerogenic CD11c CCR2 CX3CR1 counterparts, are expanded in inflammatory bowel disease". In: *Mucosal Immunology* (2018).

[216] Aleksandra S. Chikina et al. "Macrophages Maintain Epithelium Integrity by Limiting Fungal Product Absorption". In: *Cell* 183.2 (Oct. 2020), pp. 411–428.

[217] Yutao Yan et al. "Temporal and Spatial Analysis of Clinical and Molecular Parameters in Dextran Sodium Sulfate Induced Colitis". In: *PLoS ONE* 4.6 (2009).

[218] Maria Francesca Viola and Guy Boeckxstaens. "Intestinal resident macrophages: Multitaskers of the gut". In: *Neurogastroenterology and Motility* September 2019 (2020), pp. 1–12.

[219] Florent Ginhoux, Camille Bleriot, and Marc Lecuit. "Forum Dying for a Cause: Regulated Necrosis of Tissue-Resident Macrophages upon Infection". In: *Trends in Immunology* 38 (2017), pp. 693–695.

[220] Gareth-Rhys Rhys Jones et al. "Dynamics of colon monocyte and macrophage activation during colitis". In: *Frontiers in Immunology* 9.NOV (Nov. 2018), p. 2764.

[221] Ayano Kondo et al. "Highly Multiplexed Image Analysis of Intestinal Tissue Sections in Patients With Inflammatory Bowel Disease". In: *Gastroenterology* 161 (2021), pp. 1940–1952.

[222] Jillian L. Astarita et al. “The neutrophil protein CD177 is a novel PDPN receptor that regulates human cancer-associated fibroblast physiology”. In: *Plos One* 16.12 (2021), e0260800.

[223] Sarah A. Reid-Yu et al. “CXCL9 Contributes to Antimicrobial Protection of the Gut during Citrobacter rodentium Infection Independent of Chemokine-Receptor Signaling”. In: *PLOS Pathogens* 11.2 (2015), e1004648.

[224] M. Moyat et al. “IL-22-induced antimicrobial peptides are key determinants of mucosal vaccine-induced protection against H. pylori in mice”. In: *Mucosal Immunology 2017 10:1* 10.1 (May 2016), pp. 271–281.

[225] Bernard C. Lo et al. “ IL-22 Preserves Gut Epithelial Integrity and Promotes Disease Remission during Chronic Salmonella Infection ”. In: *The Journal of Immunology* 202.3 (Feb. 2019), pp. 956–965.

[226] Biana Bernshtein et al. “IL-23-producing IL-10Ra-deficient gut macrophages elicit an IL-22-driven proinflammatory epithelial cell response”. In: *Sci. Immunol* 4 (2019), p. 6571.

[227] Sebastiaan De Schepper et al. “Self-Maintaining Gut Macrophages Are Essential for Intestinal Homeostasis”. In: *Cell* 175.2 (Oct. 2018), pp. 400–415.

[228] Anna Bujko et al. “Transcriptional and functional profiling defines human small intestinal macrophage subsets”. In: *Journal of Experimental Medicine* 215.2 (Feb. 2018), pp. 441–458.

[229] Nicholas A. Scott et al. “Macrophage metabolism in the intestine is compartment specific and regulated by the microbiota”. In: *Immunology* 166.1 (May 2022), pp. 138–152.

[230] Ann-Christin Røberg Beitnes et al. “Rapid Accumulation of CD14+CD11c+ Dendritic Cells in Gut Mucosa of Celiac Disease after in vivo Gluten Challenge”. In: *PLOS ONE* 7.3 (Mar. 2012), e33556.

[231] Martin Guilliams and Freya R. Svedberg. “Does tissue imprinting restrict macrophage plasticity?” In: *Nature Immunology* 22.2 (Jan. 2021), pp. 118–127.

[232] Laween Meran et al. “Engineering transplantable jejunal mucosal grafts using patient-derived organoids from children with intestinal failure”. In: *Nature Medicine* 26.10 (Sept. 2020), pp. 1593–1601.

[233] Hong Liu et al. “Subsets of mononuclear phagocytes are enriched in the inflamed colons of patients with IBD”. In: *BMC Immunology* (2020).

[234] Vinciane Dideberg et al. “An insertion–deletion polymorphism in the Interferon Regulatory Factor 5 (IRF5) gene confers risk of inflammatory bowel diseases”. In: *Human Molecular Genetics* 16.24 (2007), pp. 3008–3016.

[235] Gang G Wang et al. “Quantitative production of macrophages or neutrophils ex vivo using conditional Hoxb8”. In: *Nature Methods* 3 (2006).

[236] Vivek Naranbhai et al. “Genomic modulators of gene expression in human neutrophils”. In: *Nature Communications* (2015).

[237] Jeffrey A. Ericson et al. “Gene Expression during the Generation and Activation of Mouse Neutrophils: Implication of Novel Functional and Regulatory Pathways”. In: *PLOS ONE* 9.10 (Oct. 2014), e108553.

[238] Nazneen R. Irani et al. “Correlation Between Endoscopic and Histological Activity in Ulcerative Colitis Using Validated Indices”. In: *Journal of Crohn’s and Colitis* 12.10 (Nov. 2018), pp. 1151–1157.

[239] A. Marchal Bressenot et al. “Review article: the histological assessment of disease activity in ulcerative colitis”. In: *Alimentary Pharmacology & Therapeutics* 42.8 (Oct. 2015), pp. 957–967.

[240] Masaaki Natsui et al. “Selective depletion of neutrophils by a monoclonal antibody, RP-3, suppresses dextran sulphate sodium-induced colitis in rats”. In: *Journal of Gastroenterology and Hepatology* 12.12 (Dec. 1997), pp. 801–808.

[241] Anja A. Kühl et al. “Aggravation of Different Types of Experimental Colitis by Depletion or Adhesion Blockade of Neutrophils”. In: *Gastroenterology* 133.6 (Dec. 2007), pp. 1882–1892.

[242] Rong Zhang et al. “Up-Regulation of Gr1+CD11b+ population in spleen of dextran sulfate sodium administered mice works to repair colitis”. In: *Inflammation and Allergy - Drug Targets* 10.1 (2011), pp. 39–46.

[243] Natalya V Serbina and Eric G Pamer. “Monocyte emigration from bone marrow during bacterial infection requires signals mediated by chemokine receptor CCR2”. In: (2006).

[244] Anja Hasenberg et al. “Catchup: A mouse model for imaging-based tracking and modulation of neutrophil granulocytes”. In: *Nature Methods* 12.5 (Apr. 2015), pp. 445–452.

[245] David F. Stroncek, Lorraine Caruccio, and Maria Bettinotti. “CD177: A member of the Ly-6 gene superfamily involved with neutrophil proliferation and polycythemia vera”. In: *Journal of Translational Medicine* 2.1 (Mar. 2004), pp. 1–9.

[246] G. Friedrich and P. Soriano. “Promoter traps in embryonic stem cells: A genetic screen to identify and mutate developmental genes in mice”. In: *Genes and Development* 5.9 (1991), pp. 1513–1523.

[247] Shankar Srinivas et al. “Cre reporter strains produced by targeted insertion of EYFP and ECFP into the ROSA26 locus”. In: *BMC Developmental Biology* 1.1 (Mar. 2001), pp. 1–8.

[248] Maureen N. Ajuebor et al. “Endogenous monocyte chemoattractant protein-1 recruits monocytes in the zymosan peritonitis model”. In: *Journal of Leukocyte Biology* 63.1 (Jan. 1998), pp. 108–116.

[249] Stephan Harm, Franz Gabor, and Jens Hartmann. “Low-dose polymyxin: an option for therapy of Gram-negative sepsis”. In: *Innate Immunity* 22.4 (May 2016), p. 274.

[250] Oliver Soehnlein et al. “Neutrophil secretion products pave the way for inflammatory monocytes”. In: *Blood* (2008).

[251] Mizuko Osaka et al. “Critical role of the C5a-activated neutrophils in high-fat diet-induced vascular inflammation”. In: *Scientific Reports* 6.1 (Feb. 2016), pp. 1–11.

[252] By Oleg Chertov et al. “Identification of Human Neutrophil-derived Cathepsin G and Azurocidin / CAP37 as Chemoattractants for”. In: 186.5 (1997).

[253] Jiehao Zhou et al. “Neutrophils Promote Mononuclear Cell Infiltration During Viral-Induced Encephalitis”. In: *The Journal of Immunology* 170.6 (Mar. 2003), pp. 3331–3336.

[254] Andrew S. Brown et al. "Cooperation between Monocyte-Derived Cells and Lymphoid Cells in the Acute Response to a Bacterial Lung Pathogen". In: *PLoS Pathogens* 12.6 (2016).

[255] Xiaoquan Rao, Jixin Zhong, and Qinghua Sun. *The heterogenic properties of monocytes/macrophages and neutrophils in inflammatory response in diabetes*. Oct. 2014.

[256] Martin Pelletier et al. "Evidence for a cross-talk between human neutrophils and Th17 cells". In: *Blood* 115.2 (Jan. 2010), pp. 335–343.

[257] Andrea Paun et al. "Functional characterization of murine interferon regulatory factor 5 (IRF5) and its role in the innate antiviral response". In: *The Journal of biological chemistry* 283.21 (May 2008), pp. 14295–14308.

[258] Annika Hausmann et al. "Intercrypt sentinel macrophages tune antibacterial NF-κB responses in gut epithelial cells via TNF". In: *Journal of Experimental Medicine* 218.11 (Nov. 2021).

[259] Mihir Pendse et al. "Macrophages regulate gastrointestinal motility through complement component 1q". In: *bioRxiv* (2022).

[260] Lisa I. Påhlman et al. "Streptococcal M Protein: A Multipotent and Powerful Inducer of Inflammation". In: *The Journal of Immunology* 177.2 (July 2006), pp. 1221–1228.

[261] Martina Beyrau, Jennifer Victoria Bodkin, and Sussan Nourshargh. "Neutrophil heterogeneity in health and disease: a revitalized avenue in inflammation and immunity". In: *Open Biology* 2.NOV (2012).

[262] Shani Talia Gal-Oz et al. "ImmGen report: sexual dimorphism in the immune system transcriptome". In: *Nature Communications* 10.1 (Sept. 2019), pp. 1–14.

[263] Hui Shen et al. "Gender-dependent Expression of Murine Irf5 Gene: Implications for Sex Bias in Autoimmunity". In: *Journal of Molecular Cell Biology* 2.5 (Oct. 2010), pp. 284–290.

[264] M. Griesbeck et al. "Sex Differences in Plasmacytoid Dendritic Cell Levels of IRF5 Drive Higher IFN- Production in Women". In: *The Journal of Immunology* 195.11 (Dec. 2015), pp. 5327–5336.

[265] Janka Bábíčková et al. "Sex Differences in Experimentally Induced Colitis in Mice: a Role for Estrogens". In: *Inflammation* 38.5 (Oct. 2015), pp. 1996–2006.

[266] Gael Boivin et al. "Durable and controlled depletion of neutrophils in mice". In: *Nature Communications* (2020).

[267] Laurent L. Reber et al. "Neutrophil myeloperoxidase diminishes the toxic effects and mortality induced by lipopolysaccharide". In: *Journal of Experimental Medicine* 214.5 (May 2017), pp. 1249–1258.

[268] Mikael G. Buell and M. Cecilia Berin. "Neutrophil-independence of the initiation of colonic injury - Comparison of results from three models of experimental colitis in the rat". In: *Digestive Diseases and Sciences* 39.12 (1994), pp. 2575–2588.

[269] Dachuan Zhang and Paul S. Frenette. "Cross talk between neutrophils and the microbiota". In: *Blood* 133.20 (May 2019), p. 2168.

[270] Jonathan R. Brestoff and David Artis. "Commensal bacteria at the interface of host metabolism and the immune system". In: *Nature Immunology 2013 14:7* 14.7 (June 2013), pp. 676–684.

[271] Michelle G. Rooks and Wendy S. Garrett. "Gut microbiota, metabolites and host immunity". In: *Nature Reviews Immunology 2016 16:6* 16.6 (May 2016), pp. 341–352.

[272] Andrew J. MacPherson et al. "The mucosal firewalls against commensal intestinal microbes". In: *Seminars in Immunopathology 2009 31:2* 31.2 (Aug. 2009), pp. 145–149.

[273] Misagh Alipour et al. "Mucosal barrier depletion and loss of bacterial diversity are primary abnormalities in paediatric ulcerative colitis". In: *Journal of Crohn's and Colitis* 10.4 (2016), pp. 462–471.

[274] Maya Saleh and Charles O. Elson. "Experimental Inflammatory Bowel Disease: Insights into the Host-Microbiota Dialog". In: *Immunity* 34.3 (Mar. 2011), pp. 293–302.

[275] Urmi Roy et al. "Distinct Microbial Communities Trigger Colitis Development upon Intestinal Barrier Damage via Innate or Adaptive Immune Cells". In: *Cell Reports* 21.4 (Oct. 2017), pp. 994–1008.

[276] J. Magarian Blander et al. "Regulation of inflammation by microbiota interactions with the host". In: *Nature Immunology* 18.8 (July 2017), pp. 851–860.

[277] F. Costa et al. "Calprotectin is a stronger predictive marker of relapse in ulcerative colitis than in Crohn's disease". In: *Gut* 54.3 (Mar. 2005), pp. 364–368.

[278] A. W. Segal and G. Loewi. "Neutrophil dysfunction in Crohn's disease". In: *The Lancet* 308.7979 (July 1976), pp. 219–221.

[279] M. W.N. Harbord et al. "Impaired neutrophil chemotaxis in Crohn's disease relates to reduced production of chemokines and can be augmented by granulocyte-colony stimulating factor". In: *Alimentary Pharmacology & Therapeutics* 24.4 (Aug. 2006), pp. 651–660.

[280] J. H. Wandall and V. Binder. "Leucocyte function in Crohn's disease. Studies on mobilisation using a quantitative skin window technique and on the function of circulating polymorphonuclear leucocytes in vitro." In: *Gut* 23.3 (Mar. 1982), pp. 173–180.

[281] Daniel J.B. Marks et al. "Defective acute inflammation in Crohn's disease: a clinical investigation". In: *The Lancet* 367.9511 (Feb. 2006), pp. 668–678.

[282] Eric L. Campbell and Sean P. Colgan. "Neutrophils and inflammatory metabolism in antimicrobial functions of the mucosa". In: *Journal of Leukocyte Biology* 98.4 (Oct. 2015), pp. 517–522.

[283] Dawei Gong et al. "Involvement of Reduced Microbial Diversity in Inflammatory Bowel Disease". In: *Gastroenterology Research and Practice* 2016 (2016).

[284] Dachuan Zhang et al. "Neutrophil ageing is regulated by the microbiome". In: *Nature* 525.7570 (Sept. 2015), pp. 528–532.

[285] Arya Khosravi et al. "Gut Microbiota Promote Hematopoiesis to Control Bacterial Infection". In: *Cell Host & Microbe* 15.3 (Mar. 2014), pp. 374–381.

[286] Hitesh S. Deshmukh et al. “The microbiota regulates neutrophil homeostasis and host resistance to Escherichia coli K1 sepsis in neonatal mice”. In: *Nature Medicine* 20.5 (Apr. 2014), pp. 524–530.

[287] Maria L. Balmer et al. “Microbiota-Derived Compounds Drive Steady-State Granulopoiesis via MyD88/TICAM Signaling”. In: *The Journal of Immunology* 193.10 (2014), pp. 5273–5283.

[288] Chiaki Iwamura et al. “Sensing of the microbiota by NOD1 in mesenchymal stromal cells regulates murine hematopoiesis”. In: *Blood* 129.2 (Jan. 2017), pp. 171–176.

[289] Chao Shi et al. “Bone Marrow Mesenchymal Stem and Progenitor Cells Induce Monocyte Emigration in Response to Circulating Toll-like Receptor Ligands”. In: *Immunity* 34.4 (Apr. 2011), pp. 590–601.

[290] Danielle G. Souza et al. “The Essential Role of the Intestinal Microbiota in Facilitating Acute Inflammatory Responses”. In: *The Journal of Immunology* 173.6 (2004), pp. 4137–4146.

[291] Caio T. Fagundes et al. “Transient TLR Activation Restores Inflammatory Response and Ability To Control Pulmonary Bacterial Infection in Germfree Mice”. In: *The Journal of Immunology* 188.3 (2012), pp. 1411–1420.

[292] T. Ohkubo et al. “Impaired Superoxide Production in Peripheral Blood Neutrophils of Germ-Free Rats”. In: *Scandinavian Journal of Immunology* 32.6 (Dec. 1990), pp. 727–729.

[293] Dipti Karmarkar and Kenneth L. Rock. “Microbiota signalling through MyD88 is necessary for a systemic neutrophilic inflammatory response”. In: *Immunology* 140.4 (Dec. 2013), pp. 483–492.

[294] Thomas B. Clarke et al. “Recognition of peptidoglycan from the microbiota by Nod1 enhances systemic innate immunity”. In: *Nature Medicine* 16.2 (Jan. 2010), pp. 228–231.

[295] Bernd Uhl et al. “Aged neutrophils contribute to the first line of defense in the acute inflammatory response”. In: *Blood* 128.19 (Nov. 2016), pp. 2327–2337.

[296] Makoto Usami et al. “Butyrate and trichostatin A attenuate nuclear factor κB activation and tumor necrosis factor α secretion and increase prostaglandin E2 secretion in human peripheral blood mononuclear cells”. In: *Nutrition Research* 28.5 (May 2008), pp. 321–328.

[297] Michiko Aoyama, Joji Kotani, and Makoto Usami. “Butyrate and propionate induced activated or non-activated neutrophil apoptosis via HDAC inhibitor activity but without activating GPR-41/GPR-43 pathways”. In: *Nutrition* 26.6 (June 2010), pp. 653–661.

[298] Marco A.R. Vinolo et al. “Suppressive effect of short-chain fatty acids on production of proinflammatory mediators by neutrophils”. In: *The Journal of Nutritional Biochemistry* 22.9 (Sept. 2011), pp. 849–855.

[299] Marjon E. Kamp et al. “G Protein-Coupled Receptor 43 Modulates Neutrophil Recruitment during Acute Inflammation”. In: *PLOS ONE* 11.9 (Sept. 2016), e0163750.

[300] Christian Sina et al. “G Protein-Coupled Receptor 43 Is Essential for Neutrophil Recruitment during Intestinal Inflammation”. In: *The Journal of Immunology* 183.11 (2009), pp. 7514–7522.

[301] Kendle M. Maslowski et al. "Regulation of inflammatory responses by gut microbiota and chemoattractant receptor GPR43". In: *Nature* 461.7268 (Oct. 2009), pp. 1282–1286.

[302] Chuansheng Guo et al. "Bile Acids Control Inflammation and Metabolic Disorder through Inhibition of NLRP3 Inflammasome". In: *Immunity* 45.4 (Oct. 2016), pp. 802–816.

[303] Lisheng Zhang et al. "FXR Protects Lung from Lipopolysaccharide-Induced Acute Injury". In: *Molecular Endocrinology* 26.1 (Jan. 2012), pp. 27–36.

[304] Jennifer A. Loughman and David A. Hunstad. "Induction of Indoleamine 2,3-Dioxygenase by Uropathogenic Bacteria Attenuates Innate Responses to Epithelial Infection". In: *The Journal of Infectious Diseases* 205.12 (June 2012), pp. 1830–1839.

[305] Jennifer A. Loughman et al. "Local generation of kynurenines mediates inhibition of neutrophil chemotaxis by uropathogenic Escherichia coli". In: *Infection and Immunity* 84.4 (2016), pp. 1176–1183.

[306] Michael J. Molloy et al. "Intraluminal Containment of Commensal Outgrowth in the Gut during Infection-Induced Dysbiosis". In: *Cell Host & Microbe* 14.3 (Sept. 2013), pp. 318–328.

[307] Luigi Franchi et al. "NLRC4-driven production of IL-1β discriminates between pathogenic and commensal bacteria and promotes host intestinal defense". In: *Nature Immunology* 13.5 (Apr. 2012), pp. 449–456.

[308] Koji Watanabe et al. "Microbiome-mediated neutrophil recruitment via CXCR2 and protection from amebic colitis". In: *PLOS Pathogens* 13.8 (Aug. 2017), e1006513.

[309] Martina E. Spehlmann et al. "CXCR2-Dependent Mucosal Neutrophil Influx Protects against Colitis-Associated Diarrhea Caused by an Attaching/Effacing Lesion-Forming Bacterial Pathogen". In: *The Journal of Immunology* 183.5 (Sept. 2009), pp. 3332–3343.

[310] Junjie Mei et al. "Cxcr2 and Cxcl5 regulate the IL-17/G-CSF axis and neutrophil homeostasis in mice". In: *The Journal of Clinical Investigation* 122.3 (Mar. 2012), pp. 974–986.

[311] Junbae Jee et al. "Cxcr2 signaling and the microbiome suppress inflammation, bile duct injury, and the phenotype of experimental biliary atresia". In: *PLoS ONE* 12.8 (2017), pp. 1–19.

[312] Nobuhiko Kamada et al. "Control of pathogens and pathobionts by the gut microbiota". In: *Nature Immunology* 14.7 (June 2013), pp. 685–690.

[313] Tsuyoshi Miki, Nobuhiko Okada, and Wolf Dietrich Hardt. "Inflammatory bactericidal lectin RegIIIβ: Friend or foe for the host?" In: *Gut microbes* 9.2 (2018), pp. 179–187.

[314] Tsuyoshi Miki, Otto Holsts, and Wolf Dietrich Hardt. "The Bactericidal Activity of the C-type Lectin RegIIIβ against Gram-negative Bacteria involves Binding to Lipid A". In: *Journal of Biological Chemistry* 287.41 (Oct. 2012), pp. 34844–34855.

[315] Heather L. Cash et al. "Symbiotic bacteria direct expression of an intestinal bactericidal lectin". In: *Science* 313.5790 (Aug. 2006), pp. 1126–1130.

[316] Marco Antonio Cassatella et al. *Biological Roles of Neutrophil-Derived Granule Proteins and Cytokines*. July 2019.

[317] A. D. Dwarakanath et al. “Differential Excretion of Leucocyte Granule Components in Inflammatory Bowel Disease: Implications for Pathogenesis”. In: *Clinical Science* 92.3 (Mar. 1997), pp. 307–313.

[318] Laurens Kruidenier et al. “Intestinal oxidative damage in inflammatory bowel disease: semi-quantification, localization, and association with mucosal antioxidants”. In: *The Journal of Pathology* 201.1 (Sept. 2003), pp. 28–36.

[319] Johannes Stallhofer et al. “Lipocalin-2 Is a Disease Activity Marker in Inflammatory Bowel Disease Regulated by IL-17A, IL-22, and TNF-α and Modulated by IL23R Genotype Status”. In: *Inflammatory Bowel Diseases* 21.10 (Oct. 2015), pp. 2327–2340.

[320] Andrea Bellés et al. “Lactoferrin modulates gut microbiota and Toll-like receptors (TLRs) in mice with dysbiosis induced by antibiotics”. In: *Food & Function* 13.10 (May 2022), pp. 5854–5869.

[321] Trude H. Flo et al. “Lipocalin 2 mediates an innate immune response to bacterial infection by sequestrating iron”. In: *Nature* 432.7019 (Nov. 2004), pp. 917–921.

[322] Martin L. Watzenboeck et al. “Lipocalin 2 modulates dendritic cell activity and shapes immunity to influenza in a microbiome dependent manner”. In: *PLOS Pathogens* 17.4 (Apr. 2021), e1009487.

[323] Xiaoxue Qiu, Chi Chen, and Xiaoli Chen. “Lipocalin 2 Deficiency Restrains Aging-Related Reshaping of Gut Microbiota Structure and Metabolism”. In: *Biomolecules* 11.9 (Aug. 2021), p. 1286.

[324] Roberta Caruso et al. “Dynamic and Asymmetric Changes of the Microbial Communities after Cohousing in Laboratory Mice”. In: *Cell Reports* 27.11 (June 2019), pp. 3401–3412.

[325] Nicholas Edward Ilott et al. “Defining the microbial transcriptional response to colitis through integrated host and microbiome profiling”. In: *ISME Journal* 10.10 (2016), pp. 2389–2404.

[326] Daniel N. Frank et al. “Molecular-phylogenetic characterization of microbial community imbalances in human inflammatory bowel diseases”. In: *PNAS* 104.34 (Aug. 2007), pp. 13780–13785.

[327] Sylwia D. Tyrkalska et al. “Neutrophils mediate Salmonella Typhimurium clearance through the GBP4 inflammasome-dependent production of prostaglandins”. In: *Nature Communications* 7.May (2016).

[328] Manfred Nairz et al. “Lipocalin-2 ensures host defense against Salmonella Typhimurium by controlling macrophage iron homeostasis and immune response”. In: *European Journal of Immunology* 45.11 (Nov. 2015), p. 3073.

[329] Ines Yang et al. “Different gastric microbiota compositions in two human populations with high and low gastric cancer risk in Colombia”. In: *Scientific Reports* 6.1 (Jan. 2016), pp. 1–10.

[330] Yu Chen Lee et al. “The Periodontopathic Pathogen, Porphyromonas gingivalis, Involves a Gut Inflammatory Response and Exacerbates Inflammatory Bowel Disease”. In: *Pathogens* 11.1 (2022).

[331] Sophie Thiemann et al. "Enhancement of IFNγ Production by Distinct Commensals Ameliorates Salmonella-Induced Disease". In: *Cell Host and Microbe* 21.6 (June 2017), pp. 682–694.

[332] Hannah M. Wexler. "Bacteroides: The good, the bad, and the nitty-gritty". In: *Clinical Microbiology Reviews* 20.4 (2007), pp. 593–621.

[333] Seth M. Bloom et al. "Commensal Bacteroides Species Induce Colitis in Host-Genotype-Specific Fashion in a Mouse Model of Inflammatory Bowel Disease". In: *Cell Host & Microbe* 9.5 (May 2011), pp. 390–403.

[334] Kei Nomura et al. "Bacteroidetes species are correlated with disease activity in ulcerative colitis". In: *Journal of Clinical Medicine* 10.8 (2021).

[335] Robert H. Mills et al. "Multi-omics analyses of the ulcerative colitis gut microbiome link Bacteroides vulgatus proteases with disease severity". In: *Nature Microbiology* 7.2 (Jan. 2022), pp. 262–276.

[336] Harrisham Kaur, Chandrani Das, and Sharmila S. Mande. "In Silico analysis of putrefaction pathways in bacteria and its implication in colorectal cancer". In: *Frontiers in Microbiology* 8.NOV (Nov. 2017), p. 2166.

[337] Bianca J Parker et al. "The Genus Alistipes : Gut Bacteria With Emerging Implications to Inflammation , Cancer , and Mental Health". In: *Frontiers in Immunology* 11.June (2020), pp. 1–15.

[338] Kim Y.C. Fung et al. "Colorectal Carcinogenesis: A Cellular Response to Sustained Risk Environment". In: *International Journal of Molecular Sciences* 14.7 (June 2013), pp. 13525–13541.

[339] Katherine Y. King and Margaret A. Goodell. "Inflammatory modulation of HSCs: viewing the HSC as a foundation for the immune response". In: *Nature Reviews Immunology* 11.10 (Sept. 2011), pp. 685–692.

[340] Arielle Glatman Zaretsky, Julie B. Engiles, and Christopher A. Hunter. "Infection-induced changes in hematopoiesis". In: *Journal of immunology* 192.1 (Jan. 2014), pp. 27–33.

[341] Katherine C. MacNamara et al. "Infection-Induced Myelopoiesis during Intracellular Bacterial Infection Is Critically Dependent upon IFN-γ Signaling". In: *Journal of immunology* 186.2 (Jan. 2011), p. 1032.

[342] Maria Casanova-Acebes et al. "Neutrophils instruct homeostatic and pathological states in naive tissues". In: *J. Exp. Med* 215.11 (2018), pp. 2778–2795.

[343] María Casanova-Acebes et al. "Rhythmic modulation of the hematopoietic niche through neutrophil clearance". In: *Cell* 153.5 (May 2013), p. 1025.

[344] Qi Chen, Sajith Nair, and Christiane Ruedl. "Microbiota regulates the turnover kinetics of gut macrophages in health and inflammation". In: *Life Science Alliance* 5.1 (Jan. 2021).

[345] X. Wang et al. "Molecular characterization of the microbial species that colonize human ileal and colonic mucosa by using 16S rDNA sequence analysis". In: *Journal of Applied Microbiology* 95.3 (Sept. 2003), pp. 508–520.

[346] Stephen M. Collins and Premsyl Bercik. "The Relationship Between Intestinal Microbiota and the Central Nervous System in Normal Gastrointestinal Function and Disease". In: *Gastroenterology* 136.6 (2009), pp. 2003–2014.

[347] Melissa A. Kinnebrew et al. "Interleukin 23 Production by Intestinal CD103 +CD11b + Dendritic Cells in Response to Bacterial Flagellin Enhances Mucosal Innate Immune Defense". In: *Immunity* 36.2 (2012), pp. 276–287.

[348] Camille Blériot et al. "Liver-Resident Macrophage Necroptosis Orchestrates Type 1 Microbicidal Inflammation and Type-2-Mediated Tissue Repair during Bacterial Infection". In: *Immunity* 42.1 (Jan. 2015), pp. 145–158.

[349] Nabeetha A. Nagalingam et al. "The effects of intestinal microbial community structure on disease manifestation in IL-10-/- mice infected with Helicobacter hepaticus". In: *Microbiome* 1.1 (May 2013), pp. 1–15.

[350] James Kinchen et al. "Structural Remodeling of the Human Colonic Mesenchyme in Inflammatory Bowel Disease". In: *Cell* 175.2 (Oct. 2018), pp. 372–386.

[351] Kaushal Parikh et al. "Colonic epithelial cell diversity in health and inflammatory bowel disease". In: *Nature* 567.7746 (2019), pp. 49–55.

[352] Elzbieta Kolaczkowska and Paul Kubes. "Neutrophil recruitment and function in health and inflammation". In: *Nature Reviews Immunology* 13.3 (Feb. 2013), pp. 159–175.

[353] Chao Shi and Eric G. Pamer. "Monocyte recruitment during infection and inflammation". In: *Nature Reviews Immunology* 11.11 (Oct. 2011), pp. 762–774.

[354] Cierra N. Casson et al. "Neutrophils and Ly6Chi monocytes collaborate in generating an optimal cytokine response that protects against pulmonary Legionella pneumophila infection". In: *PLOS Pathogens* 13.4 (Apr. 2017), e1006309.

[355] Marco A. Cassatella. "Production of Cytokines By Polymorphonuclear Neutrophils". In: *The Neutrophils: New Outlook for Old Cells* (1999), pp. 151–229.

[356] Joseph E. Qualls et al. "Suppression of experimental colitis by intestinal mononuclear phagocytes". In: *Journal of Leukocyte Biology* 80.4 (Oct. 2006), pp. 802–815.

[357] Thomas Gensollen et al. "How colonization by microbiota in early life shapes the immune system". In: *Science* 352.6285 (Apr. 2016), pp. 539–544.

[358] Yunben Yang et al. "Cross-talk between the gut microbiota and monocyte-like macrophages mediates an inflammatory response to promote colitis-associated tumourigenesis". In: *Gut* 70 (2021), pp. 1495–1506.

[359] Hao Q. Tran et al. ""Western Diet"-Induced Adipose Inflammation Requires a Complex Gut Microbiota". In: *CMGH* 9.2 (Jan. 2020), pp. 313–333.

[360] Daniela Parada Venegas et al. "Short chain fatty acids (SCFAs)mediated gut epithelial and immune regulation and its relevance for inflammatory bowel diseases". In: *Frontiers in Immunology* 10.MAR (2019), p. 277.

[361] E. Y. Lim et al. "Lactobacillus intestinalis YT2 restores the gut microbiota and improves menopausal symptoms in ovariectomized rats". In: *Beneficial Microbes* 12.5 (2021), pp. 503–516.

[362] Joanna M. Warszawska et al. “Lipocalin 2 deactivates macrophages and worsens pneumococcal pneumonia outcomes”. In: *The Journal of Clinical Investigation* 123.8 (Aug. 2013), pp. 3363–3372.

[363] Mirjana Efremova et al. “CellPhoneDB: inferring cell–cell communication from combined expression of multi-subunit ligand–receptor complexes”. In: *Nature Protocols* 15.4 (Feb. 2020), pp. 1484–1506.

[364] Noah W. Palm et al. “Immunoglobulin A coating identifies colitogenic bacteria in inflammatory bowel disease”. In: *Cell* 158.5 (Aug. 2014), p. 1000.

[365] Matthew A. Jackson et al. “Accurate identification and quantification of commensal microbiota bound by host immunoglobulins”. In: *Microbiome* 9.1 (Dec. 2021), pp. 1–22.

[366] Naama Geva-Zatorsky et al. “In vivo imaging and tracking of host–microbiota interactions via metabolic labeling of gut anaerobic bacteria”. In: *Nature Medicine* 21.9 (Aug. 2015), pp. 1091–1100.

[367] Claudia Eberl et al. “Reproducible Colonization of Germ-Free Mice With the Oligo-Mouse-Microbiota in Different Animal Facilities”. In: *Frontiers in Microbiology* 10 (Jan. 2020), p. 2999.

[368] Ilias Lagkouvardos et al. “The Mouse Intestinal Bacterial Collection (miBC) provides host-specific insight into cultured diversity and functional potential of the gut microbiota”. In: *Nature Microbiology* 1.10 (Aug. 2016), pp. 1–15.

[369] Britta Lötstedt et al. “Spatial host-microbiome sequencing”. In: *bioRxiv* (2022).